Merging Parton Showers and Matrix Elements

Nils Lavesson

Department of Theoretical Physics
Lund University

Thesis for the degree of Doctor of Philosophy

Thesis Advisor: *Leif Lönnblad*
Faculty Opponent: *Stephen Mrenna*

To be presented, with the permission of the Faculty of Science of Lund University, for public criticism in lecture hall B of the Department of Physics on Friday, the 13th of February 2009, at 10.15.

Organization	Document name
LUND UNIVERSITY Department of Theoretical Physics Sölvegatan 14A SE–223 62 LUND Sweden	**DOCTORAL DISSERTATION**
	Date of issue January 2009
	Sponsoring organization
Author(s) Nils Lavesson	

Title and subtitle
Merging Parton Showers and Matrix Elements

Abstract

This thesis considers models for describing high energy particle collisions. Existing phenomonological models are modified and new implementations made in order to achive a better description of states with several hard jets. To predict final state hadrons, parton showers are used together with pheonomenological hadronization models. These models describe a wide range of observables, but have the shortcomming that they do not describe states with several jets well. Jets are better described using matrix elements, which then needs to be merged with the parton shower description.

Paper I extends one of the earlier merging algorithms to hadron collisions. The resulting algorithm is applied to W plus jets production at the Tevatron.

Paper II is a comparison of several different algorithms from merging parton shower and matrix elements. The algorithms are compared for a range of observables for W plus jets production at the Tevatron and the LHC. The systematics of each algorithms is also studied.

Paper III deals with the more simple case of $e^+e^- \rightarrow$ jets, where the theory is better understood. Here the most simple matrix element is used for the merging and results are studied for four different algorithms. Three of the algorithms are shown to have problems not previously discussed in the literature.

Paper IV presents an extension to the merging algorithms, that allows for including matrix elements with loops. The algorithm is applied to e^+e^- with matrix element contributions of up to order α_s^2.

Key words:
QCD, Jets, Parton Model, Phenomenological Models, QCD Phenomenology

Classification system and/or index terms (if any):

Supplementary bibliographical information:		Language English
ISSN and key title:		ISBN 978-91-628-7672-2
Recipient's notes	Number of pages 190	Price
	Security classification	

Distributor
Nils Lavesson
Department of Theoretical Physics, Sölvegatan 14A, SE–223 62 Lund, Sweden

Sammanfattning

Denna avhandling handlar om modeller inom partikelfysik, vilka beskriver naturens minsta beståndsdelar. En atom består av en kärna och elektroner. Kärnan består av protoner och neutroner, vilka i sin tur består av kvarkar och gluoner. Dessa partiklar samt hela den flora av andra partiklar som bara går att skapa vid experiment är vad som studeras inom partikelfysiken.

Den dominerande teorin inom partikelfysiken är standardmodellen. Standardmodellen formulerades på 1970-talet och har sedan dess utsatts för många tester. De allra flesta delarna av teorin är bekräftade och teorin beskriver nästan all data på ett tillfredsställande sätt. Den enda partikeln som finns i standardmodellen som inte upptäckts än är Higgs-partikeln, vilken ger de andra partiklarna sin massa.

Det finns fyra krafter i naturen: starka kraften, svaga krafter, elektromagnetism och gravitation. Den starka kraften håller ihop atomkärnor och den svaga kraften ger upphov till vissa typer av radioaktiva sönderfall. Elektromagnetismen beskriver växelverkan mellan allt som har elektrisk laddning, tex. atomkärnan och elektronerna. Standardmodellen beskriver den starka, svaga och elektromagnetiska kraften, men säger ingenting om gravitation då gravitationen är mycket svagare än de andra krafterna och därför är i det närmaste omöjlig att mäta vid partikelfysikexperiment.

Hur små strukturer man kan studera är omvänt proportionellt mot den energi man använder. Det vill säga, desto större energi desto mindre skalor kan man studera. För att kunna göra kunna studera naturens minsta beståndsdelar behövs väldigt kraftfull utrustning. Metoden som används är att accelerera partiklar till mycket hög energi och låta dem kollidera. De partiklar som produceras vid kollisionen studeras sedan och kan användas för att dra slutsatser om strukturerna hos de partiklar som skapats vid kollisionen. De flesta partiklar man är intresserad av är instabila och sönderfaller snabbt vilket gör att man bara kan studera deras sönderfallsprodukter. Experimenten inom partikelfysik är ganska dyra att bygga och därför finns det endast ett fåtal i världen. Just nu håller LHC, som är det största experimentet hittills, på att starta och förhoppningsvis kommer vi att få se nya resultat inom något år.

Denna avhandling rör mest den del av standardmodellen som beskriver den starka kraften. Teorin kallas för QCD (Quantum Chromo Dyanmics) och beskriver många experiment väl. På grund av komplexiteten hos QCD använder man sig av Monte Carlo-tekniker för att simulera experimentella resultat. Monte Carlo går ut på att man genererar händelser slumpmässigt enligt en fördelning given av en modell av problemet. Inom QCD används dels rent teoretiska härledningar och dels modellering som är mer kopplade till experiment för att få en god beskrivning av fysiken. Monte Carlo-modeller har använts för att beskriva mängder av data.

En sorts observabler som används mycket i den här avhandlingen är vad som kallas för jettar. Det hela kommer från att vid en partikelkollision är de utgående partiklarna inte jämt fördelade över alla vinklar utan tenderar att klumpa ihop sig inom mindre områden. En sådan klump med partiklar kallas för en jet.

Inom partikelfysiken letar man ständigt efter ny fysik. Det finns mängder av mer eller mindre lovande kandidater att studera då data från nästa experiment kommer att börja analyseras. Partiklarna som eventuellt kommer att skapas kan bara detekteras via deras sönderfall och en stor del av dessa nya partiklar kommer, om de existerar, att visa sig i form av tillstånd med många jettar. Samma tillstånd kan dock produceras genom QCD och detta utgör den experimentella bakgrunden. För att kunna göra en noggrann mätning av signalen behöver man god kännedom om bakgrunden.

Problemet är att befintliga modeller inte beskriver tillstånd med många jettar på ett tillfredsställande sätt. Den fysik som styr skapandet av jettar har delvis approximerats bort då teorin modifierats för att kunna användas i Monte Carlo-simuleringar. Detta är ett välkänt problem inom partikelfysiken och behöver åtgärdas för att få en bra beskrivning av bakgrunden till ny fysik.

Denna avhandling handlar om att utveckla nya modeller som bättre beskriver tillstånd med många jettar. Dessa modeller implementeras sedan som en del av befintliga Monto Carlo-program och kan jämföras med data. I de första två artiklarna ligger fokus på att använda metoderna för att göra så goda förutsägelser som möjligt för observabler som är av intresse för experimentalister. De tredje artikeln är en utvärdering av befintliga metoder med hjälp av en enklare process, vilket visade på flera svagheter i algoritmerna. Den avslutande artikeln är en vidareutveckling av metoden som användes tidigare för att kunna genomföra beräkningar med ännu bättre noggranhet.

This thesis is based on the following publications:

I Nils Lavesson and Leif Lönnblad,
W+jets matrix elements and the dipole cascade
Journal of High Energy Physics **07** (2005) 054 [hep-ph/0503293].

II Johan Alwall, Stefan Hoeche, Frank Krauss, Nils Lavesson, Leif Lönnblad, Fabio Maltoni, Michelangelo Mangano, Mauro Moretti, Costas Papadopoulos, Fulvio Piccinini, Steffen Schumann, Michele Treccani, Jan Winter and Malgorzata Worek
Comparative study of various algorithms for the merging of parton showers and matrix elements in hadronic collisions
European Physical Journal **C 53** (2008) 473 [arXiv:0706.2569].

III Nils Lavesson and Leif Lönnblad,
Merging parton showers and matrix elements—back to basics
Journal of High Energy Physics **04** (2008) 085 [arXiv:0712.2966].

IV Nils Lavesson and Leif Lönnblad,
Extending CKKW-merging to one-loop matrix elements
Journal of High Energy Physics **12** (2008) 070 [arXiv:0811.2912].

Contents

i

Introduction

This thesis is about improving the precision of calculations involving the strong interaction. The strong interaction is the force that holds the nucleons (protons and neutrons) together in the nucleus and describes the interaction of particles inside the nucleons, known as quarks and gluons. The theory of the strong interaction is called Quantum Chromo Dynamics (QCD). The theory was formulated in 1970s, but even today provides us with challenges when used to describe experiments.

QCD is part of a bigger theory known as the Standard Model. The Standard Model is the dominant theory of particle physics today and can account for almost all the experimental data within particle physics. The model is described in the next section.

To probe the interactions of quarks and gluons one needs to go to energies which are high enough to break the bound states of quarks. This means going to energies that are larger than roughly 1 GeV. The highest possible energies (apart from cosmic rays) can be accessed through collider experiments, where two beams of particles are accelerated and collided head on. This produces a vast number of outgoing particles, which are tracked and measured by a detector. All the results in this thesis are calculated for collider experiments.

To be able to understand the physics in such an event one needs good tools for understanding the dynamics involved. Due to the complexity and non-linearity of QCD, the only viable way to simulate the final state particles that show up in the detector is to use Monte Carlo techniques. To do this, each part of the collision is described using different models and these are used to generate events distributed randomly in accordance with the models. In practice, complete software packages are written with the goal of producing events that resemble those recorded by the experiments as closely as possible.

One feature that is present in particle physics collisions is that particles are rarely produced isotropically, but rather appear bunched together in a region of solid angle. Such a bunch of particles is called a jet. The main goal of this thesis is to improve the description of states with several jets. The production of jets, especially at wide angles, is described by QCD at short distances. The long distance physics describes the structure within the jets and the process of

particle production known as hadronization. The methods presented in this thesis are ways of combining the short and long distance descriptions within one framework where the models has been implemented using Monte Carlo techniques.

Although events with several jets have a fairly low production rate, they are still of major importance for particle physics, since they are used as discovery channels for many proposed theories of new physics. To be able to understand the new physics one needs a good description of both the signal and the background, where the dominant background is usually multi-jet states produced through QCD. Failing to understand the background makes analysis of new physics a lot more difficult and more prone to systematic errors.

i.1 The Standard Model

The main theory of particle physics today is the Standard Model. The model includes the electromagnetic, weak and strong interactions. Gravity has not been included since the force is too weak to be seen in particle physics experiments. The Standard Model is a quantum field theory, which is a framework developed by unifying classical field theory, quantum mechanics and special relativity. The combination of the three theories leads to a general framework and specific field theories can be constructed by introducing something called gauge invariance. This means that one requires everything to be invariant both under the normal symmetries from quantum mechanics and special relativity and a chosen symmetry group. In order to maintain this new symmetry one has to introduce a specific set of dynamics, depending on which symmetry was introduced. The tricky thing is knowing which symmetries to introduce and there is no good answer to why we should use the specific symmetries present in our models apart from the fact that they describe reality well. For an introduction to particle physics and quantum field theory see [1, 2].

The symmetry group that produces the interactions in the Standard Model is $U(1) \times SU(2) \times SU(3)$. $U(1)$ is a complex phase and $SU(2)$ and $SU(3)$ are unitary matrices with determinant one and rank two and three respectively. The invariance under $U(1)$ and $SU(2)$ leads to the theory of the electroweak interaction. The particles mediating the electroweak interactions are the photon (γ), W^+, W^- and Z^0. The photon is responsible for all the electromagnetic interactions and has no mass. The other electroweak gauge particles are massive and are only seen in much rarer processes. The most widely known example of the weak interaction is the β-decay in atomic nuclei.

The symmetry group $SU(3)$ is responsible for generating the strong interaction. The strong charge is called color and can take the value of red, green, blue and their respective anti-colors. The sum of the three colors is charge neutral. The strong force only has one massless mediator known as the gluon,

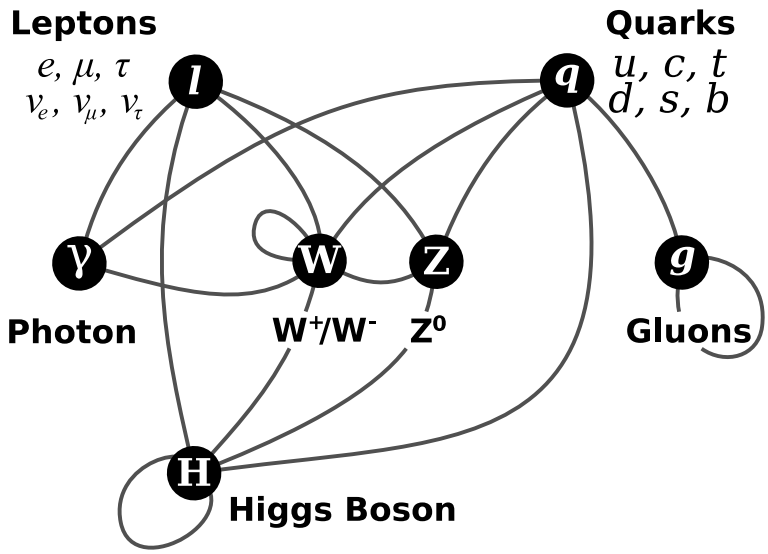

Figure *i*.1: The elementary particles and their interactions

which also carries color and anti-color charge.

The matter in the Standard Model belong to two different groups of particles, quarks and leptons. The quarks can interact through electromagnetic, weak, and strong interactions, with the strong interactions being the most dominant. The quarks come in six different flavors: down, up, strange, charm, bottom and top. The leptons include charged leptons and neutrinos. The charged leptons are the electron, muon and tau. The corresponding neutrinos are known as the electron neutrino, muon neutrino and tau neutrino. Charged leptons can interact electromagnetically and weakly, while the neutrinos can only interact weakly. Each particle also has an anti-particle with equal mass and opposite charge. The matter particles and which gauge particles they can interact with are illustrated in figure *i*.1.

The matter within the Standard Model can be split up into three generations of particles with similar properties, but with different masses. The three generations are (d, u, e, ν_e), (s, c, μ, ν_μ), and (b, t, τ, μ_e). All second and third generation quarks and charged leptons have a short lifetime and all "normal" matter is made from up and down quarks and the electron. The more exotic particles are produced in experiments through highly energetic collisions.

The final piece of the Standard Model is the Higgs particle. The role of the Higgs particle is to provide mass for the all the particles within the Standard Model (including itself). So far the Higgs particle is only a postulate and has not been confirmed experimentally. The LHC experiment (described in

section *i*.3) may provide an answer to whether the Higgs exists or not soon.

Although the Standard Model describes the vast majority of experimental data quite well, there are still several unanswered questions. Lots of theories have been proposed to extend the Standard Model, collectively known as BSM (Beyond the Standard Model) theories. This topic is very broad and has not been included in this thesis.

i.2 QCD

The particles that interact through QCD is limited to quarks, anti-quarks and gluons (collectively called partons). Quarks carry color charge, anti-quarks carry anti-color charge, and gluons have both color and anti-color charge. The gluons mediate the force, but interact through QCD themselves.

The parameter that determines the strength of a force in quantum field theory is called a coupling. The couplings in the Standard Model have a dependence on energy or distance through something called renormalization. Renormalization is a way of systematically removing infinities from the theory, where certain terms are absorbed into the couplings giving them a scale dependence. The scale is therefore referred to as the renormalization scale.

For the electromagnetic and the weak force the coupling gets stronger as one goes to higher energy or shorter distance, but for the strong force the opposite is true. The strong force is weaker at small distances and high energies and gets stronger as the distance between particles increases. The fact that in QCD the force is weak at small distances is known as asymptotic freedom and the discovery was awarded the Nobel prize in physics 2004.

The fact that the force gets stronger at large distances has profound consequences. It means that strongly interacting particles can only be observed in color-neutral bound states, which is a property known as confinement. Any attempt to separate a quark or gluon from its bound state results in the production of new color-neutral particles rather than a free quark or gluon. Although confinement is widely accepted based on experimental results, it is still an open problem to prove that the theory of QCD leads to confinement. Bound states of colored particles are called hadrons and can occur in two main varieties: baryons and mesons. Baryons are states with three quarks (or three anti-quarks) and mesons consist of one quark and one anti-quark.

The property of asymptotic freedom means that in the short distance regime, physics can be described well by perturbation theory, by expanding the problem in powers of the strong coupling. Here, everything can (in principle) be calculated from first principles. However, apart from simple cases the calculations quickly grow in complexity and there are still many challenges that remains to be solved before we have a complete understanding of perturbative QCD.

At longer distances perturbation theory no longer works and one has to use phenomenological models. The main challenge here is to describe the transition from partons to hadrons and the models are known as hadronization models. When perturbation theory no longer works, QCD can only be used as an approximate guide and the resulting models have a number of parameters that need to be fit to data.

There is, however, a strong correlation between what happens at short distances and what appears in the final state. A hard emission at high energy is believed to cause more final state hadrons to be formed in that direction. This means that the jets in the final state are correlated to reactions which have hard perturbative emissions.

The jets in the final states are defined using a jet algorithm. The most common ones are cone algorithms and clustering algorithms. Cone algorithms define a jet as a set of particles within a cone in angular space and with an energy above a certain threshold. Clustering algorithms work by computing the distance between pairs of particles according to a measure defined by the algorithm. The jets are then clustered by repeatedly merging the pair with minimum distance until a cutoff is reached.

Jets can be defined both for the perturbative emissions and the final state hadrons. The jet structure at the perturbative level is strongly correlated to the jet structure of the final hardons. Improving the description of hard emissions should also lead to a better description of jets.

i.3 Experiments

To be able to study the interactions of quarks and gluons one has to go to energies high enough to be beyond the typical energies of hadronic bound states. The main way of doing this is through collider experiments, where two beams of particles are accelerated and collided. The particles inside the beam interact and the outgoing particles are detected using various types of detectors.

Four main experiments are of interest in this thesis: LEP, HERA, Tevatron and LHC. The LEP experiment was an electron positron collider placed at CERN, outside Geneva, which operated from 1989 to 2000. The incoming particles only carry electroweak charge, providing a cleaner environment compared to situations where the incoming particles carry color charge. The LEP experiment has generated an abundance of precision measurements of the strong force and the data is still widely used to test and tune models.

The second experiment of relevance is the HERA experiment which was conducted at DESY, in Hamburg, from 1992 to 2007. The experiment collided protons with electrons or positrons. This allowed one to use the electron as a probe to determine the structure of the proton.

The largest high energy particle collider currently running is the Tevatron at FNAL, near Chicago. The experiment has been running since 1987 and is scheduled to shut down in 2009. Protons are collided with anti-protons at center of mass energies of 1.96 TeV. This experiment is famous for discovering the top quark in 1995. The use of protons in the initial state makes it possible to go to higher energies compared to using electrons, due to smaller energy losses from synchrotron radiation. However, the proton contains lots of quarks and gluons causing a lot of debris to be generated in the collisions, which makes precision measurements difficult. Machines like this are, however, well suited for discovering new physics.

The newest experiment is the LHC, also at CERN, which is currently undergoing startup. The experiment is designed to collide protons at a center of mass energy of 14 TeV. The increase in energy provides good hope that new physics can be discovered. This will be the only high energy particle collider experiment that will be running in the near future. Other experiments are planned but all decisions are postponed until the first data from the LHC arrives.

One of the big theoretical challenges within the phenomenology community is how to use all the data from LEP, HERA and the Tevatron to make the best predictions for LHC. Each experiment contributes with its own piece of information, where LEP gives you high precision and a clean environment to study QCD, HERA provides extensive studies of the proton structure and the Tevatron has a similar experimental setup to the LHC. Ideally, data from all the experiments should be considered to get the best possible predictions.

i.4 Matrix elements

To calculate a process in QCD, the Feynman diagrams for the relevant process are constructed. A Feynman diagram is a way to draw an interaction within quantum field theory. By convention, matter particles such as quarks are drawn with solid lines, gluons with spirals and other gauge bosons such as the photon with wiggly lines. Each vertex in a Feynman diagram conserves energy and momenta, but internal particles do not need to have their physical mass. Figure *i*.2 shows some examples of Feynman diagrams that contribute to e^+e^- annihilation into hadrons. Details on how to calculate Feynman diagrams can be found in [2].

For QCD purposes the way the diagrams are classified is by which order of the strong coupling (α_s) is involved and how many loops are present. The order in α_s is specified by how many strong vertices are present, and the number of loops is equal to the number of momenta that are not constrained by external legs. The diagrams are usually calculated as a function of the energy and momentum of the outgoing particles. The energy and momentum of the

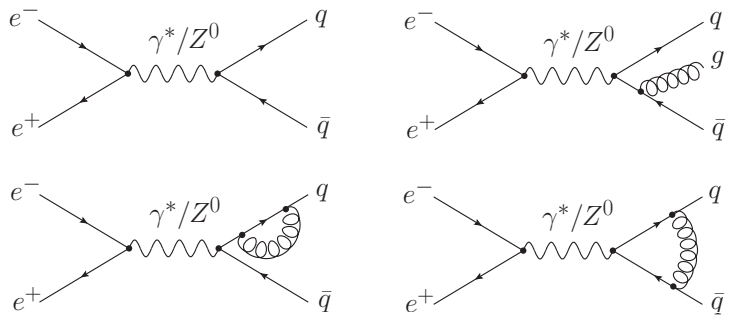

Figure *i*.2: Some of the lowest order Feynman graphs that contribute to e^+e^- to hadrons

outgoing particles is referred to as the phase space. All the outgoing particles are required to be on mass shell and energy and momentum is conserved.

The easiest diagrams to calculate are those without any loops, known as tree-level diagrams, since they do not involve any integrals over unknown momenta. For any configuration where all the particles have non-zero momentum and no particles are collinear, all tree-level diagrams are finite. However, in the phase space region where particles are either soft (low energy) or collinear the diagrams may contain poles, which lead to logarithmic divergences. The calculation needs to be regulated in these regions, usually by a cutoff in phase space which is frequently specified using a jet algorithm.

If one uses the tree-level matrix element to calculate a jet cross section by integrating over the phase space according to the jet definition, one arrives at a cross section which is the inclusive jet cross section. This means that one calculates the sum of the cross sections of all states with the number of specified jets and all higher jet multiplicities.

There have been several techniques developed to calculate tree-level matrix elements. The property most often used is to project the external legs onto helicity states, which are amplitudes where the spin is parallel or antiparallel with the momentum. When using helicity states, many of the diagrams turn out to be zero and the calculations are simplified. After the diagrams have been calculated one has to address the issue of integrating the resulting amplitude over the specified phase space, which can be quite challenging for states with several outgoing particles. The integration is usually done with Monte Carlo techniques combined with analytical calculations to determine the structure of the divergences. Some programs like MADEVENT [3] or ALPGEN [4] automatically generate and sum all the diagrams and outputs events generated randomly in accordance with the matrix element. The programs are currently limited to cases with up to 6 or 7 outgoing particles due

to the rapid increase in complexity of the calculations when increasing the number of outgoing particles.

The singularities in the soft and collinear limit indicate that there are other graphs which become important. The way to improve this situation is to include diagrams with loops. There is, however, a new difficulty arising not present in tree-level graphs, namely that all loop diagrams are infinite and frequently negative. Only the sum of all the diagrams to the same order in α_s, integrated over soft and collinear emissions, is a finite quantity. The way to do these calculations is to introduce a regularization scheme. The most common way is to do an analytical continuation of the number of space-time dimensions to $4 - \epsilon$, which makes all the loop integrals converge. The result can be summed and finally one can take the limit $\epsilon \to 0$.

The minimum expansion of the tree-level matrix element is to include the first loop. To make the one-loop matrix element calculation finite one has to include configurations with one more parton and choose a scheme to determine if the extra parton should be considered resolved or if the extra emission should be clustered and the state added to the one-loop matrix element. The scheme to determine if a parton is resolved is required to treat all configurations which contain divergences as unresolved. For example a jet algorithm might be a suitable way to classify emissions. Which scheme is suitable is also dependent on the observable one wishes to study. The observable should ideally have no dependence on unresolved partons.

Using one-loop matrix elements is a big improvement over the tree-level matrix element, since it resolves some of the issues of divergences. There is also the issue that one has to pick a renormalization scale when calculating matrix elements and the sensitivity to this scale is greatly decreased with the first loop. However, there are still ambiguities regarding how to map different parton multiplicities to one another and when to consider a parton unresolved.

One popular scheme for calculating one-loop matrix elements is known as Catani–Seymour [5, 6] dipole subtraction, which is based upon mapping between different multiplicities using phase-space maps transforming two partons into three. The scheme is used to calculate a term which is added to the one-loop matrix element and subtracted from the matrix element with one more parton in such a way that all singularities cancel. This scheme has been used for various calculation of one-loop diagrams. There are currently efforts to automate the process and to extend the calculations to processes with more external legs and hopefully in a few years we should have automated matrix element generators available just as with tree-level matrix elements.

i.5 Parton showers

Partons showers are used to provide a good description of collinear and soft emissions. The main concepts are described here and a more extensive introduction can be found in [7, 8]. To describe the soft and collinear limit one needs to correctly treat the poles that causes divergences in tree-level matrix elements. By studying a single soft or collinear emission, the probability of having such an emission can be formulated in terms of rather simple functions called splitting functions. The second ingredient in parton showers is the assumption that the emissions can be ordered by performing the emissions that are associated with a short distance first and those at longer distance later. This means that the splitting function can be used consecutively, ordered by a variable related to distance or energy.

The application of splitting functions makes the probability of emissions approximately equal to the corresponding tree-level diagram, which is known as the real part of the emissions. To approximate the effect of including all the diagrams with loops, known as virtual diagrams, one multiplies the probability of an emission by the probability of not having en emission at a higher scale. This no-emission probability is known as the Sudakov form factor and is given by exponentiating the integral of the splitting function. The procedure is similar to calculating the probability of a radioactive decay, where the probability of a decay should be multiplied by the probability that it has not already happened.

The parton shower is formulated in a probabilistic description, where one emission is considered at a time. This is ideal for implementation in a computer program using Monte Carlo techniques. At each step of the program, all the relevant emission probabilities and Sudakov form factors are calculated and an emission is generated. Using this procedure, one can build up events with many outgoing partons, which would have been impossible using the full matrix element. An illustration of a shower is shown in figure *i*.3.

If the emissions are strongly ordered, meaning that each emission happens at a much smaller value of the ordering variable compared to the previous emission, then the shower is a good approximation and this applies to the bulk of the cross section. There are important exceptions though, mainly when one has several hard partons at wide angle, which corresponds to a final states with several hard jets. In this case, the terms neglected when formulating the shower become important and the result becomes unreliable.

The parton shower also has the nice feature that the events are completely exclusive. This means that the shower determines the probability for specific parton configurations with no other emissions. The final step of producing the hadrons seen by experiments is done by more phenomenological models. The two main models used for this purpose are the ”Lund string model” [9]

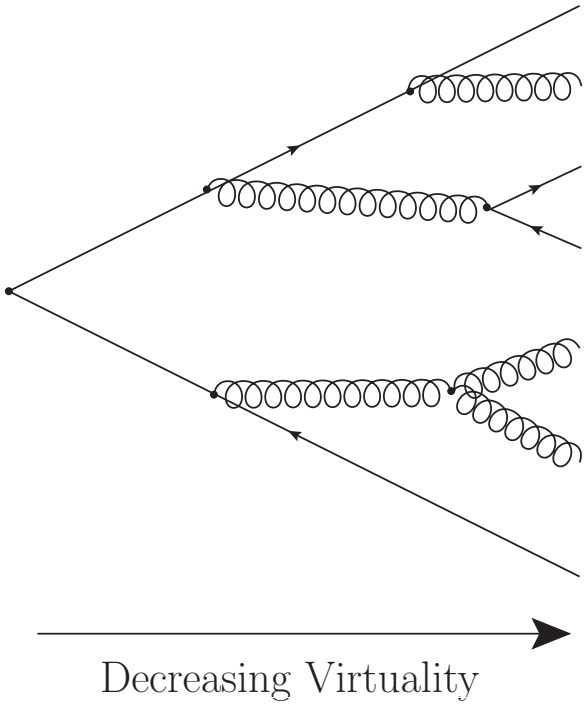

Figure *i*.3: An example of what the evolution of a quark anti-quark pair could be in a parton shower. The emissions are ordered in virtuality and as one goes to lower values more emissions are resolved.

and "Cluster fragmentation" [10]. However, both these models only work if they are provided with exclusive states where all the collinear and soft partons simulated correctly.

For the matrix elements the accuracy was described in orders of α_s, but that is clearly not the way to go for parton showers. Instead one counts which logarithms have been summed correctly. The dominant contribution to an emission probability is when the emission is both soft and collinear, which results in one order of the strong coupling and two logarithms (one from the soft pole and one from the collinear pole). One can sum the contributions from consecutive emissions including all terms of the type $\alpha_s^n \log^{2n}$, which is known as the leading-log (LL) approximation. Just about any parton shower is accurate to LL. The problem of the LL approximation is that there is a big freedom in how to do your calculations, which can lead to vastly different results. Most things measured would depend on effects that are beyond LL, but so far no one has been able to construct a shower which achieves the next

level of accuracy, which is next-to-leading log (NLL) (also correctly summing all terms of order $\alpha_s^n \log^{2n-1}$).

Beyond LL there are a number of corrections that are implemented in most parton shower algorithms, where some corrections have been derived from theory and some can be considered more as choices. The main corrections that can be derived from theory are all formally on the NLL level, but they don't make the shower accurate to NLL. Energy momentum conservation is obviously a desirable property of any program and can be included by giving a recoil to existing partons when a new parton is emitted. It does, however, leave some options for how to distribute the recoil that are not given by theory. Another effect that is also included is the running of the strong coupling by letting α_s depend on each scale of the emissions in the shower. The splitting functions contain terms beside the leading pole, which give contributions at NLL and are also included. There is also a relation between the angles of emission that can be derived from soft gluon interference, which means it is theoretically motivated to order emissions in decreasing angle (apart from the ordering already present in the cascade).

Even with these corrections implemented there are also choices to be considered. The main choice is which ordering variable to use in the shower. The most common choices are to order the shower in angles, virtuality or transverse momentum. To order the shower in angles is to promote the angular ordering discussed earlier to the level of being the ordering variable, which has some nice theoretical features, but it also has several drawbacks which include not being Lorentz invariant. Using virtuality ordering is good to cover the entire phase space, but it has a tendency to overdo it by not respecting angular ordering. This can be corrected by a separate veto on emissions. Transverse momentum has no obvious downsides, but it does lack some of the advantages of the other ordering schemes. There are many of more choices to be made in a parton shower, for further details read the manuals of the various programs.

The parton showers form the basis for the Monte Carlo event generators, which are widely used in experimental particle physics. The two most famous general purpose programs are PYTHIA [11] and HERWIG [12]. PYTHIA is available both with virtuality ordering and with transverse momentum ordering and uses Lund string fragmentation. HERWIG uses an angular ordered shower and the hadronization is done using cluster fragmentation. Another commonly used program is ARIADNE [13], which is used extensively in this thesis. The program is based on a cascade of color dipoles [14, 15] and is ordered in transverse momentum. ARIADNE does not contain any fragmentation routines and uses the PYTHIA implementation of string fragmentation instead. More recently a new program called SHERPA [16] has been written, which is mainly focused on including matrix elements together with the shower. The shower

in SHERPA is very similar to the virtuality ordered shower in PYTHIA and the PYTHIA implementation of string fragmentation is used for the hadronization.

i.6 Merging matrix elements with parton showers

In the previous two sections, two different methods for calculating cross sections for parton configurations have been described. Matrix elements have the best description for hard emissions, but cannot describe collinear and soft emissions properly. The parton shower on the other hand can handle collinear and soft emissions, but neglects terms that are important for describing hard emissions. The best thing would be if the two approaches could be combined in a consistent way, especially for observables that are dependent on hard physics such as the cross section for states with several hard jets, or jet correlations.

i.6.1 Reweighting splitting functions

The first approach that was used to improve the parton showers using matrix elements was to reweight the first branching probability [17–19]. This means that one replaces the branching probability of the first emission with the branching probability from the matrix element. This solutions corrects the first emission according to the matrix element and has become a standard feature in many of the processes in the parton shower implementations. The only problem is that the method is quite hard to generalize to more than one emission.

i.6.2 Tree-level matrix elements

More general schemes are necessary if one wants to accurately describe states with many jets. The next step to go beyond the reweighting described above, is to use tree-level matrix elements with higher parton multiplicities together with the shower. The goal of the algorithms is to be able to use the automated tools for generating events according to the matrix element and feed the results into the parton shower programs to be able to simulate final state hadrons.

There are several algorithms that address the problem and they all face the same two main issues, namely to divide the phase space for emissions between the matrix element and the parton shower and to make the matrix elements exclusive. There are a few more things that need to be included, such as reweighting the events with a running coupling, but these are straight forward to implement. The methods used in the different merging algorithms are somewhat different, but the goal of each one is the same.

The first problem of splitting the phase space is usually solved by a cut on the matrix element and the same cut as veto on the parton shower. The goal is to have two regions of phase space, one for the matrix element and one for the parton shower, that together cover the entire phase space for emissions with no overlaps. The border between the two regions is known as the merging scale.

The second problem is to make the matrix elements exclusive. This is solved by introducing (approximate) Sudakov form factors. The problem is that the matrix elements have no intrinsic ordering, which is required for the Sudakov form factors in the shower. This means that an ordered chain of emissions has to be constructed and used for the Sudakov form factors.

The first algorithm to be published was the CKKW (Catani–Krauss–Kuhn–Webber) [20] algorithm which was originally formulated for e^+e^- annihilation, but later extended to hadron collisions [21]. The CKKW algorithm is formulated using the $k_\perp$-algorithm [22, 23], which is a jet algorithm that works by merging the closest partons according to a transverse momentum ($k_\perp$) distance measure. The emission phase space is split by saying that emissions above a cut in $k_\perp$ belongs to the matrix element and below the same value the shower can perform emissions. First, events are generated according to the matrix element with a cutoff in the $k_\perp$-distance between the partons. Then the $k_\perp$-algorithm is used to construct a shower history, which in turn is used to calculate analytical Sudakov form factors and to reweight α_s. Finally, the shower is invoked with a veto on the $k_\perp$-measure of subsequent emissions.

Another algorithm was developed in parallel by Leif Lönnblad [24], which is similar to the CKKW algorithm and was later called CKKW-L. The algorithm was first published for e^+e^- and extended to hadrons collisions in paper I [25] in this thesis. In CKKW-L, any cutoff can be used to remove the divergent parts of the matrix element. First, each event is generated according to the matrix element. Then the algorithm specifies that one should construct a shower history by finding all possible ways the shower could have generated the state and pick one randomly with a probability proportional to the product of the emission probabilities involved. The aim is to calculate the best guess of how the shower could have generated the state. This has the advantage that the shower can be used to generate the Sudakov form factors, since they are by definition equal to the no emission probability of the shower. After the state has been reweighted with the Sudakov form factors, the shower is invoked with a veto on the first emission.

In [26] an algorithm called the Pseudo-Shower algorithm was introduced. This algorithm works by using a jet clustering algorithm (which could be the $k_\perp$-algorithm or something similar) both as a cutoff for the matrix element and to construct a shower history, similar to the CKKW algorithm. Then the shower is used to generate Sudakov form factors by invoking the entire

shower and clustering back to jets. The jet scale is compared to the values from the clustering, which is used to determine if the event is kept. Finally, the shower is invoked with a veto so that emissions do not go above the softest emission in the matrix element state.

The MLM [27] algorithm is the easiest one to implement. Events are generated according to the matrix elements with a cut using a jet observable. A shower history is constructed using the $k_\perp$-algorithm, but used only to reweight α_s. To generate the Sudakov form factors and to shower the event, the shower is simply invoked on the state given by the matrix element with no veto on emissions. Jets are clustered and events where the shower has created extra jets are discarded.

i.6.3 One-loop matrix elements

As one-loop calculations are becoming available it would be a logical step to use them together with the parton showers as well, which would be a significant improvement over the previously discussed algorithms. Working with one-loop matrix elements is a bit tricky since they include both the real emission terms and parts of the virtual corrections in the Sudakov form factor.

The first method for dealing with one-loop matrix element was MC@NLO [28], which uses the assumption that all the poles in the matrix element are also in the shower. Therefore the shower is used to regularize the different matrix elements. The shower term is subtracted from the real part and added to the virtual contribution. In this way, once the shower is invoked it should give a good sample back. One of the disadvantages of MC@NLO is that it can generate events with negative weights.

The other method of dealing with one-loop matrix elements is the POWHEG [29, 30] method. It works by adding together both the real and virtual contributions to one sample and then adding the emission back using the real part of the matrix element as splitting function. The shower can be added afterwards with a veto to restrict the shower to generate emissions in the phase space not covered by the first emission.

Both algorithms work adequately for the case that they address, but they are both limited by only being able to include one one-loop matrix element. One advantage of the tree-level merging algorithms discussed earlier is that they can work with many multiplicities at a time, allowing one to generate samples with matrix element corrections for several extra jets. The methods above do one order better in α_s, but can only include one specific multiplicity.

i.6.4 More general algorithms

Considering the current progress in automating various matrix element processes one would like to develop the algorithms further to include one-loop matrix elements for different multiplicities and ideally even be able to go beyond that. Such an algorithm would greatly improve the accuracy of the results once automated tools become available. There have been several attempts at more general algorithms [31–34], but these are to be considered work in progress.

Our algorithm for merging matrix elements with loops and the parton shower is presented in paper IV [35]. A method is presented for using the shower to calculate all the necessary weights for including the matrix element along the same lines as CKKW-L.

i.7 Introduction to papers

All the papers in this thesis are about improving the simulation of events using matrix elements. The main focus is getting a better description of the production of jets and associated observables such as jet scales and jet correlations. Two main processes have been studied: W production in proton collisions with extra jets (W + jets) and e^+e^- annihilation into hadrons.

The reason that W + jets was studied is that this process is the major background for top production, some Higgs production scenarios and many of the proposed discovery channels for beyond the Standard Model physics. To understand what to expect from these channels one needs accurate simulation of the background. As discussed earlier the multi-jet states are not accurately described by parton showers and matrix element corrections are therefore important.

The other process that is studied in the papers is e^+e^- annihilation into hadrons. The reason this process was chosen is since it is the cleanest and simplest possible process. There are a number of complications that have to be included in hadron collisions, related to the structure of the proton, which can be avoided entirely. There is also abundant precision data avaliable from the LEP experiment. All these properties makes the process ideal for improving the understanding of the algorithms and as a testing ground for new ideas. I belive it is important to validate all algorithms for e^+e^- before applying them to more complicated cases.

i.7.1 Paper I

Paper I is an extension of the work published by Leif Lönnblad a few years earlier [24]. In the original publication of the matrix element correction algo-

rithm, later called CKKW-L, it was described for e^+e^- and implemented for up to four outgoing partons. In this paper the same algorithm is extended to also include incoming hadrons.

Incoming hadrons lead to a number of extra complications. The most important being the structure of the partons inside the proton that needs to be modeled. This is done using parton distribution functions (PDF) which are included in the emission probability of certain types of emissions. The algorithm was applied to ARIADNE which uses semiclassical approximations for the proton structure and this is treated specifically in the paper. The solution, however, is quite general and can be used for regular PDFs as well.

There is also another challenge that only appears with incoming hadrons, which is a number of new types of diagrams. Most importantly, one of the initial state splittings is not included in ARIADNE and this issue is addressed. There is also a new class of diagrams that cannot be simulated by the cascade at all and we also introduce a prescription for how to deal with these.

The algorithm is applied to W-production with extra QCD jets and the process is simulated with up to four extra jets at Run II of the Tevatron. Several observables are plotted including jet scales and some observables showing jet correlations. It is shown in the paper that there are important effects from including matrix elements as compared to running the plain shower.

i.7.2 Paper II

Paper II is a collaboration between several of the authors of the main programs for matrix element merging. We made a collective effort to try to make the best possible prediction of W + jets. All the methods are described and results are presented for the LHC and the Tevatron. The observables chosen in this paper are typical observables that could be used by the experiments. While they may not be exactly what will be used, they should provide a good benchmark.

The rest of the paper is dedicated to investigating the systematics of the various algorithms. The effects from changing the merging scale and from changing the scale in the strong coupling constant is investigated.

To get a reasonable idea of the systematics when simulating W + jets one needs both to use different methods for the simulations and to investigate the systematics within each method. This paper includes both aspects and our goal is to deliver something that is useful for the experimentalists.

i.7.3 Paper III

In paper III we went back to e^+e^- to try to understand the algorithms better. e^+e^- is a lot simpler than hadron collisions since one does not have to include anything about the structure of the proton. This does, however, not mean that

it is easier to get good results for e^+e^-, since removing the complication of incoming hadrons also removes things that are tunable. There is also more data with better precision avaliable for e^+e^- compared to W production in hadron collisions, which leaves smaller room for error.

In this paper we use the simplest possible process, which is one extra parton, as a benchmark for the various merging algorithm. This is a convenient choice since a solution by reweighting the first splitting function is also available for this process. Ideally all algorithms should perform well for such a simple case, but we show that there are significant problems in several of the approaches.

The problems found were mostly related to using different ordering variables in the merging as compared to the shower. We show in this paper that even though one might a priori believe that these effects are small, they can vastly change the final result.

i.7.4 Paper IV

In paper IV we present a new way of doing matrix element merging, where matrix elements with loops including different parton multiplicities can be merged with a parton shower. The method presented is along the same lines as the CKKW-L algorithm, where the shower is used to calculate all the corrections to the matrix element. However, the ideas are more general and can be applied to any CKKW-like algorithm.

The method is based on the idea that one can subtract the terms corresponding to the first two orders in α_s from the parton shower. Then one can add events generated according to one-loop matrix elements and dressed with the shower. Together, the result is that the matrix element determine the two first orders in α_s, but all higher order terms are taken from the shower. Some extra complications, which occur if the ordering variable used in the shower is different from the variable used to define the merging scale, are resolved.

The explicit solutions are presented for e^+e^- collisions and the extra complications related to proton structure are to be solved in a later publication. The algorithm has been implemented in ARIADNE with the matrix elements generated by PYTHIA. It turns out that a modified treatment of α_s in the shower is required, since the matrix element contains pieces that cannot be reproduced in the shower and results in different values of the strong coupling. The algorithm is shown to be consistent with regard to changing the merging scale and changing the renormalization scale.

Finally results for hadronic jet and shape observables are presented and compared to LEP data. ARIADNE already describes these observables quite well and the results from the implementation of our algorithm in ARIADNE shows similar agreement. The implementation is intended as a proof of con-

cept and hopefully it can be extended to also include incoming protons soon.

i.7.5 List of contributions

- **Paper I:** In this paper I have contributed by doing a big part of the theoretical work and the entire computer implementation and simulation. I have made all the figures, but only written minor parts of the text.
- **Paper II:** The author list of this paper is rather long and the people are listed alphabetically, but a few of us did more work than the others. The people who had a leading role in writing the paper are Michelangelo Mangano, Leif Lönnblad and myself. Apart from taking a leading role in the collaboration, I was also responsible for producing all the results marked ARIADNE, the final data processing and making all the plots and several pieces of the text.
- **Paper III:** In this paper I have done the main part of the theoretical work and I wrote most of the computer implementation and I did most of simulations. I have also made all but one of the figures and written most of the text.
- **Paper IV:** The basic idea presented in this paper came from Leif Lönnblad. However, I have done most of the theoretical calculations and I have done all the computer simulations. I wrote most of the text and made all of the plots.

Acknowledgments

First and foremost I wish to thank Leif Lönnblad for being a great supervisor. I am happy I was given the opportunity to work with Leif, who has taught me lots of physics and always been able to find the time to answer my questions and discuss our work.

I also want to thank the other staff members of the high energy physics group namely: Torbjörn Sjöstrand, Gösta Gustafson and Johan Bijnens. Through lots of interesting discussions and by patiently answering all my questions they have provided me with lots of insight into various parts of particle physics.

My gratitude also goes to all my friends at the Department of Theoretical Physics, the Division of Mathematical Physics and the Division of Experimental High Energy Physics. It has been a pleasure knowing you all.

Finally, I wish to thank members of my family and other friends who have provided me with support over the years.

i References

[1] G. L. Kane, *Modern elementary particle physics*. Perseus Publishing, 1993. ISBN 0-201-62460-5.

[2] M. E. Peskin and D. V. Schröder, *An introduction to quantum field theory*. Westview Press, 1995. ISBN 0-201-50397-2.

[3] J. Alwall *et al.*, "MadGraph/MadEvent v4: The New Web Generation," *JHEP* **09** (2007) 028, `arXiv:0706.2334 [hep-ph]`.

[4] M. L. Mangano, M. Moretti, F. Piccinini, R. Pittau, and A. D. Polosa, "ALPGEN, a generator for hard multiparton processes in hadronic collisions," *JHEP* **07** (2003) 001, `arXiv:hep-ph/0206293`.

[5] S. Catani and M. H. Seymour, "The Dipole Formalism for the Calculation of QCD Jet Cross Sections at Next-to-Leading Order," *Phys. Lett.* **B378** (1996) 287–301, `arXiv:hep-ph/9602277`.

[6] S. Catani and M. H. Seymour, "A general algorithm for calculating jet cross sections in NLO QCD," *Nucl. Phys.* **B485** (1997) 291–419, `arXiv:hep-ph/9605323`.

[7] R. K. Ellis, W. J. Stirling, and B. R. Webber, *QCD and collider physics*. Cambridge University Press, 2003. ISBN 0-521-54589-7.

[8] G. Gustafson, "An intuitive semiclassical picture of proton structure at small x," *Acta Phys. Polon.* **B34** (2003) 2963–2988, `arXiv:hep-ph/0306108`.

[9] B. Andersson, G. Gustafson, G. Ingelman, and T. Sjostrand, "Parton fragmentation and string dyanmics," *Phys. Rept.* **97** (1983) 31.

[10] B. R. Webber, "A QCD Model for Jet Fragmentation Including Soft Gluon Interference," *Nucl. Phys.* **B238** (1984) 492.

[11] T. Sjostrand, S. Mrenna, and P. Skands, "PYTHIA 6.4 physics and manual," *JHEP* **05** (2006) 026, `arXiv:hep-ph/0603175`.

[12] G. Corcella *et al.*, "HERWIG 6.5: an event generator for Hadron Emission Reactions With Interfering Gluons (including supersymmetric processes)," *JHEP* **01** (2001) 010, `arXiv:hep-ph/0011363`.

[13] L. Lönnblad, "ARIADNE version 4 – A program for simulation of QCD cascades implementing the colour dipole model," *Comput. Phys. Commun.* **71** (1992) 15.

[14] G. Gustafson, "Dual description of a confined color field," *Phys. Lett.* **B175** (1986) 453.

[15] G. Gustafson and U. Pettersson, "Dipole formulation of QCD cascades," *Nucl. Phys.* **B306** (1988) 746.

[16] T. Gleisberg *et al.*, "SHERPA 1.alpha, a proof-of-concept version," *JHEP* **02** (2004) 056, arXiv:hep-ph/0311263.

[17] M. Bengtsson and T. Sjostrand, "Coherent parton showers versus matrix elements: implications of PETRA - PEP data," *Phys. Lett.* **B185** (1987) 435.

[18] M. H. Seymour, "A Simple prescription for first order corrections to quark scattering and annihilation processes," *Nucl. Phys.* **B436** (1995) 443–460, arXiv:hep-ph/9410244.

[19] M. H. Seymour, "Matrix element corrections to parton shower algorithms," *Comp. Phys. Commun.* **90** (1995) 95–101, arXiv:hep-ph/9410414.

[20] S. Catani, F. Krauss, R. Kuhn, and B. R. Webber, "QCD matrix elements + parton showers," *JHEP* **11** (2001) 063, arXiv:hep-ph/0109231.

[21] F. Krauss, "Matrix elements and parton showers in hadronic interactions," *JHEP* **08** (2002) 015, arXiv:hep-ph/0205283.

[22] S. Catani, Y. L. Dokshitzer, M. Olsson, G. Turnock, and B. R. Webber, "New clustering algorithm for multi - jet cross-sections in e+ e- annihilation," *Phys. Lett.* **B269** (1991) 432–438.

[23] S. Catani, Y. L. Dokshitzer, M. H. Seymour, and B. R. Webber, "Longitudinally invariant K(t) clustering algorithms for hadron hadron collisions," *Nucl. Phys.* **B406** (1993) 187–224.

[24] L. Lönnblad, "Correcting the colour-dipole cascade model with fixed order matrix elements," *JHEP* **05** (2002) 046, arXiv:hep-ph/0112284.

[25] N. Lavesson and L. Lönnblad, "W + jets matrix elements and the dipole cascade," *JHEP* **07** (2005) 054, arXiv:hep-ph/0503293.

[26] S. Mrenna and P. Richardson, "Matching matrix elements and parton showers with HERWIG and PYTHIA," *JHEP* **05** (2004) 040, arXiv:hep-ph/0312274.

[27] M. Mangano, "The so-called MLM prescription for ME/PS matching." http://www-cpd.fnal.gov/personal/mrenna/tuning/nov2002/mlm.pdf. Talk presented at the Fermilab ME/MC Tuning Workshop, October 4, 2002.

[28] S. Frixione and B. R. Webber, "Matching NLO QCD computations and parton shower simulations," *JHEP* **06** (2002) 029, arXiv:hep-ph/0204244.

[29] P. Nason, "A new method for combining NLO QCD with shower Monte Carlo algorithms," *JHEP* **11** (2004) 040, arXiv:hep-ph/0409146.

[30] S. Frixione, P. Nason, and C. Oleari, "Matching NLO QCD computations with Parton Shower simulations: the POWHEG method," *JHEP* **11** (2007) 070, arXiv:0709.2092 [hep-ph].

[31] W. T. Giele, D. A. Kosower, and P. Z. Skands, "A Simple shower and matching algorithm," *Phys. Rev.* **D78** (2008) 014026, arXiv:0707.3652 [hep-ph].

[32] Z. Nagy and D. E. Soper, "Parton showers with quantum interference," *JHEP* **09** (2007) 114, arXiv:0706.0017 [hep-ph].

[33] C. W. Bauer, F. J. Tackmann, and J. Thaler, "GenEvA (I): A new framework for event generation," *JHEP* **12** (2008) 010, arXiv:0801.4026 [hep-ph].

[34] C. W. Bauer, F. J. Tackmann, and J. Thaler, "GenEvA (II): A phase space generator from a reweighted parton shower," *JHEP* **12** (2008) 011, arXiv:0801.4028 [hep-ph].

[35] N. Lavesson and L. Lonnblad, "Extending CKKW-merging to One-Loop Matrix Elements," *JHEP* **12** (2008) 070, arXiv:0811.2912 [hep-ph].

I

W+jets matrix elements and the dipole cascade

Nils Lavesson and Leif Lönnblad

Department of Theoretical Physics, Lund University,
Sölvegatan 14A, SE–223 62 Lund, Sweden

Journal of High Energy Physics **07** (2005) 054 [hep-ph/0503293].

We extend the algorithm for matching fixed-order tree-level matrix element generators with the Dipole Cascade Model in ARIADNE to apply to processes with incoming hadrons. We test the algoritm on for the process W+n jets at the Tevatron, and find that the results are fairly insensitive to the cutoff used to regularize the soft and collinear divergencies in the tree-level matrix elements. We also investigate a few observables to check the sensitivity to the matrix element correction.

I.1 Introduction

Parton Shower based Monte Carlo Event Generators (PSEGs) have developed into essential tools in High Energy Physics. Without them it is questionable if it at all would be possible to embark on large-scale experiments such as the LHC. Although they are based on leading logarithmic approximations and phenomenological hadronization models, they are typically able to describe hadronic final states in great detail and, especially at LEP, with great precision. However, there are problems. The description of final states which include more than three hard jets is not very good, and when it comes to collisions with incoming hadrons, the precision is generally lacking, especially for small-x processes. In this article we will address both these problems.

The problem with describing several hard, well separated jets is inherent in the leading log approximations, since they assume that there is strong ordering between parton emissions, and hence only give a good description of soft inter-jet and collinear intra-jet emissions. Typically it is possible to correctly describe one additional hard jet on top of the hard sub-process used as starting point, by applying correction factors to the basic splitting functions. However, to go beyond one additional jet is more difficult.

To describe events with several hard partons we can use so-called Matrix Element Generators (MEGs), where the parton distributions can be generated according to exact tree-level matrix elements. Unfortunately these matrix elements are divergent in the soft and collinear limits and a cutoff is needed to avoid these regions of phase space. However, to generate realistic events we need to hadronize the partons into jets of hadrons, and all reasonable hadronization models require that also soft and collinear parton emissions are modeled correctly. Hence the need for combining matrix element generators with parton showers.

Combining these two approaches is, however, not trivial. The matrix elements describe inclusive events, ie. events with at least n partons above some cutoff, while parton showers are exclusive and describe events with exactly n partons. Naively adding parton showers to events generated by a MEG will therefore give a very strong dependence on the cutoff used in the MEG, even if great care is taken to avoid double-counting by only adding parton showers below that cutoff.

A solution for this problem was presented by Catani et al. in [1]. The procedure, generally referred to as CKKW, relies on applying a jet clustering algorithm to partonic event from a MEG generating zero, one, two, etc. additional hard jets above some cutoff according to exact tree-level matrix elements. The repeated clustering of two jets into one is then used to construct an ordered set of scales corresponding to consecutive parton emissions. These scales are used to calculate Sudakov form factors corresponding to no-emission probabilities,

which are used to reweight the MEG events to make them exclusive. A parton shower can then be added with a special veto to avoid double-counting of emissions above the cutoff. In this way it was shown that the dependence on the cutoff cancels to next-to-leading order accuracy. The dependence was, however, still quite visible, giving rise to annoying discontinuities in some observables.

The basic CKKW prescription was somewhat improved [2] when implemented for the Dipole Cascade model [3, 4] in the ARIADNE program [5]. Rather than using a jet clustering algorithm to construct a set of scales, the ARIADNE procedure involves constructing complete intermediate states corresponding to a series of emissions which the dipole cascade could have used to produce a given state obtained from a MEG. A special veto algorithm is used to calculate exactly the Sudakov form factors the cascade would have used to produce the state, which are then used for reweighting. In addition a special treatment of the MEG-produced states with highest multiplicity was introduced, avoiding the restriction which disallowed additional jets above the cutoff in the original CKKW paper. It should be noted that both these improvements are of "cosmetic" nature, in that the cutoff dependence is still formally only canceled to next-to-leading order accuracy.

Both these procedures were originally developed for e^+e^-. Recently there has been some developments in applying them to hadronic collisions, in particular for the W+jets process, by Krauss et al. [6–8] and Mrenna and Richardson [9]. An alternative procedure has also been developed by Mangano [10, 11], which is similar in spirit to CKKW, but which has a simpler interface between the MEG and PSEG. This development is very important for the LHC, where W+jets is an important background for almost any signal of new physics.

In this article we describe the extension of the CKKW procedure for the dipole cascade in ARIADNE to handle hadronic collisions, again concentrating on the W+jets process. The goal is to obtain a procedure which gives as small cutoff dependence as was achieved for e^+e^-. However, we also expect to see differences w.r.t. the procedures of Mrenna, Richardson and Krauss, since the dipole cascade model for collisions with incoming hadrons [12, 13] is different. The standard initial-state parton shower approaches, such as those implemented in PYTHIA [14, 15], HERWIG [16] and SHERPA/APACIC++ [17, 18], as well as the Sudakov form factors used in CKKW, correspond to a DGLAP-resummation [19–22] of leading logarithms of the hard scale. In the dipole cascade, however, also some terms corresponding to logarithms of $1/x$ are resummed. Although not formally equivalent to neither BFKL [23–25] or CCFM [26–29] evolution, it has proven to be able to describe most features small-x final states at HERA, where all DGLAP-based parton showers fail. Now, W+jets is conventionally not considered to be a small-x process because

of the hard scale, m_W, being large, but at the LHC the collision energies are so large there may be substantial effects of terms proportional to $\alpha_s^n \log(\sqrt{S}/m_W)^n$, where $m_W/\sqrt{S} \sim x \sim 0.005$.

The layout of this article is as follows. We will first recap the main points of the CKKW procedure in section II.2.1. Then, in section I.3, we describe the dipole cascade model and CKKW implementation for e^+e^- annihilation, followed by a description of the dipole cascade for incoming hadrons in section I.3.2. In section I.4 we will describe our CKKW implementation for W+jets, and hadronic collisions in general, starting with the construction of intermediate states in I.4.1, followed by the reweighting procedure in I.4.2. The results of our investigation of its performance are presented in IV.4. Finally in section IV.5 we present our conclusions.

I.2 CKKW

When generating events with a PSEG, the procedure is to start from a primary hard sub-process, typically a $2 \to 2$ process such as $e^+e^- \to q\bar{q}$ or $q\bar{q} \to W \to \bar{\nu}e$, and then to let the incoming and outgoing quarks and gluons evolve a parton cascade in an iterative $1 \to 2$ branching procedure. The emissions are ordered according to some evolution scale ρ, where the maximum scale, ρ_0 is typically given by the hardest scale in the primary sub-process, and the minimum is some cutoff scale of the order of one GeV, typically tuned to match a particular hadronization model.

We can write the exclusive cross sections for in this way generating $0, 1, 2, \ldots$ additional partons above the cutoff, ρ_c, as

$$\begin{aligned}
\sigma_{+0} &= \sigma_0\, \Delta_{S_0}(\rho_0, \rho_c) \\
d\sigma_{+1} &= \sigma_0\, \alpha_s(\rho_1) c_{11}^{PS} \Delta_{S_0}(\rho_0, \rho_1) \Delta_{S_1}(\rho_1, \rho_c) d\rho_1 d\Omega_1 \\
d\sigma_{+2} &= \sigma_0\, \alpha_s(\rho_1) \alpha_s(\rho_2) c_{22}^{PS} \Delta_{S_0}(\rho_0, \rho_1) \Delta_{S_1}(\rho_1, \rho_2) \Delta_{S_2}(\rho_2, \rho_c) d\rho_1 d\Omega_1 d\rho_2 d\Omega_2 \\
&\vdots \\
d\sigma_{+n} &= \sigma_0\, c_{nn}^{PS} \Delta_{S_n}(\rho_n, \rho_c) \prod_{i=1}^{n} \alpha_s(\rho_i) \Delta_{S_{i-1}}(\rho_{i-1}, \rho_i) d\rho_i d\Omega_i \\
&\vdots
\end{aligned} \tag{I.1}$$

where the ordering is $\rho_0 > \rho_1 > \ldots > \rho_n > \rho_c$ and Ω_i symbolizes the phase space variables defining the ith emission in addition to ρ_i (typically some momentum fraction, z_i, and some azimuth angle ϕ_i). $\Delta_{S_i}(\rho_i, \rho_{i+1})$ is the so-called Sudakov form factor giving the probability that no emissions occurred from the state with i additional partons between the scales ρ_i and ρ_{i+1}. The coefficients c_{nn}^{PS} are basically products of splitting functions which depends on ρ_i and

Ω_i, and we assume an implicit sum over all possible flavour combinations. As we will see below, the c_{nn}^{PS} may also include ratios of parton density functions (PDFs) in the case of incoming hadrons.

The Sudakov form factors are formally resummations of virtual diagrams to all orders and can, in principle, be calculated analytically. They would then only depend on the limiting scales, as is done in the standard CKKW procedure. However, when explicitly interpreted as a no-emission probability in a PSEG, as is done eg. in ARIADNE, it basically depends on all momenta in the partonic state. The typical form of the Sudakov is

$$\Delta_S(\rho_i, \rho_{i+1}) = \exp\left(-\int_{\rho_{i+1}}^{\rho_i} \frac{d\rho}{\rho}\alpha_{\mathrm{s}}(\rho)\int dz P(z)\right), \tag{I.2}$$

which, of course, can be expanded in a series in α_{s}, and we can rewrite the exclusive cross sections as

$$\begin{aligned}
\sigma_{+0} &= \sigma_0\,(1 + c_{01}^{\mathrm{PS}}\alpha_{\mathrm{s}} + c_{02}^{\mathrm{PS}}\alpha_{\mathrm{s}}^2 + \ldots)\\
d\sigma_{+1} &= \sigma_0\,\alpha_{\mathrm{s}} c_{11}^{\mathrm{PS}}(1 + c_{12}^{\mathrm{PS}}\alpha_{\mathrm{s}} + c_{13}^{\mathrm{PS}}\alpha_{\mathrm{s}}^2 + \ldots) d\rho_1 d\Omega_1\\
d\sigma_{+2} &= \sigma_0\,\alpha_{\mathrm{s}}^2 c_{22}^{\mathrm{PS}}(1 + c_{23}^{\mathrm{PS}}\alpha_{\mathrm{s}} + c_{24}^{\mathrm{PS}}\alpha_{\mathrm{s}}^2 + \ldots) d\rho_1 d\Omega_1 d\rho_2 d\Omega_2\\
&\vdots\\
d\sigma_{+n} &= \sigma_0\,\alpha_{\mathrm{s}}^n c_{nn}^{\mathrm{PS}}(1 + c_{n,n+1}^{\mathrm{PS}}\alpha_{\mathrm{s}} + c_{n,n+2}^{\mathrm{PS}}\alpha_{\mathrm{s}}^2 + \ldots)\prod_{i=1}^{n} d\rho_i d\Omega_i\\
&\vdots
\end{aligned} \tag{I.3}$$

to emphasize the resummation aspect. We note that even though all the coefficients c_{ij}^{PS} are divergent in the soft and collinear limit when $\rho_c \to 0$, the resummation to all orders in the Sudakovs gives a finite result for each of the cross sections. Also, when integrated over the allowed phase space the cross section of the primary sub process σ_0 is retained,

$$\sum_0^\infty \sigma_{+i} = \sigma_0. \tag{I.4}$$

In contrast a MEG will generate inclusive partonic states with the cross sections for generating *at least* 0, 1, 2, ... additional jets given by

$$\begin{aligned}
\sigma_{+0} &= \sigma_0 \\
d\sigma_{+1} &= \sigma_0\, \alpha_s c_{11}^{\mathrm{ME}} d\mathbf{\Omega}_1 \\
d\sigma_{+2} &= \sigma_0\, \alpha_s^2 c_{22}^{\mathrm{ME}} d\mathbf{\Omega}_1 d\mathbf{\Omega}_2 \\
&\vdots \\
d\sigma_{+n} &= \sigma_0\, \alpha_s^n c_{nn}^{\mathrm{ME}} \prod_{i=1}^{n} d\mathbf{\Omega}_i \\
&\vdots
\end{aligned} \tag{I.5}$$

where the $\mathbf{\Omega}_i$ symbolizes all phase space variables defining the ith parton, and the coefficients c_{ii}^{ME} are calculated using the exact tree-level matrix elements (including PDFs in the case of incoming hadrons). Clearly we can not simply add these cross sections, especially since each of the coefficients are divergent if the soft and collinear limits are not cut off properly.

The advantage of using a MEG is that the exact tree-level matrix elements are used, which means that also states with several hard partons are described correctly. This is not the case for the PSEG, where the coefficients are given by products of splitting functions, which is only a good approximation in the limit of strongly ordered emissions. On the other hand a MEG will not correctly treat soft and collinear partons, where the coefficients are large and need to be resummed to all orders, as in a PSEG, to give reliable results. Clearly it would be highly desirable to combine the two approaches.

It should be noted that for the first emission in a PSEG is typically quite easy to modify the splitting functions to correctly reproduce the exact matrix element, effectively replacing c_{11}^{PS} with c_{11}^{ME}, and in most PSEGs this is the default behavior for most primary sub-processes [3, 5, 13, 30–38].

I.2.1 The original CKKW procedure

Comparing eqs. IV.1 and IV.7 the solution should be obvious. Use a MEG to generate up to N additional partons above some cutoff, y_{cut}, but reweight the generated states with the Sudakov form factors, and then add a parton shower with the requirement that no partons above y_{cut} are emitted. This is the essence of the CKKW procedure. To calculate the Sudakov form factors we need an ordered set of emission scales, which is not provided by the MEG, since there all possible diagrams are added coherently and emission scales are not well defined. In the original CKKW procedure, the $k_\perp$ clustering algorithm [39, 40] was used to define an ordered set of scales which were used to analytically calculate the Sudakov form factors. A reweighting was also done to use a running α_s with the constructed scale as argument. The resolution variable of

the $k_\perp$-algorithm was also used for the cutoff in the MEG, which is not the same as the evolution variable in the PSEG. To ensure a full coverage of the phase space the parton shower was therefore added with the maximum scale as starting point, but vetoing all emissions corresponding to the $k_\perp$-algorithm resolution variable above y_{cut} to avoid double-counting.

It was shown that this procedure removes the dependence on the MEG cutoff, y_{cut}, to next-to-leading logarithmic accuracy. However, there was still a clearly visible discontinuity in some generated distributions.

I.2.2 CKKW in hadronic collisions

To extend this algorithm to be used for hadronic collisions is conceptually straight forward. In [7] and [9] the standard CKKW procedure was extended to hadronic collisions in general and for the W+jets process in particular, and implemented for the APACIC++, HERWIG and PYTHIA PSEGs. The principle is the same as for e^+e^-. Jet construction is done with the $k_\perp$-algorithm modified for hadronic collisions according to [41]. The resulting ordered set of scales is used in the analytic Sudakov form factors (in [9] a Sudakov veto algorithm similar to the one in ARIADNE was used for the PYTHIA implementation), and the events from the MEG was reweighted with these and the properly scaled α_s. The MEG states with highest multiplicity was treated in the same way as in the ARIADNE implementation above.

There are some issues which need to be treated with special care. In a PSEG, the initial states emissions are generated in a backward evolution procedure which besides the standard partonic splitting functions also involves ratios of PDFs. The leading order cross section is given by

$$d\sigma_0 = d\sigma_{hh\to W} = \sum_{q,q'} x f_q(x_+,\mu^2) x f_{q'}(x_-,\mu^2) \hat{\sigma}_{qq'\to W}(x_+x_-S)\frac{dx_+}{x_+}\frac{dx_-}{x_-}, \tag{I.6}$$

where the scale $\mu^2 = m_W^2 = x_+x_-S$. Making one step in the backward evolution with a $g \to q\bar{q}$ splitting will be performed with a probability

$$dP(Q^2,z) = \alpha_s P_{g\to q}(z)\frac{\frac{x_+}{z}f_g(\frac{x_+}{z},Q^2)}{x_+ f_q(x_+,Q^2)}\Delta_S(Q^2_{\text{max}},Q^2)\frac{dQ^2}{Q^2}dz, \tag{I.7}$$

where the Sudakov form factor can be formulated both with (PYTHIA) and without (HERWIG) ratios of PDFs. Both choices are formally equivalent in the leading-log approximation, but only the former choice corresponds exactly to a no-emission probability. The maximum scale is typically given by m_W^2, and the Sudakov form factor corresponds to a leading-log DGLAP resummation[1].

[1] Also next-to-leading logarithmic Sudakov form factors may be used [1], although these may become larger than unity, disabling the interpretation as no-emission probabilities.

However, clearly there is nothing in the real world preventing emissions with a scale above m_W^2, and such parton states will be generated by the MEG. In [7] states with one or more partons emitted at a scale above m_W^2 are treated as coming from a separate class of primary sub-processes, and the Sudakov form factors are added only for additional emissions with a maximum scale given by the smallest of the constructed scales above m_W^2.

Although the resulting procedures in [7] and [9] are shown to be fairly cutoff insensitive, there is still some dependence, and it may be worth while to extend also the ARIADNE implementation of CKKW to hadronic collisions to see if a better result can be achieved. As for the standard CKKW this extension is in principle straight forward. However, there are some tricky issues, mainly to do with the treatment of parton densities, and to describe how we deal with these, we first have to describe how hadronic collisions are implemented in ARIADNE.

I.3 The dipole cascade model

ARIADNE implements the dipole cascade model which is quite different from conventional parton cascades. Rather than iterating $1 \to 2$ parton splittings, gluons are emitted from colour-dipoles between colour-connected partons resulting in $2 \to 3$ parton splittings. This model has several advantages. Since gluons are emitted coherently by colour-connected partons, there is no need for explicit angular ordering. In addition, the evolution variable is defined as a Lorentz-invariant transverse momentum which also is a suitable scale to be used in α_s. The evolution variable is defined as (for massless partons)

$$p_\perp^2 = \frac{s_{12}s_{23}}{s_{123}}, \tag{I.8}$$

where parton 2 is the emitted one and s_{ij} and s_{ijk} are the squared invariant masses of the two- and three-parton combinations.

The probability for an emission is given in terms of the dipole splitting functions, which depend on $p_\perp^2$ and a Lorentz invariant rapidity defined as

$$y = \frac{1}{2}\ln\frac{s_{12}}{s_{23}}. \tag{I.9}$$

The probability of a gluon emission from a dipole between two partons i, j is then given by

$$\begin{aligned} dP(p_\perp^2, y) \quad &= \quad \alpha_s(p_\perp^2) D_{ij}(p_\perp^2, y) \times \\ &\quad \times \exp\left(-\int_{p_\perp^2} \frac{dp_\perp'^2}{p_\perp'^2} \int dy' \alpha_s(p_\perp'^2) D_{ij}(p_\perp'^2, y') \right) \frac{dp_\perp^2}{p_\perp^2} dy, \end{aligned} \tag{I.10}$$

where $\exp(\ldots)$ is the Sudakov form factor. The dipole splitting functions, D_{ij}, depends on which partons are involved according to

$$D_{q\bar{q}}(p_\perp^2, y) = \frac{2}{3\pi}\frac{x_1^2 + x_3^2}{(1-x_1)(1-x_3)} \tag{I.11}$$

$$D_{qg}(p_\perp^2, y) = \frac{3}{4\pi}\frac{x_1^2 + x_3^3}{(1-x_1)(1-x_3)} \tag{I.12}$$

$$D_{gg}(p_\perp^2, y) = \frac{3}{4\pi}\frac{x_1^3 + x_3^3}{(1-x_1)(1-x_3)} \tag{I.13}$$

where x_i are the resulting energy fractions of the emitting partons in the original dipole rest system, $x_i = 2E_i/\sqrt{s_{123}}$, related to $p_\perp^2$ and y according to

$$y = \frac{1}{2}\ln\left(\frac{1-x_3}{1-x_1}\right), \qquad p_\perp^2 = s_{123}(1-x_1)(1-x_3). \tag{I.14}$$

It can be shown that the dipole splitting functions are equivalent to the standard Altarelli–Parisi splitting functions in the relevant soft and collinear limits [3]. We also note that the $D_{q\bar{q}}$ exactly corresponds to the leading order $e^+e^- \to qg\bar{q}$ tree-level matrix element.

Another feature of the dipole cascade, which will turn out to be important for the CKKW implementation, is that all partons are always on shell throughout the cascade. This is possible since the recoil from the emitted parton can be absorbed by the two emitting ones. In contrast, a conventional parton cascade does not have on-shell intermediate states, and the full kinematics of an event is not constructed until all the scales in the complete shower have been generated. While the energy loss of the emitting partons are defined in the splitting functions in eqs. (I.11)–(I.13), the transverse recoil is chosen according to principles detailed in [5].

It can be noted that the "inverse" of the dipole cascade is a well-behaved jet clustering algorithm. In fact such an algorithm has been constructed, the DICLUS algorithm [42], based on successive clusterings of three jets into two, using the $p_\perp$ in eq. (I.8) as resolution scale, which has been shown to have many attractive features [43].

There are, however, also some disadvantages with the dipole cascade model, the main one being that it only deals with gluon emissions, and the splitting of gluons into $q\bar{q}$ pairs must be added by hand, both for final-state [44] and initial-state [35] splitting.

The initial-state splitting will be described in section I.3.4 below. Final-state splittings are simply added as a possibility for a dipole connected to a gluon to split this gluon into a $q\bar{q}$-pair in addition to emit a gluon. Here, the standard Altarelli–Parisi splitting function is used, divided between the two dipoles

connected to the gluon. This will result in a new dipole splitting function,

$$D_{ig}^{q\bar{q}} = \frac{\xi}{4\pi}\frac{(1-x_2)^2+(1-x_3)^2}{1-x_1}. \tag{I.15}$$

In the original formulation, the splitting was divided equally between the two dipoles connected to the gluon, ie. $\xi = 0.5$. However, in the current ARIADNE implementation, a larger fraction is given to the smaller of the dipoles ig and gj, hence for the ig dipole we have $\xi = s_{gj}/(s_{gj}+s_{ig})$.

Although these splitting do not come in naturally in the dipole picture, they can be incorporated in a consistent way and the resulting implementation in ARIADNE is probably the best model for describing both e^+e^- final states at LEP [45], and DIS final states at HERA [46].

I.3.1 ARIADNE and CKKW

The ARIADNE implementation of CKKW for e^+e^- is described in detail in [2]. Considering the nature of the dipole cascade it may seem reasonable to use the dipole clustering algorithm in DICLUS to construct scales, rather than using the $k_\perp$-algorithm. However, in the ARIADNE implementation a step further is taken. For each partonic state generated by a MEG, all possible dipole cascade histories are constructed, basically answering the question *how would ARIADNE have generated this state?* A specific history is then picked by weighting possible histories with the product of the corresponding dipole splitting functions. The implementation depends on the MEG generating specific colour connections among the partons. Although this information is not physical, it is usually provided by MEG programs. (See discussion in ref. [47]). In principle one could choose between all possible colour connections in the same way as different histories are considered, but as most MEGs supply colour information this is not necessary.

From a MEG generated state with n additional partons, we can construct, not only an ordered set of emission scales, $p^2_{\perp n}, p^2_{\perp n-1}, \dots p^2_{\perp 1}$, but also the corresponding set of intermediate states, $S_{n-1}, S_{n-2}, \dots S_0$. As in the standard CKKW, the reweighting with the correct scales in α_s is done using just the constructed scales. However, the Sudakov form factors are calculated using the fact that $\Delta_{S_i}(p^2_{\perp i}, p^2_{\perp i+1})$ exactly corresponds to the probability that no emission occurred from state S_i between the scales $p^2_{\perp i}$ and $p^2_{\perp i+1}$. Hence, letting ARIADNE make a trial emission, starting from the state S_i with $p^2_{\perp i}$ as the maximum scale and throwing away the MEG event if the trial emission was above $p^2_{\perp i+1}$, will exactly correspond to reweighting with the same Sudakov form factor, $\Delta_{S_i}(p^2_{\perp i}, p^2_{\perp i+1})$, which ARIADNE would have used when generating the event.

A special treatment is given the trial emission from the MEG generated state, S_n. Rather than using the cutoff, $p^2_{\perp c}$, from the dipole cascade, the event

is thrown if the emission is above the cutoff used in the MEG, while if the emission is below, the emission is kept and the cascade is continued down to $p_{\perp c}^2$ to produce a full ME+PS event. In addition, if $n = N$, the highest number of additional partons generated from the MEG, the emission from S_N is always kept. This was not done in the original CKKW prescription, but is clearly needed, since otherwise we would never get events with $N+1$ additional partons above the cutoff. In later developments of CKKW such a treatment has been added [7, 9, 48].

I.3.2 The dipole cascade model for incoming hadrons

In contrast to conventional parton shower models, the dipole cascade model does not separate between initial- and final-state gluon radiation. Instead, gluons are always emitted from final-state dipoles as in the e^+e^- case. The cleanest situation is in the DIS electro-production case, where the leading order process is $eq \to eq$, ie. a quark is being kicked out of a hadron. A gluon may then be emitted from the colour-dipole between the struck quark and the hadron remnant, using the same dipole splitting function as in the e^+e^- case in eq. (I.11). There is one major difference though. In the e^+e^- case, both the quark and anti-quark can be considered point-like, but in the DIS case only the struck quark is point-like (at least up to the resolution scale, Q^2, of the exchanged virtual photon) while the hadron remnant is an extended object with a size of roughly one fermi. Just as for the electromagnetic case, radiation of wavelengths much smaller than the size of the antenna is suppressed.

I.3.3 Gluon emission from an extended source

In [12] it was argued that only a fraction of the hadron remnant is effectively taking part in the emission. For a gluon emission at the scale $p_\perp^2$ this fraction is given by

$$a(p_\perp) = \left(\frac{\mu}{p_\perp}\right)^\alpha, \tag{I.16}$$

where μ parameterizes the inverse size of the remnant and α reflects the dimensionality of the emitter. If only that fraction of the remnant momentum is allowed to take part in the emissions, this corresponds to a sharp cut in the allowed phase space for gluon emission, limiting the transverse momentum mainly in the remnant direction according to

$$p_\perp < \frac{W a(p_\perp)}{e^{+y} + a(p_\perp) e^{-y}}. \tag{I.17}$$

Here we note another major difference as compared to conventional initial-state parton showers. From eq. (I.17) it is easy to see that the maximum scale

is given by

$$p_{\perp\max} = \left(\frac{W^2\mu^\alpha}{4}\right)^{\frac{1}{2+\alpha}}, \tag{I.18}$$

which may be much larger than Q^2 which is used as the maximum scale in conventional PSEGs, especially for small x values since $W^2 \approx Q^2/x$. Since the maximum scale is also used in the Sudakov form factors, these do not only correspond to a standard DGLAP resummation of leading logarithms of Q^2, but in the dipole model they also resum, at least partially, logarithms of $1/x$. Note however, that there is no formal equivalence to BFKL or CCFM evolution. There is another similarity though. Even though the emissions in the dipole model are ordered in $p_\perp$, they are not ordered in rapidity, and conversely, following the emissions in rapidity from the struck quark the transverse momenta of the gluons will be unordered as in BFKL and CCFM.

In the implementation in ARIADNE, the sharp cutoff in $p_\perp$is replaced by a smooth function, $\Theta(p_\perp^2, y)$, with some power suppression for emissions violating eq. (I.17). Concentrating on the soft and collinear limits, where the splitting function is simply $\propto d\ln p_\perp^2\, dy$, we can write the probability of emitting a gluon as

$$dP(p_\perp^2, y) = \frac{4\alpha_s}{3\pi}\Theta(p_\perp^2, y)\Delta_S(W^2, p_\perp^2)\frac{dp_\perp^2}{p_\perp^2}dy \tag{I.19}$$

Comparing this to the corresponding initial-state $q \to q$ splitting in a conventional parton shower, (cf. eq. (I.7)) where we have

$$dP(Q^2, z) = \frac{4\alpha_s}{3\pi}\frac{1}{1-z}\frac{\frac{x_+}{z}f_q(\frac{x_+}{z}, Q^2)}{x_+ f_q(x_+, Q^2)}\Delta_S(Q^2_{\max}, Q^2)\frac{dQ^2}{Q^2}dz, \tag{I.20}$$

and noting that in this limit

$$\frac{1}{z(1-z)}\frac{dQ^2}{Q^2}dz = \frac{dp_\perp^2}{p_\perp^2}dy, \tag{I.21}$$

we see that the suppression function, Θ, corresponds to the ratio of PDFs

$$\Theta(p_\perp^2, y) \to z\frac{\frac{x_+}{z}f_q(\frac{x_+}{z}, Q^2)}{x_+ f_q(x_+, Q^2)} \tag{I.22}$$

The fact that only a part of the remnant takes part in a gluon radiation also means that only a fraction of it will obtain a transverse recoil in an emission. This is handled by the addition of so-called recoil gluons and is described in some detail in [5]. These recoil gluons will not be relevant for this report, however they will play a role when implementing CKKW in ARIADNE for DIS and we will come back to them in more detail in a future publication [49].

For W production in hadronic collisions, the primary sub-process is $q\bar{q} \to W$ and the initial dipole from which gluons are radiated is between the two remnants. The model is now the same as in DIS. However, since both remnants are extended, the cutoff in eq. (I.17) becomes

$$p_\perp < \frac{W a_1(p_\perp) a_2(p_\perp)}{a_2(p_\perp)e^{+y} + a_1(p_\perp)e^{-y}}, \tag{I.23}$$

and the maximum scale is

$$p_{\perp\max} = \left(\frac{W^2 \mu_1^{\alpha_1} \mu_2^{\alpha_2}}{4}\right)^{\frac{1}{2+\alpha_1+\alpha_2}}. \tag{I.24}$$

Again the sharp cutoff is replaced by a power suppression of transverse momenta above the limit in eq. (I.23). Rather than introducing recoil gluons to absorb the transverse recoil, we note that any emission from the primary dipole corresponds to initial-state radiation, for which it is natural that the recoil is taken by the W (otherwise it would not be possible to produce a W with non-zero transverse momentum). In [13] the choice was to always transfer the transverse recoil to the W in the first emission, while in subsequent emissions, the recoil is only transferred if the emitted gluon is close to the W in phase space.

I.3.4 Sea-quark emissions from remnant dipoles

Besides gluon radiation, there is also a possibility that one of the quarks fusing into the W is a sea-quark, in which case it could have come from a perturbative splitting of a gluon as in eq. (I.7). As for the final-state gluon splitting into $q\bar{q}$, this process does not come in naturally in the dipole model. Instead it is added by hand as an explicit initial-state splitting. This procedure is detailed in [35], and is based on different treatments of the remnants depending on whether a valence- or a sea-quark entered into the primary sub-process. A sea-quark is picked with the probability $xf_{sq}(x,Q^2)/(xf_{sq}(x,Q^2) + xf_{vq}(x,Q^2))$ and in this case the complex remnant containing the anti-sea-quark and the valence quarks is split into a colour-singlet hadron containing the anti-sea-quark and a simple remnant. The sharing of longitudinal momentum is inspired by the string fragmentation function as explained in detail in [12]. A dipole connected to such a remnant is now allowed to emit the anti-sea-quark in a way similar to a standard initial-state parton shower, except that the ordering is in transverse momentum, changing eq. (I.7) to

$$dP(p_\perp^2, z) = \alpha_s P_{g\to q}(z) \frac{\frac{x_+}{z} f_g(\frac{x_+}{z}, p_\perp^2)}{x_+ f_q(x_+, p_\perp^2)} \Delta_S(p_{\perp\max}^2, p_\perp^2) \frac{dp_\perp^2}{p_\perp^2} dz. \tag{I.25}$$

As for the case of final-state gluon splitting, there is now in the W-production case several competing processes which can occur in the primary dipole, and after generating one emission of each, the one which gave the largest $p_\perp$ is chosen. If the emission of an anti-sea-quark is chosen, it will form a new dipole with the remnant of the hadron to which it previously belonged. The transverse recoil is taken by hard subsystem, just as in a standard parton shower, where the hard subsystem in our case is the W and any other parton which has been previously emitted.

It may seem counterintuitive that the essentially non-perturbative splitting of the remnant is allowed to affect perturbative emissions. However, the splitting will mainly influence the region very close to the remnant, which is typically out of reach for current experiments. Nevertheless, we will investigate alternative treatments in a future publication.

Emitting an anti-sea-quark means that we have now extracted a gluon from the incoming hadron. In a standard parton shower scenario it would then be possible to evolve this gluon backwards either with a $\mathrm{g} \to \mathrm{g}$ splitting or a $\mathrm{q} \to \mathrm{g}$ splitting. In ARIADNE, the former is modeled by gluon emissions from either of the two dipoles connected to the two remnants. In this case we use the same suppression function as in eq. (I.19), but comparing to eq. (I.25) we find that it now corresponds to the ratio of gluon densities,

$$\Theta(p_\perp^2, y) \to \frac{\frac{x_+}{z} f_\mathrm{g}(\frac{x_+}{z}, Q^2)}{x_+ f_\mathrm{g}(x_+, Q^2)}, \tag{I.26}$$

where the extra factor z in eq. (I.22) is absent since this is now included in the gluon splitting function. The initial-state $\mathrm{q} \to \mathrm{g}$ splitting is not included in the ARIADNE program, but it could in principle be added in the same way as the sea-quark emission. Again we will investigate this in a future publication.

Clearly, the dipole model for incoming hadrons has some conceptual problems, especially when it comes to initial-state $\mathrm{g} \to \mathrm{q}$ splittings. However, it also has some advantages. The first emission is quite easily modified to correctly reproduce the leading order matrix element, both for DIS and W-production. Also, a larger part of phase space is available for gluon emissions as compared to DGLAP based initial-state parton showers. This enables ARIADNE to reproduce small-x observables in DIS, such as the forward jet rates, where no conventional shower succeeds. Below we shall also see that ARIADNE gives a somewhat harder peak in the W $p_\perp$-spectrum than conventional parton showers, which we know peaks below the data measured at the Tevatron.

Now that we have explained how ARIADNE handles W-production in hadronic collisions, we can proceed with describing how to combine it with a fixed-order tree-level MEG. As for the $\mathrm{e}^+\mathrm{e}^-$ case it will involve constructing all possible cascade histories of a produced MEG state, the reweighting with Sudakov form factors using a Sudakov-veto algorithm, and finally the

reweighting with α_s as well as with ratios of PDFs and the suppression function, Θ.

I.4 ARIADNE and CKKW for W production

The states delivered by a MEG contains information about the momenta, colour connections and types of the incoming and outgoing particles in the generated sub-process. The states are generated according to exact tree-level matrix elements, using a fixed α_s evaluated at some scale Q_0^2 and weighted by the relevant parton densities typically evaluated at the same scale. Q_0^2 is usually taken to be the cutoff scale used to regularize soft and collinear divergencies.

I.4.1 Constructing the emissions

To construct a dipole cascade history of this state it is first necessary to introduce the remnants so that all outgoing coloured particles from the sub-process are connected with dipoles. This is done in the same way as for standard ARIADNE. In figure I.1 the different possible connections of dipoles to the remnants are described schematically for W-production in $p\bar{p}$ collisions. We see that if a gluon has been extracted from a baryon (lower part of figure I.1b), there are two remnants one containing a quark connected to parton in the end of anti-colour line of the gluon, and one di-quark connected to the end of the colour line. Furthermore, if a sea-quark is extracted from a proton (upper part of figure I.1a), the parton in the end of its colour line will be connected with a di-quark remnant, while the anti-sea-quark will form a hadron together with the remaining valence flavour, as described in section I.3.4 above. Similarly, if an anti-sea-quark is extracted (upper part of figure I.1b), the parton in the end of its colour line will be connected with a single quark remnant, while the sea-quark will form a hadron together with the remaining valence flavours. Finally if a valence quark is extracted (lower part of figure I.1a), the remnant is a di-quark which is connected with the parton on the end of the colour line.

The construction will now proceed iteratively, with each step corresponding to the inverse of an emission in the dipole cascade. All possible constructions will be made, and afterwards one of them will be picked. In each of the construction steps we must determine

- the scale of the corresponding emission;
- the value of splitting function to be used to give different weights to different possible construction paths;

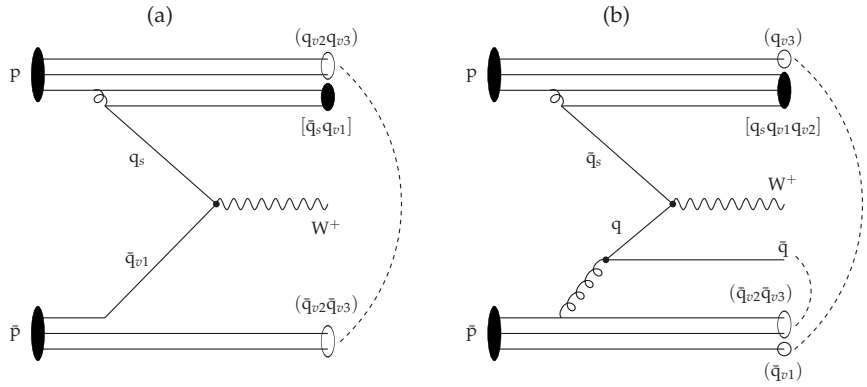

Figure I.1: Different ways dipoles are connected (dashed arcs) depending on which kind of parton is extracted from a baryon. Filled ovals corresponds to colour-singlet hadrons, while open ovals represents coloured remnants.

- the ratio of PDFs or the value of the suppression function which would have been used in the corresponding emission (which will be used to reweight the events);
- and way the momentum of the emitted parton is distributed among the emitters.

In the last point, there will usually be three partons constructed into two, which means that the total energy and momentum is always conserved with all partons staying on-shell. However, the orientation of the final two partons in the rest system of the construction needs to be specified.

Some of the possible construction steps correspond to emissions from dipoles between partons from the hard sub-process, and these are the same as in e^+e^-. Then there is a group of construction steps which involve hadron remnants, which are particular to hadronic collisions in general and to W-production in particular. In appendix III.1 we present a complete list of all possible construction steps

After the construction procedure we are normally left with several possible cascade histories. Most of these will end up in a zeroth order state containing only remnants and one W with no transverse momentum. There will be some diagrams generated by the MEG which never could have come from an ARIADNE cascade. One example is the initial-state $q \to g$ splitting discussed in the end of section I.3.4, in which case the constructed state is accepted anyway. However, there are also diagrams, such as the one in figure I.2, which could not be produced even by a conventional parton shower. In this case the construction is stopped before reaching the zeroth order state, and this state is then treated as a separate leading order process and the reweighting is only applied to additional partons (similarly to the treatment in [7] mentioned above).

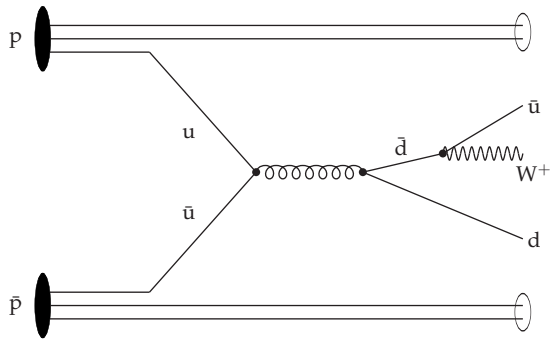

Figure I.2: An example of a W-strahlung diagram. Such diagrams are not modeled by standard ARIADNE.

The resulting alternative cascade histories may or may not have an ordered set of constructed scales. When choosing a history according to their weights given by the products of the splitting functions, we first only consider true ARIADNE histories with ordered scales. Only if no such histories were found, the other histories are considered. Histories corresponding to figure I.2 will only be considered if no full constructions are found.

I.4.2 Reweighting the events

For a given MEG state, S_n, with n additional jets, we have now constructed a dipole cascade history with complete intermediate states, $S_n, \ldots, S_0$, and the corresponding emission scales, $p_{\perp n}, \ldots, p_{\perp 1}$, and we can proceed with the reweighting.

First we note that the MEG has used PDFs typically evaluated at the cutoff scale, Q_0^2 with x_+ and x_- given by the light-cone momentum fractions of the partons, i and j, entering the hard sub-process. This should be compared with the starting point for a normal parton cascade generation, where we just have a $q\bar{q}' \to W$ sub-process, and the PDFs are evaluated at the scale m_W^2 and x'_+ and x'_- given by the corresponding momentum fractions for the q and $\bar{q}'$. Our strategy is to follow the ARIADNE cascade as closely as possible, just replacing the product of dipole splitting function with the exact tree-level matrix element, so to get the same starting point, we take the q and $\bar{q}'$ of the state S_0 and their x'_+ and x'_-, and reweight the event with

$$\omega_0 = \frac{x'_+ f_q(x'_+, m_W^2) \cdot x'_- f_{\bar{q}'}(x'_-, m_W^2)}{x_+ f_i(x_+, Q_0^2) \cdot x_- f_j(x_-, Q_0^2)}. \tag{I.27}$$

If a construction instead ended in a state such as the one in figure I.2, the

corresponding incoming partons and their momentum fractions are used instead with the scale given by m_H^2, the squared invariant mass of the hard subprocess.

Then we reweight with all the PDF ratios, R_i^{PDF}, determined in the construction,

$$\omega_1 = \prod_{i=1}^{n} R_i^{\text{PDF}}. \tag{I.28}$$

This comes about since the exact tree-level ME used corresponds to the product of splitting functions, while in a parton cascade we also have ratios of PDFs as in eqs. (I.20) and (I.25). Depending on the emission, these ratios can be either 1 for a final-state emission, the ratio of PDFs for the case of initial-state $q \to g$ and $g \to q$ splittings, the suppression function Θ for an initial-state $g \to g$ splitting and Θ/z for an initial-state $q \to q$ splitting (cf. eqs. (I.22) and (I.26)). We note that for a conventional parton cascade, where the Θ functions would be replaced by ratios of PDFs, the ω_0 and ω_1 weights would basically cancel each other, which is why these did not show up in the procedures in [7] and [9].

We then reweight with the correct scales in α_s according to

$$\omega_2 = \frac{\prod_{i=1}^{n} \alpha_s(p_{\perp i}^2)}{\alpha_s(Q_0^2)^n}. \tag{I.29}$$

Again, for the situation in figure I.2, the first two scales are taken to be m_H^2.

Finally we need to reweight with the Sudakov form factors in ARIADNE. This is done with the same Sudakov-veto algorithm as was presented in section I.3.1. There are, however a few details which should be mentioned.

The starting scale for the trial emission from the leading order state, S_0, is given by $p_{\perp\text{max}}^2 = W^2/4$, where W is the total invariant mass of the hadronic collision, ie. the same as for the standard ARIADNE treatment of W production. For the situation in figure I.2, m_H^2 is used instead.

If the constructed cascade history contains unordered scales, such that $p_{\perp i}^2 < p_{\perp i+1}^2$, the two corresponding emissions will be treated as a combined emission with $p_{\perp i+1}^2$ as the scale. The Sudakovs will be generated with a trial emission from the state S_{i-1} with a minimum scale of $p_{\perp i+1}^2$ and a trial emission from the state S_{i+1} with a maximum scale of $p_{\perp i+1}^2$, while there is no Sudakov generated from the state S_i.

Finally, in the trial emission from the state S_n, for $n < N$, when checking if the resulting partons are above the jet cutoff used in the MEG, possible recoil gluons are not considered. Such recoil gluons may appear in ARIADNE, but they are typically rather soft, and including them would very often result in the emission being below the cutoff, even if the emitted gluon is not.

I.4.3 The full algorithm

We can now summarize the full algorithm. The way it is used below results in weighted events. This is because of the complicated reweightings which takes place. However, all weights are positive, and by carefully choosing the PDFs and α_s used in the MEG, it should be possible to have a vetoing procedure so that all events end up with unit weight.

1. First the number of partons, $n \leq N$, to be generated is chosen according to the integrated tree-level matrix elements in the MEG, using a cutoff Q_0^2 in the jet resolution scale given by the longitudinally invariant $k_\perp$-algorithm. A fixed α_s is used and the PDFs are typically sampled at the Q_0^2 scale.
2. Then the MEG is told to generate the momenta of the state with n additional partons according to the tree-level matrix element. Since we do not want any events below the cutoff in the dipole cascade, the invariant $p_\perp^2$ of the partons is checked, and if anyone is below $p_{\perp c}^2$, the state is rejected and the procedure is restarted at step 1.
3. Now, all the intermediate states $S_{n-1}, \ldots, S_0$ and scales $p_{\perp n}^2, \ldots, p_{\perp 1}^2$ are constructed according to the procedure in section I.4.1, resulting in a possible dipole shower history of the generated S_n state.
4. The event is reweighted by the weight factors given in eqs. (I.27)–(I.29).
5. We now make a trial emission with the dipole cascade from the state S_0, starting from the maximum scale $p_{\perp\max}^2 = W^2/4$. If this emission is at a scale above $p_{\perp 1}^2$, the event is rejected and we restart from step 1. If not, a trial emission is performed from the state S_1 with a maximum scale of $p_{\perp 1}^2$. If this emission is at a scale above $p_{\perp 2}^2$ the event is rejected and we restart from step 1. This procedure is repeated for all states down to S_{n-1}. If no rejection has been made, a trial emission is made from the ME-generated state with n additional partons starting from the scale $p_{\perp n}^2$. There are now two cases
   (a) If $n = N$ the trial emission is always kept and the dipole cascade is allowed to continue down to the cutoff $p_{\perp c}^2$ and the event is accepted.
   (b) If $n < N$, and all parton pairs pass the cut, Q_0^2, used in the MEG, the event is rejected and we restart from step 1. If any of the partons fail the cut, the trial emission is accepted and the dipole cascade is allowed to continue down to the cutoff $p_{\perp c}^2$ and the event is accepted.

I.5 Results

To test our algorithm, we have generated W^++$n$jet events, with $n \leq N = 4$ with the MADGRAPH/MADEVENT program [50] for a $p\bar{p}$ collider at a total energy of 1960 GeV, ie. corresponding to the Tevatron run II. The longitudinally invariant $k_\perp$-algorithm was used[2] to regularize the cross section, using cutoffs $E_{\text{cut}} = 12, 22$ and 50 GeV. We used the CTEQ6L [51] PDF parameterization using E^2_{cut} as scale. E^2_{cut} was also used as the scale in α_s. The event was generated with unit weight and was then reweighted according to the algorithm in section I.4.3. To avoid wildly fluctuating weights due to the ratios of PDFs, arising from situations in which the events in MADGRAPH had large x values where the PDF is very small, the W^+ was required to have limited rapidity, $|y| < 2.5$, and all partons were required to have a limited pseudorapidity, $|\eta| < 2.5$. For the same reason, when constructing the remnants, both the valence- and sea-quark alternatives were used with appropriate weights, rather than choosing between the two as described in section I.3.4.

In the following we will use the notation MENPS for results from our new algorithm using W^++0,...,W^++N jets from MADGRAPH (the individual contributions from $W^+ + n$ jets are denoted ME$^n N$PS), while ARIADNE will denote results obtained with the default ARIADNE treatment.

As mention above, ARIADNE by default already has a matrix element correction for the first emission in W production[3]. Hence, as a first test of our new algorithm is to run it with $N = 1$, in which case we should get the same result as the standard default ARIADNE. In fact, had the construction procedure been exact, the results would be exactly the same. Of course, the construction can never be really exact, but for only one additional jet it is fairly close.

In figure I.3 we show the $p_\perp$ spectrum of the W^+ for the new algorithm with $N = 1$, ME1PS, compared to default ARIADNE. Clearly the agreement is very good. In particular we note that there is no significant discontinuity or other strange behaviors around the different cutoffs used. This agreement is not trivial, since the ME1PS curve is a sum of W^++0 and W^++1 jet event from MADGRAPH. The fact that there is a small contribution of W^++0 event above the cutoff (and vice versa, some W^++1 events below the cutoff) is an effect of the added cascade. The effect of the cutoffs is not completely invisible, however, as is clear in figure I.3d, where we enhance the effect by showing the ratio of $p_\perp$-spectra of ME1PS and ARIADNE for the different cutoffs.

We can now proceed with some confidence to investigate our new algorithm also for higher parton multiplicities in the MEG. Here we will, of course, expect differences w.r.t. ARIADNE. These differences would be the ones de-

[2] Using `MODE=4211` in the KTCLUS program [41].

[3] In fact we discovered a small bug in the default ARIADNE treatment, related to a mismatch between the invariant $p_\perp$ and the actual transverse momentum in gluon emissions. This bug has been fixed in the latest release of ARIADNE.

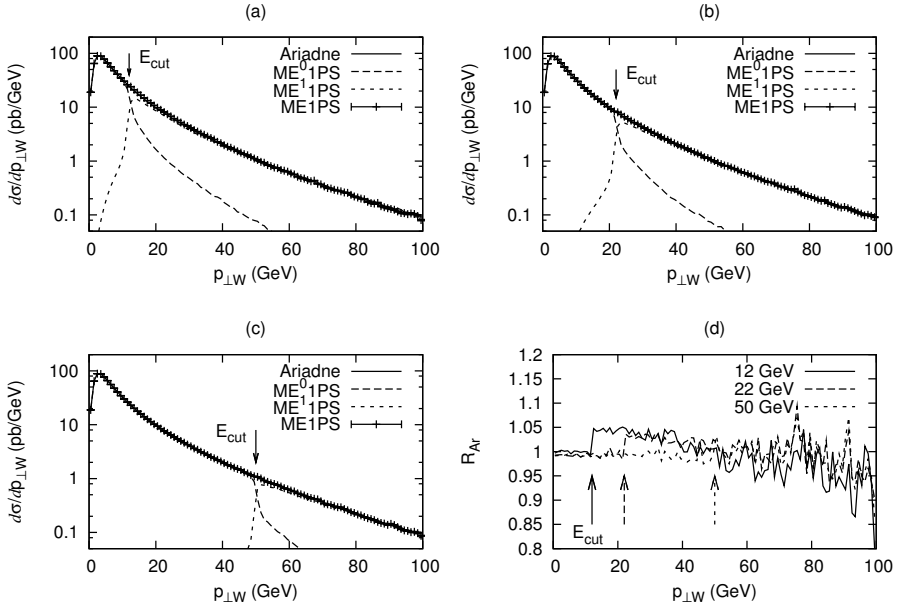

Figure I.3: Differential cross section as a function of transverse momentum of the W for standard ARIADNE compared to the first order matrix element correction for the different cutoffs (a) 12 GeV, (b) 22 GeV and (c) 50 GeV. In all cases the full line is standard ARIADNE while the error bars shows the results from ME1PS. The long-dashed and short-dashed lines indicate the contributions from W+0jet and W+1jet matrix elements to ME1PS respectively. Plot (d) shows the ratio between the ME1PS distributions and standard ARIADNE for cutoffs of 12 GeV (full line), 22 GeV (long-dashed line) and 50 GeV (short-dashed line).

sired from replacement of the products of splitting functions with the exact tree-level matrix elements, and also from the additional processes not present in the dipole cascade, such as the one in figure I.2. For small scales, these differences should be small and we would still like to have a smooth behavior of any observable sensitive to the cutoff used in MADGRAPH, at least for small enough E_{cut}. There may also be differences arising from deficiencies in our algorithm, since there are now additional construction steps possible.

In figure I.4a we again show the W^+ $p_\perp$ spectrum, but now using ME4PS and comparing with ARIADNE and also with the default PYTHIA parton shower (which also includes a tree-level matrix element correction for the first emission). We find that there is now an increase at large $p_\perp$ for the ME4PS case, which is attributed to the desired higher-order effects. We note that there is still no dramatic discontinuity around the cutoff.

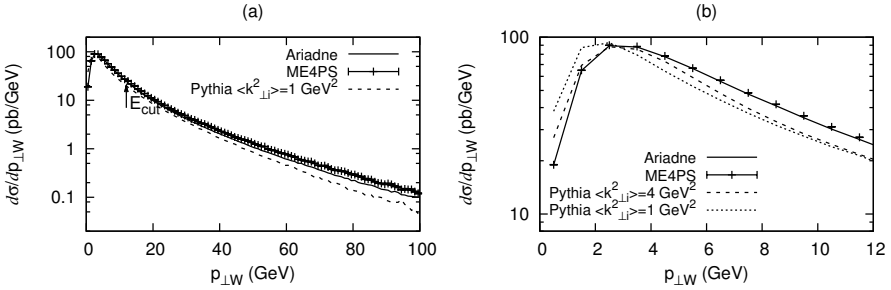

Figure I.4: (a) Differential cross section as a function of transverse momentum of the W for standard ARIADNE (full line), ARIADNE with up to fourth order matrix element corrections (error bars) and PYTHIA with intrinsic transverse momentum of $\langle k_\perp^2 \rangle = 1$ GeV^2 (short-dashed line). (b) is the same concentrating on the small $p_{\perp W}$ region, where also PYTHIA with intrinsic transverse momentum of $\langle k_\perp^2 \rangle = 4$ GeV^2 is shown (dotted line).

There is distinct difference in the small-$p_\perp$ behavior for the PYTHIA distribution. The peak in PYTHIA is shifted towards smaller $p_\perp$, as compared to ARIADNE, with or without the new matching algorithm. This is a known problem with PYTHIA, which need an uncomfortably large intrinsic transverse momentum of the proton to reproduce data. This is shown in more detail in figure I.4b where we focus on the small-$p_\perp$ part of the spectrum and where we have two curves for PYTHIA, one with an average squared intrinsic transverse momentum, $\langle k_{\perp i}^2 \rangle$, of 1 GeV^2 and one with 4 GeV^2. Note that also ARIADNE has an intrinsic transverse momentum, but this is at a typical non-perturbative value of $\langle k_{\perp i}^2 \rangle = 0.36$ GeV^2, but the increased possibility of radiating gluons in the dipole cascade, especially in the direction of the remnants, will give the slightly harder $p_\perp$ spectrum. From reference [52] we know that PYTHIA can only describe data with the higher intrinsic transverse momentum[4], which is quite close to ARIADNE[5] in figure I.4. Also other DGLAP-based parton showers need a high intrinsic transverse momentum to describe Tevatron data (HERWIG: $\langle k_\perp^2 \rangle \approx 2.6$ GeV^2 [53], APACIC++/SHERPA[6]: $\langle k_\perp^2 \rangle \approx 1.3$ GeV^2 [7]), although not as high as PYTHIA, a value above one GeV^2 is needed and well above what is required in ARIADNE.

There is still a difference in shape and with the increased statistics collected in Tevatron Run II, it may be possible to distinguish between the two.

[4] In later PYTHIA releases the higher value is the default.

[5] We have not compared directly with Tevatron results here due to uncertainties about the corrections made to the data.

[6] APACIC++/SHERPA uses a Gaussian distribution with a width of 0.8 GeV, but centered around 0.8 GeV, while the other programs use a Gaussian centered around zero.

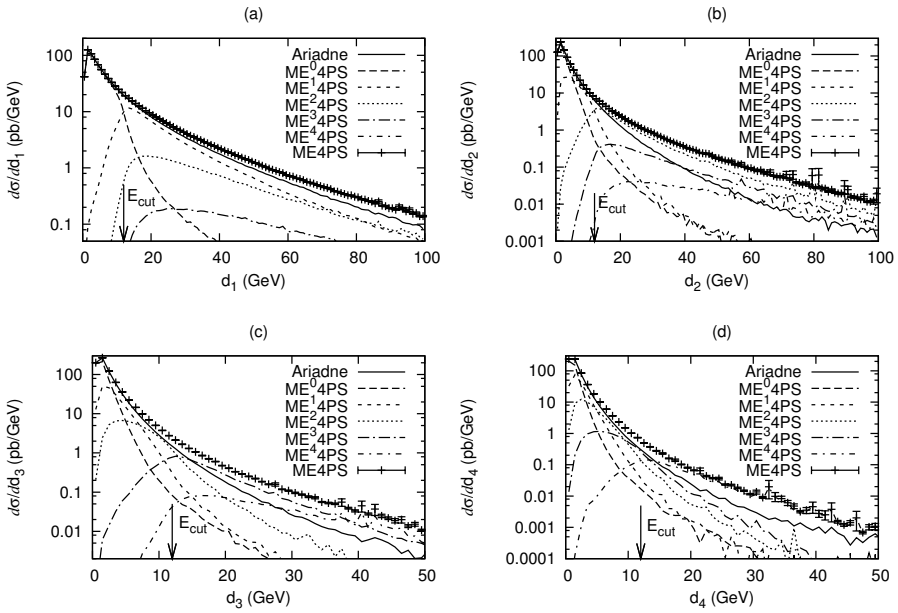

Figure I.5: Differential cross section as a function of the scale where the jets merge in the $k_\perp$-algorithm, where d_i denotes the scale when i jets merge into $i-1$ jets. Figures (a), (b), (c) and (d) shows d_1, d_2, d_3 and d_4 respectively. In all cases the error bars show the results from ARIADNE corrected with up to fourth order matrix elements (ME4PS), while the contributions from W+0jet, W+1jet,..., W+4jets matrix elements are shown with long-dashed, short-dashed, dotted, lond-dash-dotted and sort-dash-dotted lines respectively. Also shown are the results from standard ARIADNE (full line).

Next we want to check the cutoff sensitivity also for higher jet rates. We do that by taking the final events on parton level and cluster them with the same $k_\perp$-algorithm which was used for the regularization in MADGRAPH, and then look at what value of the resolution variable, d_n, an event is clustered from n-jets to $n-1$-jets. In figure I.5 we show such distributions for $n = 1, 2, 3$ and 4 for $E_{\text{cut}} = 12$ GeV, where d_3 and d_4 are only plotted for values up to 50 GeV due to limited statistics. We also show the individual contributions from different parton multiplicities delivered by MADGRAPH. We see that there is a clear difference between ME4PS and ARIADNE for large d_n values, which is expected from the improved treatment of events with several hard jets. We note that there is a rather smooth transition across E_{cut}. In figure I.6 we also show results for $E_{\text{cut}} = 22$ and 50 GeV, now presented as ratios between ME4PS and ARIADNE. As expected we here see more clearly where the new matrix element treatment sets in above E_{cut}. In figure I.6 we also show the ratio between

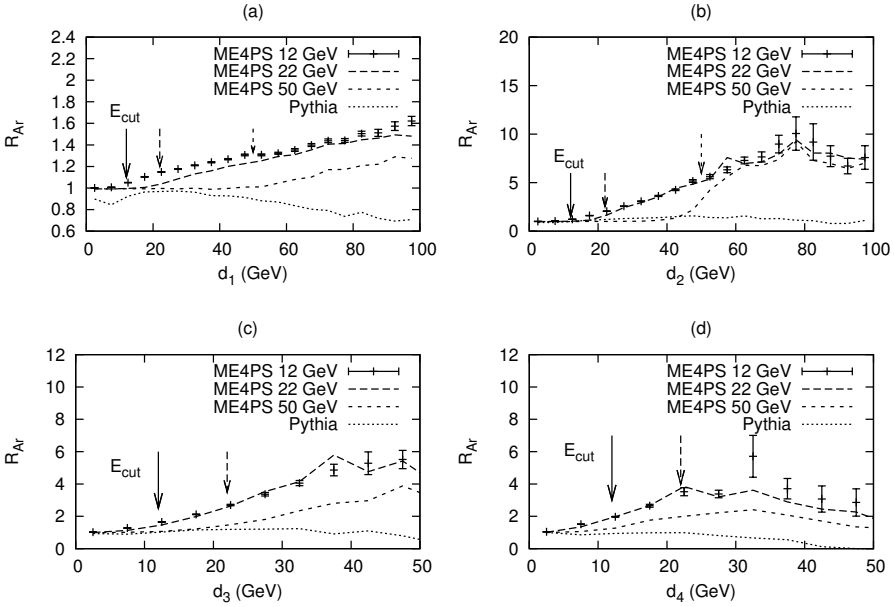

Figure I.6: Distributions in jet merging scales, d_i, given as ratios w.r.t. standard ARIADNE. Figures (a), (b), (c) and (d) shows d_1, d_2, d_3 and d_4 respectively. The ME-corrected ARIADNE (ME4PS) is shown for cutoffs of 12 GeV (error bars), 22 GeV (long-dashed line) and 50 GeV (short-dashed line). Also shown is the results for PYTHIA (dotted line).

PYTHIA and ARIADNE and we find that, as compared to the effects of the matrix element corrections, the difference between the two cascades is small.

Next we want to see if the features of the ARIADNE resummation are reflected in our new algorithm. As noted before, the emission of gluons are allowed in a larger phase space region in ARIADNE as compared to a conventional PSEG, hence the no-emission probabilities should be affected. Also, in a conventional DGLAP-based initial-state PSEG, the parton closest to the W is also the hardest one. This is not the case for ARIADNE where, effectively, contributions of emissions with lower $p_\perp$ between the hardest parton and the W is taken into account, as illustrated in figure I.7a. Possible BFKL effects in similar situations has previously been investigated in [54]. One observable which may be sensitive to this difference is the pseudorapidity difference between the W and a jet, $\Delta\eta_{Wj}$, which then should be enhanced for large $\Delta\eta_{Wj}$ in ARIADNE as compared to PYTHIA. This is also the case as shown in figure I.7b. Of course, the exact tree-level matrix element will also contain contributions such as the one in I.7a, and we see that the enhancement at large $\Delta\eta_{Wj}$ is

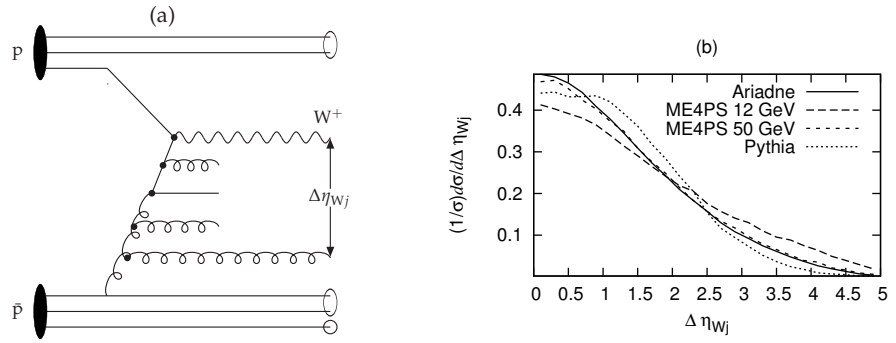

Figure I.7: Part (a) shows a typical diagram contributing to the pseudorapidity difference between the W and the hardest jet. Diagrams with soft jets between the W and the hardest jet can not be generated through DGLAP evolution, but are included in the matrix element corrections. Plot (b) is a normalized distribution of the difference in pseudorapidity between the hardest jet and the W, where the jet is defined using the $k_\perp$-algorithm with a 12 GeV cutoff and the hardest jet has a transverse momentum greater than 40 GeV. The distribution is shown for ARIADNE (full line), PYTHIA (dotted line), and ME4PS with a 12 GeV and 50 GeV cutoff (long- and short-dashed lines respectively).

even more significant, when ME corrections are added to ARIADNE with low enough cutoff. For higher cutoffs there will, of course, be much fewer events of this type generated by the MEG. It would be interesting to see if including CKKW corrections also in PYTHIA would bring it closer to ARIADNE and ME4PS. This could be expected since including higher order corrections could in the end make things more insensitive to the particular kind of resummation used.

One of the advantages of the matrix element corrections is that correlations between hard partons are more accurately described. This may be important when eg. estimating backgrounds to different searches. We will here consider the background to top production at the Tevatron for the semi-leptonic channel which corresponds to W+4-jets. In a realistic top search one would use identified b-jets, but since our MADGRAPH events do not include b-quarks we look at W+4-jets in general.

In figure I.8 we show the W+4-jets background to the top-mass distribution. We obtained it by using the $k_\perp$-algorithm to cluster four jets and required that the jet scale was above 12 GeV. Form these we found the two jets j_1 and j_2 with an invariant mass m_{12} closest to the W mass. If no jets with $|m_{12} - m_W| < 20$ GeV were found, the event was rejected. Then we selected a third jet, j_3, so that the difference $|m_{123} - m_{W4}|$ was minimized, where m_{123} is the invariant mass of jets 1, 2 and 3, and m_{W4} is the invariant mass of the $W^+$and jet 4. If the difference

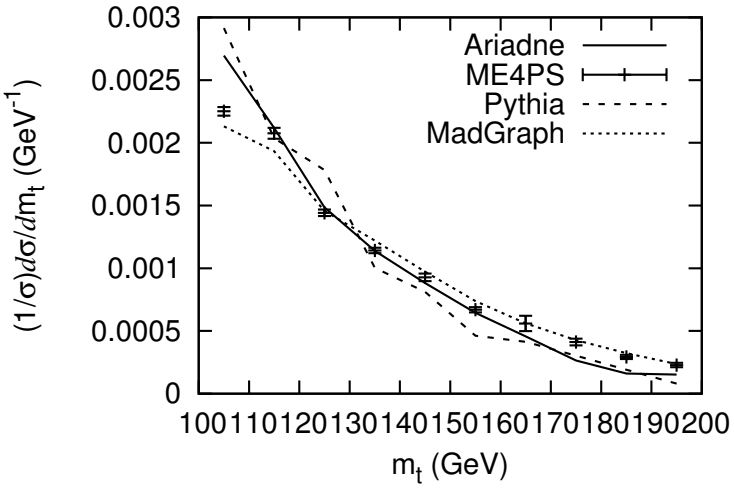

Figure I.8: The normalized differential cross section given as a function of the reconstructed top quark mass for ARIADNE (full line), PYTHIA (short-dashed line), and ME4PS with 12 GeV cutoff (long-dashed with error bars). Also shown is the results from the pure tree-level matrix element without parton showers added using a 12 GeV cutoff (dotted line).

$|m_{123} - m_{W4}| < 20$ GeV then the event was accepted and the constructed top mass is defined as the average of m_{123} and m_{W4}. Clearly the total cross section would be underestimated by the leading-order predictions of PYTHIA and ARIADNE. In figure I.8 we therefore only show the normalized shape and find that PYTHIA and ARIADNE are quite similar and that no significant change is introduced by the matrix element correction to ARIADNE. We also show the result from using the tree-level 4-jet matrix elements directly, without reweighting and adding a cascade. We find no large differences, although there is a tendency for the parton shower results to overshoot the pure matrix element result for small m_t and undershoot for large m_t. We also see that ARIADNE with matrix element corrections agree with the pure matrix elements for large m_t, while for small m_t it is slightly closer to the parton shower results.

To focus more specifically on angular correlations, we finally look at the azimuthal angle between the two hardest jets, ϕ_{12}. This observable is important for understanding how higher order emissions influence the transverse momentum of the W, $p_{\perp W}$. For $\phi_{12} \sim \pi$, the emission of a second jet decreases the $p_{\perp W}$, while for $\phi_{12} \sim 0$ the $p_{\perp W}$ is increased. In ARIADNE, after a first emission of a gluon, a second gluon will be radiated isotropically in azimuth in the

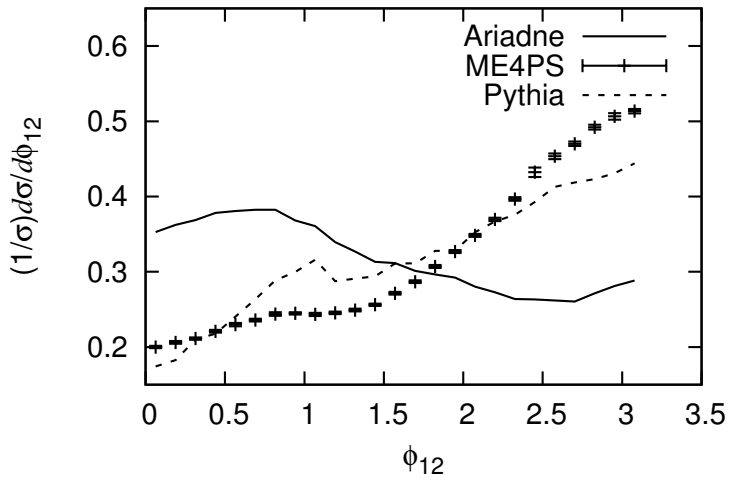

Figure I.9: Normalized distribution of the azimuthal angle difference between the two hardest jets defined using the $k_\perp$-algorithm with a 12 GeV cutoff. The distribution is shown with standard ARIADNE (full line), PYTHIA (short-dashed line), and ME4PS with 12 GeV cutoff (error bars).

rest system of the radiating dipole. Since this dipole is boosted in the direction of the first gluon, we expect that the second gluon is more likely to go in the same direction. This is not true for PYTHIA, where successive initial-state emissions are uncorrelated in azimuth (with the recoils, the net effect is a bias towards large ϕ_{12}). In figure I.9 we see the (normalized) ϕ_{12} distributions, and indeed we find that ARIADNE is more biased towards $\phi_{12} \sim 0$. Adding matrix element corrections removes this bias and brings the distribution closer to the PYTHIA result. Hence this indicates that the azimuthal correlations in standard ARIADNE are not very well modeled.

I.6 Conclusions

We have presented a way to implement a CKKW procedure for combining events generated according to tree-level matrix elements for W-production with the dipole cascade of ARIADNE. Although the basic principles are fairly simple, the details of our procedure is rather involved, which is mandated by our aim to become as insensitive as possible to the cutoff needed in the matrix element generation.

Our strategy is to take any partonic state generated by a MEG and try to

find a likely history of emissions which ARIADNE would have performed in order to generate this state. Rather than just using the constructed emission scales to calculate analytic Sudakov form factors to reweight the states, as is done in the original CKKW procedure, we find exactly the Sudakov form factors ARIADNE would have used. In addition we reweight the states with the parton densities functions and the so-called soft suppression function which ARIADNE would have used.

The PDF reweighting means that the overall normalization of cross sections are still given by the leading order diagrams used by standard ARIADNE. However, we expect an improvement of the shapes of final state distributions as compared to the standard parton shower description.

We have presented several investigations into how the ARIADNE program is improved by adding matrix element corrections. In some cases we also compared to the PYTHIA parton shower to get some insight into how well these standard cascade programs reproduces higher order matrix elements.

In one case we looked at the azimuthal correlation between the two hardest jets, and found that the difference between ARIADNE and PYTHIA was large. When corrected with matrix elements, ARIADNE came much closer to PYTHIA, indicating that such azimuthal correlations are not handled very well in standard ARIADNE.

In our quasi-realistic top-background observable we found that ARIADNE and PYTHIA were quite close and that no drastic effect was obtained by including matrix element corrections.

For the W–jet rapidity correlation we again found clear differences between ARIADNE and PYTHIA, and that these were even enhanced when correcting ARIADNE with matrix elements. This indicates that such correlations are not very well described by PYTHIA, while standard ARIADNE does a better job, although it can be improved.

We believe that the rapidity correlations indicate that non-ordered evolution is of importance for W-production at the Tevatron. Such evolution is expected to be important in small-x processes, and the fact that it shows up here, where $x \sim m_W/\sqrt{S} \approx 0.04$, may be somewhat surprising. We also believe that the inclusion of non-ordered evolution is why ARIADNE is able to reproduce experimental data on the small-$p_\perp$-distribution of the W and Z^0, distributions which can only be described by PYTHIA if an uncomfortably large intrinsic transverse momentum is added.

The fact that matrix element corrections can give us hints about where unordered evolutions may become important, is an indication that it would be very interesting to implement CKKW also for DIS[7] and compare with HERA data. Also, at the LHC where W-production may be argued to be a true small-x process ($x \sim m_W/\sqrt{S} \lesssim 0.006$), it should be interesting to study matrix element

[7] Preliminary results for DIS have already been presented in [55].

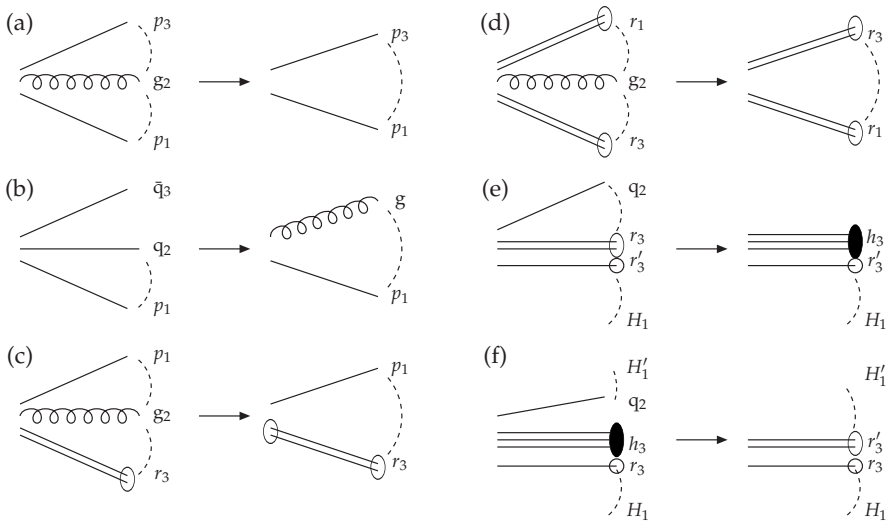

Figure I.10: Symbolic pictures of possible steps which are possible when constructing possible intermediate partonic states from events generated by a MEG. The different possibilities are described in the text. The dashed lines indicate colour-connections.

corrections. In fact also Higgs production at the LHC may be considered to be a small-x process. We will come back to these processes in future publications.

Acknowledgments

We would like to thank Stephen Mrenna, Peter Richardson, Torbjörn Sjöstrand and Christoffer Åberg for useful discussions. Special thanks to Stephen Mrenna for supplying us with event files generated with MADGRAPH/MADEVENT.

I.A Construction

Here we describe in some detail the different kinds of steps possible when constructing intermediate partonic states from events generated by a MEG. In figure I.10 the different steps are shown schematically.

(a) $p_1 - g_2 - p_3 \longrightarrow p_1 - p_3$: A gluon, colour-connected to two non-remnant partons, p_1 and p_3, is constructed to a single dipole between p_1 and p_3. The splitting function is given by one of eqs. (I.11) – (I.13) depending on whether p_1 and p_3 are gluons or quarks. The scale is given by the

invariant $p_\perp$ in eq. (I.8). No PDF ratio is relevant. In the rest frame of the construction, p_1 will retain its direction if it is a gluon and p_3 is a quark, and vice versa. If both p_1 and p_3 are gluons or both are quarks, the direction of p_1 is rotated away from the original p_3 direction with an angle $\beta x_1^2/(x_1^2+x_3^2)$, where β is the original angle between p_1 and p_3. This corresponds to the standard recoil treatment for gluon emission in ARIADNE.

(b) $p_1{-}\mathrm{q}_2\ \bar{\mathrm{q}}_3 \longrightarrow p_1{-}\mathrm{g}$. A $\mathrm{q}\bar{\mathrm{q}}$-pair is constructed into a gluon as long as they are each others anti-particles, are connected to different strings, and the end-points of these strings are not remnants of the same incoming hadron. The splitting function is given by eq. (I.15). The scale is given by the invariant $p_\perp$ in eq. (I.8). No PDF ratio is relevant. In the rest system of the construction, p_1 will retain its direction.

(c) $p_1{-}\mathrm{g}_2{-}r_3 \longrightarrow p_1{-}r_3$: A gluon, colour-connected to one remnant, r_3 and one non-remnant parton, p_1, is constructed to a single dipole between p_1 and r_3. The splitting function is given by eqs. (I.11) or (I.12) depending on whether p_1 is a quark or a gluon. If r_3 is one of two remnants of the same hadron (this corresponds to an extracted gluon), the PDF ratio is taken to be Θ, otherwise it is Θ/z. If a W is present in the event and it is *close* to g_2, the transverse momentum of the gluon in the center of mass system of p_1 and r_3 is given to the W, and the longitudinal momentum is absorbed by p_1 and r_3. The scale is given by the invariant $p_\perp$ in eq. (I.8) (calculated as if no W was close, ie. the transverse momenta of the gluon is transfered to p_1 and r_3 with the weight $x_i^2/(x_1^2+x_3^2)$). Here *close* means that $p_{+g} < p_{+\mathrm{W}}$ and $p_{-g} < p_{-\mathrm{W}}$, where $p_{\pm\mathrm{W}}$ is calculated for the constructed W momenta. If there is no W close by the momentum of the gluon is shared by p_1 and r_3, where r_3 retains its direction. The scale is given by the invariant $p_\perp$.

(d) $r_1{-}\mathrm{g}_2{-}r_3 \longrightarrow r_1{-}r_3$: A gluon connected to two remnants, one from each incoming hadron, is constructed to a single dipole between the remnants. The splitting function is given by eqs. (I.11). When calculating the scale a fraction $x_i^2/(x_1^2+x_3^2)$ of the transverse momenta from the gluon is transfered to each of the remnants and the scale is given by the invariant $p_\perp$ in eq. (I.8). The PDF ratio is given by the product of the Θ on each side, divided by z if the corresponding remnant is not one of two remnants of the same hadron. The transverse momentum of the gluon is transfered to the W if one is present, otherwise it is transfered to the hard subsystem containing the rest of the non-remnant partons in the event. The longitudinal momentum is divided between r_1 and r_3.

(e) $H_1\ r_3'\ \mathrm{q}_2{-}r_3 \longrightarrow H_1\ r_3'\ h_3$: This corresponds to the inverse of an initial-sate $\mathrm{g} \to \mathrm{q}$ splitting. For a quark, q_2, connected to a remnant, r_3, and

a hard subsystem, H_1 (which contains the W if present), connected to another remnant, r_3', from the same incoming hadron and arising from the extraction of a corresponding anti-quark, $\bar{\mathrm{q}}'$, a hadron, h_3, is formed from q_2 and r_3. The splitting function is the standard Altarelli–Parisi one, $P_{\mathrm{g}\to\mathrm{q}}(z)$. The scale is the squared transverse momentum of q_2 in the rest frame of the event. The PDF ratio is the same as would have been used in a conventional parton shower. The transverse momentum of q_2 is transfered to H_1, and the longitudinal momentum is shared between H_1, r_3' and h_3. The relative sharing of longitudinal momenta between r_3' and h_3 is the same as for the original r_3' and r_3.

(f) $H_1\ \mathrm{q}_2\ r_3\,(h_3) \longrightarrow H_1\ r_3\ r_3'$: A quark, q_2, which may have been extracted from a hadron resulting in a remnant r_3 may be absorbed into a the remnant, constructing an initial-state $\mathrm{q} \to \mathrm{g}$ splitting. The remnant is split into two, possibly together with a remnant hadron, h_3, if q_2 was a sea-quark. The splitting function is the standard Altarelli–Parisi one, $P_{\mathrm{q}\to\mathrm{g}}(z)$. The scale is the squared transverse momentum of q_2 in the rest frame of the event. The PDF ratio is the same as would have been used in a conventional parton shower. The transverse momentum of q_2 is transfered to the spectator hard subsystem, H_1, and the longitudinal momentum is shared between H_1, r_3 and r_3'. The relative sharing of longitudinal momenta between r_3 and r_3' is the same as for the original r_3 and h_3 if h_3 was present, otherwise the momenta is shared as is normally done in ARIADNE when a gluon is extracted from a hadron. Note that there is no corresponding emission in ARIADNE.

I References

[1] S. Catani, F. Krauss, R. Kuhn, and B. R. Webber, "QCD matrix elements + parton showers," *JHEP* **11** (2001) 063, arXiv:hep-ph/0109231.

[2] L. Lönnblad, "Correcting the colour-dipole cascade model with fixed order matrix elements," *JHEP* **05** (2002) 046, arXiv:hep-ph/0112284.

[3] G. Gustafson and U. Pettersson, "Dipole formulation of QCD cascades," *Nucl. Phys.* **B306** (1988) 746.

[4] G. Gustafson, "Dual description of a confined color field," *Phys. Lett.* **B175** (1986) 453.

[5] L. Lönnblad, "ARIADNE version 4: A Program for simulation of QCD cascades implementing the color dipole model," *Comput. Phys. Commun.* **71** (1992) 15–31.

[6] F. Krauss, "Matrix elements and parton showers in hadronic interactions," *JHEP* **08** (2002) 015, arXiv:hep-ph/0205283.

[7] F. Krauss, A. Schalicke, S. Schumann, and G. Soff, "Simulating W / Z + jets production at the Tevatron," *Phys. Rev.* **D70** (2004) 114009, arXiv:hep-ph/0409106.

[8] F. Krauss, A. Schalicke, S. Schumann, and G. Soff, "Simulating W / Z + jets production at the CERN LHC," *Phys. Rev.* **D72** (2005) 054017, arXiv:hep-ph/0503280.

[9] S. Mrenna and P. Richardson, "Matching matrix elements and parton showers with HERWIG and PYTHIA," *JHEP* **05** (2004) 040, arXiv:hep-ph/0312274.

[10] M. Mangano, "The so-called MLM prescription for ME/PS matching." http://www-cpd.fnal.gov/personal/mrenna/tuning/nov2002/mlm.pdf. Talk presented at the Fermilab ME/MC Tuning Workshop, October 4, 2002.

[11] M. L. Mangano, M. Moretti, and R. Pittau, "Multijet matrix elements and shower evolution in hadronic collisions: W b bbar + n jets as a case study," *Nucl. Phys.* **B632** (2002) 343–362, arXiv:hep-ph/0108069.

[12] B. Andersson, G. Gustafson, L. Lönnblad, and U. Pettersson, "Coherence effects in deep inelastic scattering," *Z. Phys.* **C43** (1989) 625.

[13] L. Lonnblad, "Small x effects in W + jets production at the Tevatron," *Nucl. Phys.* **B458** (1996) 215–230, arXiv:hep-ph/9508261.

[14] T. Sjostrand, L. Lonnblad, and S. Mrenna, "PYTHIA 6.2: Physics and manual," arXiv:hep-ph/0108264.

[15] M. Bengtsson and T. Sjöstrand, "Parton showers in leptoproduction events," *Z. Phys.* **C37** (1988) 465.

[16] G. Corcella *et al.*, "HERWIG 6.5: an event generator for Hadron Emission Reactions With Interfering Gluons (including supersymmetric processes)," *JHEP* **01** (2001) 010, arXiv:hep-ph/0011363.

[17] T. Gleisberg *et al.*, "SHERPA 1.alpha, a proof-of-concept version," *JHEP* **02** (2004) 056, arXiv:hep-ph/0311263.

[18] F. Krauss, A. Schalicke, and G. Soff, "APACIC++ 2.0: A parton cascade in C++," *Comput. Phys. Commun.* **174** (2006) 876–902, arXiv:hep-ph/0503087.

[19] V. N. Gribov and L. N. Lipatov, "Deep inelastic e p scattering in perturbation theory," *Yad. Fiz.* **15** (1972) 781–807.

[20] L. N. Lipatov, "The parton model and perturbation theory," *Sov. J. Nucl. Phys.* **20** (1975) 94–102.

[21] G. Altarelli and G. Parisi, "Asymptotic freedom in parton language," *Nucl. Phys.* **B126** (1977) 298.

[22] Y. L. Dokshitzer, "Calculation of the structure functions for deep inelastic scattering and e^+e^- annihilation by perturbation theory in quantum chromodynamics. (In Russian)," *Sov. Phys. JETP* **46** (1977) 641–653.

[23] E. A. Kuraev, L. N. Lipatov, and V. S. Fadin, "Multi-reggeon processes in the Yang-Mills theory," *Sov. Phys. JETP* **44** (1976) 443–450.

[24] E. A. Kuraev, L. N. Lipatov, and V. S. Fadin, "The Pomeranchuk singularity in nonabelian gauge theories," *Sov. Phys. JETP* **45** (1977) 199–204.

[25] I. I. Balitsky and L. N. Lipatov, "The Pomeranchuk singularity in quantum chromodynamics," *Sov. J. Nucl. Phys.* **28** (1978) 822–829.

[26] M. Ciafaloni, "Coherence effects in initial jets at small Q^2/s," *Nucl. Phys.* **B296** (1988) 49.

[27] S. Catani, F. Fiorani, and G. Marchesini, "QCD coherence in initial state radiation," *Phys. Lett.* **B234** (1990) 339.

[28] S. Catani, F. Fiorani, and G. Marchesini, "Small x behavior of initial state radiation in perturbative QCD," *Nucl. Phys.* **B336** (1990) 18.

[29] G. Marchesini, "QCD coherence in the structure function and associated distributions at small x," *Nucl. Phys.* **B445** (1995) 49–80, arXiv:hep-ph/9412327.

[30] M. Bengtsson and T. Sjostrand, "Coherent parton showers versus matrix elements: implications of PETRA - PEP data," *Phys. Lett.* **B185** (1987) 435.

[31] M. Bengtsson and T. Sjöstrand, "A comparative study of coherent and noncoherent parton shower evolution," *Nucl. Phys.* **B289** (1987) 810.

[32] M. H. Seymour, "A Simple prescription for first order corrections to quark scattering and annihilation processes," *Nucl. Phys.* **B436** (1995) 443–460, arXiv:hep-ph/9410244.

[33] M. H. Seymour, "Matrix element corrections to parton shower algorithms," *Comp. Phys. Commun.* **90** (1995) 95–101, arXiv:hep-ph/9410414.

[34] M. H. Seymour, "Matrix element corrections to parton shower simulation of deep inelastic scattering,". Contributed to 27th International Conference on High Energy Physics (ICHEP), Glasgow, Scotland, 20-27 Jul 1994.

[35] L. Lönnblad, "Rapidity gaps and other final state properties in the color dipole model for deep inelastic scattering," *Z. Phys.* **C65** (1995) 285–292.

[36] G. Miu and T. Sjostrand, "W production in an improved parton shower approach," *Phys. Lett.* **B449** (1999) 313–320, arXiv:hep-ph/9812455.

[37] S. Mrenna, "Higher order corrections to parton showering from resummation calculations," arXiv:hep-ph/9902471.

[38] G. Corcella and M. H. Seymour, "Initial state radiation in simulations of vector boson production at hadron colliders," *Nucl. Phys.* **B565** (2000) 227–244, arXiv:hep-ph/9908388.

[39] Y. L. Dokshitzer. In *Workshop on Jet studies at LEP and HERA*, durham 1990, see *J. Phys.* **G17** (1991) 1572ff.

[40] S. Catani, Y. L. Dokshitzer, M. Olsson, G. Turnock, and B. R. Webber, "New clustering algorithm for multi - jet cross-sections in e+ e- annihilation," *Phys. Lett.* **B269** (1991) 432–438.

[41] S. Catani, Y. L. Dokshitzer, M. H. Seymour, and B. R. Webber, "Longitudinally invariant K(t) clustering algorithms for hadron hadron collisions," *Nucl. Phys.* **B406** (1993) 187–224.

[42] L. Lönnblad, "ARCLUS: A New jet clustering algorithm inspired by the color dipole model," *Z. Phys.* **C58** (1993) 471–478.

[43] S. Moretti, L. Lonnblad, and T. Sjostrand, "New and old jet clustering algorithms for electron positron events," *JHEP* **08** (1998) 001, arXiv:hep-ph/9804296.

[44] B. Andersson, G. Gustafson, and L. Lönnblad, "Gluon splitting in the color dipole cascades," *Nucl. Phys.* **B339** (1990) 393–406.

[45] K. Hamacher and M. Weierstall, "The Next Round of Hadronic Generator Tuning Heavily Based on Identified Particle Data," arXiv:hep-ex/9511011.

[46] N. Brook, R. G. Waugh, T. Carli, R. Mohr, and M. Sutton, "Tuning Monte Carlo event generators to HERA data,". Prepared for Workshop on Future Physics at HERA (Preceded by meetings 25-26 Sep 1995 and 7-9 Feb 1996 at DESY), Hamburg, Germany, 30-31 May 1996.

[47] E. Boos *et al.*, "Generic user process interface for event generators," arXiv:hep-ph/0109068.

[48] A. Schalicke and F. Krauss, "Implementing the ME+PS merging algorithm," *JHEP* **07** (2005) 018, arXiv:hep-ph/0503281.

[49] N. Lavesson, L. Lönnblad, and C. Åberg. Preprint in preparation.

[50] F. Maltoni and T. Stelzer, "MadEvent: Automatic event generation with MadGraph," *JHEP* **02** (2003) 027, arXiv:hep-ph/0208156.

[51] J. Pumplin *et al.*, "New generation of parton distributions with uncertainties from global QCD analysis," *JHEP* **07** (2002) 012, arXiv:hep-ph/0201195.

[52] E. Thome, "Perturbative and nonperturbative effects in transverse momentum generation," arXiv:hep-ph/0401121.

[53] E. L. Nurse, "A measurement of the inclusive Z / gamma* → mu+ mu- cross section and study of W and Z events in p anti-p collisions at D0,". FERMILAB-THESIS-2005-05.

[54] J. R. Andersen, V. Del Duca, F. Maltoni, and W. J. Stirling, "W boson production with associated jets at large rapidities," *JHEP* **05** (2001) 048, arXiv:hep-ph/0105146.

[55] C. Åberg, "Correcting the Colour Dipole Cascade with Fixed Order Matrix Elements in Deep Inelastic Scattering." Diploma thesis, lu-tp 04-25.

II

Comparative study of various algorithms for the merging of parton showers and matrix elements in hadronic collisions

J. Alwall[1], S. Höche[2], F. Krauss[2], N. Lavesson[3], L. Lönnblad[3], F. Maltoni[4], M.L. Mangano[5], M. Moretti[6], C.G. Papadopoulos[7], F. Piccinini[8], S. Schumann[9], M. Treccani[6], J. Winter[9], M. Worek[10,11]

[1] SLAC, USA;
[2] IPPP, Durham, UK;
[3] Department of Theoretical Physics, Lund University, Sweden;
[4] Centre for Particle Physics and Phenomenology (CP3) Université Catholique de Louvain, Belgium;
[5] CERN, Geneva, Switzerland;
[6] Dipartimento di Fisica and INFN, Ferrara, Italy;
[7] Institute of Nuclear Physics, NCSR Demokritos, Athens, Greece;
[8] INFN, Pavia, Italy;
[9] Institut für Theoretische Physik, TU Dresden, Germany;
[10] ITP, Karlsruhe University, Karlsruhe, Germany;
[11] Institute of Physics, University of Silesia, Katowice, Poland.

European Physical Journal **C 53** (2008) 473 [arXiv:0706.2569].

We compare different procedures for combining fixed-order tree-level matrix-element generators with parton showers. We use the case of W-production at the Tevatron and the LHC to compare different implementations of the so-called CKKW and MLM schemes using different matrix-element generators and different parton cascades. We find that although similar results are obtained in all cases, there are important differences.

II.1 Introduction

One of the most striking features of LHC final states will be the large number of events with several hard jets. Final states with 6 jets from $t\bar{t}$ decays will have a rate of almost 1 Hz, with 10-100 times more coming from prompt QCD processes. The immense amount of available phase space, and the large acceptance of the detectors, with calorimeters covering a region of almost 10 units of pseudo-rapidity (η), will lead to production and identification of final states with 10 or more jets. These events will hide or strongly modify all possible signals of new physics, which involve the chain decay of heavy coloured particles, such as squarks, gluinos or the heavier partners of the top, which appear in little-Higgs models. Being able to predict their features is therefore essential.

To achieve this, our calculations need to describe as accurately as possible both the full matrix elements for the underlying hard processes, as well as the subsequent development of the hard partons into jets of hadrons. However, for the complex final-state topologies we are interested in, no factorization theorem exists to rigorously separate these two components. The main obstacle is the existence of several hard scales, like the jet transverse energies and di-jet invariant masses, which for a generic multi-jet event will span a wide range. This makes it difficult to unambiguously separate the components of the event, which belong to the "hard process" (to be calculated using a multi-parton amplitude) from those developing during its evolution (described by the parton shower). A given $(n+1)$-jet event can be obtained in two ways: from the collinear/soft-radiation evolution of an appropriate $(n+1)$-parton final state, or from an n-parton configuration where hard, large-angle emission during its evolution leads to the extra jet. A factorization prescription (in this context this is often called a "matching scheme" or "merging scheme") defines, on an event-by-event basis, which of the two paths should be followed. The primary goal of a merging scheme is therefore to avoid double counting (by preventing some events to appear twice, once for each path), as well as dead regions (by ensuring that each configuration is generated by at least one of the allowed paths). Furthermore, a good merging scheme will optimize the choice of the path, using the one, which guarantees the best possible approximation to a given kinematics. It is possible to consider therefore different merging schemes, all avoiding the double counting and dead regions, but leading to different results in view of the different ways the calculation is distributed between the matrix element and the shower evolution. As in any factorization scheme, the physics is independent of the separation between phases only if we have complete control over the perturbative expansion. Otherwise a residual scheme-dependence is left. Exploring different merging schemes is therefore crucial to assess the systematic uncertainties of

multi-jet calculations.

In this work we present a comprehensive comparison, for W plus multijet production, of three merging approaches: the CKKW scheme, the Lönnblad scheme, and the MLM scheme. Our investigation is an evolution and extension of the work in [1], where Mrenna and Richardson presented implementations of CKKW for HERWIG and the so-called pseudo-shower alternative to CKKW using PYTHIA, as well as the results of an approach inspired by the MLM-scheme. Our work considers the predictions of five different codes, ALPGEN, ARIADNE, HELAC, MADEVENT and SHERPA. ALPGEN implements the MLM scheme, and the results shown here are obtained with the HERWIG shower; ARIADNE the Lönnblad scheme; HELAC the MLM scheme, but will show results with the PYTHIA shower; MADEVENT uses a variant of the MLM scheme, based on the CKKW parametrization of the multiparton phase-space; SHERPA, finally, implements the CKKW scheme. This list of codes therefore covers a broad spectrum of alternative approaches and, in particular, includes all the programs used as reference event generators for multijet production by the Tevatron and LHC experimental collaborations; for those, we show results relative to publically available versions, therefore providing valuable information on the systematics involved in the generation of multijet configurations by the experiments. A preliminary study, limited to the ALPGEN, ARIADNE and SHERPA codes, was presented in [2].

While [1] devoted a large effort to discussing the internal consistency and validation of the meging schemes, we refer for these more technical aspects to the papers documenting the individual implementations of the meging algorithms in the codes we use [3–7], and we shall limit ourselves here to a short review of each implementation. We concentrate instead on comparisons among physical observables, such as cross sections or jet distributions, which we study for both the Tevatron and the LHC. The main goal is not an anatomy of the origin of possible differences, but rather the illustration of their features and their size, to provide the experimentalists with a quantitative picture of systematics associated to the use of these codes. We furthermore verify that, with only a few noteworthy exceptions, the differences among the results of the various codes are comparable in size with the intrinsic systematics of each approach, and therefore consistent with a leading-logarithmic level of accuracy. The quantaties we present correspond to experimental observables and the differences between the predictions of the various codes that we present could therefore be resolved by comparing with data.

We begin the paper with a short review of the merging prescriptions and of their implementations in the 5 codes. We then introduce the observables considered for this study, and present detailed numerical results for both the Tevatron and the LHC. We then provide with an assessment of the individual systematics of each code, and a general discusison of our findings.

II.2 Merging procedures

In general, the different merging procedures follow a similar strategy:

1. A jet measure is defined and all relevant cross sections including jets are calculated for the process under consideration. I.e. for the production of a final state X in pp-collisions, the cross sections for the processes $pp \to X + n$ jets with $n = 0, 1, \ldots, N = n_{\max}$ are evaluated.
2. Hard parton samples are produced with a probability proportional to the respective total cross section, in a corresponding kinematic configuration following the matrix element.
3. The individual configurations are accepted or rejected with a dynamical, kinematics-dependent probability that includes both effects of running coupling constants and of Sudakov form factors. In case the event is rejected, step 2 is repeated, i.e. a new parton sample is selected, possibly with a new number of jets.
4. The parton shower is invoked with suitable initial conditions for each of the legs. In some cases, like, e.g. in the MLM procedure described below, this step is performed together with the step before, i.e. the acceptance/rejection of the jet configuration. In all cases the parton shower is constrained not to produce any extra jet; stated in other words: configurations that would fall into the realm of matrix elements with a higher jet multiplicity are vetoed in the parton shower step.

The merging procedures discussed below differ mainly

- in the jet definition used in the matrix elements;
- in the way the acceptance/rejection of jet configurations stemming from the matrix element is performed;
- and in details concerning the starting conditions of and the jet vetoing inside the parton showering.

II.2.1 CKKW

The merging prescription proposed in [8, 9] is known as the CKKW scheme and has been implemented in the event generator SHERPA [10] in full generality [11].

In this scheme

- the separation of the matrix-element and parton-shower domains for different multi-jet processes is achieved through a $k_\perp$-measure [12–14], where $k_{\perp 0}$ denotes the internal separation cut, also called the merging scale;
- the acceptance/rejection of jet configurations proceeds through a

reweighting of the matrix elements with analytical Sudakov form factors and factors due to different scales in α_s;

- the starting scale for the parton shower evolution of each parton is given by the scale where it appeared first;
- a vetoed parton-shower algorithm is used to guarantee that no unwanted hard jets are produced during jet evolution.

In the original paper dealing with e^+e^- annihilations into hadrons, [8], it has been shown explicitly that in this approach the dependence on $k_{\perp 0}$ cancels to NLL accuracy. This can be achieved by combining the Sudakov-reweigthed matrix elements with a vetoed parton shower with angular ordering, subjected to appropriate starting conditions. The algorithm for the case of hadron–hadron collisions has been constructed in analogy to the e^+e^- case. However, it should be stressed that it has not been shown that the CKKW algorithm is correct at any logarithmic order in this kind of process.

For hadron-hadron collisions, the internal jet identification of the SHERPA-merging approach proceeds through a $k_\perp$-scheme, which defines two final-state particles to belong to two different jets, if their relative transverse momentum squared

$$k_{\perp ij}^2 = 2\min\left\{p_{\perp i},\, p_{\perp j}\right\}^2 \frac{\left[\cosh(\eta_i-\eta_j)-\cos(\phi_i-\phi_j)\right]}{D^2} \qquad \text{(II.1)}$$

is larger than the critical value $k_{\perp 0}^2$. In addition, the transverse momentum of each jet has to be larger than the merging scale $k_{\perp 0}$. The magnitude D, which is of order 1, is a parameter of the jet algorithm [15]. In order to completely rely on matrix elements for jet production allowed by the external analysis, the internal D should be chosen less than or equal to the D-parameter or, in case of a cone-jet algorithm, the R-parameter employed by the external analysis.

The weight attached to the generated matrix elements consists of two components, a strong-coupling weight and an analytical Sudakov form-factor weight. For their determination, a $k_\perp$-jet clustering algorithm guided by only physically allowed parton combinations is applied on the initial matrix-element configurations. The identified nodal $k_\perp$-values are taken as scales in the strong-coupling constants and replace the predefined choice in the initial generation. The Sudakov weight attached to the matrix elements accounts for having no further radiation resolveable at $k_{\perp 0}$. The NLL-Sudakov form factors employed, cf. [12], are defined by

$$\Delta_q(Q,Q_0) \quad = \quad \exp\left\{-\int_{Q_0}^{Q} dq\,\Gamma_q(Q,q)\right\}\,,$$

II

$$\Delta_g(Q,Q_0) \;=\; \exp\left\{-\int_{Q_0}^{Q} dq\,\Big[\Gamma_g(Q,q)+\Gamma_f(q)\Big]\right\}\,, \tag{II.2}$$

where $\Gamma_{q,g,f}$ are the integrated splitting functions $q\to qg$, $g\to gg$ and $g\to q\bar{q}$, which are given through

$$\Gamma_q(Q,q) \;=\; \frac{2C_F}{\pi}\frac{\alpha_s(q)}{q}\left(\ln\frac{Q}{q}-\frac{3}{4}\right)\,, \tag{II.3}$$

$$\Gamma_g(Q,q) \;=\; \frac{2C_A}{\pi}\frac{\alpha_s(q)}{q}\left(\ln\frac{Q}{q}-\frac{11}{12}\right)\,, \tag{II.4}$$

$$\Gamma_f(q) \;=\; \frac{N_f}{3\pi}\frac{\alpha_s(q)}{q}\,. \tag{II.5}$$

They contain the running coupling constant and the two leading, logarithmically enhanced terms in the limit $Q_0 \ll Q$. The single logarithmic terms $-3/4$ and $-11/12$ may spoil an interpretation of the NLL-Sudakov form factor as a non-branching probability. Therefore, $\Gamma(Q,q)$ is cut off at zero, such that $\Delta_{q,g}(Q,Q_0)$ retains its property to define the probability for having no emission resolvable at scale Q_0 during the evolution from Q to Q_0. These factors are used to reweight in accordance to the appearance of external parton lines. A ratio of two Sudakov form factors $\Delta(Q,Q_0)/\Delta(q,Q_0)$ accounts for the probability of having no emission resolvable at Q_0 during the evolution from Q to q. Hence, it is employed for the reweighting according to internal parton lines. The lower limit is taken to be $Q_0 = k_{\perp 0}$ or $Q_0 = D\,k_{\perp 0}$ for partons that are clustered to a beam or to another final state parton, respectively.

The sequence of clusterings, stopped after the eventual identification of a $2\to 2$ configuration (the core process), is used to reweight the matrix element. Moreover, this also gives a shower history, whereas the $2\to 2$ core process defines the starting conditions for the vetoed shower. For the example of an identified pure QCD $2\to 2$ core process, the four parton lines left as a result of the completed clustering will start their evolution at the corresponding hard scale. Subsequently, additional radiation is emitted from each leg by evolving under the constraint that any emission harder than the separation cut $k_{\perp 0}$ is vetoed. The starting scale of each leg is given by the invariant mass of the mother parton belonging to the identified QCD splitting, through which the considered parton has been initially formed.

Finally, it should be noted that the algorithm implemented in SHERPA does the merging of the sequence of processes $pp\to X+n$ jets with $n=0,1,\ldots,N$ fully automatically – the user is not required to generate the samples separately and mix them by hand.

II.2.2 The dipole cascade and CKKW

The merging prescription developed for the dipole cascade in the ARIADNE program [16] is similar to CKKW, but differs in the way the shower history is constructed, and in the way the Sudakov form factors are calculated. Also, since the ARIADNE cascade is ordered in transverse momentum the treatment of starting scales is simplified. Before going into details of the merging prescription, it is useful to describe some details of the dipole cascade, since it is quite different from conventional parton showers.

The dipole model [17,18] as implemented in the ARIADNE program is based around iterating $2 \to 3$ partonic splittings instead of the usual $1 \to 2$ partonic splittings in a conventional parton shower. Gluon emission is modeled as coherent radiation from colour–anti-colour charged parton pairs. This has the advantage of eg. including first order corrections to the matrix elements for $e^+e^- \to q\bar{q}$ in a natural way and it also automatically includes the coherence effects modeled by angular ordering in conventional showers. The process of quark–anti-quark production does not come in as naturally, but can be added [19]. The emissions in the dipole cascade are ordered according to an invariant transverse momentum defined as

$$q_\perp^2 = \frac{s_{12}s_{23}}{s_{123}}, \tag{II.6}$$

where s_{ij} is the squared invariant mass of parton i and j, with the emitted parton having index 2.

When applied to hadronic collisions, the dipole model does not separate between initial- and final-state gluon radiation. Instead all gluon emissions are treated as coming from final-state dipoles [20,21]. To be able to extend the dipole model to hadron collisions, spatially extended coloured objects are introduced to model the hadron remnants. Dipoles involving hadron remnants are treated in a similar manner to the normal final-state dipoles. However, since the hadron remnant is considered to be an extended object, emissions with small wavelength are suppressed. This is modeled by only allowing a fraction of the remnant to take part in the emission. The fraction that is resolved during the emission is given by

$$a(q_\perp) = \left(\frac{\mu}{q_\perp}\right)^\alpha, \tag{II.7}$$

where μ is the inverse size of the remnant and α is the dimensionality. These are semi-classical parameters, which have no correspondence in conventional parton cascades, where instead a suppression is obtained by ratios of quark densities in the backward evolution. The main effect is that the dipole cascade allows for harder gluon emissions in the beam directions, enabling it to describe properly eg. forward jet rates measured at HERA (see eg. [22]).

There are two additional forms of emissions, which need to be included in the case of hadronic collisions. One corresponds to an initial state $g \to q\bar{q}$ [23]. This does not come in naturally in the dipole model, but is added by hand in a way similar to that of a conventional initial-state parton shower [23]. The other corresponds to the initial-state $q \to gq$ (with the gluon entering into the hard sub-process), which could be added in a similar way, but this has not yet been implemented in ARIADNE.

When implementing CKKW for the dipole cascade [6, 24], the procedure is slightly different from what has been described above. Rather than using the standard $k_\perp$-algorithm to cluster the state produced by the matrix-element generator, a complete set of intermediate partonic states, S_i, and the corresponding emission scales, $q_{\perp i}$ are constructed, which correspond to a complete dipole shower history. Hence, for each state produced by the matrix-element generator, basically the question *how would ARIADNE have generated this state* is answered. Note, however, that this means that only coloured particles are clustered, which differs from eg. SHERPA, where also the W and its decay products are involved in the clustering.

The Sudakov form factors are then introduced using the Sudakov veto algorithm. The idea is that we want to reproduce the Sudakov form factors used in ARIADNE. This is done by performing a trial emission starting from each intermediate state S_i with $q_{\perp i}$ as a starting scale. If the emitted parton has a $q_\perp$ higher than $q_{\perp i+1}$ the state is rejected. This correspond to keeping the state according to the no-emission probability in ARIADNE, which is exactly the Sudakov form factor.

It should be noted that for initial-state showers, there are two alternative ways of defining the Sudakov form factor. The definition in eq. (IV.3) is used in eg. HERWIG [25], while eg. PYTHIA [26, 27] uses a form, which explicitly includes ratios of parton densities. Although formally equivalent to leading logarithmic accuracy, only the latter corresponds exactly to a no-emission probability, and this is the one generated by the Sudakov veto algorithm. This, however, also means that the constructed emissions in this case need not only be reweighted by the running α_s as in the standard CKKW procedure above, but also with ratios of parton densities, which in the case of gluon emissions correspond to the suppression due to the extended remnants in eq. (II.7) as explained in more detail in [6], where the complete algorithm is presented.

II.2.3 The MLM procedure

The so-called MLM "matching" algorithm is described below.

1. The first step is the generation of parton-level configurations for all final-state parton multiplicities n up to a given N ($W + N$ partons). They are

defined by the following kinematical cuts:

$$p_\perp^{\text{part}} > p_\perp^{\min} , \quad |\eta_{\text{part}}| < \eta_{\max} , \quad \Delta R_{jj} > R_{\min} , \tag{II.8}$$

where $p_\perp^{\text{part}}$ and η_{part} are the transverse momentum and pseudo-rapidity of the final-state partons, and ΔR_{jj} is their minimal separation in the (η, ϕ) plane. The parameters $p_\perp^{\min}$, $\eta_{\max}$ and $R_{\min}$ are called generation parameters, and are the same for all $n = 1, \ldots, N$.

2. The renormalization scale is set according to the CKKW prescription. The necessary tree branching structure is defined for each event, allowing however only for branchings, which are consistent with the colour structure of the event, which in ALPGEN is extracted from the matrix-element calculation [28]. For a pair of final-state partons i and j, we use the $k_\perp$-measure defined by

$$d_{ij} = \Delta R_{ij}^2 \min(p_{\perp i}^2, p_{\perp j}^2) , \tag{II.9}$$

where $\Delta R_{ij}^2 = \Delta\eta_{ij}^2 + \Delta\phi_{ij}^2$, while for a pair of initial/final-state partons we have

$$d_{ij} = p_\perp^2 , \tag{II.10}$$

i.e. the $p_\perp^2$ of the final-state one.

3. The $k_\perp$-value at each vertex is used as a scale for the relative power of α_s. The factorization scale for the parton densities is given by the hard scale of the process, $Q_0^2 = m_W^2 + p_{\perp W}^2$. It may happen that the clustering process stops before the lowest-order configuration is reached. This is the case, e.g., for an event like $u\bar{u} \to Wc\bar{s}g$. Flavour conservation allows only the gluon to be clustered, since $u\bar{u} \to Wc\bar{s}$ is a LO process, first appearing at $\mathcal{O}(\alpha_s^2)$. In such cases, the hard scale Q_0 is adopted for all powers of α_s corresponding to the non-merged clusters.
4. Events are then showered, using PYTHIA or HERWIG. The evolution for each parton starts at the scale determined by the default PYTHIA and HERWIG algorithms on the basis of the kinematics and colour connections of the event. The upper veto cutoff to the shower evolution is given by the hard scale of the process, Q_0. After evolution, a jet cone algorithm is applied to the partons produced in the perturbative phase of the shower. Jets are defined by a cone size R_{clus}, a minimum transverse energy $E_\perp^{\text{clus}}$ and a maximum pseudo-rapidity $\eta_{\max}^{\text{clus}}$. These parameters are called matching parameters, and should be kept the same for all samples $n = 0, 1, \ldots, N$. These jets provide the starting point for the matching procedure, described in the next bullet. In the default implementation, we take $R_{\text{clus}} = R_{\min}$, $\eta_{\max}^{\text{clus}} = \eta_{\max}$ and $E_\perp^{\text{clus}} = p_\perp^{\min} + \max(5\text{ GeV}, 0.2 \times p_\perp^{\min})$,

but these can be varied as part of the systematics assessment. To ensure a complete coverage of phase space, however, it is necessary that $R_{\text{clus}} \geq R_{\text{min}}$, $\eta_{\text{max}}^{\text{clus}} \leq \eta_{\text{max}}$ and $E_{\perp}^{\text{clus}} \geq p_{\perp}^{\text{min}}$.

5. Starting from the hardest parton, the jet, which is closest to it in (η, ϕ) is selected. If the distance between the parton and the jet centroid is smaller than $1.5 \times R_{\text{clus}}$, we say that the parton and the jet *match*. The matched jet is removed from the list of jets, and the matching test for subsequent partons is performed. The event is fully matched if each parton matches to a jet. Events, which do not match, are rejected. A typical example is when two partons are so close that they cannot generate independent jets, and therefore cannot match. Another example is when a parton is too soft to generate its own jet, again failing matching.
6. Events from the parton samples with $n < N$, which survive matching, are then required not to have extra jets. If they do, they are rejected, a suppression, which replaces the Sudakov reweighting used in the CKKW approach. This prevents the double counting of events, which will be present in, and more accurately described by, the $n+1$ sample. In the case of $n = N$, events with extra jets can be kept since they will not be generated by samples with higher n. Nevertheless, to avoid double counting, we require that their transverse momentum be smaller than that of the softest of the matched jets.

When all the resulting samples from $n = 0, \ldots, N$ are combined, we obtain an inclusive W+jets sample. The harder the threshold for the energy of the jets used in the matching, $E_{\perp}^{\text{clus}}$, the fewer the events rejected by the extra-jet veto (i.e. smaller Sudakov suppression), with a bigger role given to the shower approximation in the production of jets. Using lower thresholds would instead enhance the role of the matrix elements even at lower $E_{\perp}$, and lead to larger Sudakov suppression, reducing the role played by the shower in generating jets. The matching/rejection algorithm ensures that these two components balance each other. This algorithm is encoded in the ALPGEN generator [29,30], where evolution with both HERWIG and PYTHIA are enabled. However, in the framework of this study, the parton shower evolution has been performed by HERWIG.

II.2.4 The MADEVENT approach

The approach used in MADGRAPH/MADEVENT [31, 32] is based on the MLM prescription, but uses a different jet algorithm for defining the scales in α_s and for the jet matching. The phase-space separation between the different multi-jet processes is achieved using the $k_{\perp}$-measure as in SHERPA (eq. (II.1) with $D = 1$), while the Sudakov reweighting is performed by rejecting showered events

that do not match to the parton-level jets, as in ALPGEN. This approach allows more direct comparisons with SHERPA, including the effects of changing the $k_\perp$-cutoff scale. The details of the procedure are as follows.

Matrix-element multi-parton events are produced using MADGRAPH/ MADEVENT version 4.1 [33], with a cutoff $Q^{\rm ME}_{\rm min}$ in clustered $k_\perp$. The multi-parton state from the matrix-element calculation is clustered according to the $k_\perp$-algorithm, but allowing only clusterings that are compatible with the Feynman diagrams of the process, which are provided to MADEVENT by MADGRAPH. The factorization scale, i.e., the scale used in the parton densities, is taken to be the clustering momentum in the last $2 \to 2$ clustering (the "central process"), usually corresponding to the transverse mass, $m_\perp$, of the W boson. The $k_\perp$-scales of the QCD clustering nodes are used as scales in the calculation of the various powers of α_s.

As in the ALPGEN procedure, no Sudakov reweighting is performed. Instead, the virtuality-ordered shower of PYTHIA 6.4 [34] is used to shower the event, with the starting scale of the shower set to the factorization scale. The showered (but not yet hadronized) event is then clustered to jets using the $k_\perp$-algorithm with a jet measure cutoff $Q^{\rm jet}_{\rm min} > Q^{\rm ME}_{\rm min}$, and the matrix-element partons are matched to the resulting jets, in a way, which differs from the standard MLM procedure. A parton is considered to be matched to the closest jet if the jet measure $Q(\text{parton}, \text{jet})$ is smaller than the cutoff $Q^{\rm jet}_{\rm min}$. Events where not all partons are matched to jets are rejected. For events with parton multiplicity smaller than the highest multiplicity, the number of jets must be equal to the number of partons. For events with the highest multiplicity, N jets are reconstructed, and partons are considered to be matched if $Q(\text{parton}, \text{jet}) < Q^{\rm parton}_N$, the smallest $k_\perp$-measure in the matrix-element event. This means that extra jets below $Q^{\rm parton}_N$ are allowed, similarly to the Sherpa treatment.

Note that also the standard MLM scheme with cone jets is implemented as an alternative in MADEVENT and its PYTHIA interface.

II.2.5 HELAC implementation of the MLM procedure

In HELAC [35, 36] we have implemented the MLM procedure as described above, see section II.2.3. HELAC generates events for all possible processes at hadron and lepton colliders within the Standard Model and has been successfully tested with up to 10 particles in the final state [36–38].

The partons from the matrix-element calculation are matched to the jets constructed after the parton showering. The parton-level events are generated with a minimum $p_{\perp\rm min}$ threshold for the partons, $p_{\perp j} > p_{\perp\rm min}$, a minimum parton separation, $\Delta R_{jj} > R_{\rm min}$, and a maximum pseudo-rapidity, $|\eta_j| < \eta_{\rm max}$. In order to extract the necessary information used by the $k_\perp$-reweighting, initial- and final-state partons are clustered backwards as described in section II.2.3,

II

where again the colour flow information extracted from the matrix-element calculation is used as a constraint on the allowed clusterings. The $k_\perp$-measure, d_{ij}, for pairs of outgoing partons is given by equation (II.9) and for pairs of partons where one is incoming and one is outgoing by equation (II.10). If two outgoing partons are clustered, i.e. d_{ij} is minimal, the resulting parton is again an outgoing parton with $p = p_i + p_j$ and adjusted colour flow. In the case when incoming and outgoing partons are clustered, the new parton is incoming and its momentum is $p = p_j - p_i$. As a result we obtain a chain of d-values. For every node, a factor of $\alpha_s(d_{\text{node}})/\alpha_s(Q_0^2)$ is multiplied into the weight of the event. For the unclustered vertices as well as for the scale used in the parton density functions, the hard scale of the process $Q_0^2 = m_W^2 + p_{\perp W}^2$ is used. No Sudakov reweighting is applied. The sample of events output, which is in the latest Les Houches event file format [39], is read by the interface to PYTHIA version 6.4 [34], where the virtuality-ordered parton shower is constructed. For each event, a cone jet-algorithm is applied to all partons resulting from the shower evolution. The resulting jets are defined by $E_{\perp\text{min}}^{\text{clus}}$, $\eta_{\text{max}}^{\text{clus}}$ and by a jet cone size R_{clus}. The parton from the parton-level event is then associated to one of the constructed jets. Starting from the parton with the highest $p_\perp$ we select the closest jet ($1.5 \times R_{\text{clus}}$) in the pseudo-rapidity/azimuthal-angle space. All subsequent partons are matched iteratively to jets. If this is impossible, the event is rejected. Additionally, for $n < N$, matched events with the number of jets greater than n are rejected, whereas for $n = N$, i.e. the highest multiplicity (in this study, $N = 4$), events with extra jets are kept, only if they are softer than the N matched jets. This procedure provides the complete inclusive sample.

II.3 General properties of the event generation for the study

We present in the following sections some concrete examples. We concentrate on the case of W+multi-jet production, which is one of the most studied final states because of its important role as a background to top quark studies at the Tevatron. At the LHC, W+jets, as well as the similar Z+jets processes, will provide the main irreducible backgrounds to signals such as multi-jet plus missing transverse energy, typical of Supersymmetry and of other manifestations of new physics. The understanding of W+multi-jet production at the Tevatron is therefore an essential step towards the validation and tuning of the tools presented here, prior to their utilization at the LHC.

The CDF and DØ experiments at the Tevatron collider have reported cross-section measurements for W+multijet final states, both from Run I [40–43] and, in preliminary form, from Run II [44]. The Run I results typically refer to detector-level quantities, and a comparison with theoretical predictions

requires to process the generated events through a detector simulation. These tests were performed in the context of the quoted analyses, using the LO calculations available at the time, showing a good agreemnt within the large statistical, systematic and theoretical uncertainties. The preliminary CDF result from Run II [44] is instead corrected for all detector effects, and expressed in terms of *true* jet energies. In this form it is therefore suitable for direct comparison with theory predictions. Measurements of Z+multijet rates are also crucial, but suffer from lower statistics w.r.t. the W case. A Run II measurement of jet $p_\perp$ spectra in Z+multijet events from DØ has been compared to the predictions of SHERPA in ref. [45], showing again a very good agreement. Preliminary CDF results on the spectra of the first and second jet in Z+jet events have been compared against parton-level NLO results [46]. For both the W and Z cases, the forthcoming analyses of the high-statistics sample now available at the Tevatron will provide valuable inputs for more quantitative analyses of the codes presented here.

For each of the codes, we calculated a large set of observables, addressing inclusive properties of the events (transverse momentum spectrum of the W and of leading jets) as well as geometric correlations between the jets. What we present and discuss here is a subset of our studies, which illustrates the main features of the comparison between the different codes and of their own systematics. A preliminary account of these results, limited to the ALPGEN, ARIADNE and SHERPA codes, was presented in [2]. More complete studies of the systematics of each individual code have been [3–7] or will be presented elsewhere by the respective authors.

The existence in each of the codes of parameters specifying the details of the merging algorithms presents an opportunity to tune each code so as to best describe the data. This tuning should be seen as a prerequisite for a quantitative study of the overall theoretical systematics: after the tuning is performed on a given set of final states (e.g. the W+jets considered here), the systematics for other observables or for the extrapolation to the LHC can be obtained by comparing the difference in extrapolation between the various codes. Here it would be advantageous if future analysis of Tevatron data would provide us with spectra corrected for detector effects in a fashion suitable for a direct comparison against theoretical predictions.

The following two sections present results for the Tevatron ($p\bar{p}$ collisions at 1.96 TeV) and for the LHC (pp at 14 TeV). The elements of the analysis common to all codes are the following:

- *Event samples.* Tevatron results refer to the combination of W^+ and W^- bosons, while at the LHC only W^+ are considered. All codes have generated parton-level samples according to matrix elements with up to 4 final-state partons, i.e. $N = 4$. Partons are restricted to the light-flavour sector and are taken to be massless. The Yukawa couplings of the

quarks are neglected. The PDF set CTEQ6L has been used with $\alpha_s(m_Z) = 0.118$. Further standard-model parameters used were: $m_W = 80.419$ GeV, $\Gamma_W = 2.048$ GeV, $m_Z = 91.188$ GeV, $\Gamma_Z = 2.446$ GeV, the Fermi constant $G_\mu = 1.16639 \cdot 10^{-2}$ GeV^{-2}, $\sin^2\theta_W = 0.2222$ and $\alpha_{\rm EM} = 1/132.51$.

- *Jet definitions.* Jets were defined using Paige's `GETJET` cone-clustering algorithm, with a calorimeter segmentation of $(\Delta\eta, \Delta\phi) = (0.1, 6^\circ)$ extended over the range $|\eta| < 2.5$ ($|\eta| < 5$), and cone size of 0.7 (0.4) for the Tevatron (LHC). At the Tevatron (LHC) we require jets with $E_\perp > 10$ (20) GeV, and pseudo-rapidity $|\eta| < 2$ (4.5). For the analysis of the differential jet rates denoted as d_i, the Tevatron Run II $k_\perp$-algorithm [15][1] was applied to all final-state particles fulfilling $|\eta| < 2.5$ (5). The $k_\perp$-measure used in the algorihtm is given by equations (II.9) and (II.10).

In all cases, except the d_i plots, the analysis is done at the hadron level, but without including the underlying event. The d_i plots were done to check the details of the merging and are therefore done at parton level to avoid any smearing effects from hadronization. For all codes, the systematic uncertainties are investigated by varying the merging scale and by varying the scale in α_s and, for some codes, in the parton density functions. For ALPGEN and HELAC, the scale in α_s has been varied only in the α_s-reweighting of the matrix elements, while for the others the scale was also varied in the parton cascade. Note that varying the scale in the final-state parton showers will spoil the tuning done to LEP data for the cascades. A consistent way of testing the scale variations would require retuning of hadronization parameters. However, we do not expect a strong dependence on the hadronization parameters in the observables we consider, and no attempt to retune has been made.

The parameter choices specific to the individual codes are as follows:

- ALPGEN: The parton-level matrix elements were generated with ALPGEN [29, 30] and the subsequent evolution used the HERWIG parton shower according to the MLM procedure. Version 6.510 of HERWIG was used, with its default shower and hadronization parameters. The *default* results for the Tevatron (LHC) were obtained using parton-level cuts (see eq.(II.8)) of $p_\perp^{\rm min} = 8$ (15) GeV, $\eta_{\rm max} = 2.5$ (5), $R_{\rm min} = 0.7$ (0.4) and matching defined by $E_\perp^{\rm clus} = 10$ (20) GeV, $\eta_{\rm max}^{\rm clus} = \eta_{\rm max}$ and $R_{\rm clus} = R_{\rm min}$. The variations used in the assessment of the systematics cover:
  - different thresholds for the definition of jets used in the matching: $E_\perp^{\rm clus} = 20$ and 30 GeV for the Tevatron, and $E_\perp^{\rm clus} = 30$ and 40 GeV for the LHC. These thresholds were applied to the partonic samples produced with the default generation cuts, as well as to partonic samples produced with higher $p_\perp^{\rm min}$ values. No difference was observed in the results, aside from an obviously better generation effi-

[1] More precisely, we used the implementation in the `ktclus` package [47] (`IMODE=5`, or `4211`).

ciency in the latter case. In the following studies of the systematics, the two threshold settings will be referred to as ALPGEN parameter sets ALptX, where X labels the value of the threshold. Studies with different values of R_{clus} and R_{min} were also performed, leading to marginal changes, which will not be documented here.

- different renormalization scales at the vertices of the clustering tree: $\mu = \mu_0/2$ and $\mu = 2\,\mu_0$, where μ_0 is the default $k_\perp$-value. In the following studies of the systematics, these two settings will be referred to as ALPGEN parameter sets ALscL (for "Low") and ALscH (for "High").

The publicly available version V2.10 of the code was used to generate all the ALPGEN results.

- ARIADNE: The parton-level matrix elements were generated with MADEVENT and the subsequent evolution used the dipole shower in ARIADNE according to the procedure outlined in section II.2.2. Hadronization was performed by PYTHIA.

  For the *default* results at the Tevatron (LHC) the parton-level cuts were $p_{\perp\text{min}} = 10\ (20)$, $R_{jj} < 0.5\ (0.4)$ and, in addition, a cut on the maximum pseudo-rapidity of jets, $\eta_{j\text{max}} = 2.5\ (5.0)$. The variations used in the assessment of the systematics cover:

  - different values of the merging scales $p_{\perp\text{min}} = 20$ and 30 GeV for the Tevatron (30 and 40 GeV for the LHC). In the following studies of the systematics, these two settings will be referred to as ARIADNE parameter sets ARptX.
  - a change of the soft suppression parameters in eq. (II.7) from the default values of $\mu = 0.6$ GeV and $\alpha = 1$, to $\mu = 0.6$ GeV and $\alpha = 1.5$ (taken from a tuning to HERA data [48]). This setting will be referred to as ARs.
  - different values of the scale in α_s: $\mu = \mu_0/2$ and $\mu = 2\,\mu_0$ were used (ARscL and ARscH). This scale change was used in α_s evaluations in the program.

- HELAC: The parton-level matrix elements were generated with HELAC [35, 36] and the phase space generation is performed by PHEGAS [49]. The subsequent evolution used the default virtuality-ordered shower in PYTHIA 6.4 [34] according to the MLM procedure. Hadronization was performed by PYTHIA.

  In the present study, $e^+\nu_e + n$ jets and $e^-\bar{\nu}_e + n$ jets samples with $n = 0, \ldots, 4$ have been generated for Tevatron, while for LHC predictions only $e^+\nu_e + n$ jets final states have been considered. The number of subprocesses (i.e. $u\bar{d} \to e^+\nu_e u\bar{u}gg$ is one for the $W^+ + 4$ jets) in those cases is

II

4, 12, 94, 158 and 620 for $n = 0, 1, 2, 3, 4$ respectively, with the number of quark flavours being 4/5 for the initial/final states.

The *default* results for the Tevatron (LHC) were obtained using parton-level cuts of $p_{\perp\min} = 8\ (15)$ GeV, $\eta_{\max} = 2.5\ (5)$, $R_{\min} = 0.7\ (0.4)$ and matching defined by $E^{\text{clus}}_{\perp\min} = 10\ (20)$ GeV, $\eta^{\text{clus}}_{\max} = 2\ (4.5)$ and $R^{\text{clus}}_{\min} = 0.7\ (0.4)$. The variations used in the assessment of the systematics cover:

- different thresholds for the definition of jets used in the matching: $E^{\text{clus}}_{\perp\min} = 30$ GeV for the Tevatron, and $E^{\text{clus}}_{\perp\min} = 40$ GeV for the LHC. In the following studies of the systematics, these two settings will be referred to as HELAC parameter sets HELptX, where X labels the value of the threshold.
- different renormalization scales at the vertices of the clustering tree: $\mu = \mu_0/2$ and $\mu = 2\,\mu_0$, where μ_0 is the default $k_\perp$-value. In the following studies of the systematics, these two settings will be referred to as HELAC parameter sets HELscL and HELscH.

- MADEVENT: The parton-level matrix elements were generated with MADEVENT and the subsequent evolution used the PYTHIA shower according to the modified MLM procedure in section II.2.4. Hadronization was performed by PYTHIA.

  For the *default* results at the Tevatron (LHC) the value of the merging scale has been chosen to $k_{\perp 0} = 10\ (20)$ GeV. The variations used in the assessment of the systematics cover:

  - different values of the merging scale $k_{\perp 0} = 20$ and 30 GeV for the Tevatron, and $k_{\perp 0} = 30$ and 40 GeV for the LHC. In the following studies of the systematics, these two settings will be referred to as MADEVENT parameter sets MEktX.
  - different values of the scales used in the evaluation of α_s, in both the matrix element generation and the parton shower: $\mu = \mu_0/2$ and $\mu = 2\,\mu_0$, where μ_0 is the default $k_\perp$-value. These two settings will be referred to as MADEVENT parameter sets MEscL and MEscH.

- SHERPA: The parton-level matrix elements used within SHERPA have been obtained from the internal matrix-element generator AMEGIC++ [50]. Parton showering has been conducted by APACIC++ [51,52] whereas the combination of the matrix elements with this parton shower has been accomplished according to the CKKW procedure[2]. The hadronization of the shower configurations has been performed by PYTHIA 6.214, which has been made available through an internal interface.

[2]Beyond the comparison presented here, SHERPA predictions for W+multi-jets have already been validated and studied for Tevatron and LHC energies in [3,4]. Results for the production of pairs of W-bosons have been presented in [5].

For the *default* Tevatron (LHC) predictions, the value of the merging scale has been chosen to $k_{\perp 0} = 10\ (20)$ GeV. All SHERPA predictions for the Tevatron (LHC) have been obtained by setting the internally used D-parameter (cf. eq. (II.1) in section II.2.1) through $D = 0.7\ (0.4)$. Note that, these two choices directly determine the generation of the matrix elements in SHERPA. The variations used in the assessment of the systematics cover:

- first, different choices of the merging scale $k_{\perp 0}$. Values of 20 and 30 GeV, and 30 and 40 GeV have been used for the Tevatron and the LHC case, respectively. In the following studies of the systematics, these settings will be referred to as SHERPA parameter sets SHktX where X labels the value of the internal jet scale.
- and, second, different values of the scales used in any evaluation of the α_s *and* the parton distribution functions[3]. Two cases have been considered, $\mu = \mu_0/2$ and $\mu = 2\,\mu_0$. The choice of the merging scale is as in the default run, where μ_0 denotes the corresponding $k_\perp$-values. In the subsequent studies of the systematics these two cases are referred to as SHERPA parameter sets SHscL and SHscH. It should be stressed that these scale variations have been applied in a very comprehensive manner, i.e. in both the matrix-element and parton-showering phase of the event generation.

All SHERPA results presented in this comparison have been obtained with the publicly available version 1.0.10.

II.4 Tevatron studies

II.4.1 Event rates

We present here the comparison among inclusive jet rates. These are shown in table II.1. For each code, in addition to the default numbers, we present the results of the various individual alternative choices used to assess the systematics uncertainty. In table II.2 we show the "additional jet fractions", namely the rates $\sigma(W + n + 1\ \text{jets})/\sigma(W + n\ \text{jets})$, once again covering all systematic sets of all codes. Fig. II.1, finally, shows graphically the cross-section systematic ranges: for each multiplicity, we normalize the rates to the average of the default values of all the codes.

It should be noted that the scale changes in all codes lead to the largest rate variations. This is reflected in the growing size of the uncertainty with larger multiplicities, a consequence of the higher powers of α_s. A more de-

[3]For example, the analytical Sudakov form factors used in the matrix-element reweighting hence vary owing to their intrinsic α_s-coupling dependence.

Code	σ[tot]	$\sigma[\geq 1$ jet]	$\sigma[\geq 2$ jet]	$\sigma[\geq 3$ jet]	$\sigma[\geq 4$ jet]
ALPGEN, def	**1933**	**444**	**97.1**	**18.9**	**3.2**
ALpt20	1988	482	87.2	15.5	2.8
ALpt30	2000	491	82.9	12.8	2.1
ALscL	2035	540	135	29.7	5.5
ALscH	1860	377	72.6	12.7	2.0
ARIADNE, def	**2066**	**477**	**87.3**	**13.9**	**2.0**
ARpt20	2038	459	76.6	12.8	1.9
ARpt30	2023	446	67.9	11.3	1.7
ARscL	2087	553	116	21.2	3.6
ARscH	2051	419	67.8	9.5	1.3
ARs	2073	372	80.6	13.2	2.0
HELAC, def	**1960**	**356**	**70.8**	**13.6**	**2.4**
HELpt30	1993	373	68.0	12.5	2.4
HELscL	2028	416	95.0	20.2	3.5
HELscH	1925	324	55.1	9.4	1.4
MADEVENT, def	**2013**	**381**	**69.2**	**12.6**	**2.8**
MEkt20	2018	375	66.7	13.3	2.7
MEkt30	2017	361	64.8	11.1	2.0
MEscL	2013	444	93.6	20.0	4.8
MEscH	1944	336	53.2	8.6	1.7
SHERPA, def	**1987**	**494**	**107**	**16.6**	**2.0**
SHkt20	1968	465	85.1	12.4	1.5
SHkt30	1982	461	79.2	10.8	1.3
SHscL	1957	584	146	25.2	3.4
SHscH	2008	422	79.8	11.2	1.3

Table II.1: Cross sections (in pb) for the inclusive jet rates at the Tevatron, according to the default and alternative settings of the various codes.

tailed discussion on the effects of the scale changes can be found in section II.6. Furthermore we note that the systematic ranges of all codes have regions of overlap.

II.4.2 Kinematical distributions

We start by showing in fig. II.2 the inclusive $E_\perp$ spectra of the leading 4 jets. The absolute rate predicted by each code is used, in units of pb/GeV. The relative differences with respect to the ALPGEN results, in this figure and all other figures of this section, are shown in the lower in-sets of each plot, where for the code X we plot the quantity $(\sigma(X) - \sigma_0)/\sigma_0$, σ_0 being the values of the

Code	$\sigma^{[\geq 1]}/\sigma^{[\mathrm{tot}]}$	$\sigma^{[\geq 2]}/\sigma^{[\geq 1]}$	$\sigma^{[\geq 3]}/\sigma^{[\geq 2]}$	$\sigma^{[\geq 4]}/\sigma^{[\geq 3]}$
ALPGEN, def	**0.23**	**0.22**	**0.19**	**0.17**
ALpt20	0.24	0.18	0.18	0.18
ALpt30	0.25	0.17	0.15	0.16
ALscL	0.27	0.25	0.22	0.19
ALscH	0.20	0.19	0.17	0.16
ARIADNE, def	**0.23**	**0.18**	**0.16**	**0.15**
ARpt20	0.23	0.17	0.17	0.15
ARpt30	0.22	0.15	0.16	0.16
ARscL	0.26	0.21	0.18	0.17
ARscH	0.20	0.16	0.14	0.14
ARs	0.18	0.22	0.16	0.15
HELAC, def	**0.18**	**0.20**	**0.19**	**0.18**
HELpt30	0.19	0.19	0.18	0.19
HELscL	0.21	0.23	0.21	0.17
HELscH	0.17	0.17	0.17	0.15
MADEVENT, def	**0.19**	**0.18**	**0.18**	**0.22**
MEkt20	0.19	0.18	0.20	0.20
MEkt30	0.18	0.18	0.17	0.18
MEscL	0.22	0.21	0.21	0.24
MEscH	0.17	0.16	0.16	0.20
SHERPA, def	**0.25**	**0.22**	**0.16**	**0.12**
SHkt20	0.24	0.18	0.15	0.12
SHkt30	0.23	0.17	0.14	0.12
SHscL	0.30	0.25	0.17	0.13
SHscH	0.21	0.19	0.14	0.12

Table II.2: Cross-section ratios for $(n+1)/n$ inclusive jet rates at the Tevatron, according to the default and alternative settings of the various codes.

ALPGEN curves.

There is generally good agreement between the codes, except for ARIADNE, which has a harder $E_\perp$ spectra for the leading two jets. There we also find that SHERPA is slightly harder than ALPGEN and HELAC, while MADEVENT is slightly softer.

Fig. II.3 shows the inclusive η spectra of the leading 4 jets, all normalized to unit area. There is a good agreement between the spectra of ALPGEN, HELAC and MADEVENT, while ARIADNE and SHERPA spectra appear to be broader, in particular for the sub-leading jets. This broadening is expected for ARIADNE since the gluon emissions there are essentially unordered in rapidity, which means that the Sudakov form factors applied to the matrix-element-generated

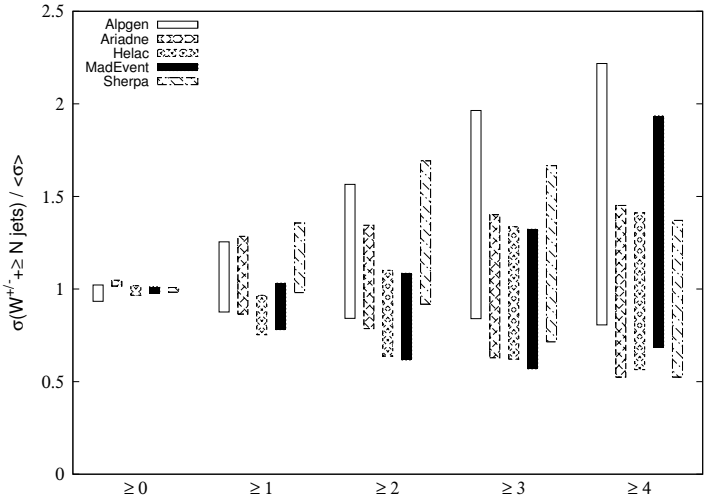

Figure II.1: Range of variation for the Tevatron cross-section rates of the five codes, normalized to the average value of the default settings for all codes in each multiplicity bin.

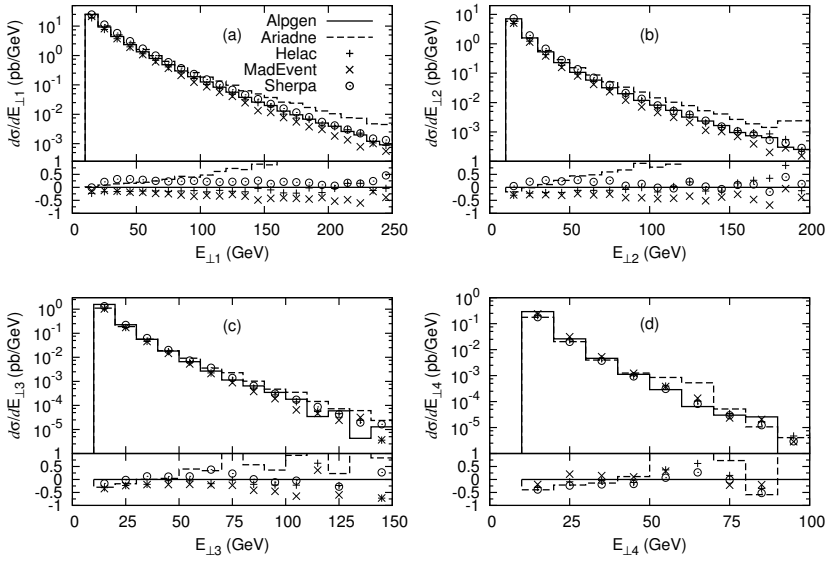

Figure II.2: Inclusive $E_\perp$ spectra of the leading 4 jets at the Tevatron (pb/GeV). In all cases the full line gives the ALPGEN results, the dashed line gives the ARIADNE results and the "+", "x" and "o" points give the HELAC, MADEVENT and SHERPA results, respectively.

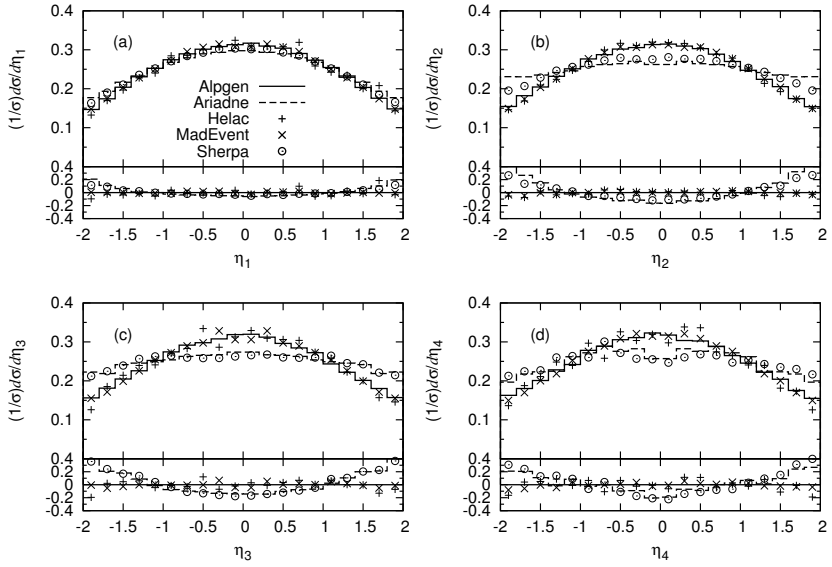

Figure II.3: Inclusive η spectra of the 4 leading jets at the Tevatron. All curves are normalized to unit area. Lines and points are as in fig. II.2.

states include also a $\log 1/x$ resummation absent in the other programs.

Fig. II.4a shows the inclusive $p_\perp$ distribution of the W boson, with absolute normalization in pb/GeV. This distribution reflects in part the behaviour observed for the spectrum of the leading jet, with ARIADNE harder than SHERPA, which, in turn, is slightly harder than ALPGEN, HELAC and MADEVENT. The region of low momenta, $p_{\perp W} < 50$ GeV, is expanded in fig. II.4b. Fig. II.4c shows the η distribution of the leading jet, η_1, when its transverse momentum is larger than 50 GeV. The curves are absolutely normalized, so that it is clear how much rate is predicted by each code to survive this harder jet cut. The $|\eta|$ separation between the W and the leading jet of the event above 30 GeV is shown in fig. II.4d, normalized to unit area. Here we find that ARIADNE has a broader correlation, while HELAC and MADEVENT are somewhat more narrow than ALPGEN and SHERPA.

In fig. II.5 we show the merging scales d_i as obtained from the $k_\perp$-algorithm, where d_i is the scale in an event where i jets are clustered into $i-1$ jets. These are parton-level distributions and are especially sensitive to the behaviour of the merging procedure close to the merging/matching scale. Note that in the plots showing the difference the wiggles stem from both the individual codes and from the ALPGEN reference. In section II.6 below, the behaviour of the individual codes is treated separately.

Also shown in fig. II.5 is the separation in $\Delta R = \sqrt{\Delta\eta^2 + \Delta\phi^2}$ between successive jet pairs ordered in hardness. The ΔR_{12} is dominated by the

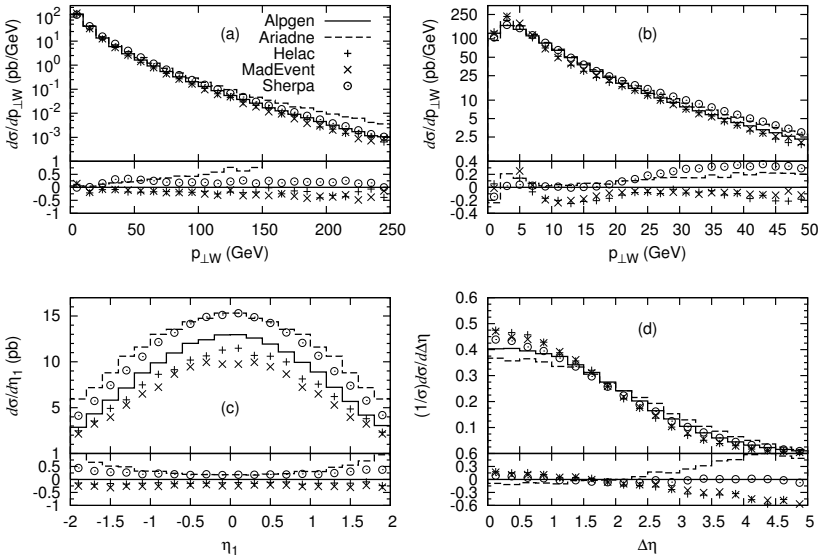

Figure II.4: (a) and (b) $p_\perp$ spectrum of $W^\pm$ bosons at the Tevatron (pb/GeV). (c) Inclusive η spectrum of the leading jet, for $p_\perp^{\text{jet1}} > 50$ GeV; absolute normalization (pb). (d) Pseudo-rapidity separation between the W and the leading jet, $\Delta\eta = |\eta_W - \eta_{\text{jet1}}|$, for $p_\perp^{\text{jet1}} > 30$ GeV, normalized to unit area. Lines and points are as in fig. II.2.

transversal-plane back-to-back peak at $\Delta R_{12} = \pi$, while for larger ΔR in all cases the behaviour is more dictated by the correlations in pseudo-rapidity. For these larger values we find a weaker correlation in ARIADNE and SHERPA, which can be expected from their broader rapidity distributions in fig. II.3.

Finally, in fig. II.6 we show $H_\perp$, the scalar sum of the transverse momenta of the charged lepton, the neutrino and the jets. This is a variable in which one often does experimental cuts in searches for new phenomena and is not expected to be very sensitive to the particulars in the merging schemes. The results show good agreement below 100 GeV, but at higher values, as expected from the differences in the hardness of the jet and $p_{\perp W}$ spectra, ARIADNE has a harder spectra than SHERPA and ALPGEN, while MADEVENT and HELAC has a slightly softer spectra.

II.5 LHC studies

II.5.1 Event rates

The tables (table II.3 and II.4) and figure (fig. II.7) of this section parallel those shown earlier for the Tevatron. The largest rate variations is, similarly to the

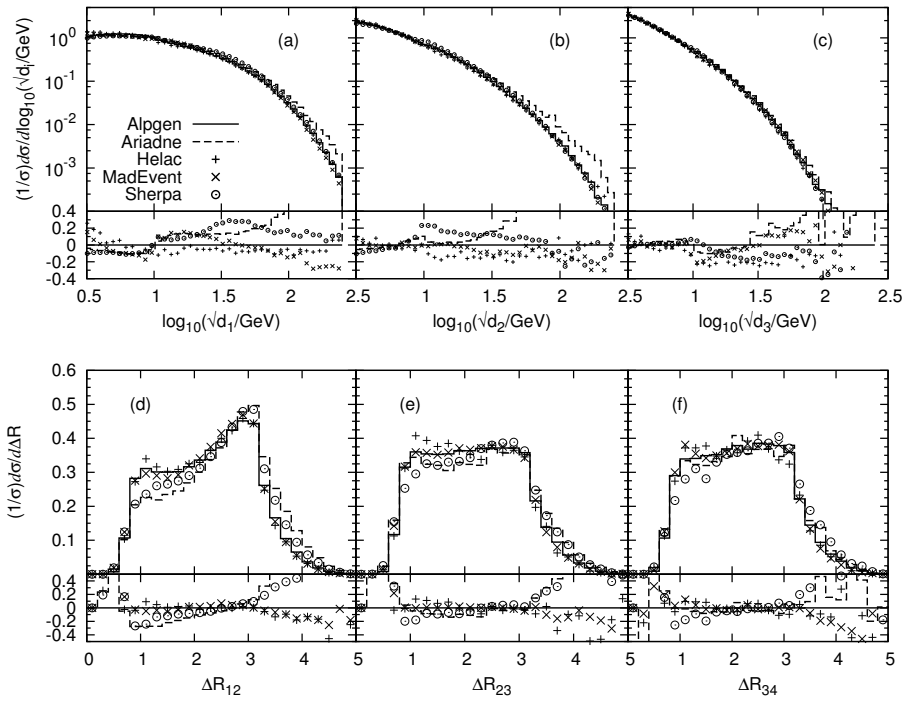

Figure II.5: (a)–(c) d_i ($i = 1, 2, 3$) spectra, where d_i is the scale in a parton-level event where i jets are clustered into $i-1$ jets using the $k_\perp$-algorithm. (d)–(f) ΔR separations at the Tevatron between jet 1 and 2, 2 and 3, and 3 and 4. All curves are normalized to unit area. Lines and points are as in fig. II.2.

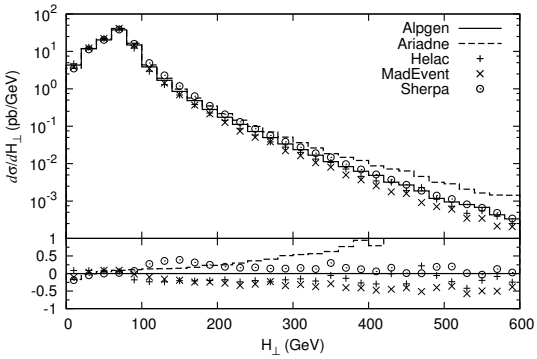

Figure II.6: The scalar sum of the transverse momentum of the charged lepton, the neutrino and the jets at the Tevatron. Lines and points are as in fig. II.2.

II

Code	σ[tot]	$\sigma[\geq 1$ jet]	$\sigma[\geq 2$ jet]	$\sigma[\geq 3$ jet]	$\sigma[\geq 4$ jet]
ALPGEN, def	**10170**	**2100**	**590**	**171**	**50**
ALpt30	10290	2200	555	155	46
ALpt40	10280	2190	513	136	41
ALscL	10590	2520	790	252	79
ALscH	9870	1810	455	121	33
ARIADNE, def	**10890**	**3840**	**1330**	**384**	**101**
ARpt30	10340	3400	1124	327	88
ARpt40	10090	3180	958	292	83
ARscL	11250	4390	1635	507	154
ARscH	10620	3380	1071	275	69
ARs	11200	3440	1398	438	130
HELAC, def	**10050**	**1680**	**442**	**118**	**36**
HELpt40	10150	1760	412	116	37
HELscL	10340	1980	585	174	57
HELscH	9820	1470	347	84	24
MADEVENT, def	**10830**	**2120**	**519**	**137**	**42**
MEkt30	10080	1750	402	111	37
MEkt40	9840	1540	311	78.6	22
MEscL	10130	2220	618	186	62
MEscH	10300	1760	384	91.8	27
SHERPA, def	**8800**	**2130**	**574**	**151**	**41**
SHkt30	8970	2020	481	120	32
SHkt40	9200	1940	436	98.5	24
SHscL	7480	2150	675	205	58
SHscH	10110	2080	489	118	30

Table II.3: Cross sections (in pb) for the inclusive jet rates at the LHC, according to the default and alternative settings of the various codes.

Tevatron rates, determined by the scale changes (described in more detail in section II.6). The main feature of the LHC results is the significantly larger rates predicted by ARIADNE (see also the discussion of its systematics, section II.6.2), which are outside the systematics ranges of the other codes. Aside from this and the fact that SHERPA gives a smaller total cross section (see also the last part of the discussion of the SHERPA systematics in section II.6.5), the comparison among the other codes shows an excellent consistency, with a pattern of the details similar to what seen for the Tevatron.

Code	$\sigma^{[\geq 1]}/\sigma^{[\mathrm{tot}]}$	$\sigma^{[\geq 2]}/\sigma^{[\geq 1]}$	$\sigma^{[\geq 3]}/\sigma^{[\geq 2]}$	$\sigma^{[\geq 4]}/\sigma^{[\geq 3]}$
ALPGEN, def	**0.21**	**0.28**	**0.29**	**0.29**
ALpt30	0.21	0.25	0.28	0.30
ALpt40	0.21	0.23	0.27	0.30
ALscL	0.24	0.31	0.32	0.31
ALscH	0.18	0.25	0.27	0.27
ARIADNE, def	**0.35**	**0.35**	**0.29**	**0.26**
ARpt30	0.33	0.33	0.29	0.27
ARpt40	0.32	0.30	0.30	0.28
ARscL	0.39	0.37	0.31	0.30
ARscH	0.32	0.32	0.26	0.24
ARs	0.31	0.41	0.31	0.30
HELAC, def	**0.17**	**0.26**	**0.27**	**0.31**
HELpt40	0.17	0.23	0.28	0.32
HELscL	0.19	0.30	0.30	0.33
HELscH	0.15	0.24	0.24	0.29
MADEVENT, def	**0.20**	**0.24**	**0.26**	**0.31**
MEkt30	0.17	0.23	0.28	0.33
MEkt40	0.16	0.20	0.25	0.28
MEscL	0.22	0.27	0.30	0.34
MEscH	0.17	0.22	0.24	0.29
SHERPA, def	**0.24**	**0.27**	**0.26**	**0.27**
SHkt30	0.23	0.24	0.25	0.27
SHkt40	0.21	0.22	0.23	0.24
SHscL	0.29	0.31	0.30	0.28
SHscH	0.21	0.24	0.24	0.25

Table II.4: Cross-section ratios for $(n+1)/n$ inclusive jet rates at the LHC, according to the default and alternative settings of the various codes.

II.5.2 Kinematical distributions

Following the same sequence of the Tevatron study, we start by showing in fig. II.8 the inclusive $E_\perp$ spectra of the leading 4 jets. The absolute rate predicted by each code is used, in units of pb/GeV.

Except for ARIADNE, we find good agreement among the codes, with ARIADNE having significantly harder leading jets, while for sub-leading jets the increased rates noted in fig. II.7 mainly come from lower $E_\perp$. Among the other codes, HELAC and SHERPA have consistently somewhat harder jets than ALPGEN, while MADEVENT is a bit softer, but these differences are not as pronounced.

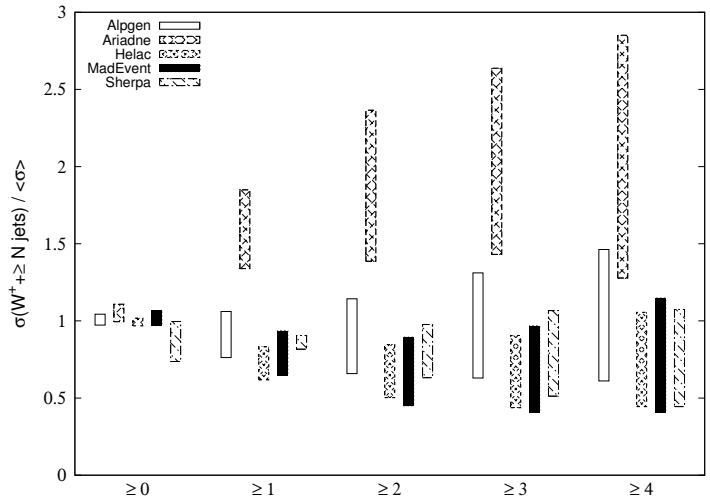

Figure II.7: Range of variation for the LHC cross-section rates of the five codes, normalized to the average value of the default settings for all codes in each multiplicity bin.

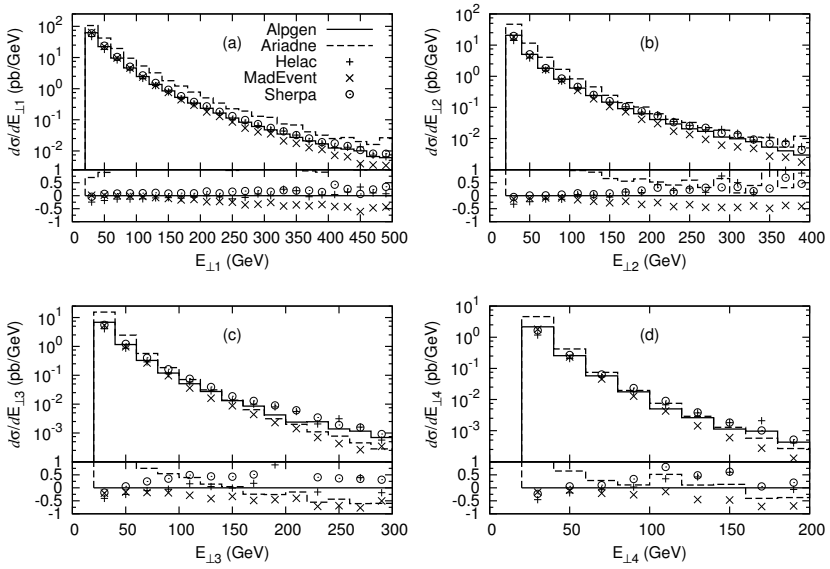

Figure II.8: Inclusive $E_\perp$ spectra of the leading 4 jets at the LHC (pb/GeV). In all cases the full line gives the ALPGEN results, the dashed line gives the ARIADNE results and the "+", "x" and "o" points give the HELAC, MADEVENT and SHERPA results respectively.

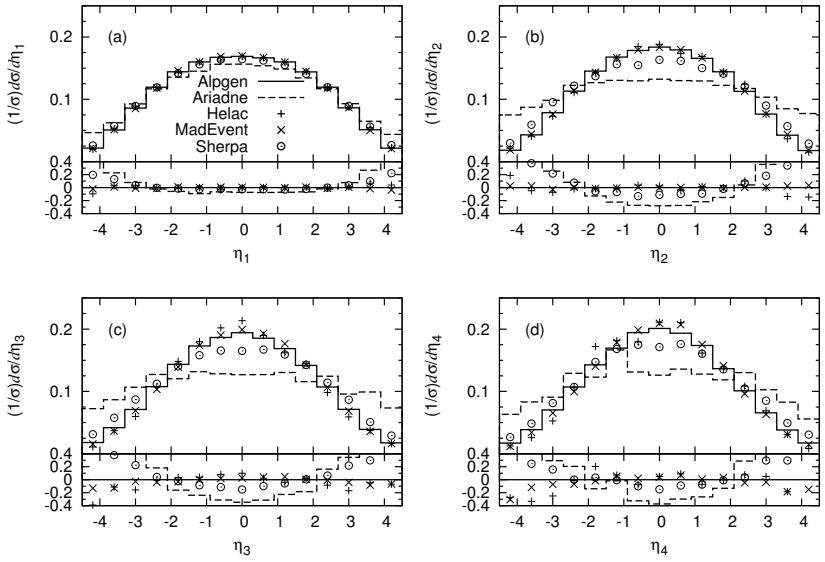

Figure II.9: Inclusive η spectra of the 4 leading jets at the LHC. All curves are normalized to unit area. Lines and points are as in fig. II.8.

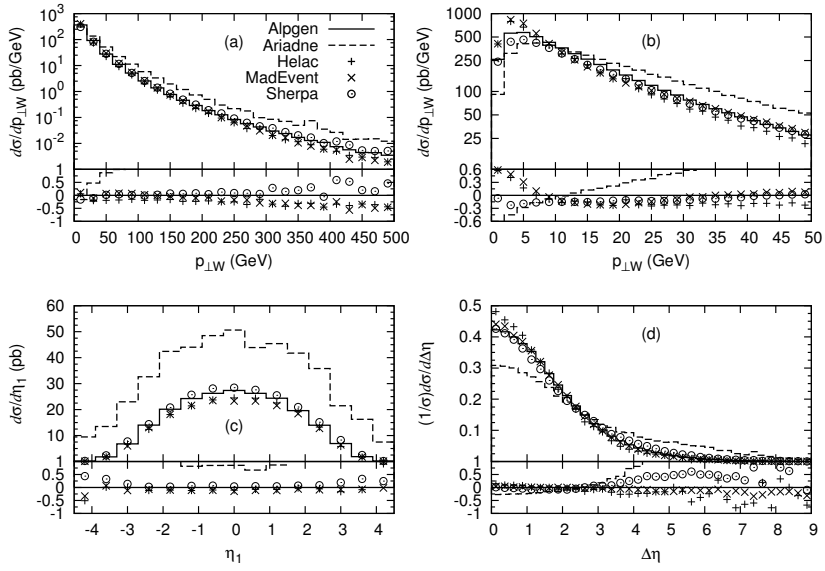

Figure II.10: (a) and (b) $p_\perp$ spectrum of W^+ bosons at the LHC (pb/GeV). (c) η spectrum of the leading jet, for $p_\perp^{\text{jet1}} > 100$ GeV; absolute normalization (pb). (d) Pseudo-rapidity separation between the W^+ and the leading jet, $\Delta\eta = |\eta_{W^+} - \eta_{\text{jet1}}|$, for $p_\perp^{\text{jet1}} > 40$ GeV, normalized to unit area. Lines and points are as in fig. II.8.

II

For the pseudo-rapidity spectra of the jets in fig. II.9 it is clear that ARIADNE has a much broader distribution in all cases. Also SHERPA has broader distributions, although not as pronounced, while the other codes are very consistent.

The $p_\perp$ distribution of W^+ bosons in fig. II.10 follows the trend of the leading-jet $E_\perp$ spectra. The differences observed in the $p_{\perp W}$ region below 10 GeV are not due to the choice of merging approach, but are entirely driven by the choice of shower algorithm. Notice for example the similarity of the HELAC and MADEVENT spectra, and their peaking at lower pt than the HERWIG spectrum built into the ALPGEN curve, a result well known from the comparison of the standard PYTHIA and HERWIG generators. Increasing the transverse momentum of the leading jet in fig. II.10a does not change the conclusions much for its pseudo-rapidity distribution. Also the rapidity correlation between the leading jet and the W^+ follows the trend found for the Tevatron, but the differences are larger, with a much weaker correlation for ARIADNE. Also SHERPA shows a somewhat weaker correlation, while HELAC is somewhat stronger than ALPGEN and MADEVENT.

For the distribution in clustering scale in fig. II.11, we find again that ARIADNE is by far the hardest. The results given by the other codes are comparable, with the only exception that for the d_1 distribution, SHERPA gives a somewhat harder prediction compared to the ones made by the MLM-based approaches.

The ΔR distributions, in fig. II.11, show at large separation a behaviour consistent with the broad rapidity distributions found for SHERPA, and in particular for ARIADNE, in fig. II.9. This increase at large ΔR is then compensated by a depletion with respect to the other codes at small separation.

The scalar transverse momentum sum in fig. II.12 shows significantly larger deviations as compared to the results for the Tevatron. ARIADNE has a much harder spectra than the other codes, while SHERPA and HELAC are slightly harder than ALPGEN and MADEVENT is significantly softer. As in the Tevatron case, it is a direct reflection of the differences in the hardness of the jet and $p_{\perp W}$ spectra, although the increased phase space for jet production at the LHC makes the $p_{\perp W}$ contribution less important at high $H_\perp$ values.

II.6 Systematic studies

In this section we present the systematic studies of each of the codes separately for both the Tevatron and the LHC, followed by some general comments on differences and similarities between the codes.

In all cases we have chosen a subset of the plots shown in the previous sections: the transverse momentum of the W, the pseudo-rapidity of the leading jet, the separation between the leading and the sub-leading jet, and the d_i

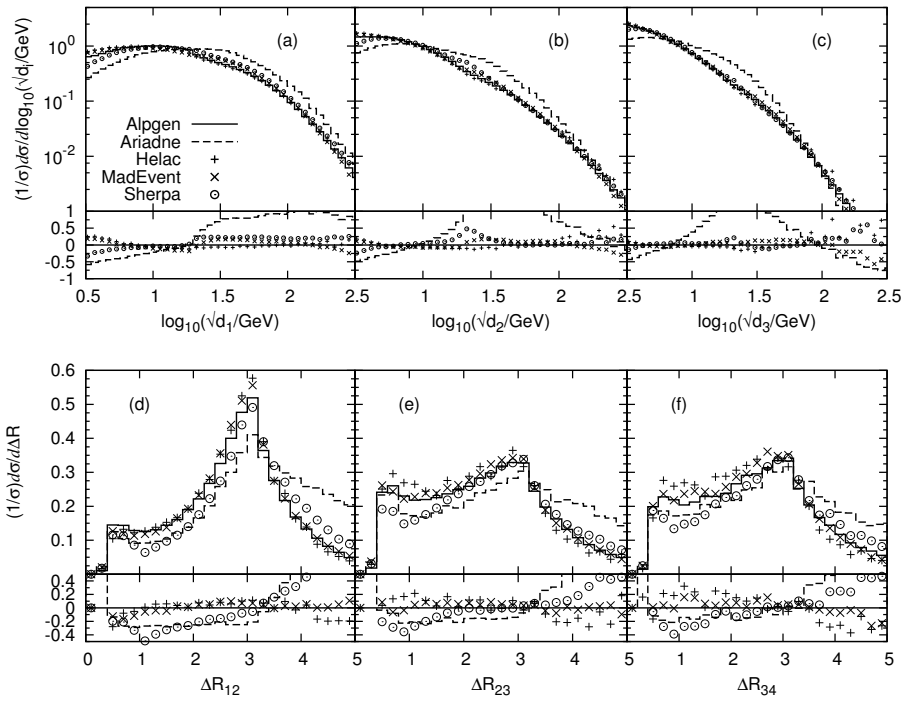

Figure II.11: (a)–(c) d_i ($i = 1, 2, 3$) spectra, where d_i is the scale in a parton-level event where i jets are clustered into $i - 1$ jets using the $k_\perp$-algorithm. (d)–(f) ΔR separations at the LHC between jet 1 and 2, 2 and 3, and 3 and 4. All curves are normalized to unit area. Lines and points are as in fig. II.8.

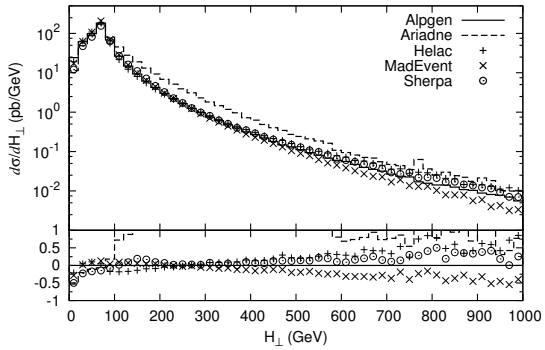

Figure II.12: The scalar sum of the transverse momentum of the charged lepton, the neutrino and the jets at the LHC. Lines and points are as in fig. II.8.

logarithmic spectra. As before, all spectra aside from $p_{\perp W}$ are normalized to unit integral over the displayed range. The variations of the inclusive jet cross sections has already been shown in table II.1-II.4 and figs. II.1 and II.7.

To estimate what systematic error can be expected from each code, the effects of varying the merging scale and changing the scale used in the determination of the strong coupling is studied (the details for each code is described in section II.3). The merging scale variations are introduced according to the definition in each algorithms and should lead to small changes in the results, although the nonleading terms from the matrix elements always lead to some residual dependence on the merging scale. In the various algorithms different choices have been made regarding how to estimate the uncertainty from α_s-scale variations and this leads to slightly different physical consequences.

In the case of ALPGEN and HELAC, the scale changes are only implemented in the strong coupling calculated in the matrix element reweighting, but the scale in the shower remains unchanged. This leads to variations of the result that are proportional to the relevant power of α_s used in the matrix element, which means that the spectra contains small deviations below the merging scale and that the deviations grow substantially above the merging scale.

In ARIADNE, MADEVENT and SHERPA both the scale in the α_s-reweighting and the scale in the α_s of the shower is changed. In addition to this the scale used in the evaluation of the parton densities is also changed in SHERPA (this is discussed further in section II.6.5). Including the scale variations in α_s in the shower changes the fraction of rejected events or the Sudakov form factors (depending on which algorithm is used), which modifies the cross section in the opposite direction compared to the scale changes in the matrix element reweighting. This leads to smaller deviations in the results above the merging scale and it is also possible to get significant deviations in the opposite direction below the merging scale, which is mainly visible in the $p_{\perp W}$ spectra.

II.6.1 ALPGEN systematics

The ALPGEN distributions for the Tevatron are shown in fig. II.13. The pattern of variations is consistent with the expectations. In the case of the $p_{\perp W}$ spectra, which are plotted in absolute scales, the larger variations are due to the change of scale, with the lower scale leading to a harder spectrum. The $\pm 20\%$ effect is consistent with the scale variation of α_s, which dominates the scale variation of the rate once $p_{\perp W}$ is larger than the Sudakov region. The change of matching scales only leads to a minor change in the region $0\ \text{GeV} < p_{\perp W} < 40\ \text{GeV}$, confirming the stability of the merging prescription.

In the case of the rapidity spectrum, we notice that the scale change leaves the shape of the distribution unaltered, while small changes appear at the edges of the η range. The d_i distributions show agreement among the var-

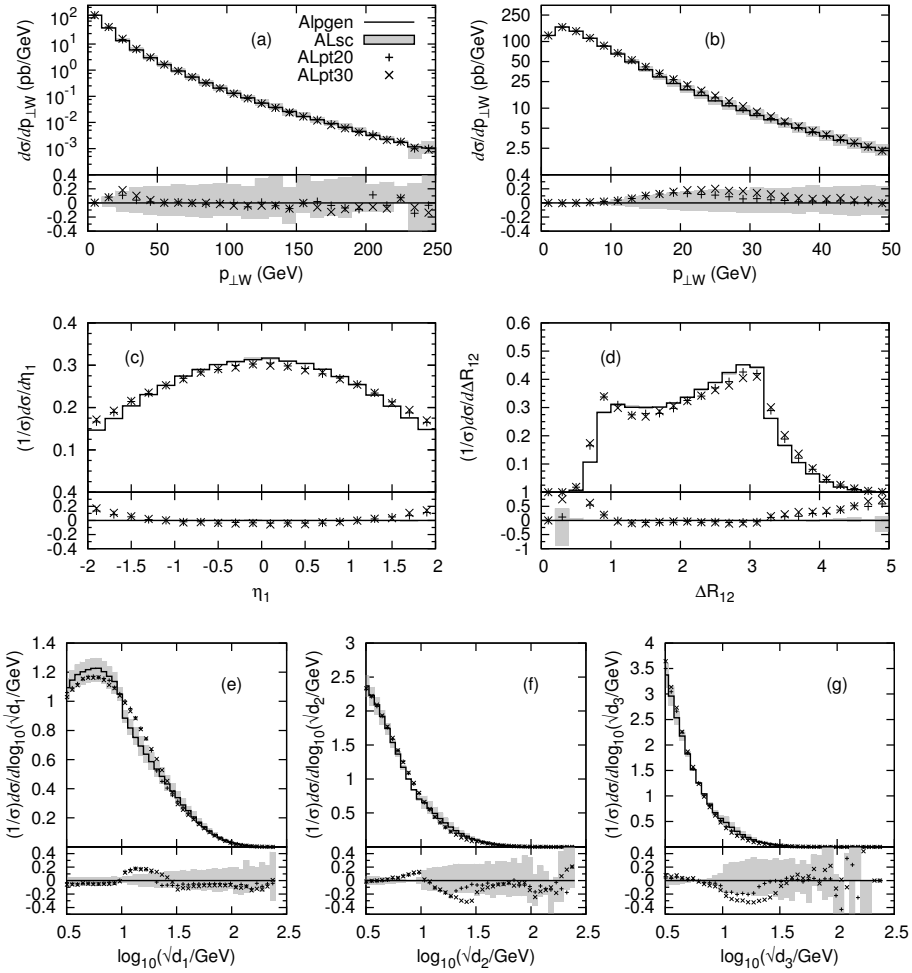

Figure II.13: ALPGEN systematics at the Tevatron. (a) and (b) show the $p_\perp$ spectrum of the W, (c) shows the pseudo-rapidity distribution of the leading jet, (d) shows the ΔR separation between the two leading jets, and (e)–(g) show the d_i ($i = 1,2,3$) spectra, where d_i is the scale in a parton-level event where i jets are clustered into $i-1$ jets using the $k_\perp$-algorithm. The full line is the default settings of ALPGEN, the shaded area is the range between ALscL and ALscH, while the points represent ALpt20 and ALpt30 as defined in section II.3.

II

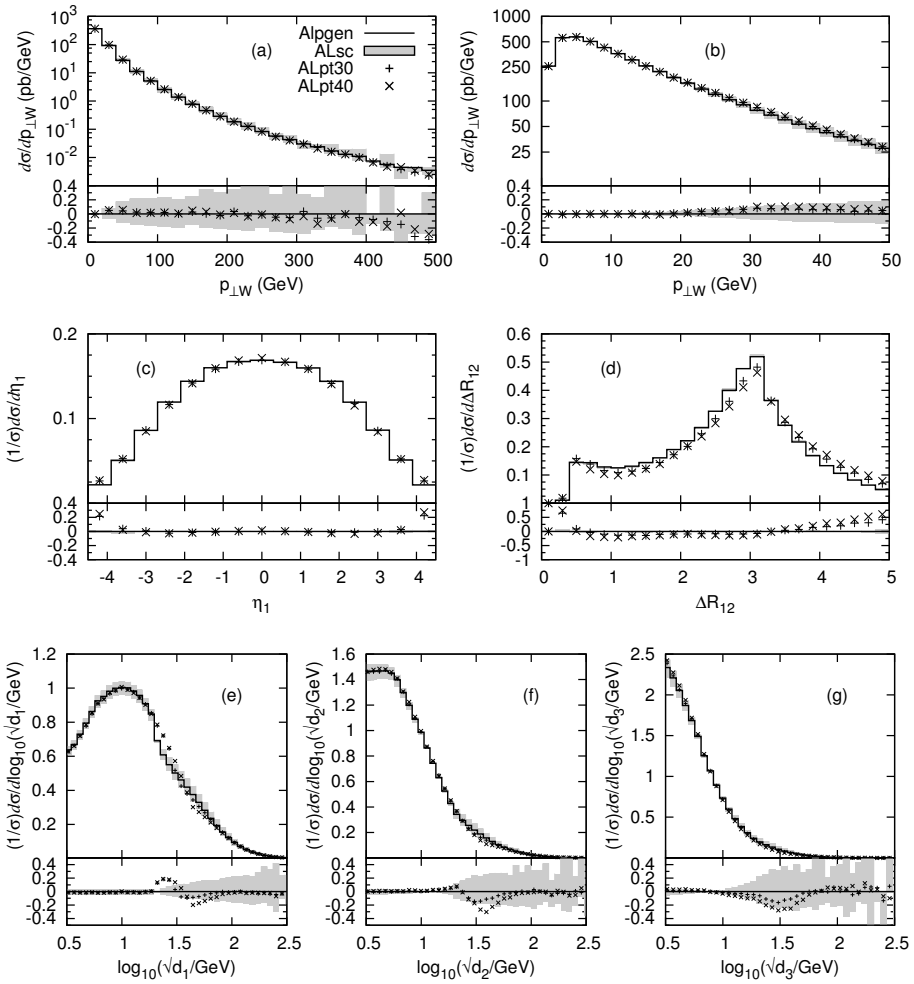

Figure II.14: ALPGEN systematics at the LHC. (a) and (b) show the $p_\perp$ spectrum of the W, (c) shows the pseudo-rapidity distribution of the leading jet, (d) shows the ΔR separation between the two leading jets, and (e)–(g) show the d_i ($i = 1, 2, 3$) spectra, where d_i is the scale in a parton-level event where i jets are clustered into $i-1$ jets using the $k_\perp$-algorithm. The full line is the default settings of ALPGEN, the shaded area is the range between ALscL and ALscH, while the points represent ALpt30 and ALpt40 as defined in section II.3.

ious options when $\sqrt{d_i} < 10$ GeV. This is due to the fact that the region $\sqrt{d_i} < 10$ GeV is dominated by the initial-state evolution of an $n = i - 1$ parton event, and both the matching and scale sensitivities are reduced. Notice that in the ALPGEN prescription the scale for the shower evolution is kept fixed when the renormalization scale of the matrix elements is changed, as a way of exploring the impact of a possible mismatch between the two.

For $\sqrt{d_i} > E_\perp^{\rm clus}$ the jet transverse energies are themselves typically above $E_\perp^{\rm clus}$, and the sensitivity to matching thresholds smaller than $E_\perp^{\rm clus}$ is reduced, since if the event matched at $E_\perp^{\rm clus}$, it will also match below that. Here the main source of systematics is therefore the scale variation, associated to the hard matrix element calculation for the $n = i$ jet multiplicity. The region 10 GeV $< \sqrt{d_i} < E_\perp^{\rm clus}$ is the transition region between the dominance of the shower and of the matrix element description of hard radiation. The structure observed in the d_i distributions in this region reflects the fact that shower and matrix element emit radiation with a slightly different probability. The selection of a matching threshold, which leads to effects at the level of $\pm 20\%$ and is therefore consistent with a LL accuracy and can be used to tune to data.

For the LHC, the ALPGEN systematics is shown in fig. II.14. The comparison of the various parameter choices is similar to what we encountered at the Tevatron, with variations in the range of $\pm 20\%$ for the matching-scale systematics, and up to 40% for the scale systematics. The pattern of the glitches in the d_i spectra for the different matching thresholds is also consistent with the explanation provided in the case of the Tevatron.

II.6.2 ARIADNE systematics

The ARIADNE systematics for the Tevatron is shown in fig. II.15. Since the dipole cascade by itself already includes a matrix-element correction for the first emission, we see no dependence on the merging scale in the $p_{\perp W}$, $\eta_{\rm jet1}$ and d_1 distributions, which are mainly sensitive to leading order corrections. For the other distributions, we become sensitive to higher-order corrections, and here the pure dipole cascade underestimates the matrix element and also tends to make the leading jets less back-to-back in azimuth. The first effect is expected for all parton showers, but is somewhat enhanced in ARIADNE due to the missing initial-state $q \to gq$ splitting, and is mostly visible in the d_2 distribution just below the merging scale. The second effect is clearly visible in the ΔR_{12} distribution, which is dominated by low $E_\perp$ jets.

The changing of the soft suppression parameter in ARs has the effect of reducing the available phase space of gluon radiation, especially for large $E_\perp$ and in the beam directions, an effect, which is mostly visible for the hardest emission and in the $p_{\perp W}$ distribution. As for ALPGEN, and also for the other codes, the change in scale mainly affects the hardness of the jets, but not the

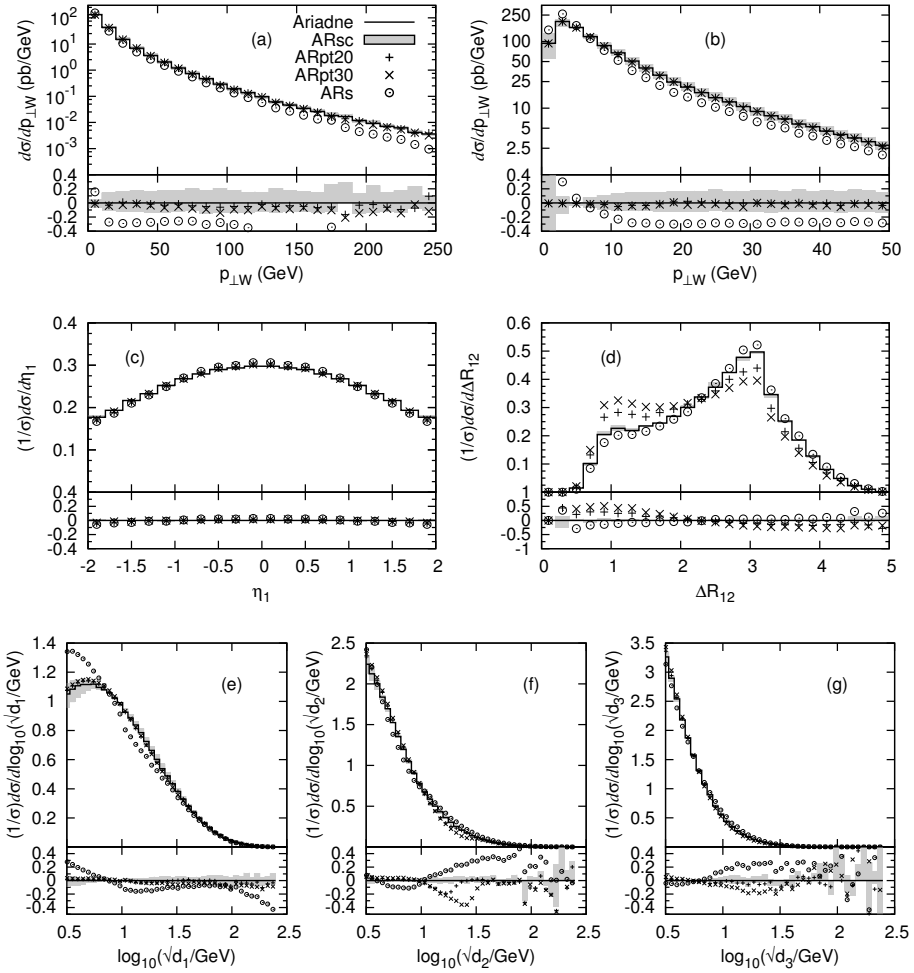

Figure II.15: ARIADNE systematics at the Tevatron. The plots are the same as in fig. II.13. The full line is the default settings of ARIADNE, the shaded area is the range between ARscL and ARscH, while the points represent ARpt20, ARpt30 and ARs as defined in section II.3.

η_{jet1} and the ΔR_{12} distribution.

For the LHC, the ARIADNE systematics is shown in fig. II.16. Qualitatively we find the same effects as in the Tevatron case. In particular we note the strong dependence on the soft suppression parameters in ARs, and it is clear that these have to be adjusted to fit Tevatron (and HERA) data before any

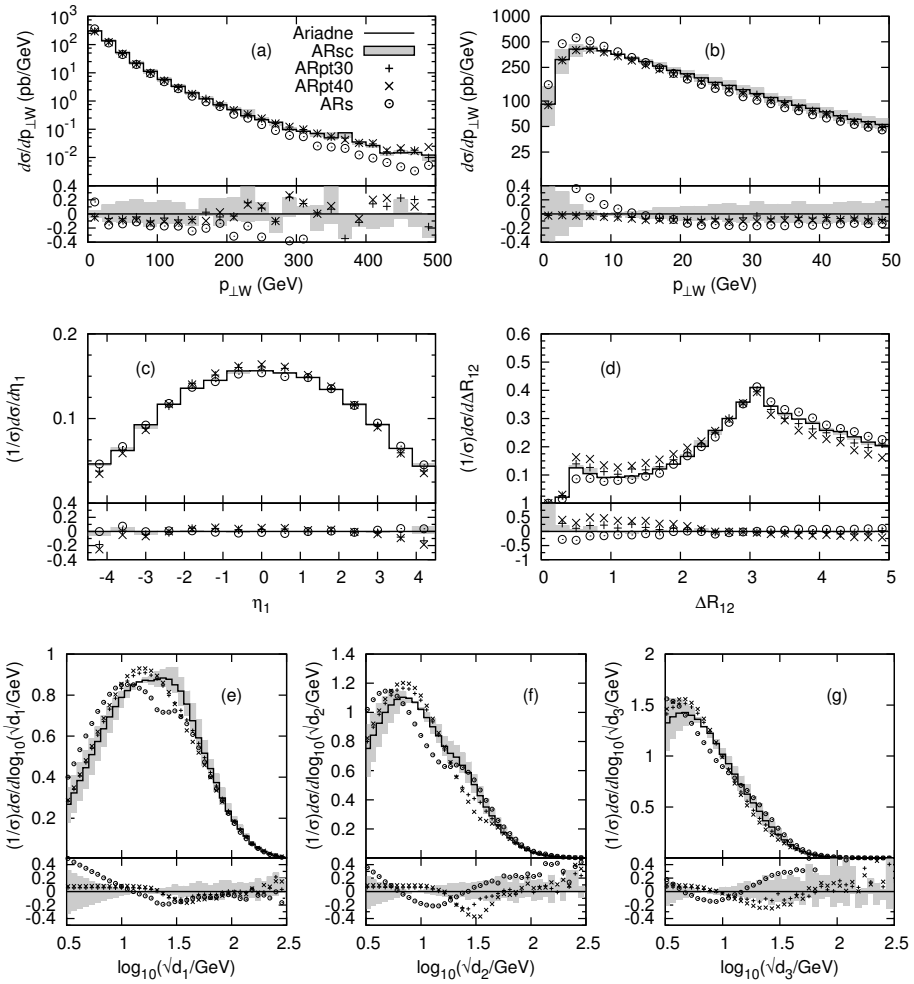

Figure II.16: ARIADNE systematics at the LHC. The plots are the same as in fig. II.14. The full line is the default settings of ARIADNE, the shaded area is the range between ARscL and ARscH, while the points represent ARpt30, ARpt40 and ARs as defined in section II.3.

predictions for the LHC can be made. It should be noted, however, that while eg. the high $p_{\perp W}$ tail in fig. II.16a for ARs is shifted down to be comparable to the other codes (cf. fig. II.10a), the medium $p_{\perp W}$ values are less affected and here the differences compared to the other codes can be expected to remain after a retuning.

This difference is mainly due to the fact that the dipole cascade in ARIADNE, contrary to the other parton showers, is not based on standard DGLAP evolution, but also allows for evolution, which is unordered in transverse momentum à la BFKL[4]. This means that in ARIADNE there is also a resummation of logs of $1/x$ besides the standard $\log Q^2$ resummation. This should not be a large effect at the Tevatron, and the differences there can be tuned away by changing the soft suppression parameters in ARIADNE. However, at the LHC we have quite small x-values, $x \sim m_W/\sqrt{S} < 0.01$, which allow for a much increased phase space for jets as compared to what is allowed by standard DGLAP evolution. As a result one obtains larger inclusive jet rates as documented in table II.3. The same effect is found in DIS at HERA, where x is even smaller as are the typical scales, Q^2. And here, all DGLAP-based parton showers fail to reproduce final-state properties, especially forward jet rates, while ARIADNE does a fairly good job.

It would be interesting to compare the merging schemes presented here also to HERA data to see if the DGLAP based shower would better reproduce data when merged with higher-order matrix elements. This would also put the extrapolations to the LHC on safer grounds. However, so far there exists one preliminary such study for the ARIADNE case only [53].

II.6.3 HELAC systematics

The Tevatron HELAC distributions are shown in fig. II.17. Since HELAC results presented in this study are based on the MLM matching prescription, we expect the HELAC systematics to follow at least qualitatively the ALPGEN ones and this is indeed the case. On the other hand the use by HELAC of PYTHIA, for parton showering as well as for hadronization, leads to differences compared to the ALPGEN results, where HERWIG is used. For the absolute rates, especially in the multi-jet regime, HELAC seems to be closer to MADEVENT that also uses PYTHIA.

For the LHC, the HELAC systematics are shown in fig. II.18. The systematics follows a similar pattern compared to that already discussed for the Tevatron case, with the expected increase of up to 40% from scale variations, due to the higher collision energy.

[4]The dipole emission of gluons in ARIADNE are ordered in transverse momentum, but not in rapidity. Translated into a conventional initial-state evolution, this corresponds to emissions ordered in rapidity but unordered in transverse momentum.

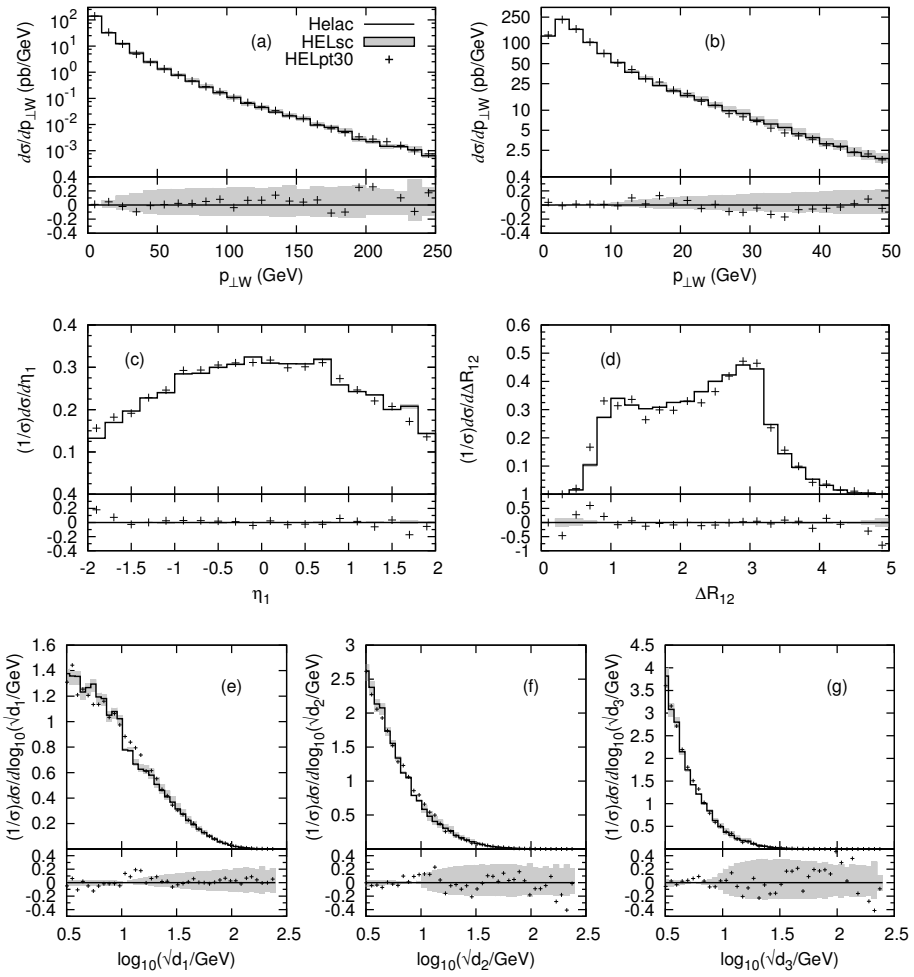

Figure II.17: HELAC systematics at the Tevatron. The plots are the same as in fig. II.13. The full line is the default settings of HELAC, the shaded area is the range between HELscL and HELscH, while the points represent HELpt30 as defined in section II.3.

II

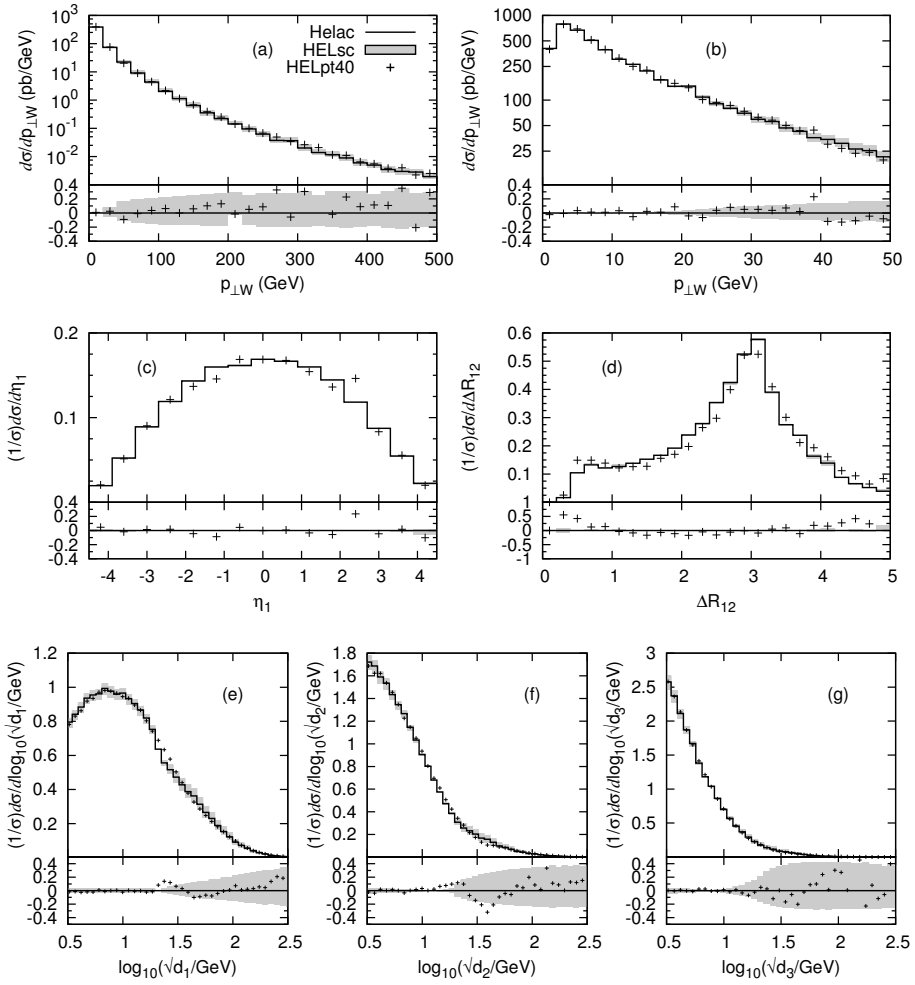

Figure II.18: HELAC systematics at the LHC. The plots are the same as in fig. II.14. The full line is the default settings of HELAC, the shaded area is the range between HELscL and HELscH, while the points represent HELpt40 as defined in section II.3.

II.6.4 MADEVENT systematics

The MADEVENT distributions for the Tevatron are shown in fig. II.19. Also here, the variations are consistent with the expectations. For the $p_{\perp W}$ spectrum, the dominant variations are due to the change of scale for α_s, with the lower scale leading to a harder spectrum. Below the $k_\perp$-cutoff, where the distribution is determined by the parton shower only, the lower scale gives the lower differential cross section.

At Tevatron energies, both the $p_{\perp W}$ spectrum and the d_i spectra are relatively stable with respect to variations of the matching scale. For the d_i spectra, the variation in matching scale gives a dip in the region $10\text{ GeV} < \sqrt{d_i} < k_{\perp 0}$, but is reduced for larger d_i. The rapidity and jet-distance spectra show a remarkable stability under both renormalization-scale changes and variations in the cutoff scale.

For the LHC, the systematics of the MADEVENT implementation are shown in fig. II.20. The variations in renormalization scale give a very similar effect as for the Tevatron, with variations up to $\pm 20\%$ on the $p_\perp$ and d_i spectra. For variations in the matching scale $k_{\perp 0}$, however, the pattern is slightly different. This can be most easily understood from looking at the d_i spectra, since, as in the Sherpa case, the cutoff scale is defined to be just the d_i, so the transition between the parton-shower and matrix-element regions is very sharp. It is clear from these distributions that the default parton shower of PYTHIA does not reproduce the shape of the matrix elements at LHC energies even for relatively small $k_\perp$, but falls off more sharply. There is therefore a dip in all the distributions around $\log k_{\perp 0}$, which gets more pronounced for the higher multiplicity distributions, and hence gives lower overall jet rates. The $p_{\perp W}$ distributions, as well as the d_1 distributions, are composed of all the different jet-multiplicity samples, which gives systematically reduced hardness of the differential cross sections for increased cutoff scales. These effects are clearly visible also in SHERPA, which uses a PYTHIA-like parton shower and $k_\perp$ as merging scale.

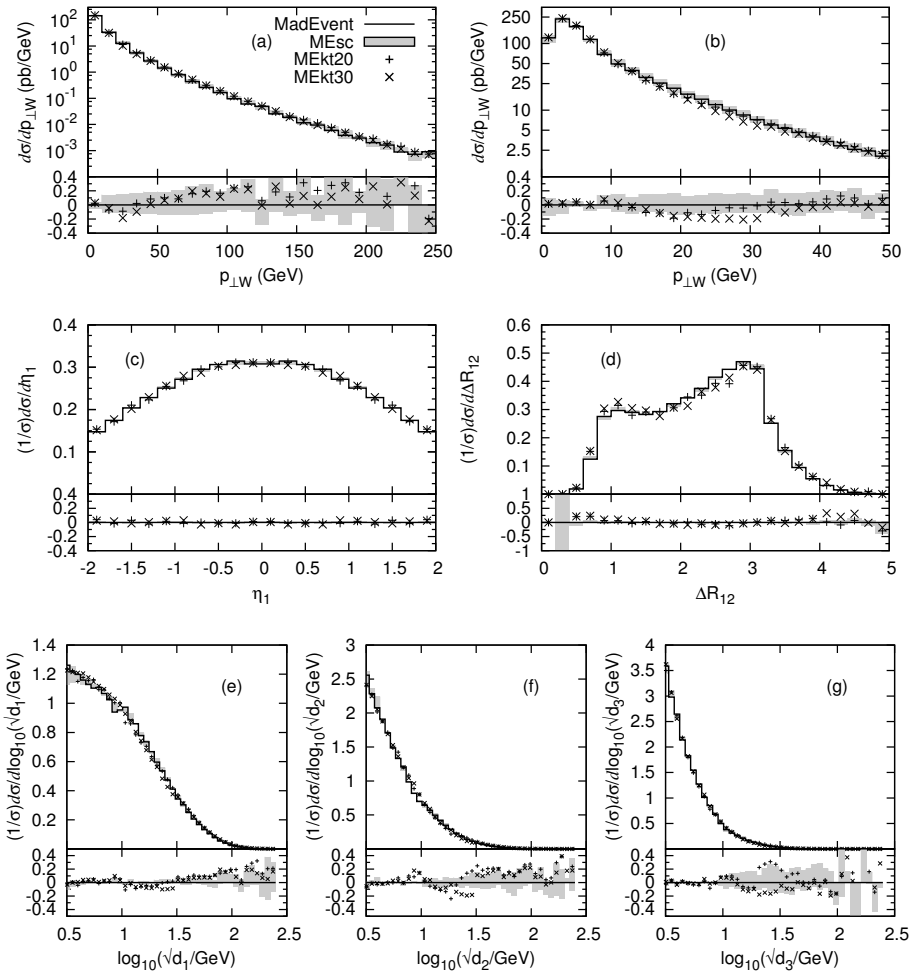

Figure II.19: MADEVENT systematics at the Tevatron. The plots are the same as in fig. II.13. The full line is the default settings of MADEVENT, the shaded area is the range between MEscL and MEscH, while the points represent MEkt20 and MEkt30 as defined in section II.3.

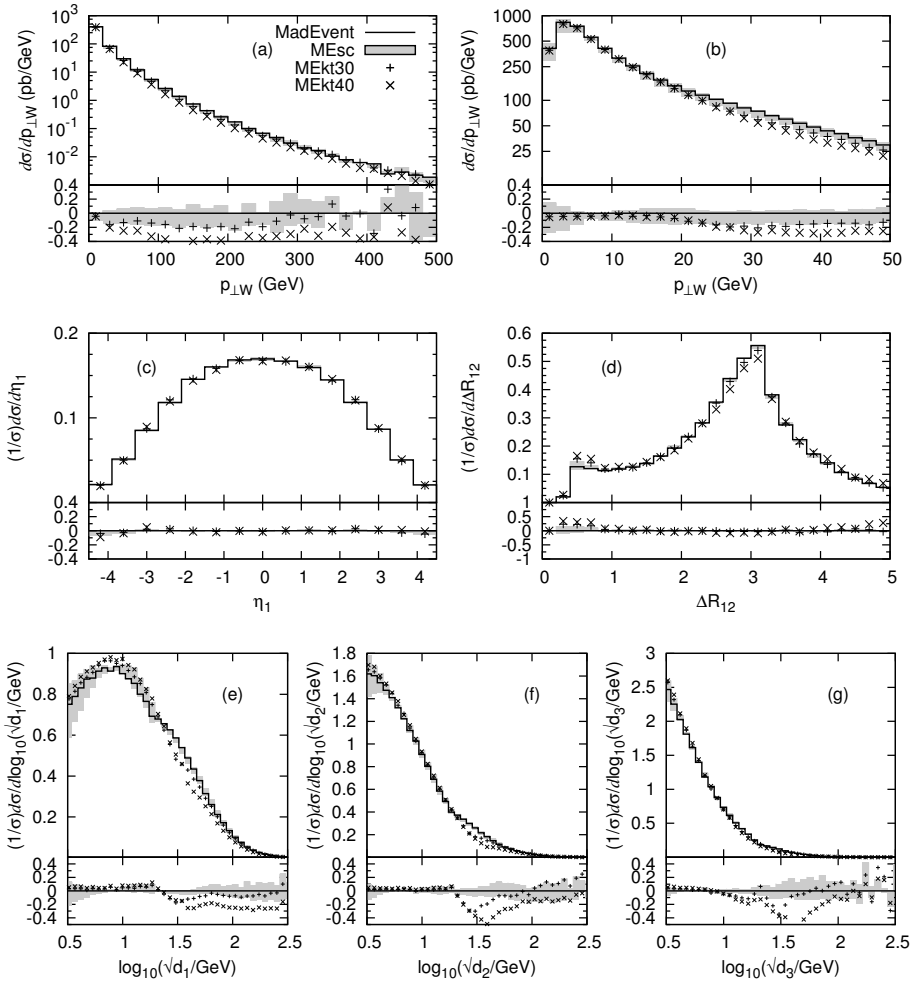

Figure II.20: MADEVENT systematics at the LHC. The plots are the same as in fig. II.14. The full line is the default settings of MADEVENT, the shaded area is the range between MEscL and MEscH, while the points represent MEkt30 and MEkt40 as defined in section II.3.

II

II.6.5 SHERPA systematics

The systematics of the CKKW algorithm as implemented in SHERPA is presented in fig. II.21 for the Tevatron case. The effect of varying the scales in the PDF *and* strong coupling evaluations by a factor of 0.5 (2.0) is that for the lower (higher) scale choice, the W-boson's $p_\perp$ spectrum becomes harder (softer). For this kind of observables the uncertainties given by scale variations dominate the ones emerging through variations of the internal separation cut. This is mainly due to a reduced (enhanced) suppression of hard-jet radiation through the α_s rejection weights. The differential jet rates, $d_{1,2,3}$, shown in fig. II.21e–g, have a more pronounced sensitivity on the choice of the merging scale, leading to variations at the 20% level. In the CKKW approach this dependence can be understood since the $k_\perp$-measure intrinsically serves as the discriminator to separate the matrix-element and parton-shower regimes. Hence, the largest deviations from the default typically appear at $d_i \approx k_{\perp 0}$. However, the results are remarkably smooth, which leads to the conclusion that the cancellation of the dominant logarithmic dependence on the merging cut is well achieved. Moreover, considering the pseudo-rapidity of the leading jet and the cone separation of the two hardest jets, these distributions show a very stable behaviour under the studied variations, since they are indirectly influenced by the cut scale only. The somewhat more pronounced deviation at low ΔR_{12} is connected to phase-space regions of jets becoming close together, which is affected by the choice of the merging scale and therefore by its variation. Taken together, SHERPA produces consistent results with relative differences of the order of or less than 20% at Tevatron energies.

The SHERPA studies of systematics for the LHC are displayed in fig. II.22. Compared to the Tevatron case, a similar pattern of variations is recognized. The $p_\perp$ spectra of the W^+ boson show deviations under cut and scale variations that remain on the same order of magnitude. However, a noticeable difference is an enhancement of uncertainties in the predictions for low $p_\perp$. This phase-space region is clearly dominated by the parton shower evolution, which in the SHERPA treatment of estimating uncertainties undergoes scale variations in the same manner as the matrix-element part. Therefore, the estimated deviations from the default given for low $p_\perp$ are very reasonable and reflect intrinsic uncertainties underlying the parton showering. For the LHC case, the effect is larger, since the evolution is dictated by steeply rising parton densities at x-values that are lower compared to the Tevatron scenario. The pseudo-rapidity of the leading jet and the cone separation of the two hardest jets show again a stable behaviour under the applied variations, the only slight exception is the regions of high $|\eta_{\text{jet1}}|$ where, using a high $k_\perp$-cut, the deviations are at the 20% level. The effect of varying the scales in the parton distributions and strong couplings now dominates the uncertainties in the differential jet rates, $d_{1,2,3}$, which are presented in fig. II.22e–g. This time, owing to

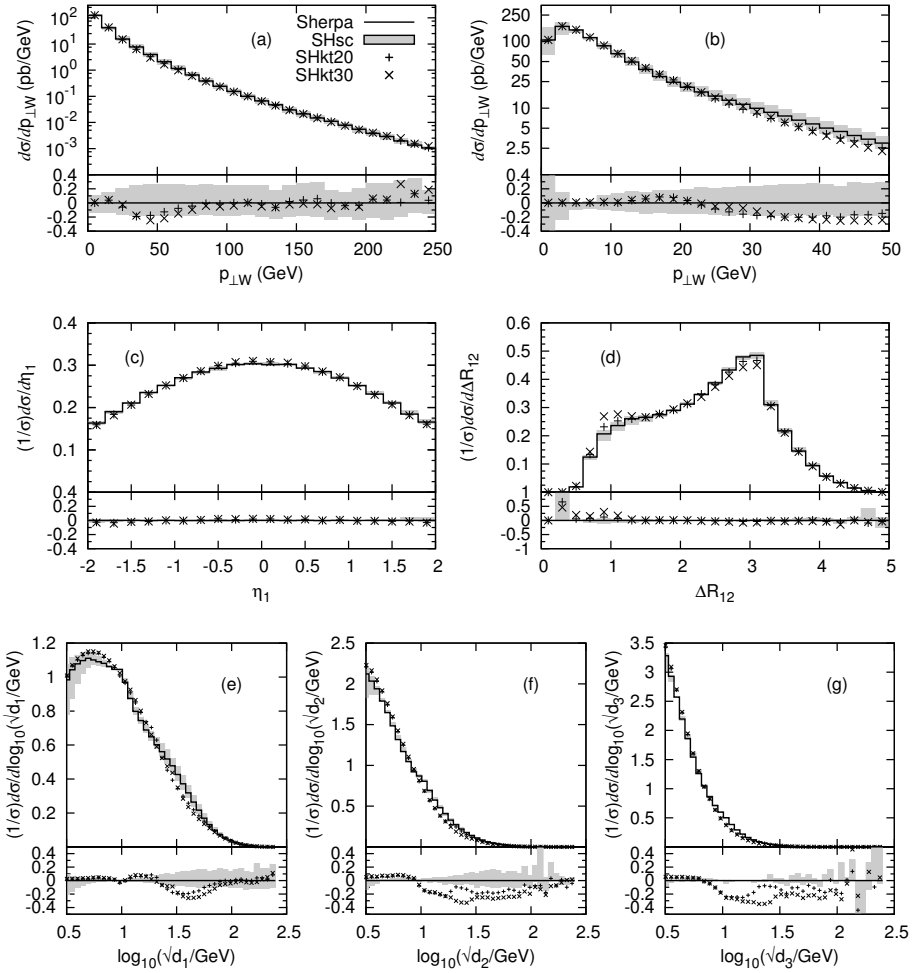

Figure II.21: SHERPA systematics at the Tevatron. The plots are the same as in fig. II.13. The full line is the default settings of SHERPA, the shaded area is the range between SHscL and SHscH, while the points represent SHkt20 and SHkt30 as defined in section II.3.

the larger phase space, for the low scale choice, $\mu = \mu_0/2$, the spectra become up to 40% harder, whereas, for the high scale choice, the spectra are up to 20% softer. The variation of the internal merging scale does not induce jumps around the cut region, however it has to be noted that for higher choices, e.g.

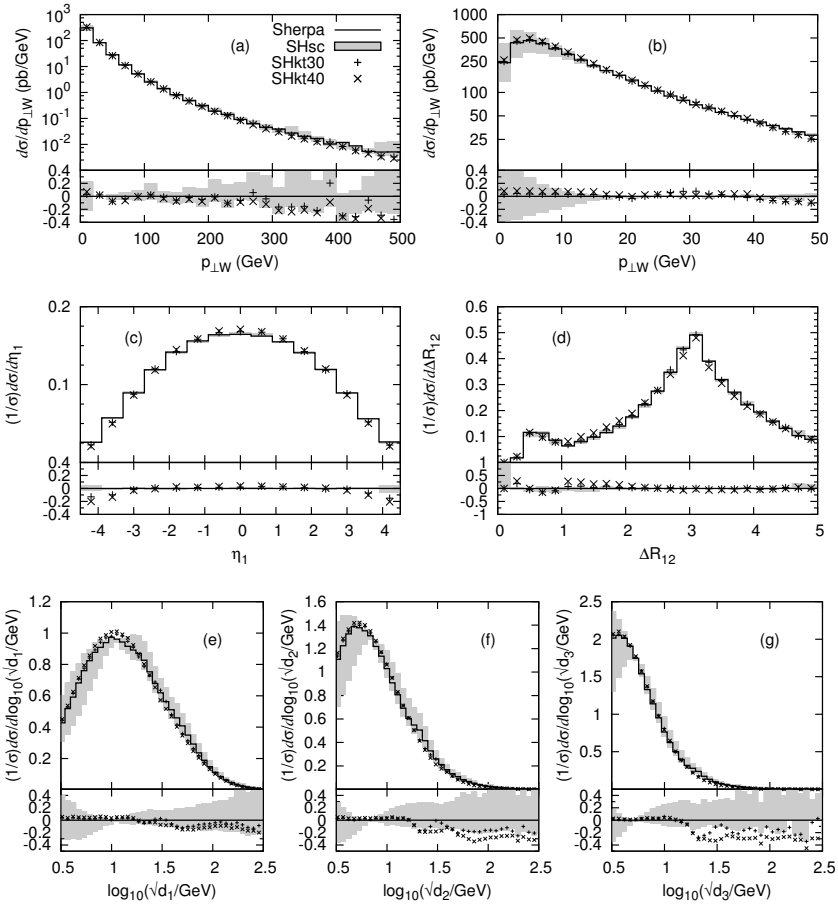

Figure II.22: SHERPA systematics at the LHC. The plots are the same as in fig. II.14. The full line is the default settings of SHERPA, the shaded area is the range between SHscL and SHscH, while the points represent SHkt30 and SHkt40 as defined in section II.3.

$k_{\perp 0} = 40$ GeV, there is a tendency to predict softer distributions in the tails compared to the default. To summarize, the extrapolation from Tevatron to LHC energies does not yield significant changes in the predictions of uncertainties under merging-cut and scale variations; for the LHC scenario, they have to be estimated slightly larger, ranging up to 40%. The results are again consistent and exhibit a well controlled behaviour when applying the CKKW approach implemented in SHERPA at LHC energies.

Giving a conservative, more reliable estimate, in SHERPA the strategy of varying the scales in the strong coupling *together with* the scales in the parton densities has been chosen to assess its systematics. So, to better estimate the impact of the additional scale variation in the parton density functions, renormalization-scale variations on its own have been studied as well. Their results show smaller deviations wrt. the default in the observables of this study with the interpretation of potentially underestimating the systematics of the merging approach. Also, then the total cross sections vary less and become 9095 pb and 8597 pb for the low- and high-scale choice, respectively. Note that, owing to the missing simultaneous factorization-scale variation, their order is now reversed compared to SHscL and SHscH, whose values are given in table II.3. Moreover, by referring to table II.4 the cross-section ratios for e.g. $\sigma^{[\geq 1]}/\sigma^{[\text{tot}]}$ now read 0.26 and 0.22 for the low- and high-scale choice, respectively. This once more emphasizes that the approach's uncertainty may be underestimated when relying on α_s-scale variations only. From table II.3 it also can be noted that the total inclusive cross section given by the full high-scale prediction SHscH is – unlike SHERPA's default – close to the ALPGEN default. In contrast to the MLM-based approaches, which prefer the factorization scale in the matrix-element evaluation set through the transverse mass of the weak boson, the SHERPA approach makes the choice of employing the merging scale $k_{\perp 0}$ instead. This has been motivated in [9] and further discussed in [3]. Eventually, it is a good result that compatibility is achieved under this additional PDF-scale variation for the total inclusive cross sections, however it also clearly stresses that there is a non-negligible residual dependence on the choice of the factorization scale in the merging approaches.

II.6.6 Summary of the systematics studies

Starting with the $p_{\perp W}$ spectra, we find a trivial $20-40\%$ effect of the scale changes, with the lower scale leading to a harder spectrum. In the case of ALPGEN and HELAC, this only affects the spectrum above the matching scale, while for ARIADNE, MADEVENT and SHERPA there is also an effect below, as there the scale change is also implemented in the parton shower. For all the codes the change in merging/matching scale gives effects smaller than or of the order of the change in α_s scale. For ARIADNE, the change in the soft suppression parameter (ARs) gives a softer spectrum, which is expected as it directly reduces the phase space for emitted gluons.

In the η_{jet1} and ΔR_{12} distributions the effects of changing the scale in α_s are negligible. In all cases, changing the merging/matching scale also has negligible effects on the rapidity spectrum, while the ΔR_{12} tends to become more peaked at small values for larger merging/matching scales, and also slightly less peaked at $\Delta R_{12} = \pi$. This effect is largest for ARIADNE while almost absent for HELAC.

Finally for the d_i distributions we clearly see wiggles of varying sizes introduced by changing the merging scales.

II.7 Conclusions

This document summarizes our comparisons of five independent approaches to the problem of merging matrix elements and parton showers. The codes under study, ALPGEN, ARIADNE, HELAC, MADEVENT and SHERPA, differ in which matrix-element generator is used, which merging scheme (CKKW or MLM) is used and the details in the implementation of these schemes, as well as in which parton shower is used.

We find that, while the three approaches (CKKW, L, and MLM) aim at a simulation based on the same idea, namely describing jet production and evolution by matrix elements and the parton shower, respectively, the corresponding algorithms are quite different. The main differences can be found in the way in which the combination of Sudakov reweighting of the matrix elements interacts with the vetoing of unwanted jet production inside the parton shower. This makes it very hard to compare those approaches analytically and to formalise the respective level of their logarithmic dependence. In addition, the different showering schemes used by the different methods blur the picture further. For instance virtuality ordering with explicit angular vetoes is used in SHERPA as well as in the HELAC and MADEVENT approach employ PYTHIA to do the showering, $p_\perp$ ordering is the characteristic feature of ARIADNE, and, through its usage of HERWIG it is angular ordering that enters into the ALPGEN merging approach. However, although the formal level of agreement between the codes is not worked out in this publication and remains unclear, the results presented in this publication show a reasonably good agreement. This proves that the variety of methods for merging matrix elements and parton showers can be employed with some confidence in vector boson plus jet production.

The comparison also points to differences, in absolute rates as well as in the shape of individual distributions, which underscore the existence of an underlying systematic uncertainty. Most of these differences are at a level that can be expected from merging tree-level matrix elements with leading-log parton showers, in the sense that they are smaller than, or of the order of, differences found by making a standard change of scale in α_s. In most cases the differences within each code are as large as the differences between the codes. And as the systematics at the Tevatron is similar to that at the LHC, it is conceivable that all the codes can be tuned to Tevatron data to give consistent predictions for the LHC. To carry out such tunings, we look forward to the publication by CDF and DØ of the measured cross sections for distributions such as those considered in this paper, fully corrected for all detector effects.

Acknowledgments

Work supported in part by the Marie Curie research training networks "MCnet" (contract number MRTN-CT-2006-035606) and "HEPTOOLS" (MRTN-CT-2006-035505).

C.G. Papadopoulos and M. Worek would like to acknowledge support from the ToK project ALGOTOOLS, "Algorithms and tools for multi-particle production and higher order corrections at high energy colliders", (contract number MTKD-CT-2004-014319).

M. Worek and S. Schumann want to thank DAAD for support through the Dresden–Crakow exchange programme.

J. Winter acknowledges financial support by the Marie Curie Fellowship program for Early Stage Research Training and thanks the CERN Theory Division for the great hospitality during the funding period.

J. Alwall acknowledges financial support by the Swedish Research Council.

II References

[1] S. Mrenna and P. Richardson, "Matching matrix elements and parton showers with HERWIG and PYTHIA," *JHEP* **05** (2004) 040, arXiv:hep-ph/0312274.

[2] S. Hoche *et al.*, "Matching parton showers and matrix elements," arXiv:hep-ph/0602031.

[3] F. Krauss, A. Schalicke, S. Schumann, and G. Soff, "Simulating W / Z + jets production at the Tevatron," *Phys. Rev.* **D70** (2004) 114009, arXiv:hep-ph/0409106.

[4] F. Krauss, A. Schalicke, S. Schumann, and G. Soff, "Simulating W / Z + jets production at the CERN LHC," *Phys. Rev.* **D72** (2005) 054017, arXiv:hep-ph/0503280.

[5] T. Gleisberg, F. Krauss, A. Schalicke, S. Schumann, and J.-C. Winter, "Studying W+ W- production at the Fermilab Tevatron with SHERPA," *Phys. Rev.* **D72** (2005) 034028, arXiv:hep-ph/0504032.

[6] N. Lavesson and L. Lönnblad, "W + jets matrix elements and the dipole cascade," *JHEP* **07** (2005) 054, arXiv:hep-ph/0503293.

[7] M. L. Mangano, M. Moretti, F. Piccinini, and M. Treccani, "Matching matrix elements and shower evolution for top- quark production in hadronic collisions," *JHEP* **01** (2007) 013, arXiv:hep-ph/0611129.

[8] S. Catani, F. Krauss, R. Kuhn, and B. R. Webber, "QCD matrix elements + parton showers," *JHEP* **11** (2001) 063, arXiv:hep-ph/0109231.

[9] F. Krauss, "Matrix elements and parton showers in hadronic interactions," *JHEP* **08** (2002) 015, arXiv:hep-ph/0205283.

[10] T. Gleisberg *et al.*, "SHERPA 1.alpha, a proof-of-concept version," *JHEP* **02** (2004) 056, arXiv:hep-ph/0311263.

[11] A. Schalicke and F. Krauss, "Implementing the ME+PS merging algorithm," *JHEP* **07** (2005) 018, arXiv:hep-ph/0503281.

[12] S. Catani, Y. L. Dokshitzer, M. Olsson, G. Turnock, and B. R. Webber, "New clustering algorithm for multi - jet cross-sections in e+ e- annihilation," *Phys. Lett.* **B269** (1991) 432–438.

[13] S. Catani, Y. L. Dokshitzer, and B. R. Webber, "The K-perpendicular clustering algorithm for jets in deep inelastic scattering and hadron collisions," *Phys. Lett.* **B285** (1992) 291–299.

[14] S. Catani, Y. L. Dokshitzer, M. H. Seymour, and B. R. Webber, "Longitudinally invariant K(t) clustering algorithms for hadron hadron collisions," *Nucl. Phys.* **B406** (1993) 187–224.

[15] G. C. Blazey *et al.*, "Run II jet physics," `arXiv:hep-ex/0005012`.

[16] L. Lönnblad, "ARIADNE version 4: A Program for simulation of QCD cascades implementing the color dipole model," *Comput. Phys. Commun.* **71** (1992) 15–31.

[17] G. Gustafson and U. Pettersson, "Dipole formulation of QCD cascades," *Nucl. Phys.* **B306** (1988) 746.

[18] G. Gustafson, "Dual description of a confined color field," *Phys. Lett.* **B175** (1986) 453.

[19] B. Andersson, G. Gustafson, and L. Lönnblad, "Gluon splitting in the color dipole cascades," *Nucl. Phys.* **B339** (1990) 393–406.

[20] B. Andersson, G. Gustafson, L. Lönnblad, and U. Pettersson, "Coherence effects in deep inelastic scattering," *Z. Phys.* **C43** (1989) 625.

[21] L. Lonnblad, "Small x effects in W + jets production at the Tevatron," *Nucl. Phys.* **B458** (1996) 215–230, `arXiv:hep-ph/9508261`.

[22] **H1** Collaboration, A. Aktas *et al.*, "Forward jet production in deep inelastic scattering at HERA," *Eur. Phys. J.* **C46** (2006) 27–42, `arXiv:hep-ex/0508055`.

[23] L. Lönnblad, "Rapidity gaps and other final state properties in the color dipole model for deep inelastic scattering," *Z. Phys.* **C65** (1995) 285–292.

[24] L. Lönnblad, "Correcting the colour-dipole cascade model with fixed order matrix elements," *JHEP* **05** (2002) 046, `arXiv:hep-ph/0112284`.

[25] G. Corcella *et al.*, "HERWIG 6.5: an event generator for Hadron Emission Reactions With Interfering Gluons (including supersymmetric processes)," *JHEP* **01** (2001) 010, `arXiv:hep-ph/0011363`.

[26] T. Sjöstrand, and others, "High-energy-physics event generation with PYTHIA 6.1," *Comput. Phys. Commun.* **135** (2001) 238–259, `arXiv:hep-ph/0010017`.

[27] T. Sjostrand, L. Lonnblad, S. Mrenna, and P. Skands, "PYTHIA 6.3: Physics and manual," `arXiv:hep-ph/0308153`.

[28] F. Caravaglios, M. L. Mangano, M. Moretti, and R. Pittau, "A new approach to multi-jet calculations in hadron collisions," *Nucl. Phys.* **B539** (1999) 215–232, arXiv:hep-ph/9807570.

[29] M. L. Mangano, M. Moretti, and R. Pittau, "Multijet matrix elements and shower evolution in hadronic collisions: W b bbar + n jets as a case study," *Nucl. Phys.* **B632** (2002) 343–362, arXiv:hep-ph/0108069.

[30] M. L. Mangano, M. Moretti, F. Piccinini, R. Pittau, and A. D. Polosa, "ALPGEN, a generator for hard multiparton processes in hadronic collisions," *JHEP* **07** (2003) 001, arXiv:hep-ph/0206293.

[31] T. Stelzer and W. F. Long, "Automatic generation of tree level helicity amplitudes," *Comput. Phys. Commun.* **81** (1994) 357–371, arXiv:hep-ph/9401258.

[32] F. Maltoni and T. Stelzer, "MadEvent: Automatic event generation with MadGraph," *JHEP* **02** (2003) 027, arXiv:hep-ph/0208156.

[33] J. Alwall *et al.*, "MadGraph/MadEvent v4: The New Web Generation," *JHEP* **09** (2007) 028, arXiv:0706.2334 [hep-ph].

[34] T. Sjostrand, S. Mrenna, and P. Skands, "PYTHIA 6.4 physics and manual," *JHEP* **05** (2006) 026, arXiv:hep-ph/0603175.

[35] A. Kanaki and C. G. Papadopoulos, "HELAC: A package to compute electroweak helicity amplitudes," *Comput. Phys. Commun.* **132** (2000) 306–315, arXiv:hep-ph/0002082.

[36] C. G. Papadopoulos and M. Worek, "Multi-parton Cross Sections at Hadron Colliders," *Eur. Phys. J.* **C50** (2007) 843–856, arXiv:hep-ph/0512150.

[37] F. Gianotti *et al.*, "Physics potential and experimental challenges of the LHC luminosity upgrade," *Eur. Phys. J.* **C39** (2005) 293–333, arXiv:hep-ph/0204087.

[38] T. Gleisberg, F. Krauss, C. G. Papadopoulos, A. Schaelicke, and S. Schumann, "Cross sections for multi-particle final states at a linear collider," *Eur. Phys. J.* **C34** (2004) 173–180, arXiv:hep-ph/0311273.

[39] J. Alwall *et al.*, "A standard format for Les Houches event files," *Comput. Phys. Commun.* **176** (2007) 300–304, arXiv:hep-ph/0609017.

[40] **CDF** Collaboration, F. Abe *et al.*, "Measurement of jet multiplicity in W events produced in $p\bar{p}$ collisions at $\sqrt{s} = 1.8-$Tev," *Phys. Rev. Lett.* **70** (1993) 4042–4046.

[41] **CDF** Collaboration, F. Abe *et al.*, "Properties of jets in W boson events from 1.8 TeV $\bar{p}p$ collisions," *Phys. Rev. Lett.* **79** (1997) 4760–4765, arXiv:hep-ex/9709016.

[42] **CDF** Collaboration, A. A. Affolder *et al.*, "Test of enhanced leading order QCD in W boson plus jets events from 1.8 TeV $\bar{p}p$ collisions," *Phys. Rev.* **D63** (2001) 072003.

[43] **D0** Collaboration, S. Abachi *et al.*, "A Study of the strong coupling constant using W + jets processes," *Phys. Rev. Lett.* **75** (1995) 3226–3231.

[44] **CDF** Collaboration, A. Messina, "Measurement of the W + Jet Cross Section at CDF," *Braz. J. Phys.* **37** (2007) 840–842, arXiv:0708.1380 [hep-ex].

[45] **D0** Collaboration, V. M. Abazov *et al.*, "Measurement of the ratios of the Z/G* + $\geq$ n jet production cross sections to the total inclusive Z/G* cross section in ppbar collisions at sqrt(s) = 1.96 TeV," *Phys. Lett.* **B658** (2008) 112–119, arXiv:hep-ex/0608052.

[46] **CDF** Collaboration. http://www-cdf.fnal.gov/physics/new/qcd/zjets_07/public.pdf, 2007.

[47] M. H. Seymour. HTTP://HEPWWW.RL.AC.UK/THEORY/SEYMOUR/KTCLUS/.

[48] N. Brook, R. G. Waugh, T. Carli, R. Mohr, and M. Sutton, "Tuning Monte Carlo event generators to HERA data,". Prepared for Workshop on Future Physics at HERA (Preceded by meetings 25-26 Sep 1995 and 7-9 Feb 1996 at DESY), Hamburg, Germany, 30-31 May 1996.

[49] C. G. Papadopoulos, "PHEGAS: A phase space generator for automatic cross- section computation," *Comput. Phys. Commun.* **137** (2001) 247–254, arXiv:hep-ph/0007335.

[50] F. Krauss, R. Kuhn, and G. Soff, "AMEGIC++ 1.0: A matrix element generator in C++," *JHEP* **02** (2002) 044, arXiv:hep-ph/0109036.

[51] R. Kuhn, F. Krauss, B. Ivanyi, and G. Soff, "APACIC++ 1.0: A Parton Cascade In C++," *Comput. Phys. Commun.* **134** (2001) 223–266, arXiv:hep-ph/0004270.

[52] F. Krauss, A. Schalicke, and G. Soff, "APACIC++ 2.0: A parton cascade in C++," *Comput. Phys. Commun.* **174** (2006) 876–902, arXiv:hep-ph/0503087.

[53] C. Åberg, "Correcting the Colour Dipole Cascade with Fixed Order Matrix Elements in Deep Inelastic Scattering." Diploma thesis, lu-tp 04-25.

III

Merging parton showers and matrix elements — back to basics

Nils Lavesson and Leif Lönnblad

Department of Theoretical Physics, Lund University,
Sölvegatan 14A, SE–223 62 Lund, Sweden

Journal of High Energy Physics **04** (2008) 085 [arXiv:0712.2966].

We make a thorough comparison between different schemes of merging fixed-order tree-level matrix element generators with parton-shower models. We use the most basic benchmark of the $\mathcal{O}(\alpha_S)$ correction to $e^+e^- \to$ jets, where the simple kinematics allows us to study in detail the transition between the matrix-element and parton-shower regions. We find that the CKKW-based schemes give a reasonably smooth transition between these regions, although problems may occur if the parton shower used is not ordered in transverse momentum. However, the so-called Pseudo-Shower and MLM schemes turn out to have potentially serious problems due to different scale definitions in different regions of phase space, and due to sensitivity to the details in the initial conditions of the parton shower programs used.

III.1 Introduction

Accurate simulations of multi-jet final states are important for current experiments and will become even more so once the LHC starts. At the LHC the production rate for such states will be large due to the huge available phase space. Hadronic multi-jet states are used for many of the discovery channels for new physics and the main irreducible background comes from QCD. A good theoretical understanding and accurate physics simulations of multi-jet QCD states are therefore essential tools for understanding and analyzing LHC data.

To be able to compare the predictions of a model with a collider experiment, a description of final state hadrons is needed. There are a few phenomenological models available to describe the production of hadrons, but they all require that the perturbative emissions are well described, especially in the soft and collinear regions, to give reliable results. These collinear and soft emissions dominate the multi-parton cross section and can be taken into account to all orders, if one approximates the emissions to be strongly ordered, as is done in parton shower models. However, when the strong ordering no longer holds, which is the case if we have several hard and widely separated jets, the parton shower models become unreliable.

In order to improve the description of multi-jet states, full matrix elements can be used. These describe the process correctly up to a given order in the strong coupling constant. However, the matrix elements become difficult to calculate for high parton multiplicities or if one goes beyond tree-level. They also contain divergences in the soft and collinear limits and need to be regulated using cutoffs.

The idea behind merging algorithms is to let the matrix elements describe the hard emissions and use the parton shower to describe the soft and collinear emissions. To accommodate this, the phase space needs to be split into two well defined regions, one where emissions are generated by tree-level matrix elements, and one where emissions are generated by the parton shower. To avoid double counting and dead regions, the two regions should have no overlaps and together cover the entire phase space. The scale that describes the border between the regions is called the merging scale.

Some extra care is needed to avoid an artificial dependence on the merging scale. The matrix elements contain divergences in the soft and collinear regions, whereas the emission probability in these regions in the parton shower is finite since it is regulated by Sudakov form factors. The effects of the Sudakov form factors need to be included in the matrix element part of the phase space as well, making the state from the matrix element exclusive. Also a running coupling similar to that of the shower needs to be introduced. If this is done correctly the dependence on the merging scale should be minimal, how-

ever, especially for corrections with several extra jets, a small residual dependence on the merging scale from sub-leading terms is basically unavoidable.

There are four main algorithms that address the problem of merging tree-level matrix elements and partons showers: CKKW [1], CKKW-L [2], Pseudo-Shower [3], and MLM [4]. CKKW was first published for e^+e^- collisions [1] and later extended to hadron collisions [5]. Implementations have been made in SHERPA [6] and in HERWIG [3, 7]. CKKW has been used in several studies of vector boson production in hadronic collisions [3, 8–11]. CKKW-L was also first published for e^+e^- [2] and later extended to hadrons and applied to W-production [11, 12]. All the CKKW-L results so far have been calculated using the ARIADNE [13] implementation. The Pseudo-Shower scheme was published in [3], where the algorithm was described, and an implementation based on PYTHIA [14] was applied to both e^+e^- and hadron collisions. The MLM algorithm has been implemented in ALPGEN [15], MADEVENT [16] and HELAC [17]. There is also one implementation based on HERWIG and MADEVENT, which was used in [3]. Several studies using MLM have been performed for heavy quark and vector boson production with incoming hadrons [3, 11, 18, 19]. To our knowledge no calculation applying MLM to e^+e^- annihilation has been published.

Of all the implementations, only the SHERPA implementation of the CKKW scheme and the ALPGEN and MADEVENT implementations of MLM are publicly available, while the others are obtainable from their respective authours upon request.

There have been some assessments of the systematics of the various algorithms done already, but the main focus so far has been the case of hadron collisions. Although collisions with incoming hadrons clearly are the most interesting in light of the upcoming LHC experiments, they also include a lot of complications, such as uncertainties from PDFs and BFKL-like corrections, that obfuscate the basic properties of the merging algorithms. e^+e^- annihilation is much simpler from a theoretical point of view and is therefore more suitable for testing the basic properties of the different algorithms. We believe it is essential to test the algorithms for e^+e^- annihilation before moving on to hadron collisions.

Systematics for e^+e^- have been published for CKKW-L [2] and for CKKW and Pseudo-Shower [3], but the systematics for the Pseudo-Shower approach was quite limited. These studies are extended in this paper, where the four algorithms listed earlier are applied to different parton shower implementations. This allows us to thoroughly test which algorithms live up to their promises.

To study systematics with as little complications as possible we only look at the simple case of $e^+e^- \to q\bar{q}g$. In this case the matrix element correction is already implemented in most of the parton showers, using a simple reweight-

ing of the hardest splitting[1] [20–23], which makes this process particularly suitable for testing the various algorithms. Ideally all the calculations should show small deviations and yield more or less trivial results. However, we find that this is not the case.

Since the process studied is rather simple, algorithms that perform well should also be tested with more complicated processes before they can be reliably used to predict experimental observables. Some of the complications that can occur during the merging do not enter if only first order corrections are applied. However, if an algorithm does not perform well for this simple process, it is improbable that it will work reliably for more complicated processes.

We note that besides the four merging algorithms presented here, there are also other ways of combining matrix elements and parton showers, *e.g.* the methods based on modifyig the tree-level or NLO matrix elements to *match* the parton shower (see *e.g.* [24–32]). Such matching algorithms may also have a dependence on an artificial matching scale. Although it may be interesting to also benchmark these algorithms using the simplest $e^+e^- \to q g \bar{q}$ process, we have not done so in this paper[2].

In this paper we will concentrate on the behavior of the merging schemes in absolute numbers. It would also be interesting to study their formal properties in terms of leading double- and single-logarithmic contributions to various cross sections, which so far has only been done for the CKKW scheme [1]. We plan to return to such issues in a future publication.

In this article we start by reviewing the theoretical aspects of the four algorithms in section IV.2. Then we move on to showing results from our implementations of the algorithms in section IV.4 and finally in section IV.5 we present our conclusions.

III.2 Theory

All of the algorithms considered in this paper aim to do a good job of merging matrix elements and partons showers. The issues that are addressed are the same, namely to split the phase space in a clean well defined way and to make the matrix element event exclusive by introducing Sudakov form factors or using some other similar suppression. The main aim is to minimize any artificial dependence on the merging scale.

[1] We refer to these matrix element corrections of only the hardest splitting as *reweighting* while the more general schemes on trial here are referred to as *merging*.

[2] After we wrote this paper a new algorithm was published [33,34] which used a similar benchmarking.

III.2.1 General scheme

The basic steps are common to all the algorithms and can be summarized as follows:

1. Select a process to be studied and choose a scheme to cutoff the divergences in the matrix elements, typically using a jet measure. Specify the maximum parton multiplicity to be generated by the matrix elements (This is currently limited to five or six extra partons for computational reasons). Calculate the cross section for all the parton multiplicities.
2. Select a parton multiplicity with a probability proportional to its integrated cross section. Generate kinematics according to the matrix element.
3. Calculate a weight for the event based on the Sudakov form factors and the running coupling. Use this weight either to reweight the event or as a probability for rejecting the event. If the event is rejected generate a new event according to step 2.
4. Find a set of initial conditions for the parton shower and invoke the shower. This may include a veto on the emissions from the shower.

All the algorithms considered in this paper do steps 1 and 2 in the same way, but steps 3 and 4 are done using rather different approaches. Each algorithm has its own way of including the Sudakov form factors and finding a good set of initial conditions for the shower.

One of the key features that distinguishes the algorithms is the choice of scales. The algorithms uses different definitions of scales when determining how to split phase space between the matrix element and the parton shower and in calculating the Sudakov form factors. Furthermore, these scale definitions may be different from what determines the ordering of emissions in the parton showers. We show later in this paper that the scale choices have significant consequences for how well the dependence on the merging scale can be minimized.

The rest of this section describes the details of each algorithm and their consequences for the physics result. The descriptions of the algorithms are limited to e^+e^- collisions, but, with a few modifications and extensions, they have all been used to calculate results for hadron collisions.

III.2.2 CKKW

The theoretical foundation for CKKW was published in [1], but the main points are repeated here for completeness. CKKW is focuses on the Durham $k_\perp$-algorithm for clustering jets in e^+e^- [35], where the distance between two

partons, i and j, is defined as

$$y_{ij} \equiv 2\min(E_i^2, E_j^2)(1 - cos\theta_{ij})/E_{\mathrm{CM}}^2. \tag{III.1}$$

The $k_\perp$-algorithm is used to construct a parton shower history from the event generated according to the matrix element. The algorithm generates a set of clusterings and corresponding scales, which are later used to calculate the Sudakov form factors and the running coupling.

Before going through the CKKW algorithm some notation needs to be introduced. Γ_q, Γ_g and Γ_f are the branching probabilities for $q \to qg$, $g \to gg$ and $g \to f\bar{f}$ respectively. The Sudakov form factors are then given by

$$\Delta_q(Q_1, Q_2) = \exp(-\int_{Q_2}^{Q_1} dq \Gamma_q(Q_1, q)) \tag{III.2}$$

$$\Delta_g(Q_1, Q_2) = \exp(-\int_{Q_2}^{Q_1} dq (\Gamma_g(Q_1, q) + \Gamma_f(Q_1, q))). \tag{III.3}$$

They can be interpreted as the probability of a parton with the production scale Q_1 not to have a branching above the scale Q_2. Note the dependency on the production scale in the branching probabilities. This means that the Sudakov form factors used in CKKW do not factorize ($\Delta(Q_1, Q_2) \cdot \Delta(Q_2, Q_3) \neq \Delta(Q_1, Q_3)$). This is also the case for the Sudakov form factors in the angular ordered shower, where the limits on the integration of the splitting functions are dependent on the production scale.

The idea of CKKW is to use the full matrix element for the branching probabilities and analytical Sudakov form factors above the merging scale, and the parton shower below the merging scale. The full CKKW algorithm is the following:

1. Calculate cross sections and generate events according to step 1 and 2 in section III.2.1. y_{MS} denotes the merging scale which is equal to the matrix element cutoff, defined in terms of the $k_\perp$-measure in eq. (III.1). The events are generated using a fixed strong coupling, α_{sME}, and a maximum multiplicity, N.
2. Construct a shower history by applying the $k_\perp$-algorithm to the state from the matrix element. The algorithm is constrained to only allow clusterings of partons which are consistent with a possible emission from the parton shower. This yields a set of clustering values $y_2, ..., y_n$, where $y_2 = 1 > y_3 > ... > y_n$ and n denotes the parton multiplicity of the event from the matrix element. Use the result from the clustering to determine a set of nodes where the partons are merged and the associated scales, $q_i^2 = y_i E_{\mathrm{CM}}^2$.
3. Calculate a weight for the running coupling given by $\prod_{i=3}^{n} \alpha_s(q_i)/\alpha_{\mathrm{sME}}^{n-2}$.

4. For each internal line of type i running between a node with scale q_j and q_k apply a factor $\Delta_i(q_j, q_{\mathrm{MS}})/\Delta_i(q_k, q_{\mathrm{MS}})$, where $q^2_{\mathrm{MS}} = y_{\mathrm{MS}} E^2_{\mathrm{CM}}$. For external lines of type i starting from a scale q_j apply the weight $\Delta_i(q_j, q_{\mathrm{MS}})$. These weights are the Sudakov form factors and they are calculated analytically.
5. Reweight the event with the product of the Sudakov form factors in step 4 and the running coupling weight in step 3.
6. Set the starting scale of each parton to the scale associated with the node in the shower history where it was produced. Invoke the shower and veto any emission which would give a $k_\perp$-measure above y_{MS}.

The original CKKW procedure [1] contained no special treatment for highest multiplicity events. This needs to be included since applying the veto on emissions in the shower down to the merging scale would prevent events with more than N jets above the merging scale from being generated. One way to resolve this is to modify the procedure for highest multiplicity events ($n = N$) and use the scale q_n instead of q_{MS} in the Sudakov form factors and the vetoed shower. This is done in [3, 36].

Another issue that needs to be addressed is effects related to the choice of ordering variable in the shower. The entire theoretical derivation in the CKKW publication [1] uses only one way of defining scales, namely the Durham $k_\perp$. While the discrepancy from using a different ordering variable in the shower may cancel to some accuracy, this is not explicitly shown or discussed, even though the shower used in the publication is ordered in virtuality. The consequences of applying the scheme to a shower not ordered in Durham $k_\perp$ are therfore somewhat unclear.

The original CKKW publication [1] claims that this procedure cancels the dependence on the merging scale to next-to-leading logarithmic (NLL) accuracy. However, this claim assumes that the formalism used, including Sudakov form factors, jet rates and generating functions, is valid at NLL, but this proof has never been published.[3]

III.2.3 CKKW-L

The CKKW-L algorithm goes through the same basic steps as CKKW, but has a different way of calculating the Sudakov form factors and implementing the veto in the shower. In the CKKW-L scheme, a full cascade history with intermediate states is constructed. What is done is basically to run the cascade backwards and answer the question "how could the shower have generated this state?". This means that the ordering scale in the shower is used when

[3] The only reference leads to reference 22 in [35], which is marked "in preparation", and it has been confirmed by one of the authors of the article that it was never completed.

clustering the partons. As in the CKKW case, only physically allowed clusterings are considered. However, contrary to CKKW where always the smallest scale is chosen for each clustering, all possible ordered shower histories are considered, and one is chosen according to a probability proportional to the product of the relevant branching probabilities. The chosen shower history is then used to calculate the Sudakov form factors and the running coupling.

To be able to use this scheme, the parton shower needs to have well defined intermediate states and it is also required that the Sudakov form factors factorize ($\Delta(Q_1, Q_2) \cdot \Delta(Q_2, Q_3) = \Delta(Q_1, Q_3)$). This is achieved if the Sudakov form factors only depend on the kinematics of the intermediate state rather than the production scale. This is for example the case in the dipole shower used in ARIADNE [13] and the $p_\perp$-ordered shower in PYTHIA [37], but not for the angular ordered shower in HERWIG [7].

The effects of the running coupling are taken into account by reweighting with the same α_s as in the shower with the constructed scales as input. The Sudakov form factors are introduced by using the shower to generate single emissions from the constructed states starting from the constructed scales and rejecting the event if the emission is above the next constructed scale. This is known as the Sudakov veto algorithm and it is equivalent to accepting events with a probability equal to the Sudakov form factor, since by definition the no emission probability of the shower is equal to the Sudakov form factor.

There are several advantages to this approach. One is that it makes sure that the Sudakov form factors above and below the merging scale match exactly and another is that any corrections introduced in the shower is also included in the Sudakov form factor. This is particularly useful if the splitting functions have been reweighted with matrix elements, since this makes it possible to completely cancel the merging scale dependence for first order correction (shown explicitly below). We also expect that the cancellation of the first order correction will lead to a smaller merging scale dependence for higher order processes even though the complete cancellation no longer holds.

We use a slightly different notation in this section to emphasize the difference in the Sudakov form factors with respect to the ones in CKKW. $\Delta_{S_n}(\rho_1, \rho_2)$ denotes a Sudakov form factor for an n-particle state giving the probability that there is no emission with a shower scale, ρ, between ρ_1 and ρ_2. The merging scale uses another notation, Q_{MS}, to emphasize that this scale does not need to be defined in terms of the emission scale in the shower. In fact, one could in principle use any partonic scale definition for the merging scale. These are the steps in the CKKW-L algorithm.

1. Calculate cross sections and generate events according to step 1 and 2 in section III.2.1. Q_{MS} denotes the merging scale which is equal to the matrix element cutoff and may be defined using any choice of scale. The events are generated using a fixed strong coupling, α_{sME}, and a maxi-

mum parton multiplicity, N.

2. Construct a full cascade history by considering all possible ordered histories and selecting one randomly with a probability proportional to the product of the branching probabilities. If no ordered histories can be constructed, unordered ones are considered. This results in a set of intermediate states $(S_2, S_3, ...S_n)$ and scales $(\rho_2 = \rho_{\max}, \rho_3, ..., \rho_n)$. S_2 denotes here denotes the constructed $2 \to 2$ process and S_n is the state given by the matrix element. n is the parton multiplicity in the event, $\rho_{\max}$ is the maximum scale of the process and ρ_i is the constructed scale where the state S_{i-1} emits a parton to produce the state S_i.
3. Reweight the events with $\prod_{i=3}^{n} \alpha_s(\rho_i)/\alpha_{\text{sME}}^{n-2}$.
4. For each state S_i (except S_n), generate an emission with ρ_i as starting scale and if this emission occurred at a scale larger than ρ_{i+1} reject the event. This is equivalent to reweighting with a factor $\prod_{i=2}^{n-1} \Delta_{S_i}(\rho_i, \rho_{i+1})$.
5. For the last step there are two cases.
   - If the event does not have the highest multiplicity $n < N$, generate an emission from the state S_n with ρ_n as starting scale. If the emission is above the merging scale Q_{MS}, reject the event. Otherwise accept the event and continue the cascade.
   - If the event has the highest possible multiplicity $n = N$, accept the event and start the cascade from the state S_n with the scale ρ_n.

The algorithm introduces all the factors that would have been present if the event had been generated by the parton shower, except the branching probability which is taken from the matrix element. To show how this comes about, a derivation of the parton multiplicity cross sections for a first order matrix element is shown below. The explicit reweighting of α_s is not shown, but is straight forward to include.

Let ρ_0 denote the parton shower cutoff and $\Gamma_{S_n}(\rho)$ denote the probability that a state S_n branches at scale ρ. The definition of the Sudakov from factor in this case is $\Delta_{S_n}(\rho_1, \rho_2) \equiv \exp(-\int_{\rho_2}^{\rho_1} d\rho\, \Gamma_{S_n}(\rho))$. The exclusive parton multiplicity cross sections generated by the standard parton shower can be written as

$$\sigma_2^{\text{PS}}(\rho_{\max}, \rho_0) = \sigma_0\, \Delta_{S_2}(\rho_{\max}, \rho_0) \tag{III.4}$$

$$\sigma_3^{\text{PS}}(\rho_{\max}, \rho_0) = \sigma_0 \int_{\rho_0}^{\rho_{\max}} d\rho\, \Delta_{S_2}(\rho_{\max}, \rho)\, \Gamma_{S_2}(\rho)\, \Delta_{S_3}(\rho, \rho_0) \tag{III.5}$$

$$\begin{aligned}\sigma_4^{\text{PS}}(\rho_{\max}, \rho_0) = {} & \sigma_0 \int_{\rho_0}^{\rho_{\max}} d\rho\, \Delta_{S_2}(\rho_{\max}, \rho)\, \Gamma_{S_2}(\rho) \times \\ & \times \int_{\rho_0}^{\rho} d\rho'\, \Delta_{S_3}(\rho, \rho')\, \Gamma_{S_3}(\rho')\, \Delta_{S_4}(\rho', \rho_0).\end{aligned} \tag{III.6}$$

This notation can be generalized to include all higher multiplicity cross sec-

III

tions. Let $f^{3\to n}(\rho,\rho_0)$ denote the probability of the three-parton state to evolve into an n parton state between the two given scales. This means that a general $n \geq 3$ parton cross section can be written as

$$\sigma_n^{\mathrm{PS}}(\rho_{\max},\rho_0) \;=\; \sigma_0 \int_{\rho_0}^{\rho_{\max}} d\rho\, \Delta_{S_2}(\rho_{\max},\rho)\, \Gamma_{S_2}(\rho) f^{3\to n}(\rho,\rho_0), \tag{III.7}$$

where

$$f^{3\to 3}(\rho,\rho_0) \;=\; \Delta_{S_3}(\rho,\rho_0). \tag{III.8}$$

$$f^{3\to 4}(\rho,\rho_0) \;=\; \int_{\rho_0}^{\rho} d\rho'\, \Delta_{S_3}(\rho,\rho')\, \Gamma_{S_3}(\rho')\, \Delta_{S_4}(\rho',\rho_0) \tag{III.9}$$

$$\vdots$$

The merging scale may be defined using a different way of mapping the phase space (denoted Q) as compared to the scale used in the shower. The value of the scale used to define the merging scale and the scale of the shower can be related if the other variables that determine the shower emission is included. Let $\vec{x}$ represent the k additional variables used in the shower, which may include energy fractions and rotation angles. The branching probability can be written in a way that it includes the dependence on these variables as long as the following is true.

$$\Gamma(\rho) = \int d^k\vec{x}\, \Gamma(\rho,\vec{x}) \tag{III.10}$$

The alternative mapping of phase space is described by the function $Q_{S_n}(\rho,\vec{x})$, which denotes the value of the merging scale measure for a given shower emission. The lowest order matrix element cross sections are equal to

$$\sigma_2^{\mathrm{ME}}(\rho_{\max},Q_{\mathrm{MS}}) \;=\; \sigma_0 \tag{III.11}$$

$$\sigma_3^{\mathrm{ME}}(\rho_{\max},Q_{\mathrm{MS}}) \;=\; \sigma_0 \int_{\rho_0}^{\rho_{\max}} d\rho \int d^k\vec{x}\, \Gamma_{S_2}^{\mathrm{ME}}(\rho,\vec{x}) \times \\ \times\Theta(Q_{S_2}(\rho,\vec{x}) - Q_{\mathrm{MS}}). \tag{III.12}$$

$\Gamma_{S_2}^{\mathrm{ME}}$ is the branching probability in the matrix element and Θ is the standard Heaviside function. Note that the equations above only hold if the matrix element merging scale is above the shower cutoff everywhere in phase space, but this can be resolved by discarding all events from the matrix element which are below the shower cutoff.

The next step is to apply the algorithm to calculate the jet rates at ρ_0 for the merged matrix element and parton shower. The two-jet state is already the lowest order process, which means no cascade history is constructed and only the final Sudakov veto down to the merging scale enters. The parton

multiplicity cross sections become equal to that of the pure shower minus the cross section for events with the first emission above Q_{MS}. The two-jet matrix-element contributions to the cross sections are equal to

$$\begin{aligned}\sigma_2(\rho_{\max},\rho_0) &= \sigma_0\,\Delta_{S_2}(\rho_{\max},\rho_0) && \text{(III.13)}\\ \sigma_n(\rho_{\max},\rho_0) &= \sigma_0\int_{\rho_0}^{\rho_{\max}} d\rho \int d^k\vec{x}\,\Theta(Q_{\mathrm{MS}}-Q_{S_2}(\rho,\vec{x}))\,\Delta_{S_2}(\rho_{\max},\rho)\times\\ &\quad\times\Gamma_{S_2}(\rho,\vec{x})f^{3\to n}(\rho,\rho_0). && \text{(III.14)}\end{aligned}$$

When the algorithm is applied to a three-jet event, an emission scale, ρ_3, is constructed. Emissions are generated from the two-jet state and events discarded according to the Sudakov veto algorithm, which is equivalent to introducing a weight $\Delta_{S_2}(\rho_{\max},\rho_3)$. The cascade is then started from the scale ρ_3 and, assuming the three-jet configuration is the highest multiplicity, no additional Sudakov suppression is included. Using the matrix element cross section from equation (III.12) and, assuming that the constructed scale ρ_3 is equal to the scale used in the matrix element, results in the following contributions to the parton multiplicity cross sections.

$$\begin{aligned}\sigma_n(\rho_{\max},\rho_0) &= \sigma_3^{\mathrm{ME}}(\rho_{\max},Q_{\mathrm{MS}})\,\Delta_{S_2}(\rho_{\max},\rho_3)\,f^{3\to n}(\rho_3,\rho_0) =\\ &= \sigma_0\int_{\rho_0}^{\rho_{\max}} d\rho\int d^k\vec{x}\,\Theta(Q_{S_2}(\rho,\vec{x})-Q_{\mathrm{MS}})\,\Gamma_{S_2}^{\mathrm{ME}}(\rho,\vec{x})\times\\ &\quad\times\Delta_{S_2}(\rho_{\max},\rho)\,f^{3\to n}(\rho,\rho_0) && \text{(III.15)}\end{aligned}$$

The following cross sections are the result from adding the contributions from the two- and three-jet processes.

$$\begin{aligned}\sigma_2^{\mathrm{ME+PS}}(\rho_{\max},\rho_0) &= \sigma_0\,\Delta_{S_2}(\rho_{\max},\rho_0) && \text{(III.16)}\\ \sigma_n^{\mathrm{ME+PS}}(\rho_{\max},\rho_0) &= \sigma_0\int_{\rho_0}^{\rho_{\max}} d\rho\int d^k\vec{x}\,[\Gamma_{S_2}^{\mathrm{ME}}(\rho,\vec{x})\,\Theta(Q_{S_2}(\rho,\vec{x})-Q_{\mathrm{MS}})+\\ &\quad+\Gamma_{S_2}^{\mathrm{PS}}(\rho,\vec{x})\Theta(Q_{\mathrm{MS}}-Q_{S_2}(\rho,\vec{x}))]\times\\ &\quad\times\Delta_{S_2}(\rho_{\max},\rho)\,f^{3\to n}(\rho,\rho_0) && \text{(III.17)}\end{aligned}$$

From the equations above one can see that the only dependence on the merging scale Q_{MS} is in the integration over the branching probabilities. This means that the merging scale dependence for this process cancels to the accuracy of which the shower generates the first emission. In fact, for the process studied in this paper, many of the parton shower implementations reweight the splitting function for the first emission with the matrix element, in which case the merging scale dependence cancels completely.

III.2.4 Pseudo-Shower

The Pseudo-Shower algorithm is similar in spirit to CKKW-L, but it uses partonic jet observables for the kinematics instead of individual partons. Where CKKW-L runs the cascade one emission at a time from a given parton state to calculate no-emission probabilities, in the Pseudo-Shower approach a full parton cascade is evolved, and the resulting partons are clustered back to jets. Any standard clustering algorithm, where in each step the pair of particles which are closest together are clustered, can be used. The same distance measure is used to define the merging scale as the one used to construct a shower history for the matrix-element state and the fully showered states. The full algorithm is defined as follows.

1. Choose a jet clustering scheme to be used in the algorithm and a merging scale, d_{MS}. Set the matrix element cutoff equal to the merging scale, calculate cross sections and generate events according to step 1 and 2 in section III.2.1. The events are generated using a fixed strong coupling, α_{sME}, and a maximum multiplicity, N.
2. Cluster the partons from the matrix element, using the selected jet scheme, until a $2 \to 2$ state is reached. As in CKKW, only clusterings corresponding to physically allowed splittings are considered. The result of the clustering is interpreted as a shower history with a set of states $(S_2, \dots S_n)$ and a set of scales $(\tilde{d}_2 = d_{\max}, \tilde{d}_3, \dots, \tilde{d}_n)$, where n is the parton multiplicity of the event.
3. For each state S_i, except S_n, perform a full shower vetoing any emission with a jet measure greater than the corresponding scale in the shower history, $d > \tilde{d}_i$. Calculate a set of clustering scales, d_j, by clustering the partons from the shower using the same algorithm as in step 2, but for practical reasons also allow clusterings corresponding to non-physical splittings. Reject the event if $\sqrt{d_{i+1}} > \sqrt{\tilde{d}_{i+1}} + \delta$ (the δ is a fudge factor to be discussed below).
4. For the final state S_n the shower is invoked, vetoing emissions with $d > \tilde{d}_n$. If the event is not a maximum multiplicity event ($n < N$), the partons are clustered and the event is rejected if the scale from the clustering is above the merging scale, $\sqrt{d_{n+1}} > \sqrt{d_{\text{MS}}} + \delta$. For $N = n$ the event is accepted except if $\sqrt{d_{n+1}} > \sqrt{\tilde{d}_n} + \delta$.

Although it was not stated in the text in [3], the implementation did include a reweighting with a running strong coupling $\prod_{i=3}^{n} \alpha_{\text{s}}(\tilde{d}_i)/\alpha_{\text{sME}}^{n-2}$. The same reweighting is also included here.

To see the similarity with CKKW-L, consider using the Pseudo-Shower using a parton shower with an ordering variable equal to the distance scale in the clustering algorithm used, and with well-defined intermediate states. In

the strongly ordered limit, the clustering algorithm would then exactly reproduce the intermediate states and branching scales in the shower. This means that evolving a full shower from the state S_i, starting from a scale $\tilde{d}_i$, clustering to find a d_{i+1} and rejecting the event if $d_{i+1} > \tilde{d}_{i+1}$ would exactly correspond to the Sudakov form factor $\Delta_{S_i}(\tilde{d}_i, \tilde{d}_{i+1})$, and the merging scale dependence for first order matrix element corrections would cancel in the same way as CKKW-L.

In reality, the clustering does not exactly reconstruct the shower splittings. If subsequent emissions are not clustered in the same way as the shower emitted them, this can affect the clustering scale of harder emissions. This means that the scale of the matrix element partons before the shower and the scale that one gets from the jet clustering after the shower are rarely the same. This is a significant problem, since the phase space cuts that separate the matrix element emissions from the partons shower emission is done using two different scales, which leads to dead regions and double counting of emissions and it also affects the calculation of the Sudakov form factors.

To moderate the effects of having two different scales, the fudge factor δ (introduced in [3]) was included whenever comparing a scale from the clustering of the matrix element state with a scale from the clustering of the fully showered state. In [3] the value $\delta = 2$ GeV was used without motivation, theoretical or otherwise, but supposedly the parameter needs to be tuned for each choice of process and merging scale to properly compensate for the mismatch in scales.

III.2.5 MLM

The MLM algorithm is similar to the Pseudo-Shower in that it also does matching with partonic jet observables. The algorithm is much simpler to implement compared to earlier schemes discussed. In the MLM merging scheme the event from the matrix element is simply fed into the parton shower program, the shower is invoked and the final state partons are clustered into jets. The algorithm then specifies that the matrix element partons should be matched to the final state partonic jets, and events are accepted only if all the jets match and the event contains no extra jets above the merging scale. In this way the Sudakov form factors are approximated by the probability that there are no emissions above the merging scale and, at the same time, the parton shower emissions are approximately constrained to be below the merging scale. The MLM algorithm is a really convenient way of doing merging since it requires no modifications to the parton shower program.

Even though MLM has been frequently used, a general version of the algorithm has never been published and all the published algorithms assume incoming hadrons. Based on [4, 11, 19], we present here our interpretation of the necessary steps needed for applying the MLM scheme to e^+e^- collisions.

The first step in an MLM implementation is to choose a jet definition to be used for the merging scale and the matrix element cutoff. The original MLM algorithm used cone jet definitions, although there have been implementations using the $k_\perp$-algorithm, *e.g.* the MADEVENT implementation in [11] and the HERWIG implementation in [3]. After specifying a cutoff, events are generated and the running coupling reweighting is calculated in the same way as in the CKKW algorithm.

Then the shower is invoked using an appropriate starting scale, which is defined for each implementations and process. For W-production in hadron collisions, the scale is set to the transverse mass of the W ($\sqrt{m_W^2 + p_{\perp W}^2}$) [11], whereas for the top production implementation it is not specified [19]. In hadron collision there is some freedom for choosing the starting scale of the shower, but for e^+e^- we think that the scale should be set to center of mass energy, to allow the shower to utilize the full phase space.

After the shower has been invoked the final state partons need to be clustered into jets and matched to the partons from the matrix element. The clustering is done with the same algorithms used to define the merging scale. The partons from the matrix element are then matched to the clustered jets, in order of decreasing energy. The measure used to match the partons to jets is some quantity related to the jet clustering. These are all the steps in the algorithm.

1. Select a merging scale, Q_{MS}, and a matrix element cutoff Q_{cut}, such that $Q_{\text{cut}} < Q_{\text{MS}}$, where the scales are defined using a jet algorithm. Calculate cross sections and generate events according to step 1 and 2 in section III.2.1. The events are generated using a fixed strong coupling, α_{sME}, and a maximum parton multiplicity, N.
2. Cluster the partons from the matrix element using the $k_\perp$-algorithm and use the clustering scales as in input to α_s and reweight the event.
3. Feed the event into a parton shower using the Les Houches interface [38], setting the scale to E_{CM}, and start the shower.
4. Cluster the partons to jets using the algorithm from step 1 with a clustering scale set to Q_{MS}. Go through the list of partons, in order of decreasing energy, and match them to the clustered jets. This is done by finding the jet with the smallest distance to the parton defined using some measure based on the jet clustering scheme[4]. If not all the partons match or there are extra jets, reject the event.

   For the highest multiplicity events either use a higher clustering scale and more relaxed matching criteria or allow extra jets that are softer than the matched jets.

[4]This cannot be exactly the same distance measure as in the jet algorithm for reasons to be discussed in section IV.4

There are several aspects of this algorithm that needs further explaining. The reason for having a cutoff below the merging scale is that events slightly below the merging scale can end up above after the shower. This leaves an arbitrary choice of matrix element cutoff, but this can be resolved if soft and collinear particles have a vanishing probability to generate an independent jet, which means that the result converge when the matrix element cutoff is lowered. This is a way of getting around the problem that occurred in the Pseudo-Shower algorithm, namely that the cuts on the matrix element state and on the partonic jets are not equivalent. However, the convergence needs to be verified for each implementation and process.

One other aspect that needs further scrutiny is what happens inside the parton shower program. The main danger is that the program may be given a state with one or more relatively soft parton and a rather high starting scale, which means that the shower often ends up emitting harder partons than the ones already present, leading to an unordered shower. This breaks the strong ordering approximation, which is fundamental to all parton showers, and the end result is heavily dependent on how unordered emissions are handled.

To derive some of the properties of MLM, let us assume (as we did in the Pseudo-Shower case) that the jet clustering is a perfect inverse of the shower and that the shower has well defined intermediate states. These assumptions are a bit crude considering the way MLM is used in current implementations, but it allows for the possibility to do analytical calculations and it should give some idea of what to expect from the algorithm. Under these assumptions parton multiplicity cross sections, including the first order matrix element corrections, can be calculated.

The calculations are performed using the same notation as in the section III.2.3. The merging scale can be defined in terms of the scale in the shower (ρ_{MS}) and starting the scale from the center of mass energy is equivalent to using the maximum scale (ρ_{max}). The two-jet matrix element contribution to the parton multiplicity cross sections becomes the same as in CKKW-L.

$$\sigma_2(\rho_{\text{max}}, \rho_0) = \sigma_0 \cdot \Delta_{S_2}(\rho_{\text{max}}, \rho_0) \tag{III.18}$$

$$\sigma_n(\rho_{\text{max}}, \rho_0) = \sigma_0 \cdot \int_{\rho_0}^{\rho_{\text{MS}}} d\rho \, \Delta_{S_2}(\rho_{\text{max}}, \rho) \, \Gamma_{S_2}(\rho) f^{3\to n}(\rho, \rho_0) \tag{III.19}$$

The contribution from the three-jet is different however. The reason is that there is no Sudakov form factor from a two-particle state included since no shower history was considered. The contribution to the cross sections is the following.

$$\sigma_n(\rho_{\text{max}}, \rho_0) = \sigma_0 \cdot \int_{\rho_{\text{MS}}}^{\rho_{\text{max}}} d\rho \, \Gamma^{\text{ME}}_{S_2}(\rho) \, \Delta_{S_3}(\rho_{\text{max}}, \rho) \, f^{3\to n}(\rho, \rho_0) \tag{III.20}$$

The sum of the two contributions become the following.

$$\sigma_2(\rho_{\max},\rho_0) = \sigma_0 \cdot \Delta_{S_2}(\rho_{\max},\rho_0) \quad \text{(III.21)}$$

$$\sigma_n(\rho_{\max},\rho_0) = \sigma_0 \cdot \int_{\rho_0}^{\rho_{\max}} d\rho \left[\Gamma^{\mathrm{ME}}_{S_2}(\rho)\,\Delta_{S_3}(\rho_{\max},\rho)\Theta(\rho-\rho_{\mathrm{MS}}) + \right. \\ \left. + \Gamma^{\mathrm{PS}}_{S_2}(\rho)\,\Delta_{S_2}(\rho_{\max},\rho)\Theta(\rho_{\mathrm{MS}}-\rho)\right] f^{3\to n}(\rho,\rho_0) \quad \text{(III.22)}$$

Comparing equation (III.21) to (III.4) one can see that the two-parton cross section becomes the correct one. Note that this would not have be the case if a lower starting scale was chosen for the shower. The higher multiplicity cross sections contain complications, which can be seen by comparing equation (III.22) to (III.7). The problem is that MLM does not include the Sudakov form factor from the S_2 state, which means that there will be an additional dependence on the merging scale as a result of the difference in the Sudakov form factors. The factor $\Delta_{S_3}(\rho_{\max},\rho)$ is where the explicitly unordered shower occurs and the results are therefore largely dependent on the parton shower implementation.

Consider, for illustration, using the $k_\perp$-ordered shower of PYTHIA on a three-parton state. Here the maximum transverse momentum of an emission is given by half the largest of the qg and $g\bar{q}$ invariant masses, which for a soft gluon can be very small. Hence, the Sudakov form factor between E_{CM} and this transverse momentum would be absent, resulting in a large dependence on the merging scale.

The actual MLM implementations contain several other complications. The jet clustering used is not the inverse of the shower and most implementations use parton showers that do not have well defined intermediate states. However, none of these aspects can resolve the problem that the Sudakov form factor is generated using a three-particle state instead of a two-particle state. The error caused by using the wrong Sudakov form factor is inherent in any MLM implementation.

III.3 Results

Each of the algorithms described above have been tested for the first order matrix element correction to $e^+e^- \to q\bar{q}$ at the Z^0 pole. As explained in the introduction, this matrix element correction can also be included by a simple reweighting of the first (or hardest) splitting in a parton cascade, thus providing us with the "correct" answer for comparison. In this way we can check whether the merging algorithms actually meet their goals of a clean cut between matrix element and parton shower phase space and a small dependence on the merging scale. Only if they do achieve these goals on this simple case,

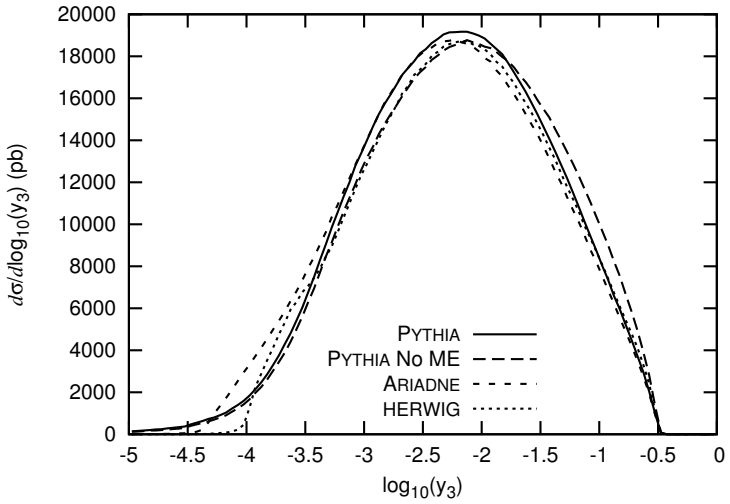

Figure III.1: The y_3 spectra at parton level for PYTHIA, PYTHIA with matrix element reweighting switched off, ARIADNE and HERWIG.

can we believe that they are likely to achieve their goals when generalized to higher order matrix elements and more complicated processes.

To have a fair comparison, we have in all cases generated matrix element events using a cut in the Durham $k_\perp$-algorithm distance measure, y, as defined in eq. (III.1). Also the merging scale is defined using this distance measure. The only exception is for the Pseudo-Shower algorithm, where a slightly different scale is used as explained below in section III.3.3. The matrix element events were generated with MADEVENT (v 4.1.31) [16].

To check the merging scale dependence we look at the distribution which should be the most sensitive, namely the y_3 scale where the $k_\perp$-algorithm clusters three jets into two, when applied to the final parton-level events. We also look at two hadron-level event shape observables, which have been well measured at LEP and corrected to hadron level. One is the normalized y_3 distribution of all final state particles measured by ALEPH [39], which shows how the dependence on the merging scale is reflected in the hadronic final state. The other is the normalized charged particle thrust distribution measured by DELPHI [40], which is not directly related to the merging scale, but is nevertheless very sensitive to the leading order matrix element correction.

In figures III.1 and III.2 we present these distributions for the four generators ARIADNE (v 4.12) [13], HERWIG (v 6.510) [7] and PYTHIA (v 6.413) [37], which all are equipped with simple matrix element reweighting. We see that

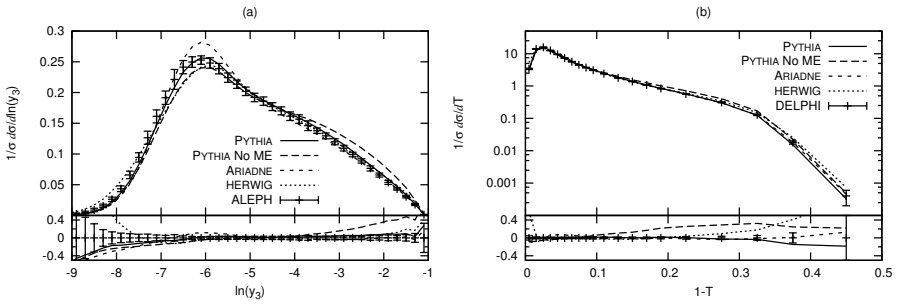

Figure III.2: The y_3 spectra for charged and neutral particles (a) and the charged particle thrust spectra (b) for PYTHIA, PYTHIA with matrix element reweighting switched off, ARIADNE and HERWIG compared to ALEPH and DELPHI data. The in-sets at the bottom of the plots show the relative differences between the Monte Carlo results and data, $(\sigma_{\mathrm{MC}} - \sigma_{\mathrm{Data}})/\sigma_{\mathrm{Data}}$.

they all agree fairly well, which should come as no surprise since they have all been tuned to fit LEP data.

In figures III.1 and III.2 we also show the results from PYTHIA, with the matrix element reweighting switched off to give a sense of how large an effects we should expect from the matrix element corrections. We see that the main effect is that these distributions are clearly harder than the ones with matrix element reweighting.

We had planed to also include SHERPA [6] in this comparison and use it for the CKKW results. Unfortunately we discovered inconsistencies[5] in the results and therefore decided not to use SHERPA at all in this study.

III.3.1 CKKW-L

We start by looking at the results from the CKKW-L scheme. Two implementations have been considered. We have used the original implementation [2] in ARIADNE and we have also made an implementation of the first order corrections using the transverse momentum ordered shower in PYTHIA [37, 41].

In ARIADNE the parton evolution is modeled by a dipole cascade [20, 42]. Unlike most other parton showers, the dipole cascade is based around $2 \to 3$ partonic splittings rather than $1 \to 2$. This model automatically includes the coherence effects from emitting gluons from colour-neighboring partons,

[5] Both the version 1.0.10 and 1.0.11 of SHERPA give different results for the cross section depending on whether weighted or unweighted events are used. Changing between weighted and unweighted events also gives two different results for the shape observables in version 1.0.10, neither being consistent with the results from version 1.0.11.

which means that explicit angular ordering is not necessary. It also means that the first order matrix element $e^+e^- \to qg\bar{q}$ is already present in the cascade by construction. The ordering variable used in the cascade is a Lorentz-invariant transverse momentum measure

$$p_\perp^2 = \frac{s_{12}s_{23}}{s_{123}}, \tag{III.23}$$

where s_{ij} are the invariant masses of the partons and index 2 indicates the emitted parton. This measure is then also used in the construction of the shower history in a procedure similar to the DICLUS jet clustering algorithm [43], but including only physically allowed clusterings.[6]

We have also implemented the CKKW-L scheme using the transverse-momentum ordered shower [41] in PYTHIA.[7] This cascade exhibits the main features required by the CKKW-L scheme, namely that it is ordered in transverse momentum and that is has well-defined on-shell intermediate states. The ordering variable (also called $p_\perp$) is defined in the following way:

$$p_\perp^2 = z(1-z)Q^2 \tag{III.24}$$

Q^2 is the invariant mass of the produced parton and radiating parton and z is the energy fraction of the radiating parton. The ordering of the shower is done in a way which incorporates coherence effects without requiring explicit angular ordering.

There is one significant difference in the PYTHIA implementation, namely that the constructed history is no longer unique. In PYTHIA there are two possible ways for the gluon to be emitted (from the quark or the anti-quark), which means that there are two possible histories to be considered. One history is selected with a probability proportional to its branching probability.

In figure III.3 we show the parton-level y_3 distribution for ARIADNE and transverse momentum ordered PYTHIA shower with matrix element reweighting.[8] Both programs are compared to their respective CKKW-L implementations with different merging scales, and the figure shows that the cancellation is almost complete. There are some small discrepancy for the lowest cutoff of the order of 2%. This is because MADEVENT generated the matrix element with massless u, d, s and c quarks, where as in ARIADNE and PYTHIA they are given a small mass, which causes a slight deviation in the emission probability. This discrepancy can be removed by setting the masses in ARIADNE and PYTHIA equal to the masses in MADEVENT. No deviations, however, are visible below the merging scale.

[6] For higher multiplicities, all possible shower histories are considered. However, for this simple case there is only one unique history

[7] Note that this is not a complete implementation, since only the leading order matrix element correction to $e^+e^- \to q\bar{q}$ is considered.

[8] We have used PYTHIA v 6.413, amended with a fix approved by the authors to avoid a bug in the built-in matrix element reweighting. This bugfix has been included v 6.414.

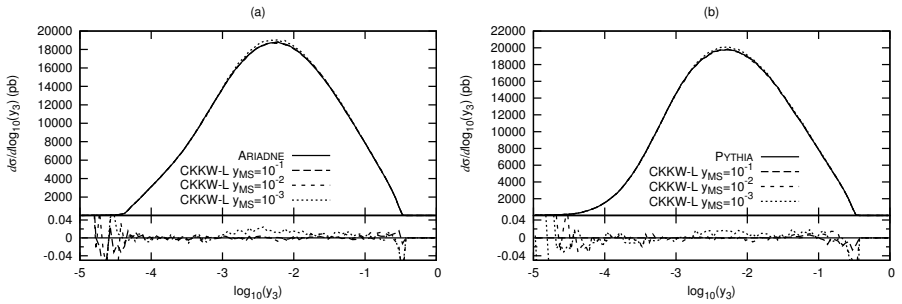

Figure III.3: (a) The y_3 spectra at parton level for ARIADNE (the first order matrix element is included by construction) and for the ARIADNE implementation of CKKW-L corrections with different merging scales. (b) is the same for our PYTHIA implementation of CKKW-L corrections with different merging scales. The in-sets at the bottom of the plots show the relative differences between the CKKW-L results and the default shower, $(\sigma_{\mathrm{CKKW-L}} - \sigma_{\mathrm{Shower}})/\sigma_{\mathrm{Shower}}$.

For completeness we show in figure III.4 the comparison for the hadron-level observables y_3 and thrust for ARIADNE and $p_\perp$-ordered PYTHIA respectively. As expected from the parton-level results, there is no serious dependence on the merging scale.[9]

III.3.2 CKKW

The CKKW algorithm has been implemented using PYTHIA, with both the $p_\perp$-ordered and the virtuality ordered shower. The implementations are done according to the scheme described in section III.2.2. The only difference is that none of the implementations use the Durham $k_\perp$ as ordering variables, therefore setting the starting scale is done differently. The scale of the quark and anti-quark is set to E_{CM} and the scale of the gluon is set to the $p_\perp$ of the reconstructed splitting for the $p_\perp$-ordered shower and the virtuality and angle[10] of the splitting for the virtuality ordered shower. For the latter, the scheme is essentially equivalent to what is implemented in SHERPA. The results are shown in figure III.5.

The results from the $p_\perp$ ordered shower show a smooth transition between the regions above and below the cutoff. This is to be expected since Durham

[9] The PYTHIA $p_\perp$-ordered shower has not been properly tuned to LEP data, and we therefore do not compare it directly to data. However, comparing with figures III.4a and b, it is clear that the variations due to the merging scale are well within the experimental errors.

[10] Besides having the virtuality as ordering variable, PYTHIA also imposes a veto on emission angles to ensure angular ordering.

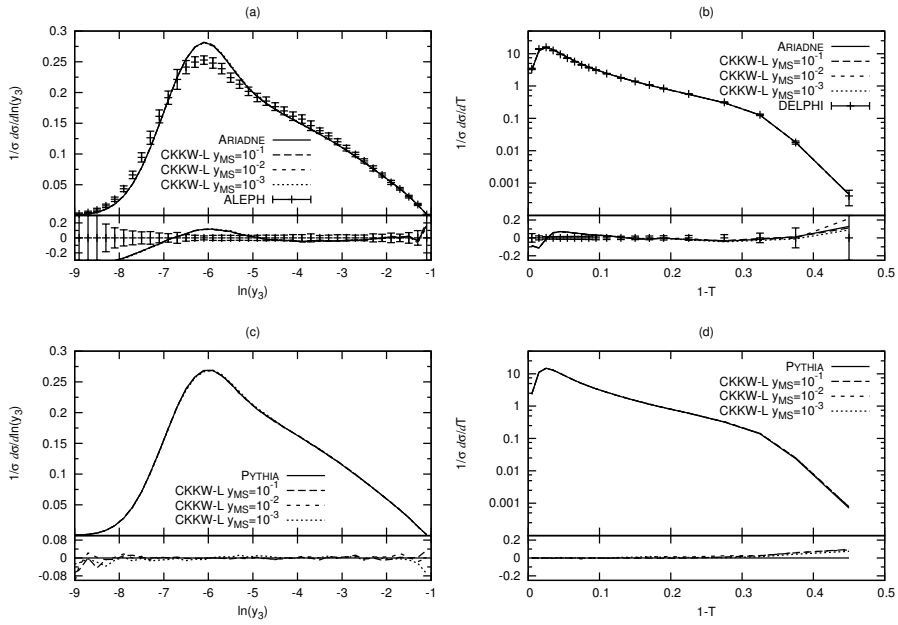

Figure III.4: Charged plus neutral particle y_3 and charged particle thrust for the ARIADNE and PYTHIA implementation of CKKW-L corrections with different merging scales. Figure (a) includes a comparison to ALEPH data and (b) a comparison to DELPHI data, where figure (c) and (d) only compare to the default PYTHIA, since the $p_\perp$-ordered shower has not yet been tuned to data.

III

$k_\perp$ is approximately equal to the $p_\perp$ in the shower, which means that the entire procedure becomes similar to CKKW-L with the exception that the Sudakov form factors are calculated according to an analytical approximation. The CKKW results show a slightly higher cross section than standard PYTHIA, which is attributed to the fact that in the analytical Sudakov form factors the approximate splitting functions are integrated over parts of phase space where they are negative. This means that Sudakov form factors cannot be interpreted as no-emission probabilities in the same way as in the shower and the end result is a slightly smaller suppression.

Figure III.5b shows the results from the virtuality ordered shower and there are clear problems. Each CKKW curve has a dip right at the merging scale and for higher values of y_3 they are significantly above the default results from PYTHIA. One source of problems is that the shower can generate unordered emissions, since an emission which has a high vitruality can have a low $k_\perp$. This also changes which Sudakov form factor is applied to each re-

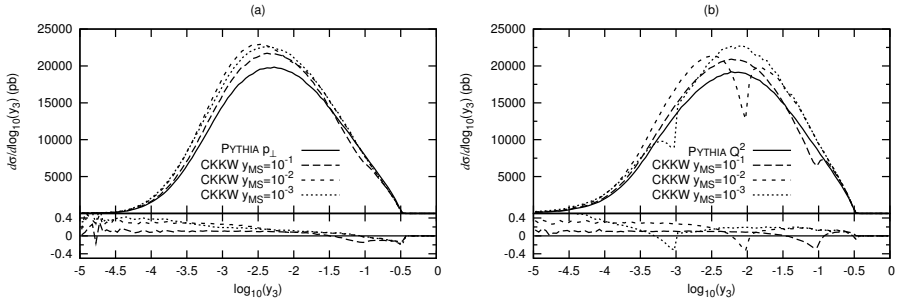

Figure III.5: The y_3 spectra at parton level for PYTHIA with $p_\perp$-ordered (a) and virtuality ordered (b) shower (and with the first order matrix element reweighting included) and for our corresponding PYTHIA implementations of CKKW corrections with different merging scales.

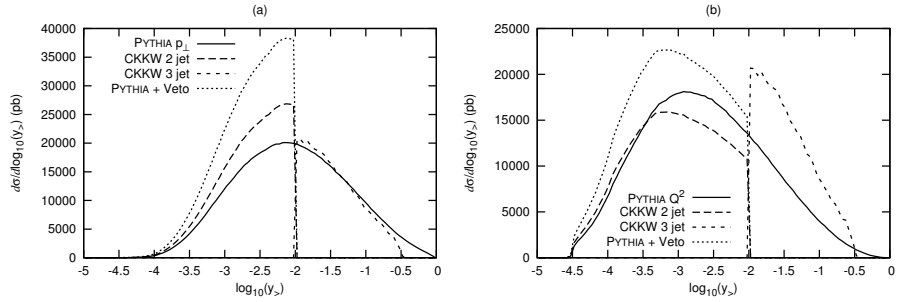

Figure III.6: The maximum Durham $k_\perp$-value of any emission in the cascade for PYTHIA with $p_\perp$-ordered shower (and with the first order matrix element reweighting included) and for the two- and three-jet components in our PYTHIA implementation of CKKW corrections with a merging scale $y_{\mathrm{MS}} = 10^{-2}$. An extra curve is included to show the two-jet contribution without the suppression from the analytic Sudakov form factor.

gion of phase space. A derivation of the problems that this can lead to for the lowest order process is presented in appendix III.1.

To further scrutinize the causes of the problems in the virtuality ordered CKKW implementation, we have studied the variable used for the shower veto which is the $k_\perp$-value of the individual emission. Figure III.6 shows the maximum Durham $k_\perp$-value for the emissions in the shower. The results have been split into two and three-jet components of the CKKW implementation using PYTHIA $p_\perp$ and virtuality ordered shower.

The two-jet events in CKKW is produced by invoking the shower vetoing emissions above the merging scale and reweighting with an analytical Sudakov form factor. These two steps can be considered separately, which is illustrated in figure III.6 by having a curve that only includes the veto and not the reweighting.

For the shower ordered in transverse momentum the three-jet contribution match the curve from running default PYTHIA fairly well above the merging scale. This is expected since the ordering in the transverse momentum ordered shower is fairly close to using Durham $k_\perp$-ordering. The two-jet contribution is similar in shape but is higher in cross section, which can be attributed to a smaller suppression from the analytical Sudakov form factors as compared to the form factors used in the shower. There is a discontinuity at the merging scale, but it is smoothed out by the shower causing the figure III.5a to appear somewhat smooth.

With the virtuality ordered shower the results are quite different, which is caused by using two rather different scales. The problem is that emissions modifies the phase space for subsequent emissions, and by emitting the partons with highest virtuality first, the hardest emissions in $k_\perp$ are no longer allowed. When studying the hardest emission according to Durham $k_\perp$, this results in a shift to smaller values. This is why the PYTHIA curve is significantly below the three-jet CKKW curve in figure III.6b. The sum of the two and three-jet contributions in figure III.6b has two peaks with a clear dip in between. When the rest of the emissions are included this structure is somewhat smothed out, but the two peaks with a dip in between are clearly visible in figure III.5b.

It is clear that one has to be a bit careful regarding the choice of shower and scales in CKKW. One CKKW implementation based on HERWIG was published in [3] and the results were consistent only after a significant amount of tuning of scale parameters. A similar procedure could probably be used to make our results more consistent, but it would add extra somewhat arbitrary parameters to the model. The problem with the ordering of the emissions also leads to a different colour structure in the events, which was pointed out in [26].

Finally we show the consequences for two experimental observables in figure III.7. Again, the results of the $p_\perp$-ordered shower has only been compared to the default PYTHIA, since it is not yet tuned to data. The $p_\perp$-ordered plots show significant lower values at high y_3 and low thrust, which is the result of the excess in cross section for two-jet events. We also see some trace of the discontinuities in figure III.6a, but they have been smoothed out by the shower and hadronization. The results from the virtuality ordred shower shows the same dips in the y_3 distribtion as in the parton-level plots. The dips are not visible in the thrust plot, but there are significant deviations from default PYTHIA.

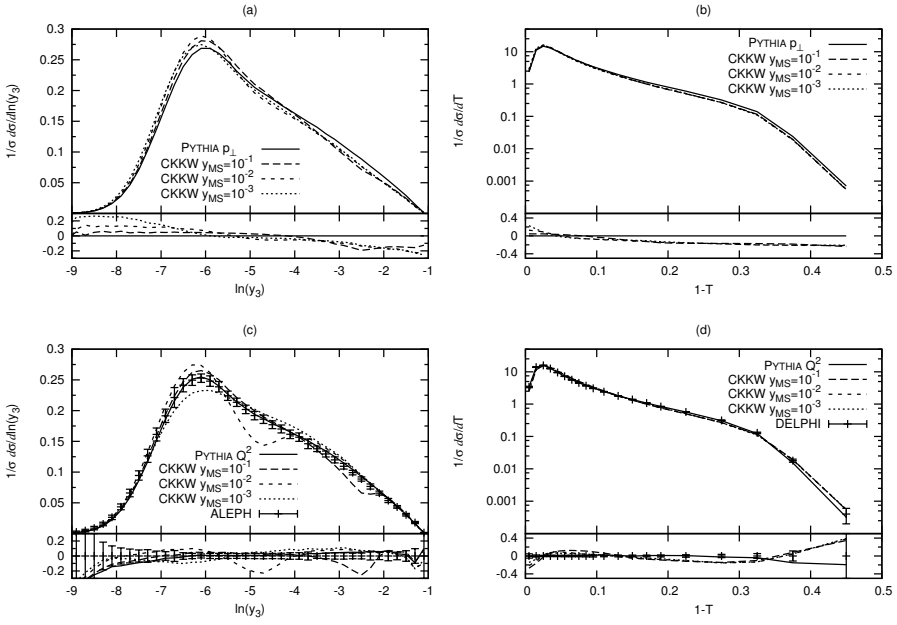

Figure III.7: Charged plus neutral particle y_3 and charged particles thrust for our PYTHIA implementation of CKKW corrections with transverse momentum and virtuality ordered showers and using different merging scales. Figure (c) includes a comparison to ALEPH data and (d) a comparison to DELPHI data, where figure (a) and (b) only compare to the default PYTHIA, since the transverse momentum ordered shower has not yet been tuned to data.

III.3.3 Pseudo-Shower

We have implemented the Pseudo-Shower [3] algorithm using matrix element events generated with MADEVENT and using PYTHIA with both virtuality ordered and $p_\perp$-ordered parton shower. The implementation has been done with the following definition for the jet clustering.

$$d_{ij} \equiv m_{ij}^2 E_i E_j / (E_i + E_j)^2 \tag{III.25}$$

This is equivalent to the measure in the LUCLUS algorithm[11] (and to the $k_\perp$-definition in eq. (III.24)) in the limit of massless particles. The jet algorithm was used both to define the merging scale and the clustering of jet observables as specified by the merging scheme. α_s-reweighting has been introduced us-

[11]Originally included in the JETSET program [44], now a part of PYTHIA as the PYCLUS routine.

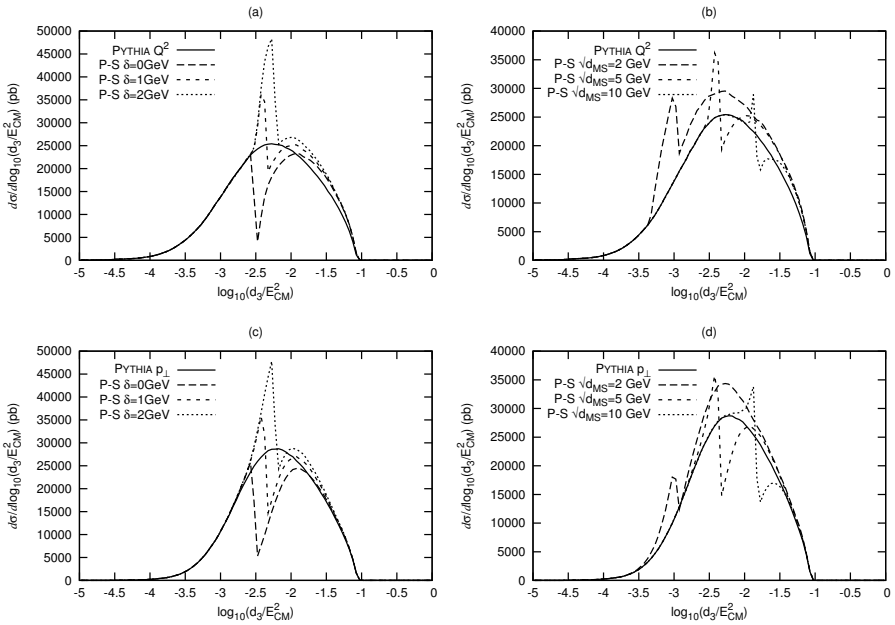

Figure III.8: The d_3 spectra at parton level for PYTHIA (with first order matrix element reweighting included) and for our implementation of the Pseudo-Shower algorithm using both the vituality ordered and the $p_\perp$-ordered shower. (a) and (c) show the effects of different valuses of the fudge factor δ with a merging scale of $\sqrt{d_{\mathrm{MS}}} = 5$ GeV. (b) and (d) show the results from different values of the merging scale d_{MS} using a fudge factor $\delta = 1$ GeV.

III

ing the scales from the jet clustering, which is happens to be the same scale definition that is used in the α_s evaluation in the PYTHIA shower.

The first thing that is investigated is the effects of different values of the fudge factor δ introduced in section III.2.4. The most sensitive distribution for checking the effects is the same variable as the merging scale. Figure III.8a and III.8c show the d_3 distribution at parton level for three different values of δ. In both figures the curve that shows the smallest deviations is $\delta = 1$ GeV, and this value is used in the rest of this section. It is clear that there is no smooth transition between the matrix element and parton shower phase space.

Figure III.8 also showes what happens if the merging scale is varied. The discontinuities persist for all three values of the merging scale and for the two different showers and the results are heavily dependent on the merging scale. The problem is a conseqence of using different ways of defining the scales in the algorithm, which we discussed in section III.2.4. The results in the rest

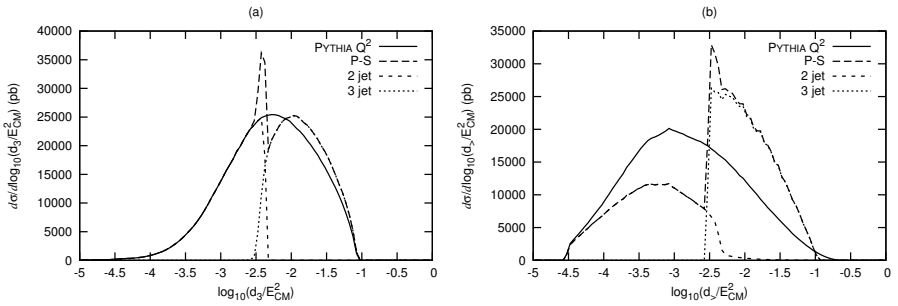

Figure III.9: The Pseudo-Shower results, with $\sqrt{d_{\mathrm{MS}}} = 5\,\mathrm{GeV}$ and $\delta = 1\,\mathrm{GeV}$, split into two- and three-jet components compared to the default shower in PYTHIA (with first order matrix element reweighting included). (a) shows the d_3 distribution at parton level and (b) is the largest d-value of the emissions in the shower.

of this section focuses on the Pseudo-Shower implemenation with a vituality ordered shower, since this was used in the original publication [3].

To demonstrate the different scales used in the algorihtm, the Pseudo-Shower results have been split up into the contributions from the two- and three-jet matrix elements. Figure III.9a shows the d_3 distribution, where it is clear that the two-jet contribution displays a sharp cut, but not the three-jet component. On the other hand, when the largest d-value of the emissions in the shower is plotted in figure III.9b, the three-jet component has a sharp cut but not the two-jet curve. This illustrates that different scales are used for the different jet multiplicities and this is the reason for the problems that appear close to the merging scale.

To further illustrate the complication with mixing scales for parton splittings and partonic jets, we show in figure III.10 the variation of the ratio between the d_3 scale on partonic jet level and the largest generated scale in the parton shower $d_>$. In a strongly ordered shower this ratio should ideally be unity, especially for the $p_\perp$-ordered PYTHIA shower in figure III.10a. However, we find that this is far from the case. Especially for the virtuality ordered shower in figure III.10b, the correlation between the different scales is very weak.

Finally two experimental observables are plotted, namely the normalized y_3 distribution for charged and neutral particles and the charged particles thrust, which are shown in figure III.11. Hadronization smoothes out most of the discontinuities shown in earlier figures, but it is clear that there are still problems. The plots show deviations from data and the results are not be independent of the merging scale.

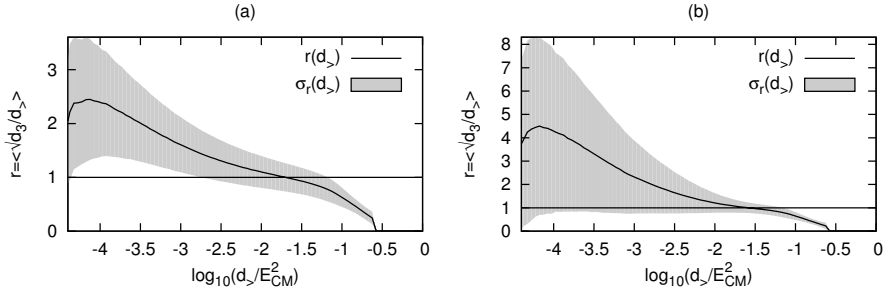

Figure III.10: The average ratio between the clustering scale d_3 for partonic jets and the generated maximum splitting scale ρ_3 in the cascade as a function of the latter. The shaded area indicates the standard deviation of the ratio. Both scales are defined as in eq. (III.25). (a) is for the $p_\perp$-ordered shower in PYTHIA, while (b) is for the virtuality ordered one.

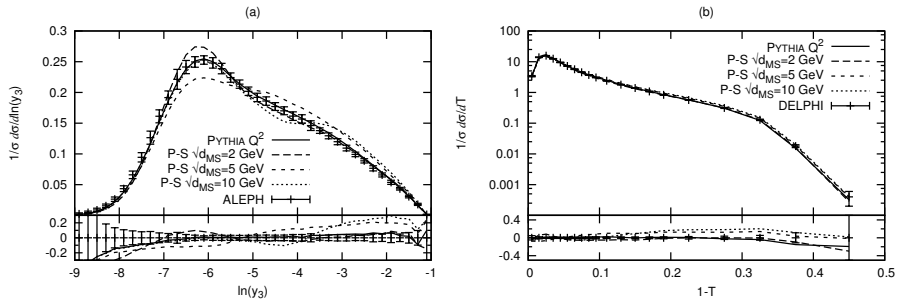

Figure III.11: The charged plus neutral particle y_3 spectra (a) and charged particle thrust spectra (b) for PYTHIA (with first order matrix element reweighting included) and for our implementation of the Pseudo-Shower algorithms with different merging scales and $\delta = 1$ GeV compared to ALEPH and DELPHI data.

III.3.4 MLM

To test MLM for e^+e^- a merging scheme and a parton–jet distance need to be chosen. Most of the MLM implementations use cone algorithms to achieve this purpose. In the case of e^+e^-, we think that a $k_\perp$-based clustering algorithm is a better choice. We have therefore decided to use the Durham $k_\perp$ algorithm to define the merging scale and matrix element cutoff.

When it comes to selecting a measure for the parton–jet distance, the natural choice would be the $k_\perp$-distance between the jet and the parton. The problem with this approach is that since the $k_\perp$-measure includes the minimum of

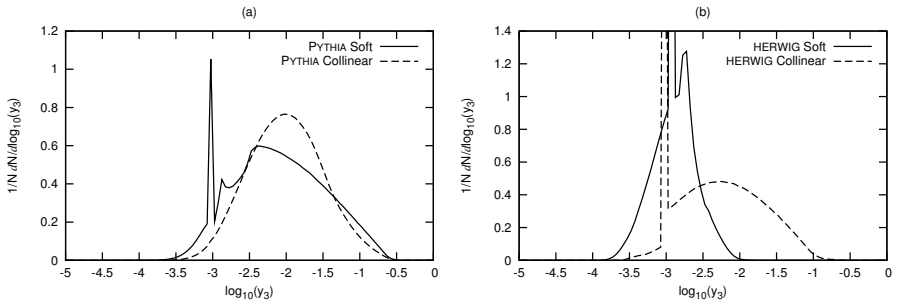

Figure III.12: The y_3 spectra at parton level for PYTHIA (a) and HERWIG (b) when starting from a state with a soft or a collinear gluon with a merging scale of $y = 10^{-3}$ and the scale in the Les Houches interface set to E_{CM}.

the two energies it means that soft partons can match jets at very wide angles, which leads to problems with convergence. Instead we modified the distance to only use the jet energy.

$$y_{\mathrm{jet,parton}} = 2E_{\mathrm{jet}}^2(1 - \cos(\theta_{\mathrm{jet,parton}}))/E_{\mathrm{CM}}^2 \tag{III.26}$$

For the highest multiplicity treatment we follow the MADEVENT implementation in [11]. For each highest multiplicity event, jets are reconstructed at a scale which is the maximum of the merging scale and the smallest distance between the partons in the matrix element level event, $\max(y_{\mathrm{MS}}, y_N)$. This scale is also used when matching the jets to partons. This allows extra jets to be produced if they are softer than those from the matrix element.

The algorithm has been implemented using MADEVENT to generate the matrix element event and both HERWIG and PYTHIA has been used to shower the events. Before we move on to the results of the merging, some important aspects of the showers need to be explained.

Step 3 in the algorithm (described in section III.2.5), where the shower is invoked, depends on how the state received from the matrix element is treated in the parton shower program. For the analysis of the merging it is important to understand how the events are treated internally. In particular the states containing soft and collinear partons require extra scrutiny since the matrix element cross section is divergent in these regions.

In the PYTHIA implementation of the Les Houches interface, the limiting factors for the radiation are the scale from the Les Houches interface, which is used as a veto, and the energy of the partons, which become the maximum kinematically allowed value for the invariant mass. No extra vetoes are applied for emissions at a wide angles. This means that even when soft or collinear partons are present some events have a lot of emissions, assuming

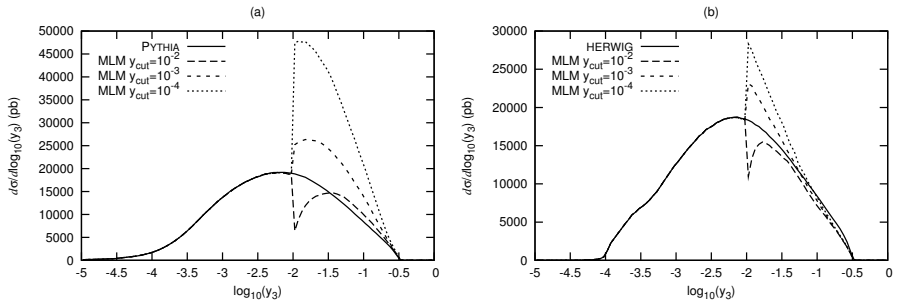

Figure III.13: (a) The y_3 spectra at parton level for default PYTHIA and our PYTHIA implementation of the MLM algorithm for $y_{\text{MS}} = 10^{-2}$ and for different values of the matrix element cutoff. (b) shows the same for HERWIG.

that the scale in the Les Houches interface is set to a high value. Figure III.12a shows the y_3 spectra for a state with a soft gluon and for one with a collinear gluon with $y_3 = 10^{-3}$ and the scale set to E_{CM}. It is obvious from the figure that a soft or collinear parton does not limit the emissions significantly.

HERWIG uses a different strategy for the internal choices of scale. Each parton is given a starting scale which is equal to the product of the four-momentum of itself and its color neighbour (if a parton has two color neighbours one is chosen at random). The parton is then boosted to the frame where it is at a right angle compared to its color neighbour and the shower invoked. Any scale set in the Les Houches interface is included as a veto on the transverse momentum (approximately given by eq. (III.25)) of the emissions. The y_3 histogram from a HERWIG shower are shown in figure III.12b starting from the same states and from the same scale as in figure III.12a. From the figure one can tell that a soft parton limits the emission from the shower quite drastically, but for a collinear parton about half of the events show significant jet activity.

Clearly, the way soft and collinear events from the matrix element give rise to hard emissions influences the jet matching veto, which is assumed to give the Sudakov suppression of these events, and the different choices of scales in the shower can have a big impact on these Sudakov form factors. This means that one has to be very careful with generalizing the MLM algorithm to different showers.

The first thing that needs to be verified with our MLM implementation is if the results converge when the matrix element cutoff is lowered. The results of the merging are shown in figure III.13 for PYTHIA and HERWIG, with a merging scale of $y_3 = 10^{-2}$ and three different values for the cutoff. No sign of convergence is visible in the figure.

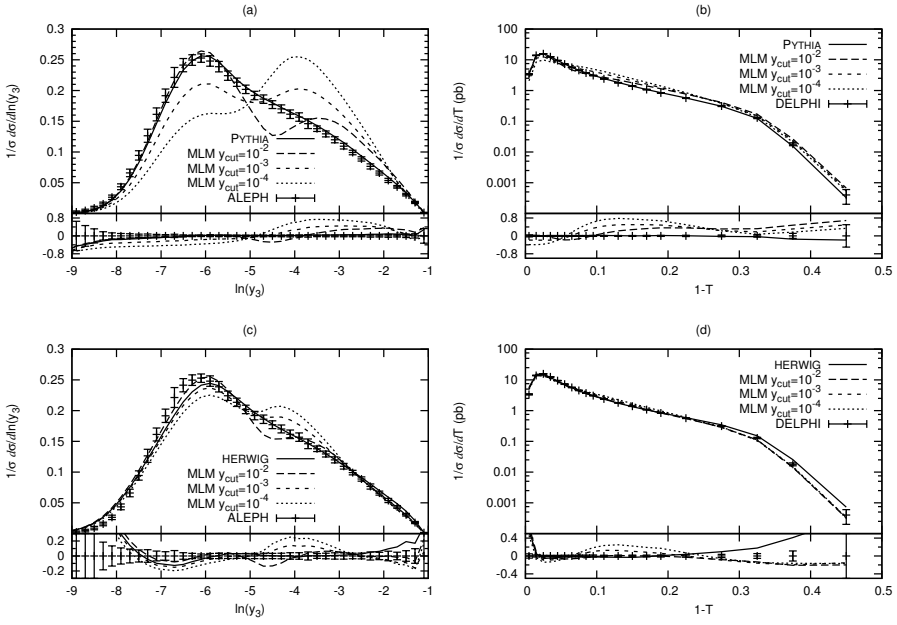

Figure III.14: The charged plus neutral particle y_3 spectra (a) and the charged particle thrust spectra (b) for default PYTHIA and our PYTHIA implementation of the MLM algorithm for three different values of the matrix element cutoff. The HERWIG results are shown in (c) and (d) respectively.

The problem is related to how HERWIG and PYTHIA treats input with soft or collinear partons. The MLM algorithm assumes that soft and collinear partons cannot produce independent jets when fed into the shower. From the earlier figures it is clear that PYTHIA can produce extra jets both for soft and collinear partons, whereas HERWIG can only produce extra jets for collinear partons. This is the reason why PYTHIA diverges faster.

The changes to the parton-level spectra is also visible in the hadron-level observables, shown in figure III.14. It is clear that changing the matrix element cutoff also affects the event shape, which diminishes the predictive power of the model.

In figure III.15 the parton-level y_3-spectra is shown with a lower merging scale. Generally one can say that the discrepancies as compared to the standard PYTHIA and HERWIG become even bigger. In HERWIG, configurations with soft gluons cannot generate hard emissions, which means a large fraction of these events are kept. There is a pole in the soft gluon limit and the cross sections for these events are therefore rather large, which leads to a continued rise

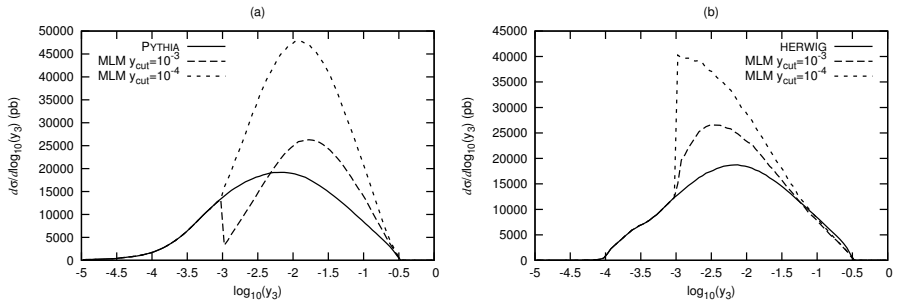

Figure III.15: (a) The y_3 spectra at parton level for default PYTHIA and our PYTHIA implementation of the MLM algorithm for $y_{\mathrm{MS}} = 10^{-3}$ and for two different values of the matrix element cutoff. (b) shows the same for HERWIG.

of the cross section of the MLM-corrected curve for low values of y_3, clearly visible in figure III.15b.

The examples above show that the MLM algorithm is very sensitive to how emission are generated and it appears to be quite tough to fix this problem. If the shower generates an emission it risks influencing things at higher jet scale and if emissions are suppressed it is not possible to control the rise of the cross section near the soft and collinear limits. In fact, even if the problems described in this section can somehow be resolved, the more fundamental problem, described in section III.2.5, that MLM uses the wrong type of Sudakov form factors remains unsolved.

III.4 Conclusions

In the previous sections, we have studied in some detail the behavior of four suggested algorithms, or schemes, for merging fixed order, tree-level matrix element generators with parton shower generators. We have done so by considering the simplest possible case of the leading order correction to the $e^+e^- \to$ hadrons process. This may not be an important use case for these merging schemes, but since it is such a simple process it is fairly easy to check whether the schemes actually accomplishes what they set out to do, namely to correctly populate the phase space above the merging scale with partons described by the full matrix element, and with emission from the parton shower below, and that they do so while correctly resumming large logarithmic contributions from soft and collinear divergencies. In addition, for this process we also have the "correct" answer available, obtained by a simple reweighting of the hardest emission in the parton shower.

Our main finding is that of the four schemes considered, only CKKW and CKKW-L meets the requirements and that even CKKW has some problems when using a parton shower with an ordering variable which is very different from the clustering variable used for the merging scale.

For CKKW-L it was claimed in [2] that the cancellation of the dependence on the merging scale is complete when using the ARIADNE dipole shower. Here we show this explicitly and also show that it is still true when using the transverse momentum ordered shower in PYTHIA. This is not a completely trivial result, because it involves an additional ambiguity in how to reconstruct the shower history for PYTHIA which is not present in ARIADNE.

In the CKKW case we also find a near complete cancellation of the merging scale dependence when using the $p_\perp$-ordered PYTHIA shower. However, when using the virtuality ordered shower in PYTHIA, we find a clear mismatch near the merging scale, and we trace this mismatch to different treatments of the no-emission probability from the gluon when it is emitted above and below the merging scale, and from possible problems in the parton shower when unordered emissions are allowed. These problems occur when the ordering variable is very different from the Durham $k_\perp$-measure used for the merging scale, which is true for the virtuality ordering, but not for the $p_\perp$-ordered shower. We expect that this is also the origin of the mismatches found in the CKKW implementation in HERWIG [3], where an elaborate tuning of the scales used in the Sudakov and α_s-reweighting was needed to minimize the merging scale dependence. Most likely a similar retuning can be done in the case of the virtuality ordered shower in PYTHIA.

For Mrennas Pseudo-Shower scheme, we find that the problems are much more severe. The main problem is that cuts made on parton level for the matrix element are made on the partonic jet level for the parton shower, and we show that this can never give the clean separation of phase spaces needed to have independence on the merging scale. This leads to a severe underestimate of the three-jet rate just above the merging scale. The fudge factor introduced in [3] can be tuned to hide the problem, but at the expense of overestimating the three-jet rate below the merging scale due to double-counting.

The MLM scheme is the simplest one to implement, in that it allows the use of any parton shower generator without modifying its internal behavior. It also uses partonic jet level cuts, but contrary to the Pseudo-Shower it tries to avoid mixing them with cuts on the few parton level. Nevertheless, an extra parton-level generation cut is needed for the matrix element. Supposedly the results should be independent on this generation cut as long as it is sufficiently smaller than the merging scale. However, we have found that this is not the case, and that the result is very sensitive to how the kinematics of the initial parton state limits emissions from the chosen parton shower. If the emissions are not limited, events generated close to the generation cut will always have a

finite possibility to end up above the merging scale, which makes the scheme very sensitive to the generation cut. If, on the other hand, the emissions are limited by the kinematics, there is no possibility to obtain the necessary Sudakov suppression of soft and collinear divergencies. It is not inconceivable that the generation cut can be tuned, possibly together with the scale used in the α_s-weighting, to get reasonably smooth distributions, but we feel that this is just hiding the fact that the MLM scheme has serious flaws.

Having done this investigation of the behavior of the algorithms for the simplest possible process, the question is if we can make some conclusions for more complicated processes. Or course, if a scheme does not handle this simple process well, it is not likely that the situation will improve for more complicated ones. But also in the case of CKKW-L, complications may occur.

As we go to higher parton multiplicities in the matrix element, we expect that the actual matrix element correction becomes larger, necessarily giving rise to discontinuities near the merging scale. These discontinuities should disappear as the merging scale is lowered and the parton shower splittings become a good approximation to the full matrix element. However, for this to work there must not be any artificial dependencies on the merging scale in the merging algorithm as such, which we have seen is not the case for all schemes.

The really interesting processes are in hadron collisions, where *e.g.* the standard model production of a W together with several hard jets is an important background to almost any search for new phenomena. Here the matching is complicated as the parton showers also includes initial state evolution of the incoming partons. Also, care must be taken to treat the parton densities in a consistent way. This was first investigated for the CKKW scheme in [5], and later for ARIADNE implementation of CKKW-L in [12]. For the latter it was shown that the merging scale dependence does indeed cancel for the leading order correction to W-production. Although it has not been checked explicitly for the other schemes, there is no reason to expect that the problems we have found in this paper will go away.

Having said all this, we must ask ourselves how severe the deficiencies we have found here would be for practical applications at *e.g.* the LHC. We are, after all, dealing with tree-level matrix elements and leading log parton showers which means we will in any case expect large scale dependencies. And surely these deficiencies results in much smaller uncertainties as compared to using parton showers without matrix element corrections. Indeed, it was shown in [11] that CKKW, CKKW-L and different MLM implementations all give consistent results for realistic experimental observables within reasonable variations of the scales used in α_s and parton densities. In fact the most severe disagreement found was for the ARIADNE implementation of CKKW-L. However, this had nothing to do with the merging scheme, but is a consequence of the radically different treatment of the phase space available

for initial-state radiation in ARIADNE as such, which includes a resummation of some logarithms of x, not present in conventional initial-state showers.

In [1] a large effort was put into showing that the dependence of the merging scale vanishes at next-to-leading logarithmic accuracy for CKKW, at least for a shower which is ordered in the Durham $k_\perp$ variable. Here we have shown that for the three-jet observables considered here, the dependence vanishes completely for CKKW-L. For the Pseudo-shower, the situation is more difficult to analyze. In the strongly ordered limit we argue that it is equivalent to CKKW-L, which indicates that the dependence on the merging scale should cancel, at least to leading double-logarithmic accuracy, nevertheless the dependence is quite large in absolute numbers. For MLM, it is clear that for the observables considered here, it is questionable if it can reproduce the correct Sudakov form factors, indicating a dependence on the merging scale (or rather the cutoff in the matrix element generation) already on the leading double-logarithmic level. We plan to return in a future publication with a more formal investigation of the logarithmic accuracy of the merging scales.

In absolute numbers, we have seen that the Pseudo-Shower and the MLM schemes, and even CKKW for some parton showers, have problems with correctly populating different regions of phase space. And even if this can be smoothed out by introducing additional cuts on the matrix element generation (for MLM), a fudge factor (for Pseudo-Shower) or separately varying the scale in the α_s and Sudakov reweighting (for CKKW with HERWIG [3]) it necessarily means introducing extra parameters which need to be tuned. Indeed, it is not inconceivable that these extra parameters need to be tuned differently for different processes and merging scales, and maybe even for different observables. As a consequence, the predictability of the models will be reduced.

Acknowledgments

We thank Frank Krauss, Peter Richardson, Torbjörn Sjöstrand and Stephen Mrenna for useful discussions. Work supported in part by the Marie Curie research training network "MCnet" (contract number MRTN-CT-2006-035606).

III.A Different scale definitions in CKKW

To illustrate the origin of the discontinuities found for CKKW when used with the virtuality-ordered shower in PYTHIA, we here look at the somewhat artificial example of calculating the differential exclusive three-jet rate, where we use the notation introduced in section III.2.3.

Assume the parton shower has ordering in ρ, and has auxiliary splitting variables, $\vec{x}$, and that the Durham $k_\perp$-measure can be written as a function of

these variables, $y = y(\rho, \vec{x})$. Now we can write the differential exclusive three-jet rate above some ρ_0 for the plain parton shower case:

$$\frac{d\sigma_3^{\mathrm{PS}}}{\sigma_0} = \Delta_{S_2}^{\mathrm{PS}}(\rho_{\max}, \rho)\Gamma_{S_2}^{\mathrm{PS}}(\rho, \vec{x})\Delta_{S_3}^{\mathrm{PS}}(\rho, \rho_0)d\rho\, d^k\vec{x} \tag{III.27}$$

where $\Delta_{S_2}(\rho_{\max}, \rho)$ is the Sudakov corresponding to the no-emission probability from the two-parton state above ρ, and $\Delta_{S_3}(\rho, \rho_0)$ is the no-emission probability from the three-parton state below ρ. We can also write the corresponding rate for the CKKW scheme:

$$\begin{aligned}\frac{d\sigma_3^{\mathrm{CKKW}}}{\sigma_0} &\approx \Delta_{S_2}^{\mathrm{CKKW}}(y_{\max}, y)\Gamma_{S_2}^{\mathrm{ME}}(\rho, \vec{x}) \times \\ &\quad \Delta_{S_2}^{\mathrm{PS}}(\rho_{\max}, \rho; < y)\Delta_{S_3}^{\mathrm{PS}}(\rho, \rho_0; < y)d\rho\, d^k\vec{x}\end{aligned} \tag{III.28}$$

where $\Delta_{S_2}^{\mathrm{CKKW}}(y_{\max}, y)$ is the analytic Sudakov form factor used for reweighting, and $\Delta_{S_3}^{\mathrm{PS}}(\rho, \rho_0; < y)$ is the parton shower no-emission probability from the three-parton state between ρ and ρ_0 excluding phase space region corresponding to the vetoed emissions with Durham $k_\perp$ above $y(\rho, \vec{x})$. $\Delta_{S_2}^{\mathrm{PS}}(\rho_{\max}, \rho; < y)$ is the corresponding no-emission probability for the two-parton state, which approximates the no-emission probability for the three-parton state above the scale ρ where the gluon is not allowed to radiate — an approximation which is valid as long as the gluon is not too hard. Now the CKKW Sudakov can be approximately written as the no-emission probability

$$\begin{aligned}\Delta_{S_2}^{\mathrm{CKKW}}(y_{\max}, y) &\approx \Delta_{S_2}^{\mathrm{PS}}(\rho_{\max}, \rho_0; > y) \\ &= \Delta_{S_2}^{\mathrm{PS}}(\rho_{\max}, \rho; > y)\Delta_{S_2}^{\mathrm{PS}}(\rho, \rho_0; > y),\end{aligned} \tag{III.29}$$

where the $> y$ notation indicates that only emissions with Durham $k_\perp$ above y are considered. Also, we can write

$$\Delta_{S_2}^{\mathrm{PS}}(\rho_{\max}, \rho) = \Delta_{S_2}^{\mathrm{PS}}(\rho_{\max}, \rho; > y)\Delta_{S_2}^{\mathrm{PS}}(\rho_{\max}, \rho; < y) \tag{III.30}$$

and

$$\Delta_{S_3}^{\mathrm{PS}}(\rho, \rho_0) = \Delta_{S_3}^{\mathrm{PS}}(\rho, \rho_0; > y)\Delta_{S_3}^{\mathrm{PS}}(\rho, \rho_0; < y) \tag{III.31}$$

We can now rewrite the two three-jet rates as

$$\begin{aligned}\frac{d\sigma_3^{\mathrm{PS}}}{\sigma_0} &= \Gamma_{S_2}^{\mathrm{PS}}(\rho, \vec{x})\Delta_{S_2}^{\mathrm{PS}}(\rho_{\max}, \rho; > y)\Delta_{S_2}^{\mathrm{PS}}(\rho_{\max}, \rho; < y) \times \\ &\quad \Delta_{S_3}^{\mathrm{PS}}(\rho, \rho_0; > y)\Delta_{S_3}^{\mathrm{PS}}(\rho, \rho_0; < y)d\rho\, d^k\vec{x} \\ \frac{d\sigma_3^{\mathrm{CKKW}}}{\sigma_0} &= \Gamma_{S_2}^{\mathrm{ME}}(\rho, \vec{x})\Delta_{S_2}^{\mathrm{PS}}(\rho_{\max}, \rho; > y)\Delta_{S_2}^{\mathrm{PS}}(\rho, \rho_0; > y) \times \\ &\quad \Delta_{S_2}^{\mathrm{PS}}(\rho_{\max}, \rho; < y)\Delta_{S_3}^{\mathrm{PS}}(\rho, \rho_0; < y)d\rho\, d^k\vec{x}\end{aligned} \tag{III.32}$$

And we find that the only difference, besides the desired $\Gamma^{\mathrm{PS}}_{S_2} \to \Gamma^{\mathrm{ME}}_{S_2}$, is that in the plain shower has a no-emission probability $\Delta^{\mathrm{PS}}_{S_3}(\rho, \rho_0; > y)$ where CKKW has $\Delta^{\mathrm{PS}}_{S_2}(\rho, \rho_0; > y)$. This can be seen as an extra suppression in the plain parton shower due to the no-emission probability from the gluon at a shower scale below ρ but at a Durham $k_\perp$-scale above y. Now if the ordering variable ρ is close to the Durham $k_\perp$, this region will be very small and the mismatch will be small, as we saw in the case of the $p_\perp$-ordered PYTHIA shower. But for the virtuality ordering in PYTHIA we have

$$y = \min\left(\frac{z}{1-z}, \frac{1-z}{z}\right)\frac{Q^2}{E^2_{\mathrm{CM}}} \tag{III.33}$$

and similarly for the angular ordering variable, ξ, in HERWIG we have

$$y = \min(z^2, (1-z)^2)\frac{E^2\xi}{E^2_{\mathrm{CM}}}, \tag{III.34}$$

(where E is the energy of the parent parton in the splitting) and, hence, the region can become quite large, especially in the regions $z \to 0$ or 1, where the probability of an emission is large. We note, however, that in PYTHIA the effect is limited by the presence of an additional angular ordering veto in addition to the virtuality ordering.

III References

[1] S. Catani, F. Krauss, R. Kuhn, and B. R. Webber, "QCD matrix elements + parton showers," *JHEP* **11** (2001) 063, arXiv:hep-ph/0109231.

[2] L. Lönnblad, "Correcting the colour-dipole cascade model with fixed order matrix elements," *JHEP* **05** (2002) 046, arXiv:hep-ph/0112284.

[3] S. Mrenna and P. Richardson, "Matching matrix elements and parton showers with HERWIG and PYTHIA," *JHEP* **05** (2004) 040, arXiv:hep-ph/0312274.

[4] M. Mangano, "The so-called MLM prescription for ME/PS matching." http://www-cpd.fnal.gov/personal/mrenna/tuning/nov2002/mlm.pdf. Talk presented at the Fermilab ME/MC Tuning Workshop, October 4, 2002.

[5] F. Krauss, "Matrix elements and parton showers in hadronic interactions," *JHEP* **08** (2002) 015, arXiv:hep-ph/0205283.

[6] T. Gleisberg *et al.*, "SHERPA 1.alpha, a proof-of-concept version," *JHEP* **02** (2004) 056, arXiv:hep-ph/0311263.

[7] G. Corcella *et al.*, "HERWIG 6.5: an event generator for Hadron Emission Reactions With Interfering Gluons (including supersymmetric processes)," *JHEP* **01** (2001) 010, arXiv:hep-ph/0011363.

[8] F. Krauss, A. Schalicke, S. Schumann, and G. Soff, "Simulating W / Z + jets production at the Tevatron," *Phys. Rev.* **D70** (2004) 114009, arXiv:hep-ph/0409106.

[9] F. Krauss, A. Schalicke, S. Schumann, and G. Soff, "Simulating W / Z + jets production at the CERN LHC," *Phys. Rev.* **D72** (2005) 054017, arXiv:hep-ph/0503280.

[10] T. Gleisberg, F. Krauss, A. Schalicke, S. Schumann, and J.-C. Winter, "Studying W+ W- production at the Fermilab Tevatron with SHERPA," *Phys. Rev.* **D72** (2005) 034028, arXiv:hep-ph/0504032.

[11] J. Alwall *et al.*, "Comparative study of various algorithms for the merging of parton showers and matrix elements in hadronic collisions," *Eur. Phys. J.* **C53** (2008) 473–500, arXiv:0706.2569 [hep-ph].

[12] N. Lavesson and L. Lönnblad, "W + jets matrix elements and the dipole cascade," *JHEP* **07** (2005) 054, arXiv:hep-ph/0503293.

[13] L. Lönnblad, "ARIADNE version 4: A Program for simulation of QCD cascades implementing the color dipole model," *Comput. Phys. Commun.* **71** (1992) 15–31.

[14] T. Sjostrand, L. Lonnblad, S. Mrenna, and P. Skands, "PYTHIA 6.3: Physics and manual," arXiv:hep-ph/0308153.

[15] M. L. Mangano, M. Moretti, F. Piccinini, R. Pittau, and A. D. Polosa, "ALPGEN, a generator for hard multiparton processes in hadronic collisions," *JHEP* **07** (2003) 001, arXiv:hep-ph/0206293.

[16] J. Alwall *et al.*, "MadGraph/MadEvent v4: The New Web Generation," *JHEP* **09** (2007) 028, arXiv:0706.2334 [hep-ph].

[17] A. Cafarella, C. G. Papadopoulos, and M. Worek, "Helac-Phegas: a generator for all parton level processes," arXiv:0710.2427 [hep-ph].

[18] M. L. Mangano, M. Moretti, and R. Pittau, "Multijet matrix elements and shower evolution in hadronic collisions: W b bbar + n jets as a case study," *Nucl. Phys.* **B632** (2002) 343–362, arXiv:hep-ph/0108069.

[19] M. L. Mangano, M. Moretti, F. Piccinini, and M. Treccani, "Matching matrix elements and shower evolution for top- quark production in hadronic collisions," *JHEP* **01** (2007) 013, arXiv:hep-ph/0611129.

[20] G. Gustafson and U. Pettersson, "Dipole formulation of QCD cascades," *Nucl. Phys.* **B306** (1988) 746.

[21] M. Bengtsson and T. Sjostrand, "Coherent parton showers versus matrix elements: implications of PETRA - PEP data," *Phys. Lett.* **B185** (1987) 435.

[22] M. H. Seymour, "A Simple prescription for first order corrections to quark scattering and annihilation processes," *Nucl. Phys.* **B436** (1995) 443–460, arXiv:hep-ph/9410244.

[23] M. H. Seymour, "Matrix element corrections to parton shower algorithms," *Comp. Phys. Commun.* **90** (1995) 95–101, arXiv:hep-ph/9410414.

[24] S. Frixione and B. R. Webber, "Matching NLO QCD computations and parton shower simulations," *JHEP* **06** (2002) 029, arXiv:hep-ph/0204244.

[25] S. Frixione and B. R. Webber, "The MC@NLO 3.3 event generator," arXiv:hep-ph/0612272.

[26] P. Nason, "A new method for combining NLO QCD with shower Monte Carlo algorithms," *JHEP* **11** (2004) 040, arXiv:hep-ph/0409146.

[27] P. Nason and G. Ridolfi, "A positive-weight next-to-leading-order Monte Carlo for Z pair hadroproduction," *JHEP* **08** (2006) 077, arXiv:hep-ph/0606275.

[28] S. Frixione, P. Nason, and C. Oleari, "Matching NLO QCD computations with Parton Shower simulations: the POWHEG method," *JHEP* **11** (2007) 070, arXiv:0709.2092 [hep-ph].

[29] M. Kramer, S. Mrenna, and D. E. Soper, "Next-to-leading order QCD jet production with parton showers and hadronization," *Phys. Rev.* **D73** (2006) 014022, arXiv:hep-ph/0509127.

[30] Z. Nagy and D. E. Soper, "Matching parton showers to NLO computations," *JHEP* **10** (2005) 024, arXiv:hep-ph/0503053.

[31] Z. Nagy and D. E. Soper, "Parton showers with quantum interference," *JHEP* **09** (2007) 114, arXiv:0706.0017 [hep-ph].

[32] W. T. Giele, D. A. Kosower, and P. Z. Skands, "A Simple shower and matching algorithm," *Phys. Rev.* **D78** (2008) 014026, arXiv:0707.3652 [hep-ph].

[33] C. W. Bauer, F. J. Tackmann, and J. Thaler, "GenEvA (I): A new framework for event generation," *JHEP* **12** (2008) 010, arXiv:0801.4026 [hep-ph].

[34] C. W. Bauer, F. J. Tackmann, and J. Thaler, "GenEvA (II): A phase space generator from a reweighted parton shower," *JHEP* **12** (2008) 011, arXiv:0801.4028 [hep-ph].

[35] S. Catani, Y. L. Dokshitzer, M. Olsson, G. Turnock, and B. R. Webber, "New clustering algorithm for multi - jet cross-sections in e+ e- annihilation," *Phys. Lett.* **B269** (1991) 432–438.

[36] A. Schalicke and F. Krauss, "Implementing the ME+PS merging algorithm," *JHEP* **07** (2005) 018, arXiv:hep-ph/0503281.

[37] T. Sjostrand, S. Mrenna, and P. Skands, "PYTHIA 6.4 physics and manual," *JHEP* **05** (2006) 026, arXiv:hep-ph/0603175.

[38] E. Boos *et al.*, "Generic user process interface for event generators," arXiv:hep-ph/0109068.

[39] **ALEPH** Collaboration, A. Heister *et al.*, "Studies of QCD at e+ e- centre-of-mass energies between 91-GeV and 209-GeV," *Eur. Phys. J.* **C35** (2004) 457–486.

[40] **DELPHI** Collaboration, P. Abreu *et al.*, "Tuning and test of fragmentation models based on identified particles and precision event shape data," *Z. Phys.* **C73** (1996) 11–60.

[41] T. Sjostrand and P. Z. Skands, "Transverse-momentum-ordered showers and interleaved multiple interactions," *Eur. Phys. J.* **C39** (2005) 129–154, `arXiv:hep-ph/0408302`.

[42] G. Gustafson, "Dual description of a confined color field," *Phys. Lett.* **B175** (1986) 453.

[43] L. Lönnblad, "ARCLUS: A New jet clustering algorithm inspired by the color dipole model," *Z. Phys.* **C58** (1993) 471–478.

[44] T. Sjostrand, "The Lund Monte Carlo for e+ e- Jet Physics," *Comput. Phys. Commun.* **28** (1983) 229.

IV

Extending CKKW-merging to one-loop matrix elements

Nils Lavesson and Leif Lönnblad

Department of Theoretical Physics, Lund University,
Sölvegatan 14A, SE–223 62 Lund, Sweden

Journal of High Energy Physics **12** (2008) 070 [arXiv:0811.2912].

We extend earlier schemes for merging tree-level matrix elements with parton showers to include also merging with one-loop matrix elements. In this paper we make a first study on how to include one-loop corrections, not only for events with a given jet multiplicity, but simultaneously for several different jet multiplicities. Results are presented for the simplest non-trivial case of hadronic events at LEP as a proof of concept.

IV.1 Introduction

One of the big theoretical challanges with LHC physics is the description of states with many hard jets. The high energy and large rapidity range for jets at the LHC means that producing multi-jet events from QCD processes is more likely than ever before. These states compose the background for many of the channels that could contain new physics. It is therefore important to get as good description as possible for the multi-jet states within QCD.

Monte Carlo event generators have become standard tools for simulating events in a particle collider. These event generators try to simulate events with all the characteristics of a real event. The theoretical basis is a parton shower, which is combinded with hadronization models to produce the final-state hadrons. The hadronization models are phenomenological models that only work reliably when all the partons in the soft and collinear limit have been simulated corretly in the shower. Parton showers are based on expanding the emission probabilities in this limit, which makes them suitable to use together with the hadronization models. Although parton showers have been used to describe a wide range of results with good accuracy, it is well known that they cannot give a good description of observables sensitive to emissions away from the collinear and soft regions.

The way to improve the description of multi-jet states is to include exact matrix elements. The matrix elements describe these states well, but do not provide a way of describing emissions in the soft or collinear limit. In fact, the matrix elements are divergent in these limits and have to be regulated using a cutoff. To correctly describe the final-state hadrons in multi-jet events, the matrix elements and the parton shower descriptions need to be combined. This has been done for tree-level matrix elements using algorithms such as CKKW [1, 2], CKKW-L [3, 4], MLM [5, 6] and Pseudo-Shower [7].

In recent years a lot of effort has been put into calculating one-loop matrix elements to be able to predict observables to next-to-leading order (NLO) accuracy. There are several program available to do this, *e.g.* MCFM [8] and NLOJET++ [9]. Currently efforts are being made to automate the whole procedure and make more processes available, including significantly higher parton muliplicities (MCFM and BlackHat [10]). The one-loop matrix element calculations contain important QCD contributions which cannot be simulated with tree-level matrix elements nor with parton showers. Preferably both the tree-level and one-loop matrix elements as well as the parton shower should be used consistently together. Lacking such a complete description, the uncertainties in a given NLO calculation due to parton showers and hadronization are typically estimated using a separate approximate Monte Carlo simulation. Alternatively, for certain observables, it is possible to combine a NLO calculation with analytically resummed parton-shower correction together with a

semi-universal power correction giving the hadronization correction. However, it would clearly be advantegous if the one-loop matrix elements could be used together with parton showers and hadronization models in a more consistent manner.

A few algorithms have been presented to merge one-loop matrix elements with parton showers. The two main algorithms are MC@NLO [11, 12] and POWHEG [13, 14], but they are limited to only include the one-loop matrix element for the lowest order process. A similar algorihtm for e^+e^- to three jets was presented in [15–17]. Other groups have made proposals on how to go beyond this and include one-loop matrix elements also for higher multiplicities [18–21][1], but none have so far presented a complete implementation.

In this paper we present a general algorithm to include one-loop matrix elements of any order in the strong coupling together with parton showers. The idea is to take the first two terms in orders of α_s from the one-loop matrix element and all higher order terms from the parton shower. Two different events samples are generated. The first sample consists of events which are generated according to one-loop matrix elements and dressed using a parton shower. The second sample are events generated with a parton shower corrected with tree-level matrix elements, where the first two terms in the α_s-expansion has been subtracted. The procedure is applied to all the different multiplicities one wishes to calculate and in the end all the samples are added.

Calculating the first two terms in orders of α_s in the shower introduces complications because they include the first term in an expansion of the Sudakov form factor. In addition the running α_s used in the shower also gives a contribution to the terms at this order. These complications need to be dealt with in order to have a consistent algorithm.

Our method uses the same philosophy as CKKW-L, which means that phase space is split up in two different regions using a merging scale, and the corrections to the matrix elements are simulated using the shower. However, it should be noted that most of what is presented here could also be used together with the CKKW algorithm, where the corrections are calculated analytically. Using the shower rather than doing analytical calculation means that non-leading terms, such as energy–momentum conservation and recoil treatments, included in the shower, are also included in the corrections to the matrix elements.

Although it would be more interesting to simulate jets at the LHC, we limit ourselves to LEP physics in this paper. The reason is that the inclusion of parton densities causes a number of additional complications that needs to be studied further before an algorithm valid also for incoming hadrons can be presented.

The outline of this paper is the following. In section IV.2 some key concepts

[1] In particular [18] is very close in spirit to the strategy presented here.

of parton shower and matrix elments are reviewed, which are then used in the description of the merging. Section IV.3 describes the various steps in the algorithm and how to calculate all the terms needed. The algorithm is implemented toghether with ARIADNE [22] and the results are presented in section IV.4. Finally in section IV.5 our conclusions are presented.

IV.2 Theory

This section contains some basic properties of parton showers and matrix elements, including both tree-level and one-loop matrix elements. After the theoretical background has been established our algorithm for merging one-loop matrix elements and parton shower is presented.

IV.2.1 Parton showers

Emissions in the soft and collinear limit can be resummed to all orders using a parton shower. This is done using only the dominant behavior in this limit, which is translated into an emission probablility. The other main component is the assumption that the emissions can be ordered. To make the results exclusive, the probability for emitting a parton also includes the probability that no emission has occured at a higher scale, which is known as a Sudakov form factor. The result is a formalism where each emission can be considered individually and generated according to a resonably simple probability distribution, which is ideal for computer simulations.

The parton shower is a good approximation for emissions near the soft and collinear limits and can give a nice description for a large range of observables, since the approximation is valid for the bulk of the cross section. There are important exceptions though, which occur mainly when you have several hard partons emitted at wide angle.

Different shower models use different choices to specify the ordering variable, the most common choices being transverse momentum, angle and virtuality. To formulate the parton cross sections in a general way we simply denote the ordering variable ρ. The emission probability is the product of a splitting function, which is a function of the emissions kinematics, and the stong coupling α_s. Most showers use a running α_s with a transverse momentum as the scale, which is not necessarily equal to the ordering variable. However, here we assume that the ordering variable is the same as the scale in α_s for notiational convenience. The cross sections for the parton multiplicities for a shower that has evolved down to the shower cutoff (ρ_c) can be written in the following way.

$$
\begin{aligned}
d\sigma_0 &= C_0^{\mathrm{PS}}(\Omega_0^{\mathrm{PS}})\,\Delta_{S_0}(\rho_0,\rho_c)d\Omega_0^{\mathrm{PS}}\\
d\sigma_1 &= C_1^{\mathrm{PS}}(\Omega_1^{\mathrm{PS}})\,\alpha_{\mathrm{s}}(\rho_1)\Delta_{S_0}(\rho_0,\rho_1)\Delta_{S_1}(\rho_1,\rho_c)d\Omega_1^{\mathrm{PS}}\\
d\sigma_2 &= C_2^{\mathrm{PS}}(\Omega_2^{\mathrm{PS}})\,\alpha_{\mathrm{s}}(\rho_1)\alpha_{\mathrm{s}}(\rho_2)\Delta_{S_0}(\rho_0,\rho_1)\Delta_{S_1}(\rho_1,\rho_2)\Delta_{S_2}(\rho_2,\rho_c)d\Omega_2^{\mathrm{PS}}\\
&\vdots\\
d\sigma_n &= C_n^{\mathrm{PS}}(\Omega_n^{\mathrm{PS}})\Delta_{S_n}(\rho_n,\rho_c)\prod_{i=1}^{n}\alpha_{\mathrm{s}}(\rho_i)\Delta_{S_{i-1}}(\rho_{i-1},\rho_i)d\Omega_n^{\mathrm{PS}}\\
&\vdots
\end{aligned}
\tag{IV.1}
$$

The parton shower phase space is described by

$$
\Omega_n^{\mathrm{PS}} = (\mathbf{q}_1,\ldots,\mathbf{q}_m,\rho_1,\vec{x}_1,\rho_2,\vec{x}_2,\ldots,\rho_n,\vec{x}_n), \tag{IV.2}
$$

where $\mathbf{q}$ denotes the momenta of the m (usually two) outgoing partons at Born level, ρ is the value of the ordering variable and $\vec{x}$ are the other kinematical variables that describe each emission. $\Delta_{S_n}(\rho_n,\rho_{n+1})$ denotes the Sudakov form factor, which is the probability that no emission occurs from the n-parton state, S_n, between the scales ρ_n and ρ_{n+1}, and the C_n^{PS}-coefficients are the Born-level matrix element multiplied with the products of splitting functions in the shower and depend on all ρ_i and $\vec{x}_i$ with $i \leq n$.

The Sudakov form factors in the shower is an approximate way of calculating the virtual diagrams to all orders. In the angular ordered shower in HERWIG this is done by an analytical calculation based on the production scales of the various partons, but other showers, such as the parton showers in PYTHIA and the dipole shower in ARIADNE, uses the actual parton state when calculating the Sudakov form factor as an explicit no-emission probability. The algorithm described in later sections require Sudakov form factors that factorize ($\Delta_{S_i}(\rho_1,\rho_2)\Delta_{S_i}(\rho_2,\rho_3) = \Delta_{S_i}(\rho_1,\rho_3)$), which is the case if the Sudakov form factors only depend on the intermediate state. In this paper the notation used reflects the dependency on the parton state, which is denoted by a subscript. The Sudakov form factors can explicitly be written

$$
\Delta_{S_n}(\rho_i,\rho_{i+1}) = \exp\left(-\int_{\rho_{i+1}}^{\rho_i} d\rho\alpha_{\mathrm{s}}(\rho)\Gamma_{S_n}(\rho)\right), \tag{IV.3}
$$

where Γ denotes the branching probability for the specific parton state.

It should be noted that the way the virtual corrections are approximated in the shower means that the sum of all the parton cross sections is equal to the Born cross section:

$$
\sum_{i=0}^{\infty}\sigma_i = \int C_0^{\mathrm{PS}}(\Omega_0^{\mathrm{PS}})d\Omega_0^{\mathrm{PS}} = \sigma_{\mathrm{Born}}. \tag{IV.4}
$$

This means that the parton shower does not properly approximate the higher-order corrections to the total cross section. Instead it is common to include a *K*-factor by scaling all the cross sections with the N^{l}LO cross section divided by the Born cross section. However, it does nothing to improve the shape observables or the relative abundance of different parton multiplicities.

Measurements of α_s have been done with better and better accuracy, typically using precision data from LEP (see *e.g.* [23]). If the same values of α_s would be used within a parton shower it would not describe data well. The reason is that the shower has a tendency to underestimate emission probabilities, especially for hard emissions. The shower therefore gives a better description of data if a higher value of α_s is used. To get the best possible fit, the parton shower implementations usually make α_s tunable. This is frequently done by doing a one- or two-loop α_s evolution and making Λ_{QCD} a parameter to be fit to data.

Making α_s tunable is equal to modifying the scale used in the evaluation of α_s, apart from corrections related to flavour thresholds. This means that it is possible to use a different scale when evaluating α_s and use the world average α_s from precision measurements, which is illustrated in the equation below.

$$\alpha_s^{\text{PS}}(\rho) \quad = \quad \alpha_s^{\text{WA}}(b\rho) \tag{IV.5}$$

This is something that is used in later sections of this paper.

It is possible to expand the parton cross sections in the shower in powers of α_s. To do this the exponential in each Sudakov form factors has to be expanded and the running of the coupling taken into account. The relative change of the cross section at each order of α_s is denoted by $c_{n,m}$, where n is the order in α_s of the relevant tree diagram and m is the number of loops. Using a renormalization scale, μ, the parton cross sections in eq. (IV.1) can be written as

$$\begin{aligned}
d\sigma_0 &= C_0^{\text{PS}}(\Omega_0^{\text{PS}})\,(1 + c_{0,1}^{\text{PS}}(\Omega_0^{\text{PS}})\alpha_s(\mu) + c_{0,2}^{\text{PS}}(\Omega_0^{\text{PS}},\mu)\alpha_s^2(\mu) + \ldots)d\Omega_0^{\text{PS}} \\
d\sigma_1 &= C_1^{\text{PS}}(\Omega_1^{\text{PS}})\,\alpha_s(\mu)(1 + c_{1,1}^{\text{PS}}(\Omega_1^{\text{PS}},\mu)\alpha_s(\mu) + c_{1,2}^{\text{PS}}(\Omega_1^{\text{PS}},\mu)\alpha_s^2(\mu) + \ldots)d\Omega_1^{\text{PS}} \\
d\sigma_2 &= C_2^{\text{PS}}(\Omega_2^{\text{PS}})\,\alpha_s^2(\mu)(1 + c_{2,1}^{\text{PS}}(\Omega_2^{\text{PS}},\mu)\alpha_s(\mu) + c_{2,2}^{\text{PS}}(\Omega_2^{\text{PS}},\mu)\alpha_s^2(\mu) + \ldots)d\Omega_2^{\text{PS}} \\
&\vdots \\
d\sigma_n &= C_n^{\text{PS}}(\Omega_2^{\text{PS}})\alpha_s^n(\mu)(1 + c_{n,1}^{\text{PS}}(\Omega_n^{\text{PS}},\mu)\alpha_s(\mu) + c_{n,2}^{\text{PS}}(\Omega_n^{\text{PS}},\mu)\alpha_s^2(\mu) + \ldots)d\Omega_n^{\text{PS}} \\
&\vdots
\end{aligned} \tag{IV.6}$$

All the higher order changes to the cross section (except $c_{0,1}$ in case the Born level contains no powers of α_s, which is assumed here) have a dependence on

the renormalization scale, when one expands in terms of a fixed coupling constant. This happens because the shower uses a running α_s and when changing the scale to μ there are residual terms that needs to be absorbed into the parton shower coefficients. These effects are described further in later sections.

Note that the parton shower provides a value for the parton cross sections that includes terms of all orders in α_s, but the coefficients are only approximately correct. The goal of merging algorithms is to replace some of the coefficients by the exact results in order to minimize the effects of the approximations done in the parton shower. In the following we discuss how these terms can be calculated and what kind of results one can achieve.

IV.2.2 Matrix elements

Processes calculated through matrix elements means that one is calculating the amplitudes of the Feynman diagrams directly. This is easy to do for $2 \to 2$ processes, but gets increasingly difficult for larger number of external legs or if one includes loops.

To calculate an observable using matrix elements is equivalent to exactly calculating the terms in an α_s expansion one term at a time. The advantage of matrix elements is that they are exact up to the calculated order. In certain regions of phase space this approach works fine, but for collinear and soft emissions there are divergencies in the matrix elements which prevents the α_s expansion from converging.

The leading order term for final states with several outgoing partons are tree-level matrix elements (no loops). If one expands the differential cross sections in different multiplicities one arrives at the following

$$\begin{aligned} d\sigma_0 &= C_0^{\mathrm{ME}}(\Omega_0)\, d\Omega_0 \\ d\sigma_1 &= C_1^{\mathrm{ME}}(\Omega_1)\, \alpha_s d\Omega_1 \\ d\sigma_2 &= C_2^{\mathrm{ME}}(\Omega_2)\, \alpha_s^2 d\Omega_2 \\ &\vdots \\ d\sigma_n &= C_n^{\mathrm{ME}}(\Omega_n)\, \alpha_s^n d\Omega_n \\ &\vdots \end{aligned} \tag{IV.7}$$

where we have used the short-hand notation

$$\Omega_n = (\mathbf{p}_1, \ldots, \mathbf{p}_{n+m}). \tag{IV.8}$$

Here $\mathbf{p}$ is used to denote the momenta of the outgoing partons in the matrix element. The Born-level diagram considered has m outgoing partons and

n denotes the number of extra outgoing partons. For simplicity we assume throughout that the Born-level cross sections does not contain any powers of α_s, but this requirement can easily be relaxed.

The tree-level expansion is divergent and one needs to introduce a phase-space cut to avoid collinear and soft configurations. Another important property of tree-level matrix elements is that they describe inclusive quantities. If one, *e.g.*, integrates the three-parton matrix element according to a jet definition, this yields the cross section for a configuration with *at least* three jets.

There a several methods for calculating tree-level matrix elements which have been implemented as parts of automated programs. These programs generate all the possible diagrams, sum them and generate events accordingly. Examples of such programs include MADEVENT [24] and ALPGEN [25].

There are many uncertainties associated with tree-level matrix element that can be better controlled if one could include the next order in the α_s expansion, which would mean including one-loop matrix elements. One of the problems with loop matrix elements is that they are infinite and frequently negative. Only the sum of the associated real emission with the virtual one is a finite quantity. In practice one assumes that emissions within a region are unresolved and that their amplitude can be added to the virtual contribution. There are a few choices to be made, depending on when to consider an emission unresolved and how to map the unresolved contribution onto the virtual one.

Most one-loop matrix elements are calculated with a method called Catani–Seymour dipole subtraction [26, 27]. This method uses a function calculated analytically from dipoles that is added to the virtual contribution and subtracted from the real contribution. This way of calculating one-loop matrix elements has been proven to work quite well, but it needs to be modified to be applied to our algorithm. The reason is that for our matching algorithms to work, a strict phase space cut is needed to separate resolved and unresolved emissions. This can be accomplished by modifying the subtraction scheme outside the singular regions.

If a jet cutoff, y_{cut}, is used to determine when an emission is resolved, and the renormalization scale is set to μ, one can formulate the cross sections for one-loop matrix elements in the following way.

$$
\begin{aligned}
d\sigma_0 &= C_0^{\text{ME}}(\Omega_0)(1+\alpha_s(\mu)c_{0,1}^{\text{ME}}(\Omega_0, y_{\text{cut}}))\, d\Omega_0 \\
d\sigma_1 &= C_1^{\text{ME}}(\Omega_1)\,\alpha_s(\mu)(1+\alpha_s(\mu)c_{1,1}^{\text{ME}}(\Omega_1, \mu, y_{\text{cut}}))\Theta(y-y_{\text{cut}})d\Omega_1 \\
d\sigma_2 &= C_2^{\text{ME}}(\Omega_2)\,\alpha_s^2(\mu)(1+\alpha_s(\mu)c_{2,1}^{\text{ME}}(\Omega_2, \mu, y_{\text{cut}}))\Theta(y-y_{\text{cut}})d\Omega_2 \\
&\vdots \\
d\sigma_{n-1} &= C_{n-1}^{\text{ME}}(\Omega_{n-1})\,\alpha_s^{n-1}(\mu)(1+\alpha_s(\mu)c_{n-1,1}^{\text{ME}}(\Omega_{n-1}, \mu, y_{\text{cut}}))\Theta(y-y_{\text{cut}})d\Omega_{n-1}
\end{aligned}
$$

$$d\sigma_n = C_n^{\mathrm{ME}}(\Omega_n)\,\alpha_s^n(\mu)\Theta(y - y_{\mathrm{cut}})d\Omega_n \quad \text{(IV.9)}$$

When one-loop matrix elements are calculated, the unresolved parton of the tree-level matrix element with one more outgoing particles needs to be added. The resolved part is considered to have a higher multiplicity but also needs to be included in the calculation. This means that the highest multiplicity is always calculated to tree-level accuracy.

The renormalization scale used in the calculation enters not only as a scale in α_s, but also affects the one-loop terms (except for $c_{0,1}^{\mathrm{ME}}$ in case the Born level contains no powers of α_s). It is quite simple to see how the renormalization scale enter if one considers the running coupling, which can be expanded as

$$\begin{aligned} \alpha_s(\mu') &= \alpha_s(\mu)\left(1 + \alpha_s(\mu)\frac{\log(\mu/\mu')}{\alpha_0} + \mathcal{O}(\alpha_s^2(\mu))\right) \\ \alpha_0 &= \frac{2\pi}{\beta_0} = \frac{6\pi}{33 - 2n_f} \end{aligned} \quad \text{(IV.10)}$$

This means that a change in the renormalization scale of the first term leaves a remnant term in the next order in α_s simply through the running, which is something that needs to be taken into account if one varies the renormalization scale. The effect can be studied by expanding α_s explicitly for one of the multiplicities

$$\begin{aligned} &\alpha_s^l(\mu)(1 + \alpha_s(\mu)c_{l,1}^{\mathrm{ME}}(\Omega_l, \mu, y_{\mathrm{cut}})) = \quad \text{(IV.11)} \\ &\alpha_s^l(\mu')(1 + l\alpha_s(\mu')\frac{\log(\mu'/\mu)}{\alpha_0} + \alpha_s(\mu')c_{l,1}^{\mathrm{ME}}(\Omega_l, \mu, y_{\mathrm{cut}}) + \mathcal{O}(\alpha_s^2(\mu'))), \end{aligned}$$

which leads to the following scale dependence

$$c_{l,1}^{\mathrm{ME}}(\Omega_l, \mu', y_{\mathrm{cut}})) = c_{l,1}^{\mathrm{ME}}(\Omega_l, \mu, y_{\mathrm{cut}}) + l\frac{\log(\mu'/\mu)}{\alpha_0} + \mathcal{O}(\alpha_s(\mu'))). \quad \text{(IV.12)}$$

The renormalization scale can also be used to tune the different jet fractions, which is known as optimized perturbation theory [28]. Going beyond one-loop matrix elements or going to processes with incoming hadrons, there is also a renormalization scheme dependence to be considered.

IV.2.3 Merging parton showers and tree-level matrix elements

The purpose of merging algorithms is to improve the description of jet observables without changing things such as the internal jet structure, which is described well by the shower. At a more formal level the goal is to replace some coefficients in the expansion of the parton shower with their correct counterparts from the matrix elements.

There are several algorithms formulated with this purpose in mind. The main ones are CKKW [1, 2], CKKW-L [3, 4], MLM [5, 6] and Pseudo-Shower [7]. Their advantages and disadvantages when applied to e^+e^- annihilation is discussed thoroughly in [29]. Here the discussion is limited to how the CKKW-L algorithm can be extended to also include one-loop matrix elements, but most of the general ideas can be applied also to CKKW.

Before going to one-loop matrix element, the mechanism used to merge tree-level matrix elements needs to be understood. With tree-level matrix elements two issues need to be resolved, namely to divide the phase space for emissions between the parton shower and the matrix element and to introduce Sudakov form factors to make the matrix elements exclusive. Essentially one would like to replace the product of splitting functions present in the cross sections for various processes in the parton shower with the correct tree-level matrix element.

The phase space is to be divided in such a way that the region for allowed emissions from the matrix element and the parton shower cover the entire phase space with no overlaps. Failing to do this consistently results in double counting or dead regions. The scale that defines the border between the matrix-element and the parton-shower phase space is known as the merging scale, and is usually defined using a jet clustering algorithm.

The Sudakov form factors are introduced by using a constructed shower history, which is done by considering all possible shower histories for the states generated according to the matrix element and selecting one with a probability proportional to the product of the corresponding splitting functions in the shower. The actual shower is then used for calculating the Sudakov form factors, which has the advantage that any non-leading effects that were introduced in the shower are also included. For further details on this procedure we refer the reader to [3, 4].

A particular shower scenario is dependent on the emission scales of the shower (denoted ρ) and other shower variables such as energy fraction and angular orientation, which are denoted simply by $\vec{x}$. A complete set of scales and other variables can be used to yield a shower history composed of specific states, denoted S_i. Looking at the differential exclusive cross section for n emitted partons, the parton shower yields the following

$$\frac{d\sigma_n^{\mathrm{PS}}}{d\Omega_n^{\mathrm{PS}}} = KC_n^{\mathrm{PS}}(\Omega_n^{\mathrm{PS}})\Delta_{S_n}(\rho_n,\rho_c)\prod_{i=1}^{n}\alpha_{\mathrm{s}}(b\rho_i)\Delta_{S_{i-1}}(\rho_{i-1},\rho_i), \qquad \text{(IV.13)}$$

where ρ_0 is the maximum scale, ρ_c is the shower cutoff scale and b is the parameter introduced in equation (IV.5). An overall N^{l}LO K-factor, $K = 1+\sum_{i=1}^{l} k_i\alpha_{\mathrm{s}}^i(\mu)$, has also been included.

The above expression is to be compared with the appropriate tree-level matrix element. The tree-level matrix element is an inclusive quantity and do

not cover the full phase space, which is denoted by including a step function with the matrix element cutoff which is set equal to the merging scale, y_{MS}. The cross section for the tree-level matrix element can be formulated in the following way.

$$\frac{d\sigma_n^{\mathrm{ME}}(y_{\mathrm{MS}})}{d\Omega_n} = C_n^{\mathrm{ME}}(\Omega_n)\alpha_{\mathrm{s}}^n(\mu)\Theta(y(\Omega_n) - y_{\mathrm{MS}}) \quad \text{(IV.14)}$$

By selecting one history out of all possible histories, the matrix element can be mapped onto the shower phase space formulation, which can be described by the mapping $\Omega_n \mapsto \Omega_n^{\mathrm{PS}}$. The matrix element cross section can be written in terms of parton shower phase space in the following way.

$$\frac{d\sigma_n^{\mathrm{ME}}(y_{\mathrm{MS}})}{d\Omega_n^{\mathrm{PS}}} = C_n^{\mathrm{ME}}(\Omega_n^{\mathrm{PS}})\alpha_{\mathrm{s}}^n(\mu)\Theta(y(S_n) - y_{\mathrm{MS}}) \quad \text{(IV.15)}$$

The Sudakov form factors are then introduced in the same way as in equation (IV.13). In addition, the coupling constant is reweighted to use the emission scales instead of a fixed renormalization scale. The procedure results in the following exclusive cross section.

$$\begin{aligned}\frac{d\sigma_n(y_{\mathrm{MS}})}{d\Omega_n^{\mathrm{PS}}} = {} & KC_n^{\mathrm{ME}}(\Omega_n^{\mathrm{PS}})\alpha_{\mathrm{s}}^n(\mu)\Theta(y(S_n) - y_{\mathrm{MS}})\Delta_{S_n}(\rho_n, \rho_c) \times \\ & \prod_{i=1}^{n} \frac{\alpha_{\mathrm{s}}(b\rho_i)}{\alpha_{\mathrm{s}}(\mu)}\Delta_{S_{i-1}}(\rho_{i-1}, \rho_i) \quad \text{(IV.16)}\end{aligned}$$

This expression is fully exclusive in the same way as a state generated by the shower. However, the tree-level matrix element is only allowed to generate emissions above the merging scale. The scheme therefore needs to be supplemented by introducing a way of allowing the shower to generate extra emissions below the merging scale and the methods for accomplishing this is the subject of the next section.

IV.2.4 Adding parton showers to multi-parton states

If the merging scale, y_{MS}, is defined in the same way as the parton shower ordering variable, the adding of a parton shower is fairly trivial. For most parton showers you can simply shower each parton individually and use y_{MS} as the maximum scale for the ordering variable.

If, however, the merging scale and ordering scale are different, *e.g.* the merging scale is defined in invariant mass, while the shower ordering is in

transverse momentum (as is the case in our studies below in section IV.4), the problem becomes non-trivial.

In the original CKKW formulation, the problem was solved by introducing the concept of a "vetoed shower". Here, each parton is allowed to shower, starting from a value of the ordering variable typically given by the maximum possible scale in the Born-level process. Each emission is then checked so that it if is above the merging scale, y_{MS}, the emission is discarded, allowing the shower to continue to evolve down to lower evolution scales.

There is, however, a problem with this procedure, as was noted in [13] and [29], related to the fact that the shower may be allowed to make effectively unordered emissions. To understand the problem, we consider a partonic state corresponding to n parton emissions beyond the Born level. The state can be mapped onto a set of intermediate states and scales, where ρ_n represents the scale of the last emission. Now if the merging scale is very different from the ordering scale, it may very well happen in a vetoed shower that an emission with $y < y_{\mathrm{MS}}$ and $\rho > \rho_n$ is generated, which breaks the ordering, since in the shower such an emission should have been emitted from an intermediate state. Breaking the ordering results in the wrong colour structure, which may result in incorrect treatment of coherence effect, and different kinematics, which may give unwanted suppressions in some regions of phase space.

So far, two solutions to this problem has been presented. The CKKW-L approach and the so-called "truncated" vetoed shower. Both approaches requires that not only emission scales are reconstructed as in CKKW, but also the full kinematics of the complete shower history with on-shell intermediate states, S_i.

The truncated shower [13][2] is a way of allowing the shower to generate emissions from the intermediate states in the shower history and thereby preserve the ordering. The vetoed shower is started from the Born-level state, S_0 with the corresponding maximum scale ρ_0 and is vetoed in the same way as above. When the shower evolution comes down to ρ_1, it is stopped and the reconstructed emission $(\rho_1, \vec{x}_1)$ that was generated by the matrix element is inserted by hand. The vetoed evolution is then continued down to ρ_2, where the next reconstructed emission is inserted, and so on, in a way such that the kinematics of the partons in the original state is minimally disturbed.

The philosophy of the CKKW-L approach is quite different, in that unordered emissions are simply forbidden. This means that as soon as there is one emission below the merging scale, that emission and all subsequent emission (above and below the merging scale) are generated by the shower. When adding a shower to a n-parton state with the reconstructed scale ρ_n, the

[2]Here we only give our rough interpretation of the truncated shower. For a more detailed description we refer to [13]

shower is started from ρ_n and the first emission is forced to be below the merging scale, but later emissions have no such restrictions. The reweighting for the same state is done by using the full Sudakov form factor down to the scale ρ_n. The state which are thus forbidden can be generated by matrix elements for lower multiplicity together with the shower.

The CKKW-L approach can be applied to the cross section in equation (IV.16) modifying the last Sudakov form factor and adding a shower. The first emission is added with the restriction that it should be below ρ_n and the merging scale. The emission probability can be described as

$$dP = \alpha_s(b\rho)\Gamma_{S_n}(\rho,\vec{x})\Theta(y_{\rm MS}-y(S_n,\rho,\vec{x}))\Delta_{S_n}(\rho_n,\rho;<y_{\rm MS})d\rho d\vec{x}, \quad \text{(IV.17)}$$

where

$$\Delta_{S_n}(\rho_n,\rho;<y_{\rm MS}) = \exp\left(-\int_\rho^{\rho_n} d\rho' d\vec{x}\alpha_s(b\rho')\Gamma_{S_i}(\rho',\vec{x})\times \right.$$
$$\left. \times\Theta(y_{\rm MS}-y(S_n,\rho',\vec{x}))\right). \quad \text{(IV.18)}$$

In addition to the probability described above the CKKW-L procedure specifies that one should also include the Sudakov form factor between the generated emission ρ_{n+1} and the previous emission ρ_n and above the merging scale, $\Delta_{S_n}(\rho_n,\rho_{n+1};>y_{\rm MS})$. The cascade is then continued from ρ_{n+1} with no veto.

An alternative way of performing the same calculation is to generate one emission starting from ρ_n and discard the entire event if the emission was above the merging scale. It is equivalent to the above procedure since the probability for discarding the event is equal to the Sudakov form factor calculated at the end. This is the way the algorithm was formulated in [3]

The exclusive cross section in equation (IV.16) should be modified accordingly. Assuming that one emission has been added using the procedure describe above, one can formulate the cross section in the following way.

$$\frac{d\sigma_n(y_{\rm MS})}{d\Omega_n^{\rm PS}} = KC_n^{\rm ME}(\Omega_n^{\rm PS})\alpha_s^n(\mu)\Theta(y(S_n)-y_{\rm MS})\Delta_{S_n}(\rho_n,\rho_{n+1};>y_{\rm MS})\times$$
$$\times\prod_{i=1}^{n}\frac{\alpha_s(b\rho_i)}{\alpha_s(\mu)}\Delta_{S_{i-1}}(\rho_{i-1},\rho_i) \quad \text{(IV.19)}$$

Another important issue to consider when adding a parton shower is how to handle the highest multiplicity states with $n = N$. Clearly we must here not veto emissions above $y_{\rm MS}$, since this would artificially suppress final states with more than N emissions above this scale. In this case no extra Sudakov

form factors needs to be included and the cross section is given by

$$\begin{aligned}\frac{d\sigma_n(y_{\mathrm{MS}})}{d\Omega_n^{\mathrm{PS}}} &= KC_n^{\mathrm{ME}}(\Omega_n^{\mathrm{PS}})\alpha_{\mathrm{s}}^n(\mu)\Theta(y(S_n)-y_{\mathrm{MS}})\times \\ &\quad\times\prod_{i=1}^{n}\frac{\alpha_{\mathrm{s}}(b\rho_i)}{\alpha_{\mathrm{s}}(\mu)}\Delta_{S_{i-1}}(\rho_{i-1},\rho_i). \qquad \text{(IV.20)}\end{aligned}$$

The only constraint on the shower is that the first emission should be below ρ_n.

In the CKKW-L algorithm, emissions are thus corrected with the full matrix element only if they are among the N hardest (according to the parton shower ordering) *and* are all above the merging scale.

IV.2.5 Extending to one-loop MEs

To be able to extend the algorithm to also include one-loop matrix elements a new set of issues has to be addressed. First and foremost, the one-loop matrix element contains a terms which is one order higher in α_{s}. To be able to apply a correction, the shower cross section, eq. (IV.13), therefore needs to be expanded to that level, with a fixed renormalization scale μ. The α_{s} expansion of the Sudakov form factor and the running coupling can be written

$$\begin{aligned}\Delta_{S_i}(\rho_i,\rho_{i+1}) &= 1-\int_{\rho_{i+1}}^{\rho_i}d\rho\alpha_{\mathrm{s}}(b\rho)\Gamma_{S_i}^{\mathrm{PS}}(\rho)+\ldots \\ &= 1-\alpha_{\mathrm{s}}(\mu)\int_{\rho_{i+1}}^{\rho_i}d\rho\Gamma_{S_i}^{\mathrm{PS}}(\rho)+\mathcal{O}(\alpha_{\mathrm{s}}^2(\mu)) \qquad \text{(IV.21)} \\ \alpha_{\mathrm{s}}(b\rho) &= \alpha_{\mathrm{s}}(\mu)\left(1+\alpha_{\mathrm{s}}(\mu)\frac{\log(\mu/(b\rho))}{\alpha_0}+\mathcal{O}(\alpha_{\mathrm{s}}^2(\mu))\right), \qquad \text{(IV.22)}\end{aligned}$$

where the possibility of modifying the scale used in α_{s} in the shower has been included from equation (IV.5).

This means the parton shower cross section in eq. (IV.13) can be rewritten as

$$\begin{aligned}\frac{d\sigma_n^{\mathrm{PS}}}{d\Omega_n^{\mathrm{PS}}} &= C_n^{\mathrm{PS}}(\Omega_n^{\mathrm{PS}})\alpha_{\mathrm{s}}^n(\mu)\left[1+\alpha_{\mathrm{s}}(\mu)\left\{k_1+\sum_{i=1}^{n}\frac{\log(\mu/(b\rho_i))}{\alpha_0}\right.\right. \qquad \text{(IV.23)} \\ &\quad\left.\left.-\sum_{i=0}^{n-1}\int_{\rho_{i+1}}^{\rho_i}d\rho\Gamma_{S_i}(\rho)-\int_{\rho_c}^{\rho_n}d\rho\Gamma_{S_n}(\rho)\right\}+\mathcal{O}(\alpha_{\mathrm{s}}^2(\mu))\right].\end{aligned}$$

Note that the extra term that appears because of the running coupling is equivalent to the term which appears if the renormalization scale of the one-loop matrix element is changed, derived explicity in equation (IV.12).

The one-loop matrix elements need to be put through the procedure described earlier to construct a shower history. The procedure yields the following form for the cross section.

$$\begin{aligned}\frac{d\sigma_n^{\mathrm{ME}}(y_{\mathrm{MS}})}{d\Omega_n^{\mathrm{PS}}} &= C_n^{\mathrm{ME}}(\Omega_n^{\mathrm{PS}})\alpha_{\mathrm{s}}^n(\mu)\left[1+\alpha_{\mathrm{s}}(\mu)c_{n,1}^{\mathrm{ME}}(\Omega_n^{\mathrm{PS}},\mu,y_{\mathrm{MS}})\right]\times \\ &\quad \times\Theta(y(S_n)-y_{\mathrm{MS}}) \qquad \text{(IV.24)}\end{aligned}$$

The cross section contains the same terms as the tree-level cross section plus the next order correction to the matrix element, which is a sum of the virtual diagrams of multiplicity n and the real diagrams with multiplicity $n+1$ kinematics below the merging scale y_{MS}.

If the merging scale is defined using the same scale as the ordering variable in the shower, no further modifications to the matrix element would have been necessary. However, to preserve the ordering of the shower, extra Sudakov form factors need to be included. The phase space in question is where emissions have a higher ordering variable (ρ) than the last emission of the matrix element (ρ_n) and are below the merging scale. These emissions would violate the shower ordering and are therefore forbidden, but one still needs to include virtual corrections in this region, which is done using Sudakov form factors. The reweighted one-loop cross sections can be written as

$$\begin{aligned}\frac{d\sigma_n(y_{\mathrm{MS}})}{d\Omega_n^{\mathrm{PS}}} &= C_n^{\mathrm{ME}}(\Omega_n^{\mathrm{PS}})\alpha_{\mathrm{s}}^n(\mu)\left[1+\alpha_{\mathrm{s}}(\mu)c_{n,1}^{\mathrm{ME}}(\Omega_n^{\mathrm{PS}},\mu,y_{\mathrm{MS}})\right]\times \\ &\quad \times\Theta(y(S_n)-y_{\mathrm{MS}})\prod_{i=0}^{n-1}\Delta_{S_i}(\rho_i,\rho_{i+1};<y_{\mathrm{MS}}), \qquad \text{(IV.25)}\end{aligned}$$

where the definition for the Sudakov from factor was presented in equation (IV.18). Note that no reweighting is necessary for the lowest multiplicity processes, since if there are no emissions in the matrix element state, there are no regions of phase space where the shower can generate emissions violating the ordering requirement.

The other component that goes into the merging is the shower where all the terms corresponding to the one-loop matrix element have been subtracted. When doing the subtraction we choose to work with a cascade which is already corrected with tree-level matrix elements. The idea is to reweight the tree-level matrix element the same way as CKKW-L, which is described by equation (IV.19), and then subtract the terms corresponding to the one-loop matrix element. Note that one of the Sudakov form factors has a dependency on the scale of the next emission performed by the shower ρ_{n+1}, which was described in section IV.2.4.

The terms of order $\alpha_{\mathrm{s}}^{n+1}$ in equation (IV.23) needs to modified to comply with the phase space restrictions of the one-loop matrix element. The shower

is formulated in a way where emissions can be anywhere within the allowed shower phase space, whereas the matrix element is restricted to emissions above the merging scale. This difference in phase space does not affect the expansion of the running coupling, but must be included in the integration over the branching probability. The full formula including tree-level matrix element corrected with CKKW-L and the subtraction of the one-loop terms is the following.

$$\begin{aligned}\frac{d\sigma_n^{\mathrm{PScorr}}(y_{\mathrm{MS}})}{d\Omega_n^{\mathrm{PS}}} &= C_n^{\mathrm{ME}}(\Omega_n^{\mathrm{PS}})\alpha_s^n(\mu)\times \\ &\Bigg[K\Delta_{S_n}(\rho_n,\rho_{n+1};>y_{\mathrm{MS}})\prod_{i=1}^{n}\frac{\alpha_s(b\rho_i)}{\alpha_s(\mu)}\Delta_{S_{i-1}}(\rho_{i-1},\rho_i) \\ &-\prod_{i=0}^{n-1}\Delta_{S_i}(\rho_i,\rho_{i+1};<y_{\mathrm{MS}})\times \\ &\times\Bigg\{1+k_1\alpha_s(\mu)+\alpha_s(\mu)\sum_{i=1}^{n}\frac{\log(\mu/(b\rho_i))}{\alpha_0} \\ &-\alpha_s(\mu)\sum_{i=0}^{n-1}\int_{\rho_{i+1}}^{\rho_i}d\rho d\vec{x}\,\Gamma_{S_i}(\rho,\vec{x})\Theta(y(S_i,\rho,\vec{x})-y_{\mathrm{MS}}) \\ &-\alpha_s(\mu)\int_{\rho_c}^{\rho_n}d\rho d\vec{x}\,\Gamma_{S_n}(\rho,\vec{x})\Theta(y(S_i,\rho,\vec{x})-y_{\mathrm{MS}})\Bigg\}\Bigg] \quad \text{(IV.26)}\end{aligned}$$

The samples described by eq. (IV.25) and eq. (IV.26) are added together in the end to form the parton multiplicity cross section for one-loop matrix elements merged together with parton showers. When implementing the algorithms one also allows for extra emissions generated by the shower with the requirement that the first such emission should have a lower scale than ρ_n and be below the merging scale. The details of the entire procedure is described in section IV.3.

IV.2.6 Two partons at two loops

In the case of $e^+e^- \to$ hadrons, there is an additional matrix element that can be included without considering higher order terms in the running of α_s, which is the two-loop matrix element for two partons. The reason is that the leading-order term for the two-parton cross section does not include α_s. The matrix element is also fairly easy to simulate if one knows the other components at order α_s^2. Working with two-loop terms means that the equation (IV.21) needs to be expanded one more order including the parameter b, defined in equation

(IV.5). The expanded Sudakov form factor can be written in the following way.

$$\begin{aligned}\Delta_{S_i}(\rho_i,\rho_{i+1}) &= 1-\int_{\rho_{i+1}}^{\rho_i} d\rho\alpha_s(b\rho)\Gamma^{PS}_{S_i}(\rho)+\frac{1}{2!}\left(\int_{\rho_{i+1}}^{\rho_i} d\rho\alpha_s(b\rho)\Gamma^{PS}_{S_i}(\rho)\right)^2-\dots \\ &= 1-\alpha_s(\mu)\int_{\rho_{i+1}}^{\rho_i} d\rho\Gamma^{PS}_{S_i}(\rho)-\alpha_s^2(\mu)\int_{\rho_{i+1}}^{\rho_i} d\rho\frac{\log(\mu/(b\rho))}{\alpha_0}\Gamma^{PS}_{S_i}(\rho)+ \\ &\quad +\frac{1}{2}\alpha_s^2(\mu)\left(\int_{\rho_{i+1}}^{\rho_i} d\rho\Gamma^{PS}_{S_i}(\rho)\right)^2+\mathcal{O}(\alpha_s^3(\mu)) \qquad \text{(IV.27)}\end{aligned}$$

Apart from the terms above, the K-factor of order α_s^2 needs to be included, but for the running α_s it is sufficient to include the first order expansion of α_s given by equation (IV.22). The tree-level matrix element can be modified in the following fashion, which is to be added to the event generated according to the two loop matrix element.

$$\begin{aligned}\frac{d\sigma_2^{PScorr}(y_{MS})}{d\Omega_0^{PS}} &= C_0^{ME}(\Omega_0^{PS})\left[K\Delta_{S_0}(\rho_0,\rho_1;>y_{MS})-\left\{1+k_1\alpha_s(\mu)+k_2\alpha_s^2(\mu)\right.\right. \\ &\quad -\alpha_s(\mu)(1+k_1\alpha_s(\mu))\int_{\rho_c}^{\rho_0} d\rho d\vec{x}\,\Gamma_{S_0}(\rho,\vec{x})\Theta(y(S_i,\rho,\vec{x})-y_{MS}) \\ &\quad -\alpha_s^2(\mu)\int_{\rho_c}^{\rho_0} d\rho d\vec{x}\,\frac{\log(\mu/\rho)}{\alpha_0}\Gamma_{S_0}(\rho,\vec{x})\Theta(y(S_i,\rho,\vec{x})-y_{MS}) \\ &\quad \left.\left.+\frac{\alpha_s^2(\mu)}{2}\left(\int_{\rho_c}^{\rho_0} d\rho d\vec{x}\,\Gamma_{S_0}(\rho,\vec{x})\Theta(y(S_i,\rho,\vec{x})-y_{MS})\right)^2\right\}\right] \qquad \text{(IV.28)}\end{aligned}$$

This term represents the modified parton shower and added to the two-parton matrix element calculated at two loops, the cascade becomes corrected at one order higher in α_s. Note that there is a dependence on the scale of the next emission generated by the shower, in this case ρ_1, in the same way as in equations (IV.19) and (IV.26).

The term described above should be added to the two-parton matrix element calculated at two-loop accuracy. Since the two-loop matrix element considered has the lowest multiplicity, no reweighting due to the ordering requirement is necessary. If two-loop matrix elements with higher parton multiplicity were to be included, they would have to be reweighted in the same way as the one-loop matrix elements, described in eq. (IV.25).

IV.3 The algorithm

This section describes all the necessary steps needed to generate the actual events. First the methods for calculating each individual weight is presented and then each step in the algorithm is described.

IV.3.1 Calculating the terms

Each of the weights that need to be calculated consists of a number of common elements. This section describes how to calculate each individual piece. All the terms are calculated similarly to the CKKW-L approach, which means that the actual shower is used. However, it should be noted that it is possible to do calculations along the same lines using the analytical weights in the CKKW algorithm. Using the actual shower puts a constraint on which parton showers can be used. The algorithm can only be applied to showers with well defined intermediate states and Sudakov form factors that factorizes, which is the same requirement as the CKKW-L algorithm.

The weights described in this section are calculated using Monte Carlo techniques, which means that there is an element of randomness in each weight. The calculations presented give the correct value for each weight if an average value is calculated. In the general framework of Monte Carlo event generators this does not present a problem.

The simplest weight to be calculated is the plain Sudakov form factor, denoted $\Delta_{S_i}(\rho_i, \rho_{i+1})$. This is done by generating one emission with the shower starting from the state S_i and the scale ρ_i. If the emission is above the scale ρ_{i+1} set the weight to zero, otherwise set it equal to one. This gives the correct behavior since by definition the no-emission probability of the shower is equal to the Sudakov form factor.

The next weight to be described is the Sudakov form factor that is modified to exclude emissions above the merging scale denoted $\Delta_{S_i}(\rho_i, \rho_{i+1}; < y_{\mathrm{MS}})$, defined in equation (IV.18), and is used to reweight the states generated according to one-loop matrix elements. In this case two different scales are mixed and the scheme for the plain Sudakov form factor needs to be supplemented with an accept/reject scheme. The calculation is described in the following steps.

1. Feed the state S_i into the shower and generate one emissions starting from a scale ρ_i. This yields an emission scale ρ and a new state S.
2. Depending on the emission there are three options.
   - If the scale of the generated emission ρ is above ρ_{i+1} and if the emission is above the merging scale ($y(S) > y_{\mathrm{MS}}$) generate a new emission from the state S_i, but this time using ρ as the starting scale. Repeat step 2.
   - If the scale of the generated emission ρ is below ρ_{i+1} set the weight to one.
   - If the scale of the generated emission ρ is above ρ_{i+1} and if the emission is below the merging scale ($y(S) < y_{\mathrm{MS}}$) set the weight to zero.

The only other terms that need to be calculated are the integrated branching probabilities. First the calculation of the term

$$\alpha_s(\mu)\int_{\rho_{i+1}}^{\rho_i} d\rho d\vec{x}\,\Gamma_{S_i}(\rho,\vec{x})\Theta(y(S_i,\rho,\vec{x})-y_{\mathrm{MS}}) \tag{IV.29}$$

is described and later it is shown how to extend the calculation to the other related terms. The calculation is done by generating emissions in the entire avaliable phase space and counting the total number. The procedure is described in the following steps.

1. Use a fixed value for $\alpha_s = \alpha_s(\mu)$ (usually avaliable as an option in a parton shower program) and generate one emission from the state S_i with a starting scale ρ_i. This yields an emission scale ρ and a new state S.
2. If the emission has a scale $\rho > \rho_{i+1}$ and is above the merging scale $y(S) > y_{\mathrm{MS}}$ count the emission.
3. Depending on the scale of the emission stop the algorithm or generate another emission.
   - If the scale of the generated emission ρ is above ρ_{i+1} generate a new emission from the state S_i, but this time using ρ as the starting scale. Repeat step 2 and 3.
   - If the scale of the generated emission ρ is below ρ_{i+1} set the weight to the total number of emission counted in step 2.

The average number of emissions in the algorithm above gives the correct value for the integral. To show that this is the case consider the probability of n emissions.

$$P(n) = \Delta_{S_i}(\rho_i,\rho_{i+1};>y_{\mathrm{MS}})\frac{1}{n!}\left(\alpha_s(\mu)\int_{\rho_{i+1}}^{\rho_i} d\rho d\vec{x}\,\Gamma_{S_i}(\rho,\vec{x})\Theta(y(S_i,\rho,\vec{x})-y_{\mathrm{MS}})\right)^n. \tag{IV.30}$$

The average number of emission can be written as

$$\begin{aligned}\sum_{n=0}^{\infty} nP(n) &= \Delta_{S_i}(\rho_i,\rho_{i+1};>y_{\mathrm{MS}})\alpha_s(\mu)\int_{\rho_{i+1}}^{\rho_i} d\rho d\vec{x}\,\Gamma_{S_i}(\rho,\vec{x})\Theta(y(S_i,\rho,\vec{x})-y_{\mathrm{MS}})\times \\ &\quad \sum_{n=1}^{\infty}\frac{1}{(n-1)!}\left(\alpha_s(\mu)\int_{\rho_{i+1}}^{\rho_i} d\rho d\vec{x}\,\Gamma_{S_i}(\rho,\vec{x})\Theta(y(S_i,\rho,\vec{x})-y_{\mathrm{MS}})\right)^{n-1} \\ &= \alpha_s(\mu)\int_{\rho_{i+1}}^{\rho_i} d\rho d\vec{x}\,\Gamma_{S_i}(\rho,\vec{x})\Theta(y(S_i,\rho,\vec{x})-y_{\mathrm{MS}}).\end{aligned} \tag{IV.31}$$

The same algorithm can also be used to calculate the higher order terms present in equation (IV.28). The integrated branching probability squared can be calculated by setting the weight to $n(n-1)$, where n is the number of emis-

sions, which gives the correct average since

$$\sum_{n=0}^{\infty} n(n-1)P(n) \quad = \quad \left(\alpha_s(\mu)\int_{\rho_{i+1}}^{\rho_i} d\rho d\vec{x}\,\Gamma_{S_i}(\rho,\vec{x})\Theta(y(S_i,\rho,\vec{x})-y_{\mathrm{MS}})\right)^2. \quad \text{(IV.32)}$$

There is one more term to be considered in equation (IV.28), which is

$$\alpha_s^2(\mu)\int_{\rho_{i+1}}^{\rho_i} d\rho d\vec{x}\,\frac{\log(\mu/(b\rho))}{\alpha_0}\Gamma_{S_i}(\rho,\vec{x})\Theta(y(S_i,\rho,\vec{x})-y_{\mathrm{MS}}). \quad \text{(IV.33)}$$

The way this integral is calculated is by an accept/reject scheme. The first step is to rewrite the term where the value of the logarithm has been divided by its maximum, which occurs for the minimum possible value of ρ.

$$\left(\frac{\alpha_s(\mu)\log(\mu/(b\rho_{i+1}))}{\alpha_0}\right)\times$$
$$\times\left(\alpha_s(\mu)\int_{\rho_{i+1}}^{\rho_i} d\rho d\vec{x}\,\frac{\log(\mu/(b\rho))}{\log(\mu/(b\rho_{i+1}))}\Gamma_{S_i}(\rho,\vec{x})\Theta(y(S_i,\rho,\vec{x})-y_{\mathrm{MS}})\right) \quad \text{(IV.34)}$$

The second factor can now be simulated with a scheme simular to the one described earlier. The only addition is that emissions are only counted if $\log(\mu/(b\rho))/\log(\mu/(b\rho_{i+1})) > R$, where R is a random number between 0 and 1.

IV.3.2 The steps

To generate the actual events we start with two different samples. One is generated according to the one-loop matrix element and one generated with tree-level matrix elements, where both samples are generated using the same cutoff, y_{MS}. The two samples are generated for all multiplicates except for the highest one, where only the tree-level matrix element is used. Different weights are calculated for the events depending on if they were generated according to a one-loop matrix element or a tree-level matrix element. Event are generated according to the following steps:

1. Choose a merging scale y_{MS} and use the same scale as matrix element cutoff. Calculate the cross section for the one-loop matrix element with multiplicities $n < N$ and for tree-level matrix elements with multiplicities $n \leq N$. Choose a matrix element with a probability proportional to its cross section.
2. Generate an event with a kinematic distribution in accordance with the chosen matrix element.
3. Construct a shower history by considering all possible histories and selection one with a probability proportional to the corresponding product of splitting functions. This leads to a set of states $S_n \ldots S_0$ and scales $\rho_n \ldots \rho_0$.

4. When generating the first emission from the shower, there are two cases to be considered.
   - If the event was generated according to a one-loop matrix element or according to a tree-level matrix element with a multiplicity less than the maximum ($n < N$), generate one emission starting from the state S_n with a starting scale ρ_n, but veto any emission which is above the merging scale y_{MS}
   - If the event was generated according to a tree-level matrix element and had the highest multiplicity ($n = N$), generate one emission from the state S_n with a starting scale ρ_n.
5. The events are reweighted depending on type:
   - If the event was generated according to a one-loop matrix element, reweight the event with a factor $\prod_{i=0}^{n-1}\Delta_{S_i}(\rho_i,\rho_{i+1};<y_{\text{MS}})$ according to the steps in subsection IV.3.1.
   - If the event was generated according to a tree-level matrix element, but did not have the highest multiplicity ($n < N$), then the the weight depends on the scale of the emission in step 4, ρ_{n+1}. (If the shower cutoff was reached and no emission generated, set $\rho_{n+1} = \rho_c$.) Reweight the event with

$$
\begin{aligned}
&K\Delta_{S_n}(\rho_n,\rho_{n+1};>y_{\text{MS}})\prod_{i=1}^{n}\frac{\alpha_{\text{s}}(b\rho_i)}{\alpha_{\text{s}}(\mu)}\Delta_{S_{i-1}}(\rho_{i-1},\rho_i)\\
&-\prod_{i=0}^{n-1}\Delta_{S_i}(\rho_i,\rho_{i+1};<y_{\text{MS}})\left\{1+k_1\alpha_{\text{s}}(\mu)+\alpha_{\text{s}}(\mu)\sum_{i=1}^{n}\frac{\log(\mu/(b\rho_i))}{\alpha_0}\right.\\
&\qquad-\alpha_{\text{s}}(\mu)\sum_{i=0}^{n-1}\int_{\rho_{i+1}}^{\rho_i}d\rho d\vec{x}\,\Gamma_{S_i}(\rho,\vec{x})\Theta(y(S_i,\rho,\vec{x})-y_{\text{MS}})\\
&\qquad\left.-\alpha_{\text{s}}(\mu)\int_{\rho_c}^{\rho_n}d\rho d\vec{x}\,\Gamma_{S_i}(\rho,\vec{x})\Theta(y(S_i,\rho,\vec{x})-y_{\text{MS}})\right\},
\end{aligned}
\tag{IV.35}
$$

     according to the steps in subsection IV.3.1.
   - If the event was generated according to a tree-level matrix element, but had the highest multiplicity ($n = N$), then the event is reweighted by $\prod_{i=1}^{n}\frac{\alpha_{\text{s}}(b\rho_i)}{\alpha_{\text{s}}(\mu)}\Delta_{S_{i-1}}(\rho_{i-1},\rho_i)$.
6. Continue the cascade below ρ_{n+1}

IV.4 Results

Our algorithm has been implemented using ARIADNE version 4.12 [22], which has been modified to include the possibility of calculating the different

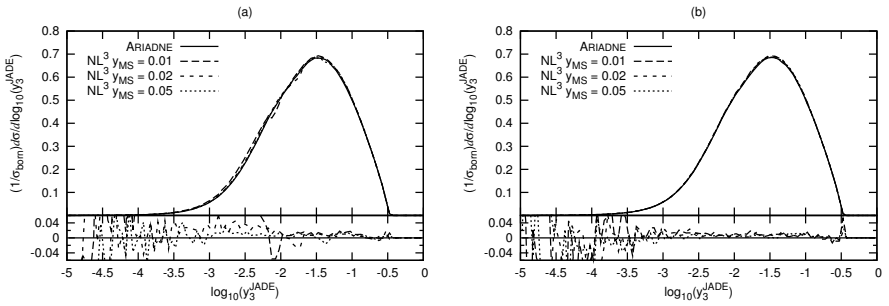

Figure IV.1: The parton-level y_3 spectra according to the JADE definition for the samples corrected with one-loop two-parton matrix element and tree-level three-parton matrix element. (a) includes all flavours and masses and (b) is with only massless d-quarks. The in-sets at the bottom of the plots show the relative differences between the results from NL^3 and default ARIADNE, $(\sigma_{\mathrm{NL}^3} - \sigma_{\mathrm{ARIADNE}})/\sigma_{\mathrm{ARIADNE}}$.

weights needed. The matrix elements used is taken from an implementation in PYTHIA version 6.414 [3] [30], where the e^+e^- matrix elements were calculated in [31] and parameterized in [32]. The implementation includes the possibility of generating e^+e^- events according to zero, one, or two orders in α_s. This means that the four jets can only be generated according to the tree-level matrix element, whereas the three jet contribution can be generated using the one-loop contribution and the two jet can include up to two loops. The different multiplicities are separated using a cutoff in invariant mass divided by center of mass energy (Q^2/s), which can be varied between 0.01 and 0.05. The process considered throughout this section is e^+e^- to hadrons at the Z^0 mass peak.

The first thing to be studied is how the algorithm behaves for the somewhat trivial case of calculating three partons with a tree-level matrix element and two partons to one loop. To study the effects of the cutoff, the JADE [33] jet clustering algorithm is used, since it has a jet scale which closely resembles the scale used for the cutoff, y_{MS}. The matrix elements are calculated using a fixed value of the α_s used in ARIADNE at the renormalization scale, which is set to m_Z (*i.e.* not using eq. (IV.5) and setting $b = 1$ in the rest of section IV.2 and IV.3). The distribution in clustering scale for the third jet for our new procedure[4] is shown in figure IV.1 with three different values of the merging scale, 0.01, 0.02 and 0.05 and is compared to the standard ARIADNE shower. The figure includes one plot with all flavours and masses and one where only massless d-quarks was used. Including quark masses there are some deviations,

[3] PYTHIA has been modified to allow renormalization scales bigger than the center of mass energy and to return negative weights instead of rounding to zero for three partons at one loop.

[4] The results for our new procedure is throughout denoted NL^3.

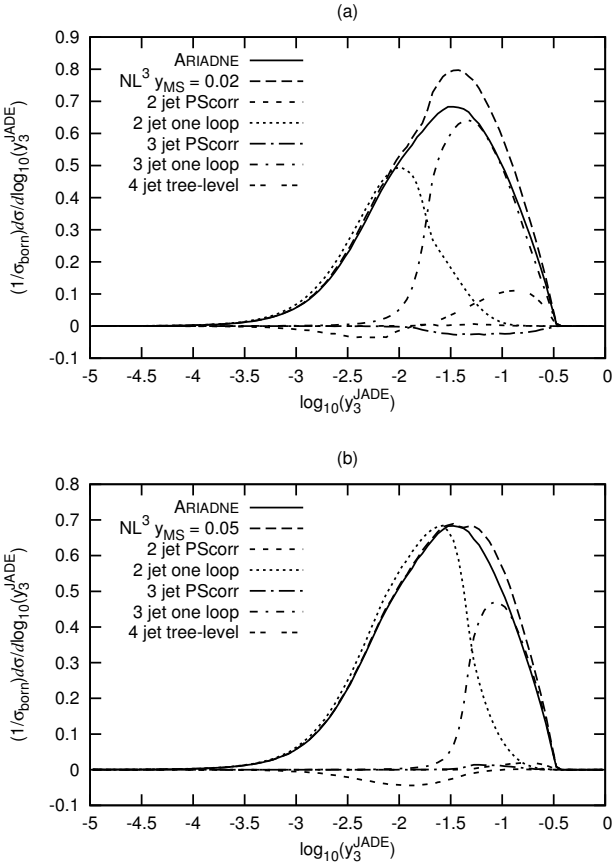

Figure IV.2: The parton-level y_3 spectra according to the JADE definition for the samples corrected with matrix elements describing two partons at one loop, three partons at one loop and four partons at tree level. (a) shows the curves for a cutoff of 0.02 and (b) for a cutoff 0.05. Both figures include curves displaying the various components of the NL^3 samples.

IV

especially close to the cutoff. This is due to slightly different treatments of the suppression of radiation from heavy quarks (the dead-cone effect). The matrix element in PYTHIA uses the exact formula, whereas in ARIADNE a more general approximate formula is used. However, when masses are not included no deviations are visible, which should be the case since both the K-factor and the matrix element correction are present in the shower to this order.

Moving on to the simplest non-trivial case which includes two partons to one loop, three partons to one loop and four partons to tree level. Also here

the clustering scale of the third jet using JADE is studied for the same α_s, renormalization scale and merging scales. The distribution is shown in figure IV.2 together with the various components that make up each distribution. The cutoff 0.01 is not included since it would have a negative two-parton cross section, which is not allowed in the PYTHIA routines.

The different components in figure IV.2 can be identified in the following way. The curves marked *one loop* are simply the contributions from the one-loop matrix elements with a Sudakov form factor according to equation (IV.25) and a shower added below the merging scale, the curves marked *PScorr* are the contribution calculated from the tree-level matrix elements according to equation (IV.26) and the curve marked *4 jet tree-level* is the highest multiplicity contribution which is calculated according to equation (IV.20). The dominant contributions are clearly the one-loop matrix elements for two-parton and three-parton configurations. The four-parton matrix element is also significant at the hard end of the spectrum, but the contributions from the modified tree-level distributions are generally small.

We also note that the modified tree-level contribution (*PScorr*) have a slightly negative value. This is a result of the expansion of the Sudakov form factor together with the running coupling. However, negative weights can be avoided if one chooses a merging scale defined using the ordering variable in the shower, and a renormalization scale equal to the merging scale. As long as the one-loop matrix elements are not themselves negative, which happens for small enough merging scales, all events would then have positive weights.

One important feature of the algorithm is the possibility of including several multiplicities together. The importance of this is illustrated in figure IV.2 by the fact that the two-parton components give a contribution which extend significantly above the merging scale (while the opposite is true for the three parton contribution). Clearly it would be problematic to try to describe the jet distribution using only three- and four-parton matrix elements, although the calculation would be formally correct to NLO accuracy.

Another thing that is noticeable is that there is a significant overshoot above the cutoff in figure IV.2. This is attributed to the one-loop term of the three parton matrix element, which can not be accurately reproduced in the cascade. The equivalent term in the cascade is calculated using the Sudakov form factors and the value is significantly smaller than the matrix element.

The whole issue of the one-loop contribution being significantly larger than the parton shower counterpart has another consequence, namely that the α_s used in the shower is higher than what is fitted to precision calculations, which include both fixed-order matrix elements and logarithmic resummations. However, simply lowering α_s everywhere would destroy the agreement between the curves below the cutoff. We therefore both lower the value of α_s and modify the scale used as a argument in the shower by using the param-

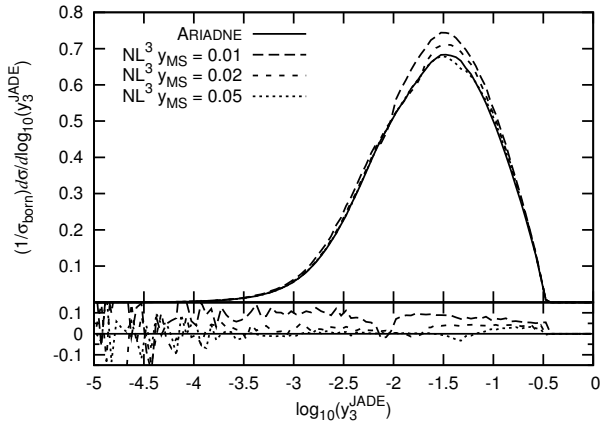

Figure IV.3: The parton-level y_3 spectra according to the JADE definition for the NL^3 algorithm including a modified way of treating α_s.

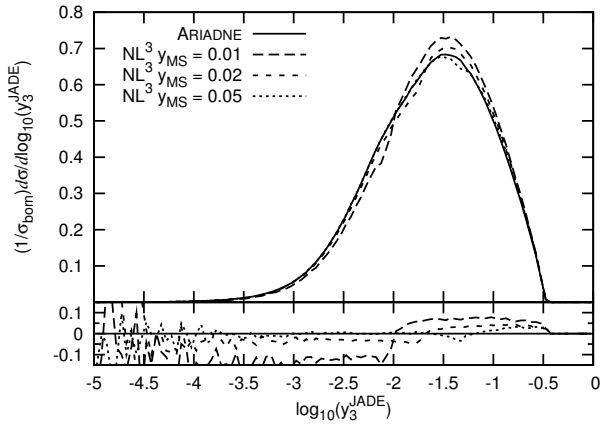

Figure IV.4: The parton-level y_3 spectra according to the JADE definition for the NL^3 algorithm including a modified way of treating α_s and the two-parton matrix element at two loops.

eter b (defined in equation (IV.5)). The value of α_s from the PDG [34] which is $\alpha_s(m_Z) = 0.1176$ which corresponds to $\Lambda_{QCD} = 85.8$ MeV (assuming a leading order α_s which is used in ARIADNE), which should be compared to the ARIADNE default $\Lambda_{QCD} = 220$ MeV. Figure IV.3 shows the curves using the PDG value for α_s and $b = 85.8/220 = 0.389$. There is a much better agreement for values above the cutoff, but there are still some discrepancies.

For the two-parton matrix element the calculation is also available at two

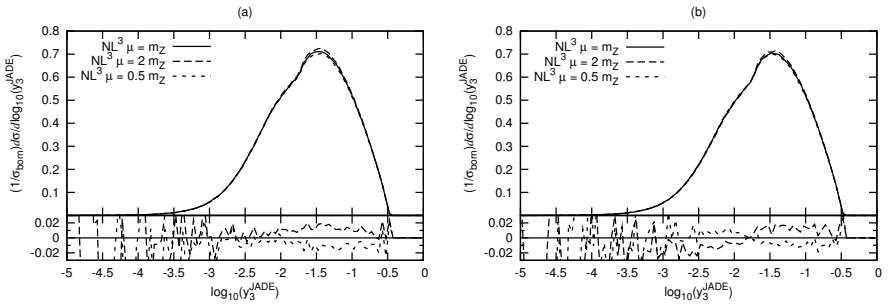

Figure IV.5: The parton-level y_3 spectra according to the JADE definition for the NL^3 algorithm including a modified way of treating α_s where the renormalization scale has been varied up and down by a factor of two. (a) includes the one-loop corrections and (b) includes the two-parton matrix element at two loops.

loops. This was discussed in general in section IV.2.6. In figure IV.4 the two-loop corrections have been included, still using the same α_s treatment as described above. There is a clear difference in that the curves no longer overlap with ARIADNE for values below the merging scale. This happens since the two-loop contribution is beyond what can be reproduced by ARIADNE.

To check the consistency of the algorithm we have studied the sensitivity to changes in the renormalization scale. In figure IV.5 the renormalization scale has been varied up and down by a factor of two, both for the case of one-loop correction and including two partons at two loops. Overall, the sensitivity to changes in the renormalization scale is small, with variations of around two percent in the results. This is expected since all the higher order terms comes from the shower which is unaffected by the renormalization scale.

Finally our algorithm is compared to data from the DELPHI [35] experiment. It should be noted that all the data are quite well reproduced by ARIADNE and since we get small deviations in the previous plot, we expect small differences here as well. The data to be studied are all corrected to the particle level and includes only charged particles. Figure IV.6 shows the jet distributions for the third and fourth jet according to the JADE [33] definition and the Durham [36] definition. The curves include the central merging scale value of 0.02 with and without the extra two-loop correction. All the results reproduce the data quite well.

The results from the algorithm has also been compared to the shape observables thrust and oblateness, which is shown in figure IV.7. The agreement is again quite good. The curves including the matrix element corrections actually do a bit better for oblateness, which is to be expected since it is sensitive to distributions including four jets where we have included the exact tree-level matrix elements.

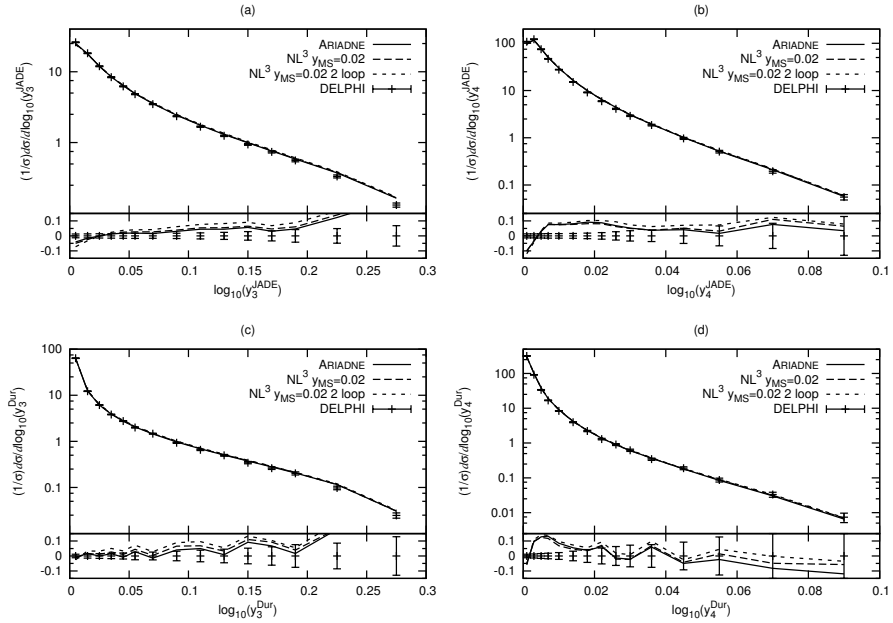

Figure IV.6: Charged particle jet observables compared to DELPHI data and the standard ARIADNE shower for the NL^3 algorithm using a merging scale of 0.02. The following jet observables are shown: (a) 3 jet JADE, (b) 4 jet JADE, (c) 3 jet Durham and (d) 4 jet Durham.

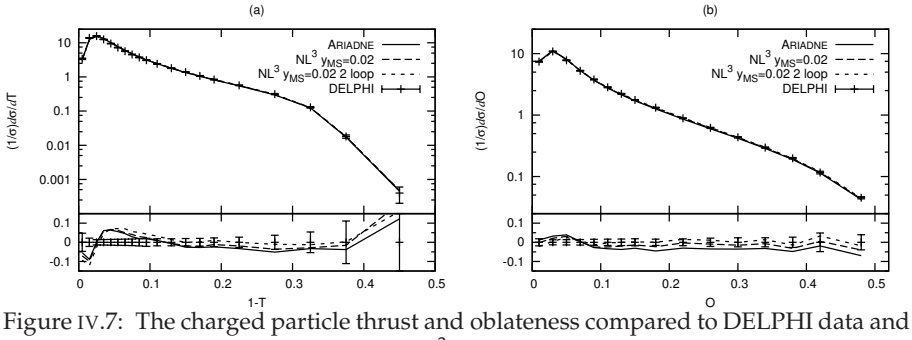

Figure IV.7: The charged particle thrust and oblateness compared to DELPHI data and the standard ARIADNE shower for the NL^3 algorithm using a merging scale of 0.02.

IV.5 Conclusions

We have presented an algorithm for merging one-loop and tree-level matrix elements with parton showers. The algorithm allows for the inclusion of sev-

eral different multiplicities, which is important for simulating an entire process. For observables where the combination of tree-level and one-loop matrix elements used gives the correct NLO prediction, our procedure will also give correct NLO predictions but with a resummation of leading logarithms which is of the same accuracy as in the parton shower used. The basic principle of the procedure is quite simple. The first two terms in the α_s expansion is subtracted from the shower and the corresponding one-loop matrix element is added. Although a simple idea, it leads to some complicated issues.

To calculate the first two terms in powers of α_s in a parton shower requires that several different terms are taken into account. Both the first term in the expansion of the Sudakov form factor and the first term in the running coupling contributes at this level. In this paper these terms were derived and subtracted from the shower. The calculation was done within a framework similar to the CKKW-L method, but it is also applicable to CKKW algorithms in general.

The modified shower is then added to a sample calculated according to one-loop matrix elements. The requirement on the matrix elements is that one should be able to specify a phase-space cut which separates the parton multiplicities and decides whether or not a parton is to be considered unresolved. This is not done within the commonly used subtraction schemes, but can be solved by a modifying the subtraction scheme outside the singular regions.

We have explicitly calculated all the weights without taking into account the possibility of incoming hadrons, which is going to be the topic of a future publication. We then implemented the procedure and applied it to the process e^+e^- to hadrons. The shower in ARIADNE was used and PYTHIA was used to generate the matrix elements.

To test the consistency of the algorithm, jet distributions at parton level were studied. The trivial case of two partons at one loop and three partons at tree level was found to have only small deviations, which disappeared if quark masses were excluded. The first nontrivial case was how the algorithm behaves for two partons at one loop, three partons at one loop and four partons at tree level. This led to a clear overshoot due to the fact that the terms in the matrix element is significantly bigger than those in the shower, which is compensated by using a much larger α_s in the shower compared to fits using matrix elements including loops. If the value of α_s is adjusted according to our prescription, the agreement is quite good.

One important aspect of our procedure is the ability to combine several different parton multiplicities in a consistent way. This allows us to obtain corrections to a NLO prediction for a given n-jet observable, stemming from cumulative sub-leading effects from the parton shower added to the $(n-1)$-jet states.

Other aspects of the algorithms was explored, such as including the two-

parton matrix element to two-loop accuracy, which only led to slight changes below the merging scale. The sensitivity to the choice of renormalization scale was tested and a change of a factor of two in the renormalization scale results in changes of around two percent in the results.

The predictions of the algorithm has also been compared to four different jets observables and two shape observables measured at LEP. ARIADNE already provides a good description of the data and including the matrix element corrections gives similar agreement.

Overall, the procedure has been shown to be consistent and give good results at hadron level. These relatively simple cases establish a proof of concept and a good staring point to explore the additional pieces needed to simulate processes with incoming hadrons. If the algorithm is developed further and the matrix element generators improved, then there are good prospects for being able to merge one-loop matrix elements and partons shower for the more interesting LHC processes.

IV.6 Acknowledgments

We thank Torbjörn Sjöstrand for useful discussions. Work supported in part by the Marie Curie research training network "MCnet" (contract number MRTN-CT-2006-035606).

IV References

[1] S. Catani, F. Krauss, R. Kuhn, and B. R. Webber, "QCD matrix elements + parton showers," *JHEP* **11** (2001) 063, arXiv:hep-ph/0109231.

[2] F. Krauss, "Matrix elements and parton showers in hadronic interactions," *JHEP* **08** (2002) 015, arXiv:hep-ph/0205283.

[3] L. Lönnblad, "Correcting the colour-dipole cascade model with fixed order matrix elements," *JHEP* **05** (2002) 046, arXiv:hep-ph/0112284.

[4] N. Lavesson and L. Lönnblad, "W + jets matrix elements and the dipole cascade," *JHEP* **07** (2005) 054, arXiv:hep-ph/0503293.

[5] M. Mangano, "The so-called MLM prescription for ME/PS matching." http://www-cpd.fnal.gov/personal/mrenna/tuning/nov2002/mlm.pdf. Talk presented at the Fermilab ME/MC Tuning Workshop, October 4, 2002.

[6] M. L. Mangano, M. Moretti, F. Piccinini, and M. Treccani, "Matching matrix elements and shower evolution for top- quark production in hadronic collisions," *JHEP* **01** (2007) 013, arXiv:hep-ph/0611129.

[7] S. Mrenna and P. Richardson, "Matching matrix elements and parton showers with HERWIG and PYTHIA," *JHEP* **05** (2004) 040, arXiv:hep-ph/0312274.

[8] J. Campbell and K. Ellis, "MCFM - Monte Carlo for FeMtobarn processes." http://mcfm.fnal.gov/.

[9] Z. Nagy, "Next-to-leading order calculation of three-jet observables in hadron hadron collision," *Phys. Rev.* **D68** (2003) 094002, arXiv:hep-ph/0307268.

[10] C. F. Berger *et al.*, "An Automated Implementation of On-Shell Methods for One- Loop Amplitudes," *Phys. Rev.* **D78** (2008) 036003, arXiv:0803.4180 [hep-ph].

[11] S. Frixione and B. R. Webber, "Matching NLO QCD computations and parton shower simulations," *JHEP* **06** (2002) 029, arXiv:hep-ph/0204244.

[12] S. Frixione and B. R. Webber, "The MC@NLO 3.3 event generator," arXiv:hep-ph/0612272.

[13] P. Nason, "A new method for combining NLO QCD with shower Monte Carlo algorithms," *JHEP* **11** (2004) 040, arXiv:hep-ph/0409146.

[14] S. Frixione, P. Nason, and C. Oleari, "Matching NLO QCD computations with Parton Shower simulations: the POWHEG method," *JHEP* **11** (2007) 070, arXiv:0709.2092 [hep-ph].

[15] M. Kramer and D. E. Soper, "Next-to-leading order QCD calculations with parton showers. I: Collinear singularities," *Phys. Rev.* **D69** (2004) 054019, arXiv:hep-ph/0306222.

[16] D. E. Soper, "Next-to-leading order QCD calculations with parton showers. II: Soft singularities," *Phys. Rev.* **D69** (2004) 054020, arXiv:hep-ph/0306268.

[17] M. Kramer, S. Mrenna, and D. E. Soper, "Next-to-leading order QCD jet production with parton showers and hadronization," *Phys. Rev.* **D73** (2006) 014022, arXiv:hep-ph/0509127.

[18] Z. Nagy and D. E. Soper, "Parton showers with quantum interference," *JHEP* **09** (2007) 114, arXiv:0706.0017 [hep-ph].

[19] W. T. Giele, D. A. Kosower, and P. Z. Skands, "A Simple shower and matching algorithm," *Phys. Rev.* **D78** (2008) 014026, arXiv:0707.3652 [hep-ph].

[20] C. W. Bauer, F. J. Tackmann, and J. Thaler, "GenEvA (I): A new framework for event generation," *JHEP* **12** (2008) 010, arXiv:0801.4026 [hep-ph].

[21] C. W. Bauer, F. J. Tackmann, and J. Thaler, "GenEvA (II): A phase space generator from a reweighted parton shower," *JHEP* **12** (2008) 011, arXiv:0801.4028 [hep-ph].

[22] L. Lönnblad, "ARIADNE version 4: A Program for simulation of QCD cascades implementing the color dipole model," *Comput. Phys. Commun.* **71** (1992) 15–31.

[23] T. Becher and M. D. Schwartz, "A precise determination of α_s from LEP thrust data using effective field theory," *JHEP* **07** (2008) 034, arXiv:0803.0342 [hep-ph].

[24] J. Alwall *et al.*, "MadGraph/MadEvent v4: The New Web Generation," *JHEP* **09** (2007) 028, arXiv:0706.2334 [hep-ph].

[25] M. L. Mangano, M. Moretti, F. Piccinini, R. Pittau, and A. D. Polosa, "ALPGEN, a generator for hard multiparton processes in hadronic collisions," *JHEP* **07** (2003) 001, arXiv:hep-ph/0206293.

[26] S. Catani and M. H. Seymour, "The Dipole Formalism for the Calculation of QCD Jet Cross Sections at Next-to-Leading Order," *Phys. Lett.* **B378** (1996) 287–301, arXiv:hep-ph/9602277.

[27] S. Catani and M. H. Seymour, "A general algorithm for calculating jet cross sections in NLO QCD," *Nucl. Phys.* **B485** (1997) 291–419, arXiv:hep-ph/9605323.

[28] P. M. Stevenson, "Optimized Perturbation Theory," *Phys. Rev.* **D23** (1981) 2916.

[29] N. Lavesson and L. Lönnblad, "Merging parton showers and matrix elements – back to basics," *JHEP* **04** (2008) 085, arXiv:0712.2966 [hep-ph].

[30] T. Sjostrand, S. Mrenna, and P. Skands, "PYTHIA 6.4 physics and manual," *JHEP* **05** (2006) 026, arXiv:hep-ph/0603175.

[31] R. K. Ellis, D. A. Ross, and A. E. Terrano, "The Perturbative Calculation of Jet Structure in e+ e- Annihilation," *Nucl. Phys.* **B178** (1981) 421.

[32] R.-Y. Zhu, *Determination of the strong coupling constant up to complete second order in QCD*. Ph.d. thesis, MIT, 1983. MIT-LNS Report RX-1033.

[33] **JADE** Collaboration, W. Bartel *et al.*, "Experimental Studies on Multi-Jet Production in e+ e- Annihilation at PETRA Energies," *Z. Phys.* **C33** (1986) 23. See also S. Bethke, Habilitation thesis, LBL 50-208 (1987).

[34] **Particle Data Group** Collaboration, C. Amsler *et al.*, "Review of particle physics," *Phys. Lett.* **B667** (2008) 1.

[35] **DELPHI** Collaboration, P. Abreu *et al.*, "Tuning and test of fragmentation models based on identified particles and precision event shape data," *Z. Phys.* **C73** (1996) 11–60.

[36] S. Catani, Y. L. Dokshitzer, M. Olsson, G. Turnock, and B. R. Webber, "New clustering algorithm for multi - jet cross-sections in e+ e- annihilation," *Phys. Lett.* **B269** (1991) 432–438.